Identification of disease modifiers and novel treatment targets in hypertrophic cardiomyopathy

Schuldt, Maike

2021

document version
Publisher's PDF, also known as Version of record

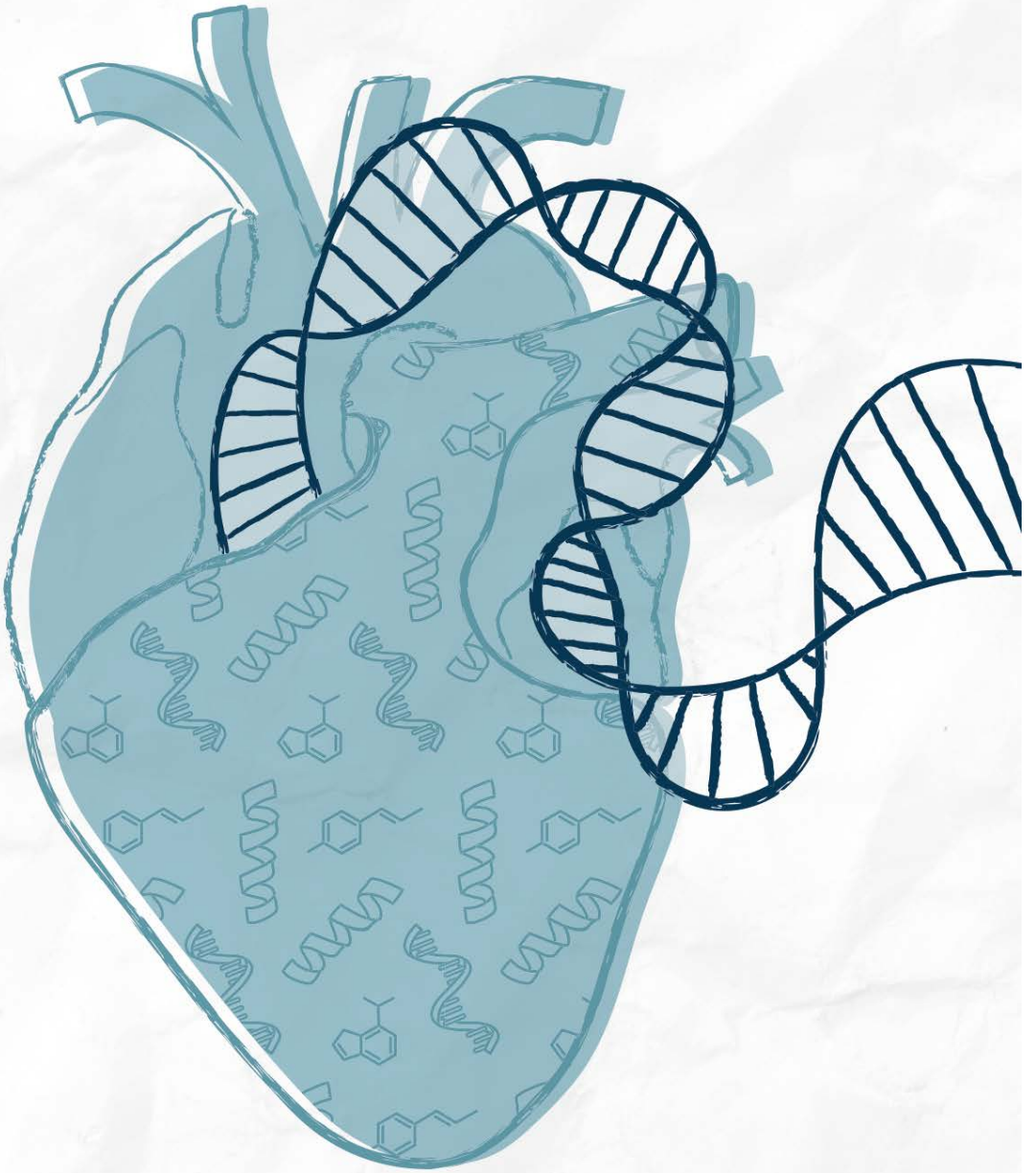

IDENTIFICATION OF DISEASE MODIFIERS AND NOVEL TREATMENT TARGETS IN HYPERTROPHIC CARDIOMYOPATHY

Maike Schuldt

Identification of disease modifiers and novel treatment targets in hypertrophic cardiomyopathy

Maike Schuldt

The work presented in this thesis was performed at the Amsterdam UMC, Vrije Universiteit, Department of Physiology, Amsterdam Cardiovascular Sciences Research Institute, Amsterdam, The Netherlands.

Cover design: Daniëlle Balk | www.daniellebalk.com
Layout: Daniëlle Balk | www.persoonlijkproefschrift.com
Printing: Ridderprint | www.ridderprint.nl

ISBN: 978-94-6416-436-7

VRIJE UNIVERSITEIT

Identification of disease modifiers and novel treatment targets in hypertrophic cardiomyopathy

ACADEMISCH PROEFSCHRIFT

ter verkrijging van de graad Doctor
aan de Vrije Universiteit Amsterdam,
op gezag van de rector magnificus
prof.dr. V. Subramaniam
in het openbaar te verdedigen
ten overstaan van de promotiecommissie
van de Faculteit der Geneeskunde
op vrijdag 28 mei 2021 om 9.45 uur
in de aula van de universiteit,
De Boelelaan 1105

door

Maike Schuldt
geboren te Einbeck, Duitsland

promotor: prof.dr. J. van der Velden

copromotor: dr. DWD. Kuster

Overige leden promotiecommissie:

prof. Bianca JJM. Brundel
prof. Connie R. Jimenez
prof. Reinier A. Boon
prof. Rudolf A. de Boer
dr. Annette Baas
dr. Magdalena Harakalova

The research described in this thesis was supported by a grant of the Dutch Heart Foundation (CVON2014-40 DOSIS). Financial support by the Dutch Heart Foundation for the publication of this thesis is gratefully acknowledged.

"Everything must be made as simple as possible. But not simpler."
- Albert Einstein

TABLE OF CONTENTS

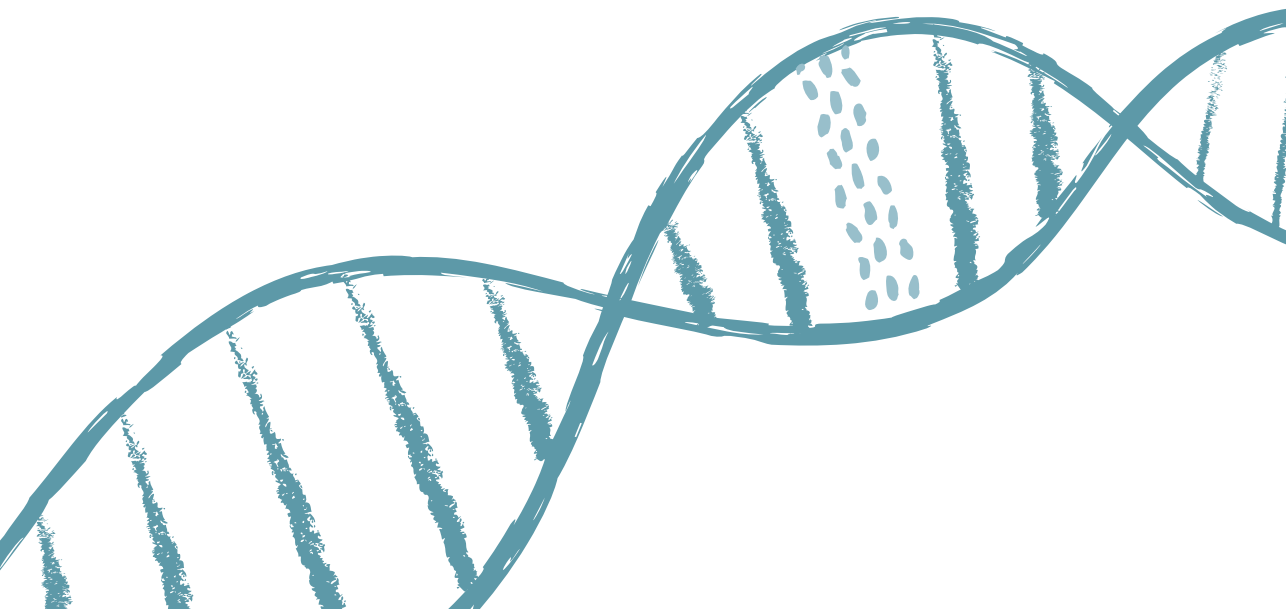

GENERAL INTRODUCTION AND THESIS OUTLINE

STRENGTH OF PATIENT COHORTS AND BIOBANKS FOR CARDIOMYOPATHY RESEARCH

R.A. de Boer, L.L.A.M. Nijenkamp, H.H.W. Silljé, T.R. Eijgenraam, R. Parbhudayal, B. van Driel, R. Huurman, M. Michels, J. Pei, M. Harakalova, F.H.M. van Lint, M. Jansen, A.F. Baas, F.W. Asselbergs, J.P. van Tintelen, B.J.J.M. Brundel, L.M. Dorsch, **M. Schuldt**, D.W.D. Kuster, J. van der Velden (DOSIS consortium)

Adjusted based on the publication in the Netherlands Heart Journal, 2020 Aug; 28(Suppl 1):50–56.

1

ABSTRACT

In 2011 the Netherlands Heart Foundation initiated consortium funding (CVON, Cardiovasculair Onderzoek Nederland) to stimulate collaboration between clinical and basic (preclinical) researchers on specific areas of research. One of those areas involves genetic heart diseases, which are frequently caused by pathogenic variants in genes that encode sarcomere proteins. In 2014, the DOSIS (**D**eterminants **o**f **s**usceptibility **i**n inherited cardiomyopathy: towards novel therapeutic approache**s**) consortium was initiated, focusing their research on secondary disease hits involved in the initiation and progression of cardiomyopathies. Here we highlight several recent observations from our consortium and collaborators which may ultimately be relevant for clinical practice.

Inherited cardiomyopathies, caused by pathogenic variants in genes encoding proteins that regulate cardiomyocyte contractility, are a major cause of morbidity and mortality. In 50-60% of familial hypertrophic (HCM) and 30-40% of dilated (DCM) cardiomyopathy, a pathogenic gene variant can be identified. The most common genes that are affected in HCM are *MYH7, MYBPC3* and *TNNT2,* which encode the thick filament proteins myosin heavy chain, cardiac myosin-binding protein-C (cMyBP-C), and the thin filament protein troponin T. In DCM the titin (*TTN)* gene, which encodes the giant myofilament protein titin, is the most frequently affected gene (~15-20% of all gene variants)[1]; in particular gene variants that lead to *TTN* truncation have been shown to be pathogenic [2]. In addition, in the Netherlands, a founder mutation in the *PLN* gene, which encodes the calcium-handling protein phospholamban, was identified in 2012 as a now well-known cause of DCM and arrhythmogenic cardiomyopathy [3,4]. Figure 1 depicts a cardiomyocyte to illustrate the affected proteins involved in cardiomyopathies. Upon activation of a cardiomyocyte, calcium enters the cell via the L-type calcium channel, which subsequently releases calcium from the intracellular calcium store, the sarcoplasmic reticulum. Calcium binds to the troponin complex, which induced a conformational change of troponin-tropomyosin, and thereby releases binding sites for myosin heads on the thin actin filament. Binding of myosin to actin (so-called cross-bridge) results in force development. The kinetics of cross-bridge cycling is regulated by cMyBP-C, and the giant protein titin, encoded by *TTN* and linked with DCM, underlies passive stiffness of sarcomeres [5].

In past years the number of genes in genetic diagnostic panels increased with the hope to identify a disease-causing variant in a larger group of patients and their family members. However, recent studies conclude that the additional benefit of screening large numbers of genes is disappointingly low and of marginal clinical utility [6,7]. Numerous new *TTN* gene variants have been identified mainly because of its large size. A study in 3 European cardiogenic centers showed that missense and non-frameshifting insertions/deletions variants are most likely benign, as reference populations showed comparable frequencies of these rare *TTN* variants [8]. The current panels thus rather increase the number of variants with unknown significance (VUS), which are likely benign, though they may have a modifier role in disease. Cardiomyopathy patients with a suspected genetic etiology should be referred for genetic screening. For HCM this includes patients with (usually asymmetric) left ventricular hypertrophy, not (fully) explained by abnormal loading conditions, with or without a clear family history. For DCM this includes patients with non-ischemic DCM, not (fully) explained by other etiological factors. Young age of onset and familial occurrence are important parameters that hint towards a genetic etiology. However, late onset in seemingly sporadic cases does not exclude a genetic origin due to the reduced penetrance and variable disease expression. All HCM and DCM patients in whom genetic screening was performed can be added to the biobanks, including their relatives (asymptomatic mutation carriers).

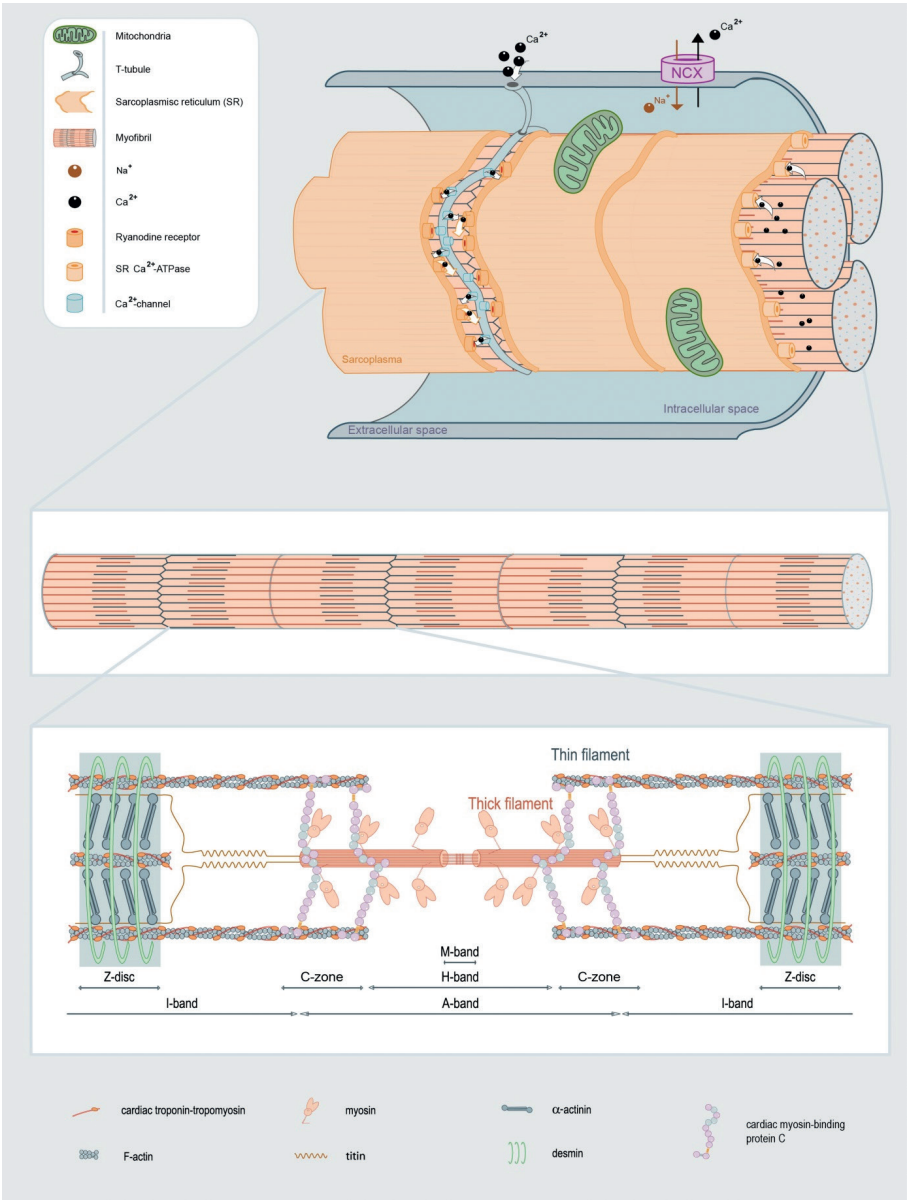

FIGURE 1. Activation of a cardiomyocyte triggers calcium entry and release of calcium from the sarcoplasmic reticulum (*SR*), which results in contraction of the cardiac myofibrils. To relax the cardiomyocyte, calcium is pumped back into the SR, and out of the cell via the sodium-calcium exchanger (*NCX*). Myofibrils consist of sarcomeres composed of the thin actin and thick myosin filament, and the third filament titin. Sarcomeres consist of sub-regions (depicted by the different bands), which underlie the striated pattern of cardiac muscle. Gene variants that cause cardiomyopathies are frequently found in myosin heavy chain, troponin T, cardiac myosin-binding protein-C (located in the Z-zone) and titin. (Figure is adapted from Sequeira at al. [30]).

Since cardiomyopathies remain to constitute one of the most common causes of sudden cardiac death in the young and still represent major causes for cardiac transplantation, adequate identification of additional disease triggers and understanding the pathomechanisms is of utmost importance. The clinical approach is furthermore complicated since inherited cardiomyopathies are clinically heterogeneous: age-dependent penetrance and disease-severity differ greatly between patients with the identical genetic variant. The mechanisms that underlie the variation in disease expression are still largely unknown. By combining cellular, genetic and clinical data from well-phenotyped national patient cohorts, DOSIS strived to define disease factors (i.e. secondary hits) that in addition to the pathogenic gene variant cause and aggravate cardiac disease in cardiomyopathy patients (Table 1; Figure 2). Several recent observations are highlighted below.

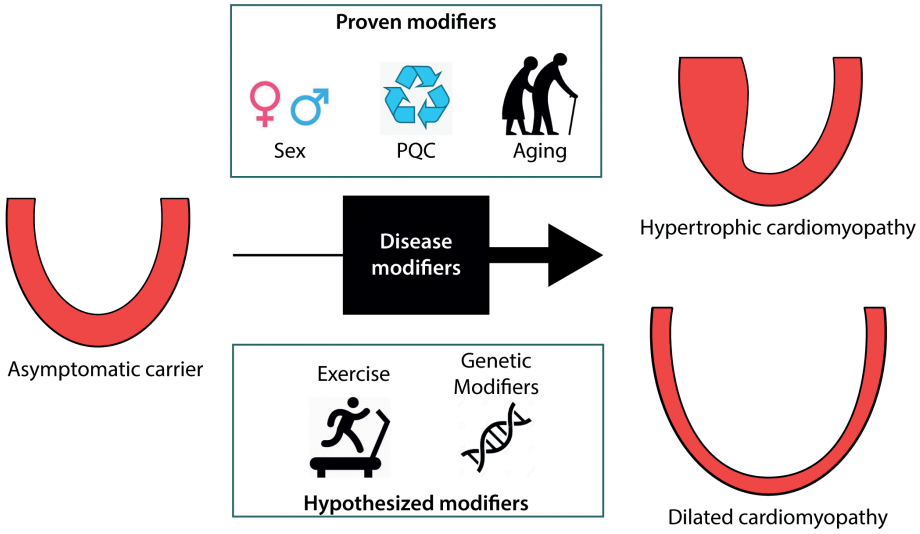

FIGURE 2. Disease modifiers in inherited cardiomyopathies (PQC, protein quality control).

TABLE 1. Cohorts of DOSIS

Cohort	Participating centres	Population	Biobank collection	Aim
Erasmus HCM observational cohort	Erasmus MC	HCM patients and gene variant carriers	DNA	Identify predictive clinical markers for major cardiac events
BIO FOr CARe observational cohort	UMC Utrecht, UMC Groningen, Amsterdam UMC, Erasmus MC	All sarcomere gene variants	DNA, RNA (from blood), plasma and serum	Identify predictive biomarkers for major cardiac events
Telephone interviews	UMC Utrecht, UMC Groningen, Amsterdam UMC	*MYBPC3* founder gene variant carriers	n.a.	Determine predictive value of environmental factors (especially exercise) for major cardiac events
ENERGY randomised placebo-controlled trial	Amsterdam UMC, Erasmus MC	Preclinical *MYH7* gene variant carriers	serum	Determine effects of trimetazidine on improving myocardial energy efficiency in the pre-clinical disease stage
Myectomy cohort	Erasmus MC, UMC Utrecht	HCM patients undergoing septal myectomy	DNA, cardiac tissue	Collect myocardial tissue for use in etiological studies

Indexation for body size to set the diagnostic threshold for left ventricular thickening

Using a large collection of myectomy samples from patients with obstructive HCM, we have shown that there is a sex-specific difference in diastolic function at the time of myectomy in HCM patients carrying pathogenic variants in *MYH7* and *MYBPC3* [9]. Women showed more diastolic dysfunction evident from significantly higher E/e' ratios, impaired left ventricular filling patterns, and higher tricuspid regurgitation velocities. Of the female patients, 50% showed grade III diastolic dysfunction, while the majority of male patients (56%) had only mild (grade I) diastolic dysfunction. Correction of maximal septal thickness and left atrial diameter for body surface area (BSA) resulted in significantly *higher* values in female compared to male patients. Histological and protein analyses revealed more advanced remodeling of the heart in female compared to male HCM patients evident from higher levels of fibrosis and activation of the cardiac fetal gene program, which is characteristic of heart failure. In addition to genetic screening, the current diagnostic criterion of hypertrophy is a maximal LV wall thickness of ≥15mm, or ≥13mm in first-degree relatives of HCM patients. As the heart of women, and in general relatively small persons, is smaller compared to the heart of men, this threshold for the diagnosis of HCM probably should be corrected for body size [10]. The current diagnostic threshold, which does not take into account body size,

may likely explain the male predominance in HCM patient cohorts, simply because males in general have larger hearts. A recent study in a Dutch cohort of 199 genotype-positive subjects, family members of HCM patients, who were referred for cardiac screening between 1995 and 2018, indexation of wall thickness by BSA decreased the number of HCM diagnoses [11]. Moreover, predictive accuracy for HCM-related events (mortality, cardiac transplantation, implantable cardioverter-defibrillator implantation and septal reduction therapy) improved significantly after indexation by BSA. These studies indicate that correcting LV thickness for body size should be considered for the diagnosis of HCM and longitudinal follow-up studies in larger cohorts of preclinical genotype-positive individuals are needed to confirm this.

Altered metabolism as key driver of disease in cardiomyopathies

Several studies suggest an important role for secondary disease-modifiers such as additional (epi)genetic variations and environmental disease triggers. Compelling data have accumulated that obesity is an overarching risk factor, also for age-of-onset and severity of cardiomyopathies. Proof that obesity contributes to disease onset and severity comes from cohort studies. The international HCM Share registry showed that patients with a high body mass index have a significantly increased risk of heart failure, more advanced left ventricular outflow tract obstruction and arrhythmias (i.e. HCM-related outcomes)[12]. Moreover, a prospective study in adolescent men demonstrated that even mildly elevated body weight in late adolescence significantly increased the risk to develop dilated cardiomyopathy in adulthood [13]. At the heart level, a recent proteomics study in human HCM tissue samples showed reduced levels of energy metabolism proteins [14].This observation is in line with studies in human HCM showing energy deficiency of the heart [15,16]. Energy deficiency has been proposed as the primary variant-induced pathomechanism of HCM [17], which is supported by studies showing reduced cardiac efficiency in preclinical asymptomatic carriers of sarcomere gene variants in the absence of cardiac hypertrophy [16,18]. Accordingly, DCM caused by *TTN* gene variants has been linked with mitochondrial dysfunction and metabolic perturbations as cause of disease progression [19]. Overall, these studies indicate that timely (disease stage-specific) treatment of metabolic perturbations may slow down disease progression in cardiomyopathy patients [20]. An observational cohort to determine the predictive value of metabolic biomarkers (BIO FOr CARe: identification of biomarkers for development and progression of HCM in carriers of the Dutch *MYBPC3* founder carriers) and a clinical trial using metabolic drug therapy aimed to improve energetics of the heart at preclinical stage in HCM gene variant carriers are currently performed by several DOSIS PIs (ENERGY trial)[21].

Altered protein quality control as disease modifier in cardiomyopathy

An age-related decline in protein quality control (PQC) has been proposed as contributor to disease progression in cardiomyopathy. As sarcomere proteins are the most abundant proteins in the heart, maintenance of sarcomere structure and function

depends on PQC mechanisms. Pathogenic gene variants result in poison polypeptides or reduced protein levels (haploinsufficiency) and may trigger PQC and/or stress cellular protein homeostasis. DCM patients with truncating *TTN* variants show a relatively mild disease course, though with significant excess mortality in elderly patients. The latter may be explained by an age-related deterioration of the PQC mechanisms. As life expectancy increases, *TTN*-associated morbidity and mortality will likely become more prevalent [22]. Also in PLN-associated cardiomyopathy protein aggregation and activation of PQC pathways has been observed in end-stage disease [23].

Terminally misfolded and aggregation-prone (mutant) proteins are cleared by the two degradation systems, UPS and autophagy. Furthermore, pathways of PQC are strongly linked to cell architecture, such as the microtubules network. DOSIS studies in a large set of cardiac tissues from a well-characterized HCM patient group showed altered PQC with several specific changes in gene-variant positive patients (genotype-positive) compared to genotype-negative patients and non-failing controls. An introduction to the role of PCQ control in the heart is given in **Chapter 3**, and DOSIS results on PQC in HCM patient samples are described in **Chapters 4 and 7**.

Cell-to-cell mRNA/protein variability as pathomechanism in cardiomyopathy

As familial cardiomyopathies represent an autosomal dominant genetic disorder, most patients are heterozygous for the mutation and carry one variant and one normal (wild-type) allele. In cardiomyopathy patients, the heart of a genotype-positive individual produces the variant protein in addition to the normal protein. As indicated above, the homeostasis of cellular proteins is tightly regulated by the PQC system, but it is also regulated at the mRNA level by non-sense mediated mRNA decay. Both systems are needed to suppress the accumulation of variant protein while keeping the normal protein at sufficient levels in cardiac muscle cells. It was recently shown that transcription of both alleles occurs independently and in a stochastic manner, where one cell favors one allele and the next cell favors the other allele [24]. This burst-like, stochastic on/off-switching of allele transcription does not affect mRNA and protein levels in case of homozygous wild-type alleles. However, heterozygosity of alleles as present in genotype-positive individuals may introduce cell-to-cell variation with one cardiomyocyte expressing high levels of variant protein, while variant levels may be low in another cardiomyocyte [25]. Indeed, Kraft and colleagues showed that *MYH7* gene variants cause a variable variant to wild-type ratio of mRNA expression in cardiomyocytes from the same heart [24,26]. The DOSIS consortium showed intercellular variation of cMyBP-C myofilament protein expression due to truncating *MYBPC3* variants in the myocardium of HCM patients [27]. The functional consequences of the variable protein expression, which results in a mosaic pattern of cardiomyocytes with low and high variant/wild-type expression remain to be determined. Loss of cMyBP-C causes severe dysfunction in mouse studies and engineered heart tissue [28,29]. We propose that the intercellular variation of cMyBP-C protein levels cause

inhomogeneous contraction and relaxation and underlies the formation of myofibrillar disarray, a currently unexplained disease characteristics of HCM. As aging reduces the quality of PQC, an age-dependent progression of the degree of allelic imbalance and cell-to-cell variation may contribute to cardiomyopathy development.

In conclusion, monogenetic cardiomyopathies have been intensely studied in the last 3 decades, and this has resulted in major progress in understanding what genes are involved. On the other hand, the striking heterogeneity, the highly variable age of onset, and the presence of gene variant carriers that never develop disease is as of yet largely unexplained. Given the profound repercussion for carriers, patients and family members we must improve to better understand the individual's response to the presence of a pathogenic gene variant.

DOSIS aims for hitherto unexplored mechanisms that probably will modify the pathogenic gene variant (Figure 3). We have set up important initiatives and collaborations and have generated preliminary results showing that environmental and genetic modifiers indeed are important in our understanding. In the future we will step up our initiatives and projects and have identified an agenda, that contains - what we feel - important additional factors that when fully understood will guide clinicians in proper diagnosis, risk prediction, prognostication and, ultimately, cause-specific novel treatments.

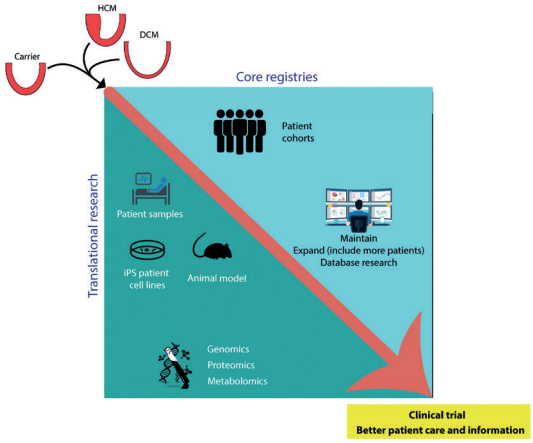

FIGURE 3. By combining cellular, genetic and clinical data from well-phenotyped national patient cohorts, DOSIS strives to define disease factors that in addition to the pathogenic gene variant cause and aggravate cardiac disease in cardiomyopathy patients.

Sources of funding: CVON-DOSIS consortium 2014-40 Netherlands Heart Foundation

Acknowledgements: We thank Salva R. Yurista and Vasco Sequeira with the design of the Figures.

AIM AND OUTLINE OF THIS THESIS

As described above, HCM is clinically heterogeneous and disease penetrance and severity differs greatly even between individuals carrying the same sarcomere gene mutation. Within the scope of the DOSIS consortium (Figure 2), we explored disease modifiers of HCM in this thesis, that may influence disease onset and disease phenotype. Therefore, we performed functional studies in isolated cardiomyocytes of myectomy tissue from the Erasmus MC myectomy cohort and determined protein levels of modifiers in these tissues. We pursued a targeted approach exploring known or hypothesized modifiers (part 1) as well as an unbiased approach using different omics techniques to identify novel modifiers (part 2).

Part 1: Targeted analysis of known and hypothesized disease modifiers

In part 1 of this thesis we explored disease modifiers in myectomy tissue of HCM patients for which we already had evidence from studies in animal models or other cardiac pathologies.

The DOSIS consortium has shown intercellular variability in cMyBP-C protein expression due to truncating *MYBPC3* mutations in the myocardium of HCM patients [27], but the functional consequences still remain to be elucidated. In line with variable levels (dose) of healthy and mutant protein in the myocardium, we defined the functional impact of mutant protein dose and mutation location in **Chapter 2.** Therefore, we assessed the mutant protein dose effect of the pathogenic *TNNT2* variants I79N, R94C and R278C on contractile function of cardiomyocytes in functional single cell studies. We performed troponin exchange experiments to introduce defined levels of mutant protein into healthy cardiomyocytes. Furthermore, we determined levels of mutant cardiac troponin T in patient tissues with the *TNNT2* R278C mutation and combined it with functional data.

The following two chapters focus on the role of the cellular protein quality control (PQC) system in disease progression. As mutant proteins are often misfolded and aggregation-prone, they likely trigger the PQC to maintain a healthy protein homeostasis. **Chapter 3** gives an overview about the different components of the cellular protein quality control system and summarizes the current knowledge of its involvement in inherited cardiomyopathies. It further highlights pharmacological targeting of the PQC as potential novel therapeutic strategy in cardiomyopathies.

In **Chapter 4** we determined the expression levels of different heat shock proteins involved in protein stabilization (HSPB1, HSPB5, HSPB7) and refolding (HSPD1, HSPA1, HSPA2) in myectomy tissue of HCM patients. Thereby we also looked at differences between genotype-positive and genotype-negative HCM patients. As PQC function is also linked to the microtubule network, we also assessed levels of α-tubulin and acetylated α-tubulin.

Part 2: Omics-studies to identify novel disease modifiers

In part 2 we used proteomics, transcriptomics and metabolomics to identify novel disease modifiers and biomarkers, that may represent potential novel treatment targets and may be used for early diagnosis of cardiac dysfunction.

In **Chapter 5** we performed a proteomics screen on a large and clinically well-characterized set of myectomy tissues from the Erasmus MC myectomy cohort. By comparing to non-failing controls, we defined major HCM disease-specific changes on the protein level. As genotype-specific differences were low, we compared in particular genotype-positive and genotype-negative samples. We validated our top candidate in a novel *MYBPC3*$_{2373insG}$ mouse model to demonstrate functional relevance.

In **Chapter 6** we applied a multi-omics approach on a set of myectomy samples harboring a *MYBPC3* mutation by integrating the proteomics data with the histone acetylome and transcriptomics data in close collaboration with colleagues from Utrecht. In this study we aimed to identify disease markers that are consistently changed on three levels of regulation, the chromatin level, the RNA level and the protein level.

As the DOSIS consortium has shown that there is a sex-specific difference in diastolic function at the time of myectomy, with women having more severe diastolic dysfunction [9], we analyzed sex differences in the proteomics data set in **Chapter 7**. Thereby we aimed to identify changes on the protein level that may underlie the sex-specific differences in clinical presentation of male and female HCM patients.

In **Chapter 8** we performed a metabolomics screen in serum of healthy controls, asymptomatic mutation carriers and symptomatic obstructive HCM patients, that were part of the ENGINE study [15]. As advanced imaging techniques have shown disease stage-dependent differences in myocardial oxygen consumption and efficiency, we aimed to identify serum biomarker panels that are able to distinguish healthy controls, asymptomatic mutation carriers and symptomatic patients.

In **Chapter 9** we summarize and discuss our findings and point out future perspectives.

REFERENCES

1. Walsh R, Thomson KL, Ware JS et al. Reassessment of Mendelian gene pathogenicity using 7,855 cardiomyopathy cases and 60,706 reference samples. Genet Med. 2017;19:192-203.
2. Herman DS, Lam L, Taylor MR et al. Truncations of titin causing dilated cardiomyopathy. N Engl J Med. 2012;366:619-28.
3. van der Zwaag PA, van Rijsingen IA, Asimaki A et al. Phospholamban R14del mutation in patients diagnosed with dilated cardiomyopathy or arrhythmogenic right ventricular cardiomyopathy: evidence supporting the concept of arrhythmogenic cardiomyopathy. Eur J Heart Fail. 2012;14:1199-207.
4. van Spaendonck-Zwarts KY, van Rijsingen IA, van den Berg MP et al. Genetic analysis in 418 index patients with idiopathic dilated cardiomyopathy: overview of 10 years' experience. Eur J Heart Fail. 2013;15:628-36.
5. van der Velden J, Stienen GJM. Cardiac Disorders and Pathophysiology of Sarcomeric Proteins. Physiol Rev. 2019;99:381-426.
6. Thomson KL, Ormondroyd E, Harper AR et al; NIHR BioResource – Rare Diseases Consortium. Analysis of 51 proposed hypertrophic cardiomyopathy genes from genome sequencing data in sarcomere negative cases has negligible diagnostic yield. Genet Med. 2019;21:1576-84.
7. van Lint FHM, Mook ORF, Alders M, Bikker H, Lekanne Dit Deprez RH, Christiaans I. Large next-generation sequencing gene panels in genetic heart disease: yield of pathogenic variants and variants of unknown significance. Neth Heart J. 2019;27:304-09.
8. Akinrinade O, Heliö T, Lekanne Deprez RH et al. Relevance of titin missense and non-frameshifting insertions/deletions variants in dilated cardiomyopathy. Sci Rep. 2019;9:4093.
9. Nijenkamp LLAM, Bollen IAE, van Velzen HG et al. Sex differences at the time of myectomy in hypertrophic cardiomyopathy. Circ Heart Fail. 2018;11:e004133.
10. van Driel B, Nijenkamp L, Huurman R, Michels M, van der Velden J. Sex differences in hypertrophic cardiomyopathy: new insights. Curr Opin Cardiol. 2019;34:254-59.
11. Huurman R, Schinkel AFL, van der Velde N et al. Effect of body surface area and gender on wall thickness thresholds in hypertrophic cardiomyopathy. Neth Heart J. 2020;28:37-43.
12. Fumagalli C, Maurizi N, Day SM et al; SHARE Investigators. Association of obesity with adverse long-term outcomes in hypertrophic cardiomyopathy. JAMA Cardiol. 2019;6:1-8.
13. Robertson J, Schaufelberger M, Lindgren M et al. Higher body mass index in adolescence predicts cardiomyopathy risk in midlife. Circulation. 2019;140:117-25.
14. Coats CJ, Heywood WE, Virasami A et al. Proteomic analysis of the myocardium in Hypertrophic Obstructive Cardiomyopathy. Circ Genom Precis Med. 2018;11:e001974.
15. Guclu A, Knaapen P, Harms HJ et al. Disease stage-dependent changes in cardiac contractile performance and oxygen utilization underlie reduced myocardial efficiency in human inherited hypertrophic cardiomyopathy. Circ Cardiovasc Imaging. 2017;10(5).
16. Crilley JG, Boehm EA, Blair E et al. Hypertrophic cardiomyopathy due to sarcomeric gene mutations is characterized by impaired energy metabolism irrespective of the degree of hypertrophy. J Am Coll Cardiol. 2003;41:1776-82.
17. Ashrafian H, Redwood C, Blair E, and Watkins H. Hypertrophic cardiomyopathy:a paradigm for myocardial energy depletion. Trends Genet. 2003;19:263-8.

18. Witjas-Paalberends ER, Guclu A et al. Gene-specific increase in the energetic cost of contraction in hypertrophic cardiomyopathy caused by thick filament mutations. Cardiovasc Res. 2014;103:248-57.
19. Verdonschot JAJ, Hazebroek MR, Derks KWJ et al. Titin cardiomyopathy leads to altered mitochondrial energetics, increased fibrosis and long-term life-threatening arrhythmias. Eur Heart J. 2018;39:864-73.
20. van der Velden J, Tocchetti CG, Varricchi G et al. Metabolic changes in hypertrophic cardiomyopathies. Scientific update from the Working Group of Myocardial Function of the ESC. Cardiovasc Res. 2018;114:1273-80.
21. van Driel BO, Rossum AC, Michels M, Huurman R, van der Velden. J. Extra energy for hearts with a genetic defect: ENERGY trial. Neth Heart J. 2019;27:200-05.
22. Jansen M, Baas AF, van Spaendonck-Zwarts KY et al. Mortality risk associated with truncating founder mutations in titin. Circ Genom Precis Med. 2019;12:e002436.
23. Te Rijdt WP, van der Klooster ZJ, Hoorntje ET et al. Phospholamban immunostaining is a highly sensitive and specific method for diagnosing phospholamban p.Arg14del cardiomyopathy. Cardiovasc Pathol. 2017;30:23-26.
24. Montag J, Kowalski K, Makul M et al. Burst-like transcription of mutant and wildtype MYH7-alleles as possible origin of cell-to-cell contractile imbalance in hypertrophic cardiomyopathy. Front Physiol. 2018;9:359.
25. Kraft T, Montag J, Radocaj A, Brenner B. Hypertrophic cardiomyopathy: cell-to- cell imbalance in gene expression and contraction force as trigger for disease phenotype development. Circ Res. 2016;119:992–95.
26. Brenner B, Seebohm B, Tripathi S, Montag J, Kraft T. Familial hypertrophic cardiomyopathy: functional variance among individual cardiomyocytes as a trigger of FHC-phenotype development. Front Physiol. 2014;5:392.
27. Parbhudayal RY, Garra A, Götte MJW et al. Variable cardiac myosin binding protein-C expression in the myofilaments due to MYBPC3 mutations in hypertrophic cardiomyopathy. J Mol Cell Cardiol. 2018;123:59-63.
28. McConnell BK, Jones KA, Fatkin D et al. Dilated cardiomyopathy in homozygous myosin-binding protein-C mutant mice. J Clin Invest. 1999;104:1235–44.
29. Wijnker PJM, Friedrich FW, Dutsch A et al. Comparison of the effects of a truncating and a missense *MYBPC3* mutations on contractile parameters of engineered heart tissue. J Mol Cell Cardiol. 2016;97:82-92.
30. Sequeira V, Nijenkamp LL, Regan JA, van der Velden J. The physiological role of cardiac cytoskeleton and its alterations in heart failure. Biochim Biophys Acta. 2014;1838:700-22.

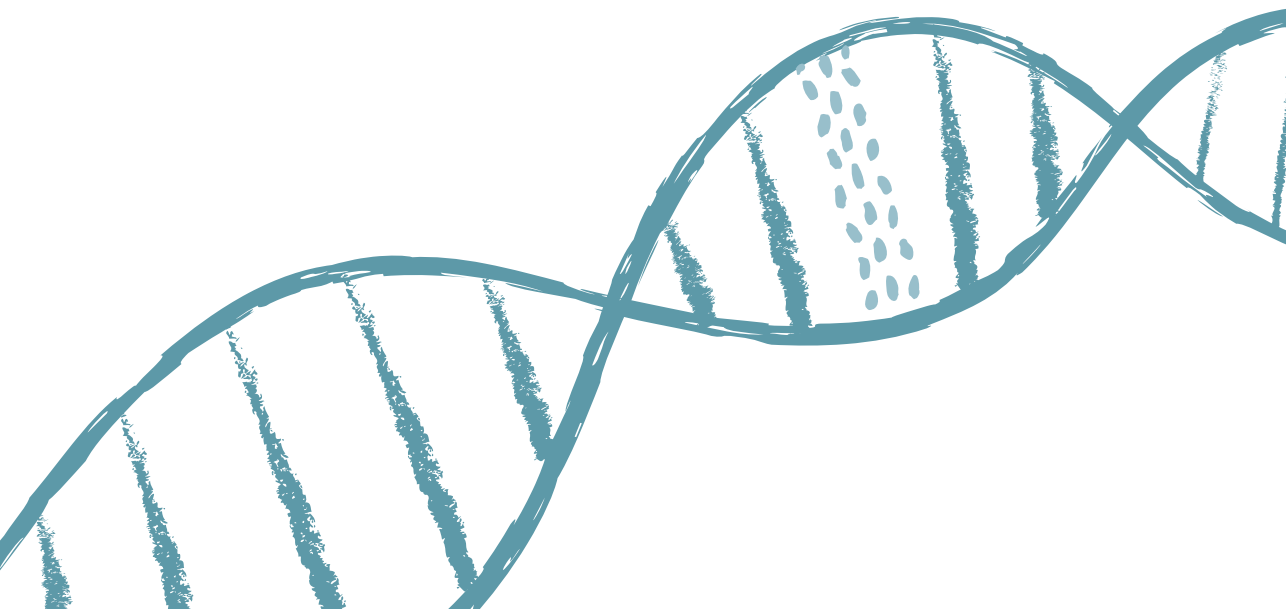

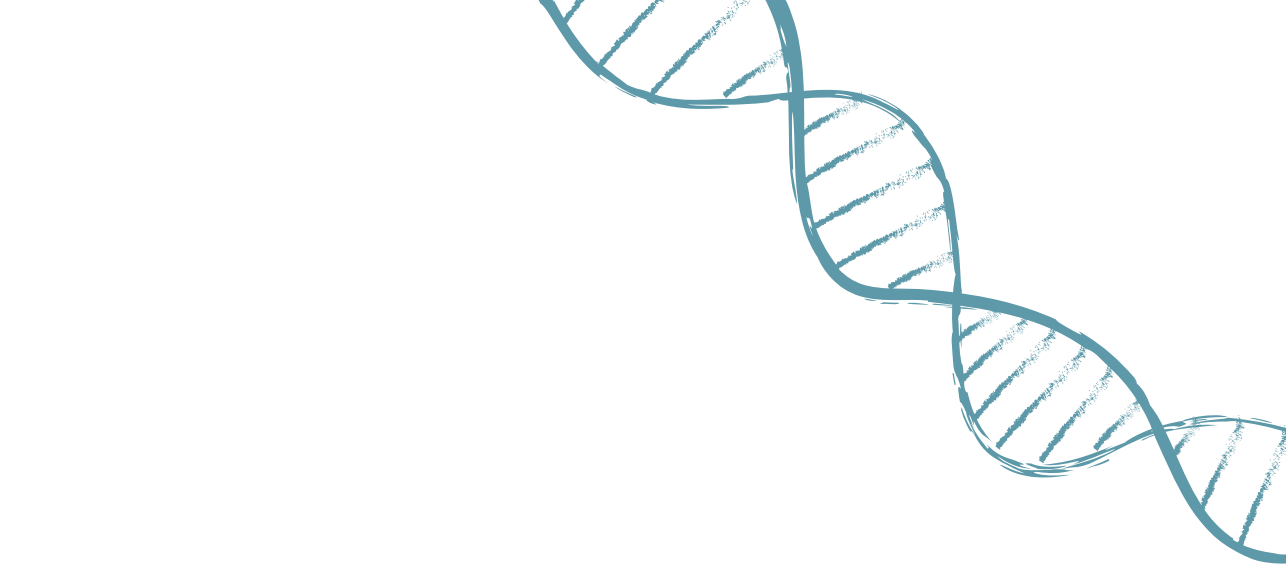

PART 1
TARGETED ANALYSIS OF KNOWN AND HYPOTHESIZED DISEASE MODIFIERS

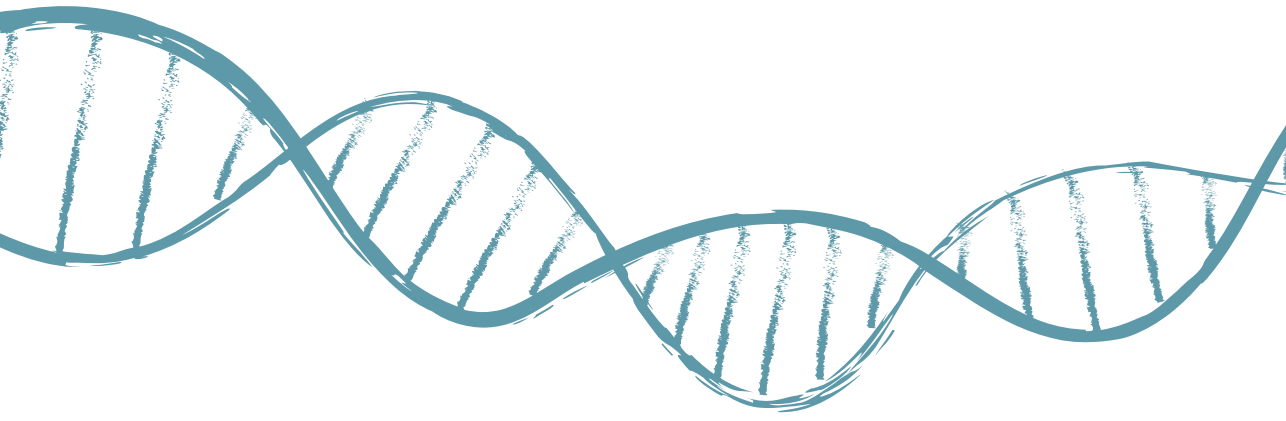

MUTATION LOCATION OF HCM-CAUSING TROPONIN T MUTATIONS DEFINES THE DEGREE OF MYOFILAMENT DYSFUNCTION IN HUMAN CARDIOMYOCYTES

Maike Schuldt, Jamie R. Johnston, Huan He, Roy Huurman, Jiayi Pei, Magdalena Harakalova, Corrado Poggesi, Michelle Michels, Diederik W.D. Kuster, Jose R. Pinto, Jolanda van der Velden

Journal of Molecular and Cellular Cardiology, 2020. 150: p. 77-90.

2

ABSTRACT

Background: The clinical outcome of hypertrophic cardiomyopathy patients is not only determined by the disease-causing mutation but influenced by a variety of disease modifiers. Here, we defined the role of the mutation location and the mutant protein dose of the troponin T mutations I79N, R94C and R278C.

Methods and results: We determined myofilament function after troponin exchange in permeabilized single human cardiomyocytes as well as in cardiac patient samples harboring the R278C mutation. Notably, we found that a small dose of mutant protein is sufficient for the maximal effect on myofilament Ca^{2+}-sensitivity for the I79N and R94C mutation while the mutation location determines the magnitude of this effect. While incorporation of I79N and R94C increased myofilament Ca^{2+}-sensitivity, incorporation of R278C increased Ca^{2+}- sensitivity at low and intermediate dose, while it decreased Ca^{2+}-sensitivity at high dose. All three cTnT mutants showed reduced thin filament binding affinity, which coincided with a relatively low maximal exchange (50.5 ± 5.2%) of mutant troponin complex in cardiomyocytes. In accordance, 32.2 ± 4.0% mutant R278C was found in two patient samples which showed 50.0 ± 3.7% mutant mRNA. In accordance with studies that showed clinical variability in patients with the exact same mutation, we observed variability on the functional single cell level in patients with the R278C mutation. These differences in myofilament properties could not be explained by differences in the amount of mutant protein.

Conclusions: Using troponin exchange in single human cardiomyocytes, we show that TNNT2 mutation-induced changes in myofilament Ca^{2+}-sensitivity depend on mutation location, while all mutants show reduced thin filament binding affinity. The specific mutation-effect observed for R278C could not be translated to myofilament function of cardiomyocytes from patients, and is most likely explained by other (post)-translational troponin modifications. Overall, our studies illustrate that mutation location underlies variability in myofilament Ca^{2+}-sensitivity, while only the R278C mutation shows a highly dose-dependent effect on myofilament function.

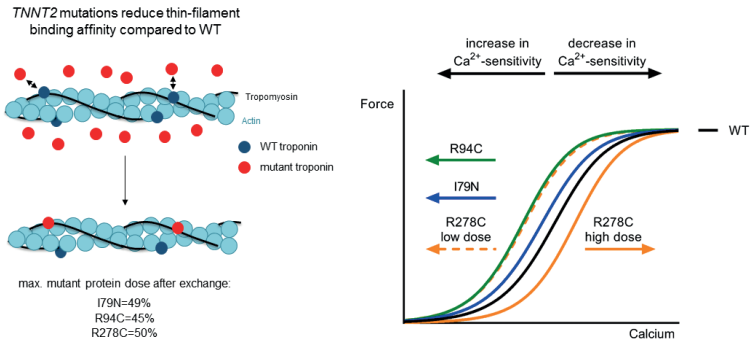

INTRODUCTION

Hypertrophic cardiomyopathy (HCM) is the most prevalent inherited heart disease affecting 1:500 to 1:200 individuals in the general population [1,2]. Current genetic screening identifies a pathogenic gene variant (further referred to as mutation) in ~50–60% of all patients [3]. Despite improved genotyping, prediction of disease based on genotype is challenging as the HCM population shows large clinical variability. This is evident from large differences in disease onset and severity, even in individuals carrying the exact same mutation. There is thus no clear frequent affected sarcomere genes [4]. As the majority of genotype-positive individuals are heterozygous for a gene mutation, carrying one normal and one mutant allele, clinical heterogeneity may be explained by the abundance (dose) of the mutant protein. Although 50% of healthy and 50% of mutant protein would be expected with a heterozygous mutation, this ratio can change due to allelic expression being stochastic, which can result in variable expression levels of healthy and mutant protein [5,6]. Accordingly, 43% of mutant protein has been shown in human induced pluripotent stem cell-derived cardiomyocytes carrying the I79N mutation in the gene (TNNT2) encoding cardiac troponin T (cTnT) [7], whereas heterozygous Tnnc1-A8V mice only showed 21% of mutant protein [8]. Furthermore, mutant protein dose can be influenced by changes in protein stability and/or degradation. A mutant protein dose-dependent increase in myofilament Ca2+-sensitivity was reported in a transgene (Tg) mouse model with a α-tropomyosin mutation [9]. Another study showed a dose-dependent effect of the Tnnt2 mutation R92Q on morphological and structural abnormalities as well as hypertrophy markers in Tg mice [10]. In addition to mutant protein dose, location of the mutation in the gene may explain the degree of cardiac muscle dysfunction. A mutation location effect has been observed in a study comparing two mouse models with different Tnnt2 mutations, a missense and a truncation mutation, that differ in their degree of hypertrophy and fibrosis development [11]. Furthermore, studies in transgenic mice found that the Tnnt2 mutation I79N increased Ca^{2+}-sensitivity [12], whereas the R278C mutation did not [13]. Differences in Ca^{2+}-sensitivity and Ca^{2+}- binding affinity have also been demonstrated in a study comparing the mouse models for Tnnt2 I79N, F110I and R278C [14]. Similarly, in vitro studies using recombinant proteins have shown that the HCM-associated increase in Ca^{2+}-sensitivity differs for different human TNNT2 mutations incorporated into porcine fibers [15], strengthening the concept of mutation location as a disease modifier. Based on these previous studies, we hypothesize that the degree of myofilament dysfunction depends on both the mutant protein dose and mutation location. To test our hypothesis we make use of the troponin exchange method in human cardiomyocytes, which enables us to control the dose of mutant protein in single cardiac muscle cells and study the effects on myofilament Ca^{2+}-sensitivity. We compared three pathogenic TNNT2 mutations I79N, R94C and R278C. Furthermore, we were able to characterize myofilament function in three human myectomy samples of patients carrying the R278C mutation, which enabled us to compare the effects of this specific mutation in the absence (exchange experiments) and presence (myectomy samples) of secondary disease remodeling.

METHODS

Human cardiac samples

Exchange experiments were performed in the human sample 2.114 which had a high endogenous phosphorylation background and was obtained from the Sydney Heart Bank. HCM tissue samples from the interventricular septum of patients harboring the *TNNT2* R278C mutation were obtained during myectomy surgery to relieve LV outflow tract obstruction and collected by the Erasmus University Medical Center Rotterdam and the University of Florence. HCM samples from patients with other mutations and without a sarcomere mutation (sarcomere mutation-negative) were used as controls in our protein analyses studies (samples from Erasmus Medical Center and Sydney Heart Bank). Table 1 provides an overview, including clinical characteristics, of all HCM samples used in this study. The samples 4.021, 5.033, 6.034, 7.012 and 7.040 were used as non-failing controls for single cardiomyocyte measurements and/or western blot analysis. They originate from the LV free wall of donor hearts without history of cardiac disease and were obtained from the Sydney Heart Bank. Written informed consent was obtained from each patient prior to myectomy and the study protocol was approved by the local medical ethics review committees. All samples were stored in liquid nitrogen until use.

Cardiomyocyte force measurements

Single cardiomyocytes were mechanically isolated from frozen cardiac tissue and functional myofilament measurements performed as described previously [16]. Briefly, the membrane of isolated cardiomyocytes was permeabilized with 0.5% Triton X-100 and single cardiomyocytes were attached to a force transducer and a motor needle. To determine the force-calcium relation, the force development of the cell was measured at different calcium concentrations. Ca^{2+}-sensitivity of myofilaments was determined as the [Ca^{2+}] needed to achieve half-maximal force (EC_{50}). The protocol was performed at 1.8 and 2.2 µm sarcomere length of the cell to determine length-dependent activation (LDA), which was measured as the difference in EC_{50} at both sarcomere lengths. Only cells with a maximal force >10 kN/m^2 were included in the analysis to ensure good quality of the cells.

TABLE 1. Clinical characteristics of HCM samples. Clinical characteristics of human HCM samples that were used in this study. Abbreviations: sarcomere mutation negative (SMN), interventricular septum (IVS), left atrial diameter (LAD), enddiastolic diameter (EDD), left ventricular outflow tract obstruction (LVOTO). FL, samples from Florence; SHB, explanted heart sample from Sydney Heart Bank.

Sample ID	Age (yrs, at myectomy)	Sex	Genotype	IVS (mm)	LAD (mm)	EDD (mm)	E/A ratio	E/e' ratio	Diastolic dysfunction (stage)	LVOTO (mmHg)
HCM 173	58	M	*TNNT2* R278C	18	51	40	1.5	15.7	2	74
HCM 175	61	M	*TNNT2* R278C	16	46	50	0.75	12.5	2	31
HCM 234	72	M	*TNNT2* R278C	19	62	38	*NA*	20.8	2 or 3	96
FL 1084	49	M	*TNNT2* R278C & *MYBPC3* T1095M	*NA*	*NA*	*NA*	*NA*	*NA*	*NA*	*NA*
FL 1097	60	F	*TNNT2* R278C	*NA*	*NA*	*NA*	*NA*	*NA*	*NA*	*NA*
FL 10112	73	F	*TNNT2* R278C & *MYBPC3* K814del	*NA*	*NA*	*NA*	*NA*	*NA*	*NA*	*NA*
HCM 132	15	F	*TNNT2* Gln272*	19	37	39	2.33	17.5	3	81
SHB 3166	26	M	*TNNT2* K280N	37	*NA*	*NA*	*NA*	*NA*	*NA*	*NA*
HCM 109	71	F	SMN	22	52	53	1.30	33.6	2	130
HCM 168	46	M	SMN	15	49	41	1.00	20.4	2	92
HCM 222	68	M	SMN	15	45	49	1.39	27.2	2	61
HCM 169	52	M	*MYBPC3* 2373insG	21	45	43	0.87	15.9	1	100
HCM 204	30	M	*MYBPC3* 2373insG	19	37	37	1.14	16.3	2	100
HCM 219	44	F	*MYBPC3* 2373insG	19	48	43	1.5	12.5	3	74
HCM 163	64	F	*TNNI3* R145W	23	46	42	0.52	16.3	1	125
HCM 236	29	M	*MYH7* T1377M	26	52	44	1.83	18.3	2	104
HCM 246	25	M	*MYH7* R663C	28	34	*NA*	*NA*	*NA*	*NA*	38

* Indicates a truncation after the amino acid.

Troponin exchange in cardiomyocytes

Troponin exchange in permeabilized cardiomyocytes was performed as described previously [17]. The recombinant troponin complex was expressed and assembled as reported before [18]. The membrane-permeabilized cells of a highly phosphorylated human sample were incubated with non-phosphorylated recombinant troponin complex at the concentrations 0.01, 0.1 and 1.5 mg/ml, resembling a low, intermediate and high mutant protein concentration, respectively. Functional measurements after exchange were performed after incubation with protein kinase A (PKA) because the incorporated recombinant troponin complex was non-phosphorylated. The amount of troponin replacement was determined by phos-tag analysis of cardiac troponin I (cTnI) using the phosphorylation difference between the endogenous and the recombinant troponin complex, the former being highly phosphorylated and the latter being non-phosphorylated (example shown in Fig. 1B for the *TNNT2* I79N mutation). The percentage of troponin replacement after exchange was quantified as the percentage of non-phosphorylated cardiac troponin I (cTnI) of the total non-, mono- and bis-phosphorylated cTnI levels.

Co-sedimentation assay

Thin filament co-sedimentation assays were carried out using rabbit skeletal muscle filamentous actin (F-actin), recombinant human tropomyosin (Tm), and recombinant human troponin complexes as previously described [19,20] with a few modifications. Recombinant human cardiac tropomyosin was expressed with the N-terminal tag alanine-serine after the initiatior methione to mimic N-terminal acetylation [21]. Prior remove potential precipitates and the resultant supernatants were resolved on a denaturing gel to assess purity. Protein concentrations were determined using Pierce Coomassie Plus/Bradford assay (Thermo Fisher Scientific). F-actin, Tm, and troponin complexes were combined at a molar ratio of 7:1:1, respectively, into a final volume of 100 µl co-sed buffer (25 mM HEPES, 60 mM NaCl, 3 mM $MgCl_2$, 0.5 mM EGTA, 1 mM DTT, 0.5 mM $CaCl_2$, 2 mM β-mercaptoethanol, pH 7.0) resulting in a final concentration of 20 µmol/l F-actin, 2.86 µmol/l Tm and 2.86 µmol/l troponin complex. The samples were centrifuged for 30 min at 120,000 × g in a TLA-100 rotor (Beckman Coulter) at 21 °C. The pellets (P) and supernatants (S) were subsequently diluted with reducing Laemmli buffer, boiled, and resolved on 12% SDS-PAGE gels. The proteins were stained with Coomassie, destained, and imaged on an Odyssey IR system (LI-COR Biosciences) followed by densitometric quantification using Image Studio V5.2 (LI-COR Biosciences).

Phosphorylation assays

Tissue samples were homogenized to a concentration of 2.5 µg/µl, and 100 µl of the homogenate was incubated with 10 units of protein kinase A (PKA; Sigma, P5511) and 0.006 mM cAMP for 40 min at 25 °C. The phosphorylation level before and after PKA incubation was assessed with ProQ phosphostaining and phos-tag gel analysis of

cTnI. Troponin complexes were incubated with 0.5 units of PKA/µg and incubated at room temperature for 1, 5, 10, 20, 40 and 60 min. The phosphorylation level of cTnI was determined with phos-tag gel analysis.

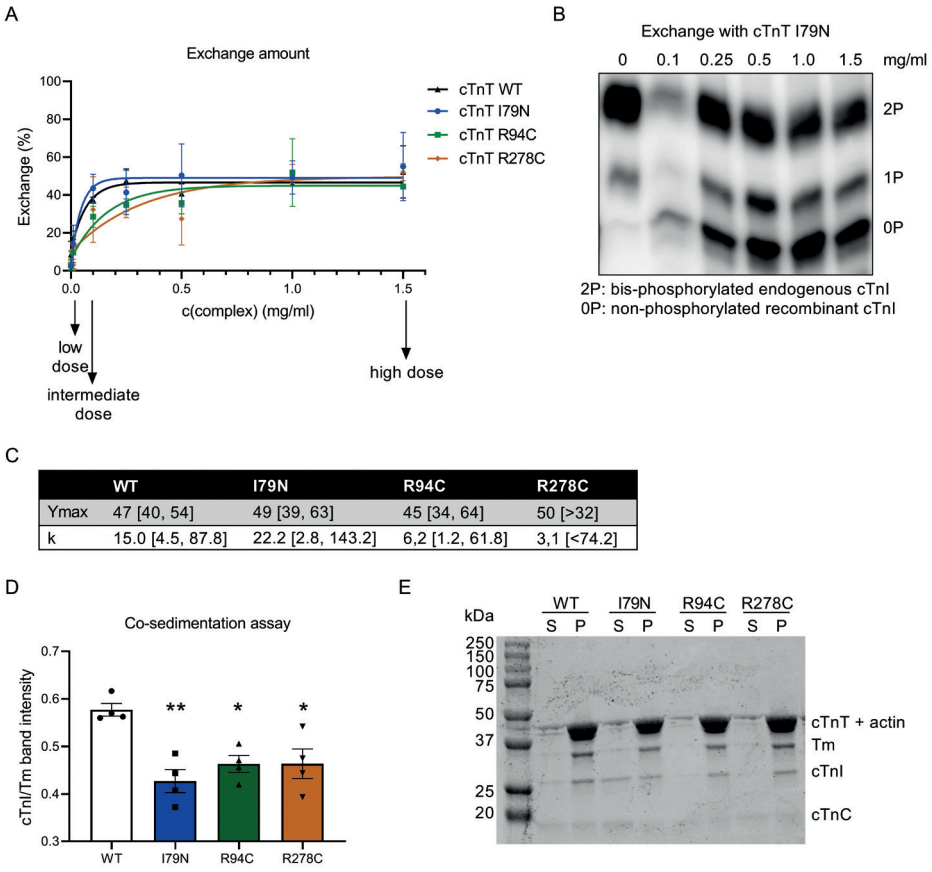

	WT	I79N	R94C	R278C
Ymax	47 [40, 54]	49 [39, 63]	45 [34, 64]	50 [>32]
k	15.0 [4.5, 87.8]	22.2 [2.8, 143.2]	6,2 [1.2, 61.8]	3,1 [<74.2]

FIGURE 1. (A) Exchange of endogenous troponin complex with different concentrations of recombinant WT and mutant complex harboring the mutations I79N, R94C and R278C. Exchange percentage was analyzed by phos-tag gel analysis. (B) Representative image of phos-tag gel analysis for exchange curves in (A). (C) Ymax and k represent parameters of the exponential plateau curve fit with the 95% confidence interval (please note that an upper limit of Ymax and a lower limit of k for R278C could not be determined), $n = 2$. (D-E) Co-sedimentation assay. (D) Quantification of thin filament co-sedimentation assay results. Vertical axis is the band intensity ratio of cardiac troponin I to tropomyosin. (E) Representative image of an SDS-PAGE gel (12%) containing thin filament co-sedimentation products for WT and mutant troponin complexes. Abbreviations: S, supernatant; P, pellet; WT, wild-type; Tm, tropomyosin; cTnT, cardiac troponin T; cTnI, cardiac troponin I; cTnC, cardiac troponin C; one-way ANOVA with Dunnett's multiple comparisons test, $*p < 0.05$, $**p < 0.01$ compared to WT. $n = 4$ for each condition.

Protein analysis

Protein phosphorylation

Non-, mono- and bis-phosphorylated forms of cTnI (Pierce, MA1- 22700) were quantified by phos-tag gel analysis as described previously [22]. It was used to assess the percentage of troponin replacement after exchange and to assess the cTnI phosphorylation level of human cardiac tissue samples.

Protein levels

Whole tissue lysates were prepared to determine troponin protein levels. Therefore, pulverized frozen tissue was homogenized in 40 µl/mg tissue 1× reducing sample buffer (106 mM Tris-HCl, 141 mM Tris-base, 2% lithium dodecyl sulfate (LDS), 10% glycerol, 0.51 mM EDTA, 0.22 mM SERVA Blue G250, 0.18 mM Phenol Red, 100 mM DTT) using a glass tissue grinder. Proteins were denatured by heating to 99 °C for 5 min and debris was removed by centrifugation at maximum speed for 10 min in a microcentrifuge (Sigma, 1–15 K). For analysis of troponin protein levels by Western blot, 5 µg of protein were separated on a 4–15% TGX gradient-gel (Biorad) and transferred to a polyvinylidene difluoride membrane. Site-specific antibodies directed to cTnT (ab10214, Abcam), cTnT (T6277, Sigma-Aldrich), cTnT (ab8295, Abcam), cTnI (ab10231, Abcam), cardiac Troponin C (cTnC, sc48347, Santa Cruz) and α-actinin (A7811, Sigma-Aldrich) were used to detect the proteins which were visualized with an enhanced chemiluminescence detection kit (Amersham) and scanned with Amersham Imager 600. Protein levels were determined by densitometric analysis. Protein levels were normalized to α-actinin or cTnI when appropriate. Equal loading of troponin complexes was verified with Imperial protein stain (Thermo Scientific).

Mass spectrometry to determine mutant protein dose in human tissue samples

Whole tissue lysates were run on 13% SDS gels to achieve a good separation of the cTnT and the actin band. Thereto approximately 15 µg of protein were loaded for each sample. The gel was stained with coomassie to visualize the protein bands and the cTnT band was cut out of the gel. Subsequently, a wash buffer (50% aqueous acetonitrile with 50 mM ammonium bicarbonate) was used to de-stain cut gel bands. De-stained gel bands were then cut into ~1 mm pieces and shrunk by incubation with acetonitrile at 37 °C for 10 min. Gel pieces were further dried in SpeedVac (Thermo Fisher Scientific, Waltham, MA). A digestion buffer (10% aqueous acetonitrile with 50 mM ammonium bicarbonate) was added to rehydrate the gel pieces. Reductive alkylation of cysteine was carried out by mixing with 1,4-dithiothreitol (DTT, Sigma-Aldrich, catalog #: 11583786001, St. Louis, MO) at 37 °C for 10 min followed by mixing with iodoacetamide (IAA, Sigma-Aldrich, catalog #: I1149, St. Louis, MO) at room temperature for 10 min. Afterwards, endoproteinase Glu-C (catalog number 90054, Thermo Fisher Scientific, Waltham, MA) was added and the mixture was incubated at 37 °C overnight. The supernatant was collected and the digestion was quenched by addition of a 0.5% formic acid aqueous

solution. After incubation at 37 °C for 10 min, the supernatant was collected. The gel pieces were dried by incubation with acetonitrile at 37 °C for 15 min and the supernatant was collected. The combined supernatant was dried in the SpeedVac. A series of calibration curve standards of varying mutant/wild-type (WT) cTnT ratios (0.05, 0.1, 0.2 and 1), but of a fixed total concentration of 20 μM cTnT, was reductively alkylated with DTT and IAA with the same procedure as the in-gel digestion. After mixing with Glu-C and incubation at 37 °C overnight, the digestion reaction was quenched by addition of a 0.5% formic acid aqueous solution. The mixture was then dried in the SpeedVac. The dried peptides mixture was dissolved in a 0.1% formic acid aqueous solution and the mixture was injected to an Easy Nano-Liquid Chromatography (nLC) II system (Thermo Fisher Scientific, Waltham, MA) equipped with a 75 μm × 10 cm C18AQ analytical column (catalog # SC003, Thermo Fisher Scientific, Waltham, MA) and a 100 μm × 2 cm trap column (catalog # SC001, Thermo Fisher Scientific, Waltham, MA). Mobile phase composition is as follows – A: H2O with 0.1% formic acid; B: acetonitrile with 0.1% formic acid. The gradient profile is linear from 1% B to 35% B in 90 min at 0.3 μl/min. The nLC was online coupled with a Hybrid Velos LTQ-Orbitrap Mass Spectrometer (Thermo Fisher Scientific, Waltham, MA). Eluates from nLC were electrospray-ionized with a 2.2 kV spray voltage. For the initial peptide identification, precursor full mass scans (m/z 350–2000, mass resolution of 60,000 at m/z 400, automatic gain control – AGC target 1 × 106 ions and maximum ionization time 500 ms) were followed by data-dependent collisional-induced-dissociation (CID) MS2 of the top 9 most abundant precursor ions (AGC target 1 × 105 ions, maximum ionization time 100 ms, isolation window of 2 m/z, normalized collision energy NCE 35 and dynamic exclusion of 60 s). For quantification of percentage of mutant proteins, targeted FT scan (m/z 390–440, mass resolution of 60,000 at m/z 400, AGC target 1 × 106 ions, maximum ionization time 200 ms) were carried out in triplicates for each gel band samples and calibration curve standards. For initial peptide identification, the acquired Xcalibur. raw files were analyzed by Proteome Discoverer 1.4 with Sequest HT (Thermo Fisher Scientific) against a modified human proteome database with troponin T R278C mutant sequence. Variable modification of methionine oxidation and cysteine carboxymethylation were included. Mass tolerance was set with a precursor mass error of less than 5 ppm and MS2 fragment ion mass error of less than 0.8 Da. Peptides with sequence of NQKVSKTRGKAKVTGRWK (TnT WT 271–288, [M + 5H]5+ m/z 415.2498) and NQKVSKTCGKAKVTGRWK (TnT R278C MT 271–288, C278 is carboxylated, [M + 5H]5+ m/z 416.0357) were identified as the R/C278 containing peptides with the highest S/N best suited for quantification. For quantification, the acquired Xcalibur.raw files with the targeted FT scan of m/z 390–440 were manually analyzed in the Xcalibur Qual Browser. Since the retention time (RT) of WT or mutant TnT 271–288 peptides overlaps, the MS signal over the RT with those MS (WT: m/z 415.2498; mutant: m/z 416.0357) signals were averaged and the ratio of mutant/WT MS signals calculated. A calibration curve was established with the above mentioned mutant/WT MS signals ratio and the actual mutant/WT concentration ratio. A linear regression calibration curve was generated with R2 of 0.9964.

RNA sequencing

RNA was isolated using ISOLATE II RNA Mini Kit (Bioline) according to the manufacturer's instructions with minor adjustments (10 min digestion using 20 µg proteinase K and a subsequent washing step using 100% ethanol were added after the lysis step). Sample quality and quantity was assessed using the 2100 Bioanalyzer with a RNA 6000 Pico Kit (Agilent), and Qubit Flourometer with a HS RNA Assay (Thermo Fisher). After selecting the polyadenylated fraction of RNA, libraries were prepared using the NEXTflexTM Rapid RNA-seq Kit (Bioo Scientific). Libraries were sequenced on the Nextseq500 Illumina platform, producing 75 bp long single end reads. Reads were aligned to the human reference genome GRCh37 using STAR v2.4.2a [23]. Picard's AddOrReplaceReadGroups v1.98 (http://broadinstitute.github.io/picard/) was used to add read groups to the BAM files, which were sorted with Sambamba v0.4.5 [24] and transcript abundances were quantified with HTSeq-count v0.6.1p1 [25] using the union mode. Subsequently, reads per kilobase million reads sequenced (RPKMs) were calculated with edgeR's RPKM function [26]. The secondary structure of mRNAs were predicted using the RNAfold software, with the minimum free energy (MFE) and partition function option selected (URL: http://rna.tbi.univi e.ac.at/cgi-bin/RNAWebSuite/RNAfold.cgi) [27]. WT or mutant full-length human *TNNT2* mRNA sequence corresponding to the adult-expressed isoform of cTnT (NCBI Reference Sequence: NM_001276347.2) was used for the prediction.

Immunofluorescence

Slides were thawed at RT for 20 min inside a closed a box. Tissue sections were washed with PBS-T, permeabilized with 0.25% PBS-Triton and blocked with 1% BSA and 10% donkey serum for 30 min. Primary antibodies for α-actinin (ACTN2, 14221-1-AP, Proteintech, dilution 1:100) and cTnT (TNNT2 [1C11], ab8295, Abcam, dilution 1:250) were incubated overnight at 4 °C. Afterwards tissue sections were washed and incubated with suitable secondary Alexa fluor antibodies for 30 min. The sections were washed in PBS and mounted with Mowiol. Images were acquired with a Nikon A1 confocal microscope and analysis and quantifications were performed with FIJI software.

Statistics

Graphpad Prism v8 software was used for statistical analysis. Data were statistically analyzed using unpaired *t*-test, one-way ANOVA with Dunnett's or Tukey's multiple comparisons post hoc test or 2way-ANOVA when appropriate. All values are shown as mean ± standard error of the mean. A p-value ≤ 0.05 was considered as significantly different.

RESULTS

Lower thin filament-binding affinity of mutant compared to WT troponin complex

We performed troponin exchange in permeabilized human cardiomyocytes to test the direct effect of mutation location and mutant protein dose on myofilament function. Therefore we used the HCM-causing troponin T mutations I79N, R94C and R278C. To analyze their ability to incorporate into the myofilaments and to determine the required complex concentration for a low, intermediate and high protein dose, we exchanged endogenous troponin with different concentrations of recombinant WT and mutant troponin complex. All complexes incorporated to a similar degree (Fig. 1A, C), with a maximum incorporation (Ymax) of 47% for WT, 49% for I79N, 45% for R94C and 50% for R278C. Dose dependency of incorporation appeared to be slightly different for the different complexes. WT and I79N showed almost maximal incorporation at very low concentrations, while R94C and R278C reached the maximal incorporation at higher concentrations (Fig. 1A), which is also illustrated by the difference in k representing the rate constant (k_{WT} = 15.0, k_{I79N} = 22.2, k_{R94C} = 6.2 and k_{R278C} = 3.1) (Fig. 1C). However, the variation is too large to assess whether the complexes exchange differently at low and intermediate dose. Additionally, we performed a co-sedimentation assay with the three complexes to determine their binding affinity to isolated thin filaments. While we observed reduced binding affinity of all three mutants compared to WT, no differences were observed in thin filament binding affinity between the three mutants (Fig. 1D, E, Table S1).

Mutation location determines degree of myofilament dysfunction

Based on the obtained percentage of exchange at different concentrations of recombinant troponin complex we selected 0.01 mg/ml, 0.1 mg/ml and 1.5 mg/ml for subsequent functional experiments, which are indicated as low, intermediate and high dose, respectively. Exchange of cTn complex containing the *TNNT2* mutants were compared to cells exchanged with cTn complex containing WT recombinant cTnT (1.5 mg/ml). To avoid that PKA-mediated cTnI phosphorylation differences may mask mutant-related changes in myofilament function, all functional measurements were performed in troponin-exchanged cells after treatment with exogenous PKA. A time-dependent PKA phosphorylation assay of the isolated recombinant complexes confirmed that the cTnI phosphorylation level of the recombinant complex after 40 min of PKA incubation is comparable to that of non-failing donors (Fig. S1). There was no difference in PKA's ability to phosphorylate the different troponin complexes (Fig. S1E). Moreover, to further minimalize an interfering effect of myofilament protein phosphorylation background, exchange with all 4 troponin complexes (WT and 3 mutants) were performed in the same human sample (sample 2.114). Interestingly, we did not see a mutant protein dose effect for the I79N and R94C mutations (Fig. 2A, B, D, E; Table S2). For the R94C mutation, a significant increase in Ca^{2+}-sensitivity was seen at low dose of mutant protein, which did not increase further when increasing

the dose (Fig. 2E), indicating that the maximal increase in myofilament Ca^{2+}-sensitivity was already achieved at low dose. A similar pattern with a dose-independent trend to increased Ca^{2+}-sensitivity (not significant) was observed for I79N (Fig. 2D). The magnitude of the increase in Ca^{2+}-sensitivity is determined by the mutation location. We found that R94C increases Ca^{2+}- sensitivity to a larger extent than I79N, depicted by the larger curve shift of R94C compared to I79N (Fig. 2G). Interestingly, we observed strikingly different results for the R278C complex. While the low and intermediate dose led to an increase in Ca^{2+}-sensitivity to a similar level as R94C, we observed significantly decreased Ca^{2+}-sensitivity for the high dose (Fig. 2C, F; Table S2). This is also demonstrated by the large difference in EC_{50} at low and high dose (Fig. 2F). In several exchange experiments we were able to determine the exchange efficiency in the remaining cell suspension after functional measurements of single cardiomyocytes. In Fig. 2I we plotted myofilament Ca^{2+}-sensitivity data relative to the troponin exchange efficiency obtained in experiments in which we collected both data sets. This figure illustrates the mutation location-specific effects on EC_{50}. LDA, the cellular analogue for the Frank-Starling mechanism of the heart, was assessed for all three mutations at low, intermediate and high dose of mutant protein (Fig. 3A-C, Table S3). The variability between cells was large and we did not observe differences in LDA for all three mutations compared to cardiomyocytes exchanged with wild-type troponin complex. Maximal force did not differ between the different mutations and mutant protein dosages (Fig. 3D-F, Table S4).

Expression of R278C at mRNA and protein level in human patient samples

In patients, the percentage of mutant protein in the cell and its contribution to disease variability is unknown. We collected myocardial tissue from the interventricular septum of three obstructive HCM patients carrying the R278C mutation during myectomy surgery (HCM 173, HCM 175 and HCM 234). In these tissues we performed protein analysis and functional measurements to investigate the variability in patients with the exact same mutation. Western blot analysis revealed a 5.20 ± 0.37 fold increase in total cTnT protein levels in the three human *TNNT2*-R278C mutant samples compared to donor tissue, sarcomere mutation-negative (SMN) samples, samples with a truncating *MYBPC3* mutation and samples with missense mutations in genes other than *TNNT2*, when analyzed with the ab10214 antibody (abcam) (Fig. 4A, B). Levels of cTnI and cTnC were not changed in the *TNNT2*-R278C samples compared to all other groups (Fig. 4C, D), implying that the presence of mutation R278C in *TNNT2* leads to elevated cTnT levels only.

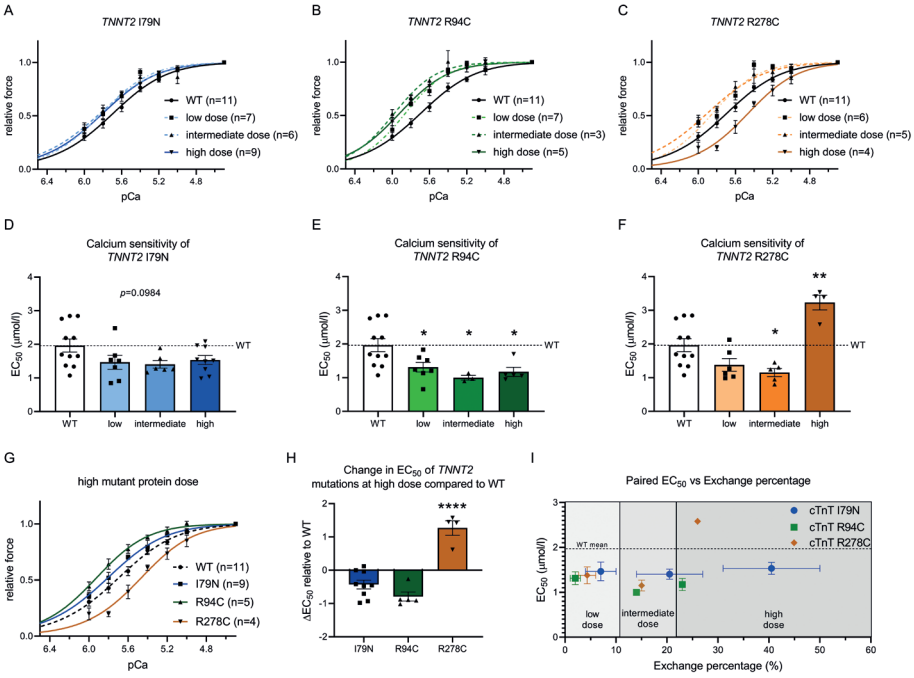

FIGURE 2. (A-C) Force-calcium relations after exchange with cTnT I79N (A), R94C (B) and R278C (C) complex at low, intermediate and high dose. (D-F) EC_{50} values after exchange with I79N (D), R94C (E) and R278C (F) at low, intermediate and high mutant protein dose. (G) Comparison of force-calcium relation of the different mutants at high dose. (H) Change in EC_{50} (ΔEC_{50}) of mutants at high dose compared to WT. (I) Relation of EC_{50} and exchange percentage defined in the same exchange experiments. In (I) n(I79N) = 2/2/2, n(R94C) = 2/1/1, n(R278C) = 3/1/1 for low/intermediate/high dose, respectively. *$p < 0.05$, **$p < 0.01$ compared to WT in (D-F); ****$p < 0.0001$ compared to I79N and R94C in H, one-way ANOVA with Dunnett's (D-F) or Tukey's (H) multiple comparisons test.

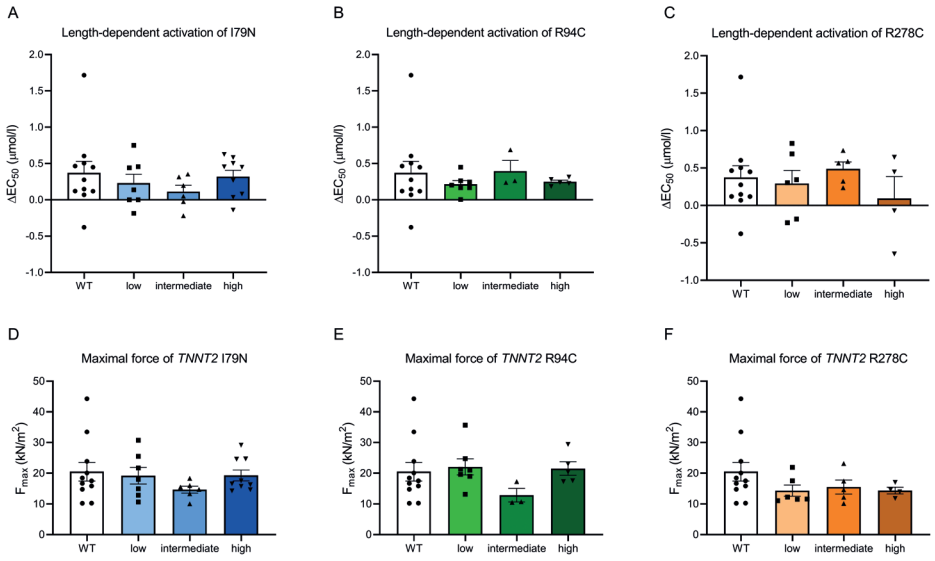

FIGURE 3. (A), (B) and (C) show length-dependent activation after exchange with cTnT I79N, R94C and R278C, respectively. (D), (E) and (F) show maximal force development after exchange with cTnT I79N, R94C and R278C, respectively. Low, intermediate and high mutant protein dose are depicted for each mutation compared to WT. n(WT) = 11, n(I79N) = 7/6/9, n(R94C) = 7/3/5, n(R278C) = 6/5/4 for low/intermediate/high dose, respectively.

This deviation from the expected troponin stoichiometry of 1:1:1 for cTnT, cTnI and cTnC would be an unexpected unique finding. Therefore, we also determined the cTnT protein levels with the T6277 (Sigma) and the ab8295 (abcam) antibodies to validate the results. Interestingly, the analysis revealed elevated levels of cTnT but with a smaller fold change of 2.09 ± 0.13 for the T6277 antibody (Fig. 4E) and unchanged levels of cTnT with the ab8295 antibody (Fig. 4F). Because of these divergent results, we determined whether the antibodies have the same affinity to recombinant WT and R278C cTnT protein, or whether the mutation affects antibody binding. To do so, we performed western blot analysis on different amounts of recombinant WT and R278C troponin complex. For the two antibodies ab10214 and T6277 we found an approximately 2- fold increase of the cTnT/cTnI signal for the R278C compared to WT, whereas the ab8295 antibody showed an increased cTnT/cTnI signal only at low protein concentrations (Fig. S2A-B).

This indicates that the R278C mutation influences antibody binding of all three antibodies, in a possibly protein concentration-dependent manner. We obtained 3 more human *TNNT2*-R278C samples from an Italian patient cohort and compared all available *TNNT2*-R278C samples to two patient samples with other *TNNT2* mutations (Gln272* and K280N) and could show that the increased cTnT signal is specific for

tissue samples harboring the R278C mutation (Fig. S2C). Based on these western blot analyses we cannot make a confident statement about troponin stoichiometry in the *TNNT2* R278C samples. Consequently, we performed immunofluorescence (IF) for cTnT and α-actinin on a selection of the human samples (3 *TNNT2* R278C, 1 Donor, 2 SMN, 2 $MYBPC3_{2373insG}$ and 2 missense mutation samples) to determine cTnT protein levels with a different method. Due to the poor performance of the ab10214 and T6277 antibodies in IF, we only used the ab8295 (abcam) antibody for the stainings. In contrast to the western blot analysis of the ab10214 and T6277 antibodies but in line with the results from the ab8295 antibody, IF did not show a significant difference in cTnT protein levels compared to the non-failing donor sample ($p = 0.0777$, Fig. 5A-B). Overall, our data show that the R278C mutation alters cTnT antibody-binding, and cannot be used to determine cTnT protein levels. We further performed RNA sequencing and mass spectrometry on two HCM tissue samples with the R278C mutation to assess the percentage of the mutant cTnT-R278C mRNA and protein levels in the samples. While *TNNT2*-R278C mRNA levels were close to 50%, the levels of mutant protein were 36% in HCM 173 and 28% in HCM 175 (please note that we were not able to define levels in HCM 234 upon several attempts) (Fig. 5C and Fig. S3). This supports the results from the IF analysis that do not show elevated total cTnT levels in the *TNNT2*-R278C tissues.

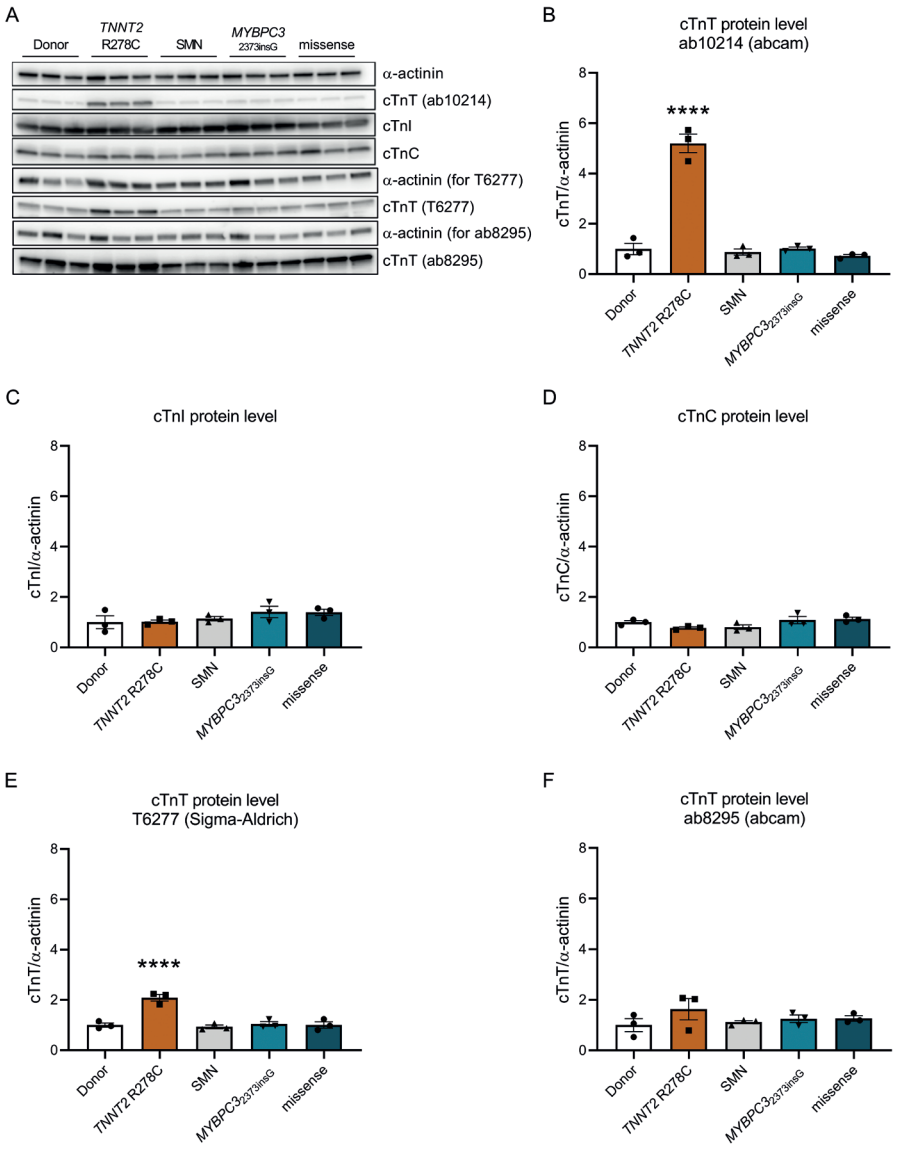

FIGURE 4. (A) shows representative western blot images of troponin protein levels in the three human samples harboring the *TNNT2* R278C mutation compared to control and other HCM patient samples with the cardiac troponin T (cTnT) antibodies ab10214, T6277 and ab8295. cTnT protein levels with the ab10214 antibody are quantified in (B). (C) shows quantified protein levels of cardiac troponin I (cTnI) and (D) of cardiac troponin C (cTnC). (E) displays quantified cTnT protein levels with the antibody T6277 and (F) with the antibody ab8295. Every dot represents the average of 2 data points per sample in (B), (E) and (F) and the average of 4 data points in (C) and (D). Data is normalized to Donor which is set to 1. ****$p < 0.0001$ compared to WT, one-way ANOVA with Dunnett's multiple comparisons test.

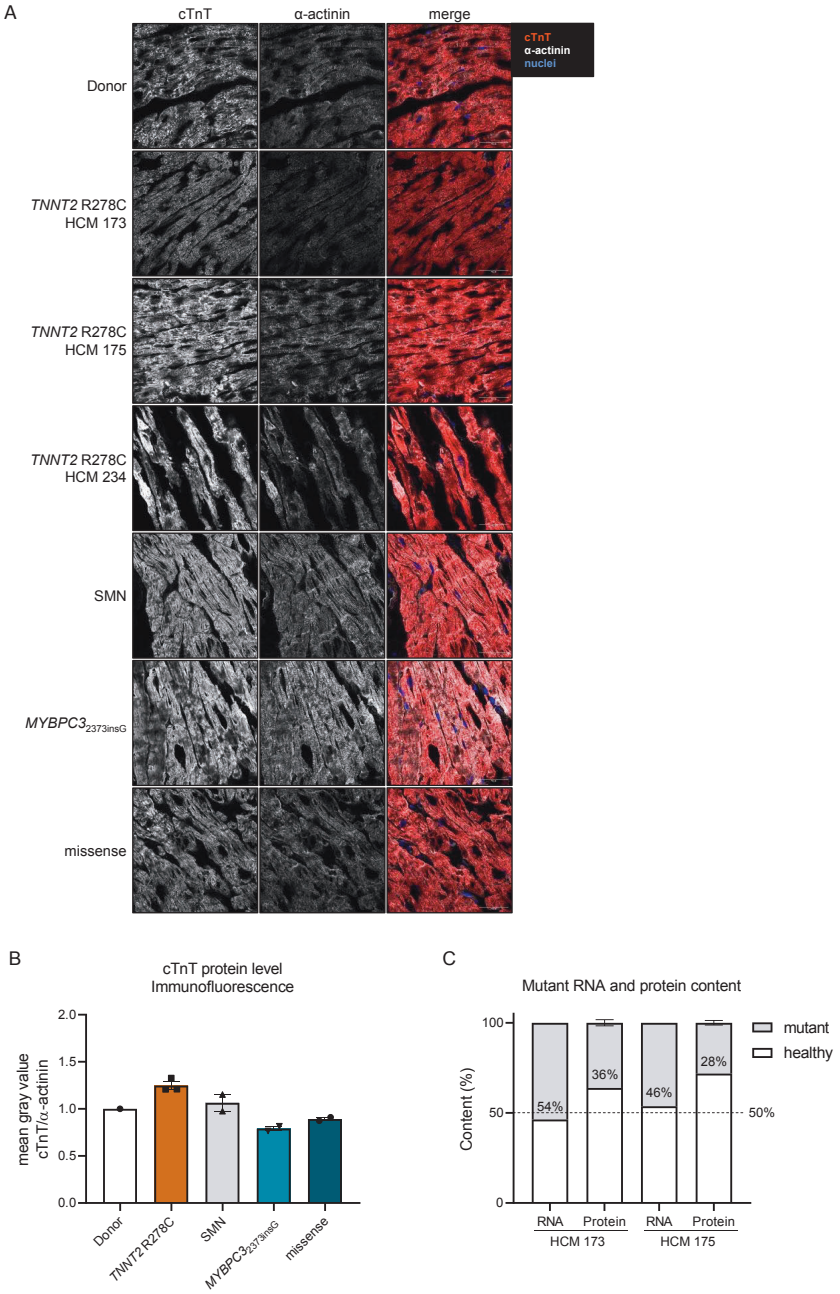

FIGURE 5. (A) Representative immunofluorescence images of human cardiac tissue stained for cardiac troponin T (cTnT), α-actinin and nuclei. (B) Quantified intensity of cTnT staining normalized to α-actinin staining. Every dot represents one sample and is an average of 3 images. (C) shows the content of mutant cTnT mRNA and protein in the human tissue samples determined by RNA sequencing and mass spectrometry.

R278C mutant human samples differ on a functional level

We compared myofilament function of the three patient samples in isolated membrane-permeabilized cardiomyocytes. While the difference in percentage of mutant protein was only slightly different between HCM 173 (36%) and HCM 175 (28%), the direction of the change in Ca^{2+}-sensitivity compared to non-failing donors was opposite in these samples, showing a trend to an increase and a decrease, respectively (Figs. 6A-B, Table S5). HCM 234 shows a significant increase in Ca^{2+}-sensitivity compared to donor samples (Fig. 6C, Table S5). Analysis of cTnI phosphorylation revealed reduced levels of phosphorylation in all three patient samples compared to donors, shown by lower levels of the highly phosphorylated 2P band and increased levels of the 1P and 0P bands (Fig. 6G-H). The lowest level of cTnI phosphorylation was observed in HCM 234. Since it is well-known that reduced cTnI phosphorylation increases myofilament Ca^{2+}-sensitivity [16], we repeated the functional measurements after incubation with PKA to increase cTnI phosphorylation in HCM samples to levels observed in non-failing donor samples. First of all we determined with a phosphorylation assay if cTnI is still PKA responsive in these patients. As seen in Fig. 6G-H, cTnI phosphorylation increases after treatment with PKA in the *TNNT2* mutant samples, indicating that PKA-mediated phosphorylation of cTnI is not hampered by the presence of the *TNNT2* mutation. Accordingly, PKA treatment of isolated cardiomyocytes decreases myofilament calcium sensitivity significantly in HCM 173 and with a strong trend in HCM 234 (Fig. 6D-F, Table S5). In line with these results, we observed a blunted LDA in all three patient samples compared to donor, but detected a statistically significant difference only for HCM 173 (Fig. 6I-K, Table S6). LDA was enhanced only in HCM 173 after PKA-mediated phosphorylation of cTnI (Fig. 6L-N, Table S6). Overall, our data suggest that perturbations in myofilament function in samples harboring the R278C mutation can be corrected to values that are seen in non-failing samples by PKA treatment.

DISCUSSION

In this study we investigated the mutation location and mutant protein dose effect of three HCM-causing *TNNT2* mutations. We proposed that the mutation location and mutant protein dose are potential disease modifiers via specific changes in myofilament function. While our exchange experiments show a more important role for the mutation location than for the mutant protein dose for mutations I79N and R94C, the functional consequences of R278C are highly dose-dependent.

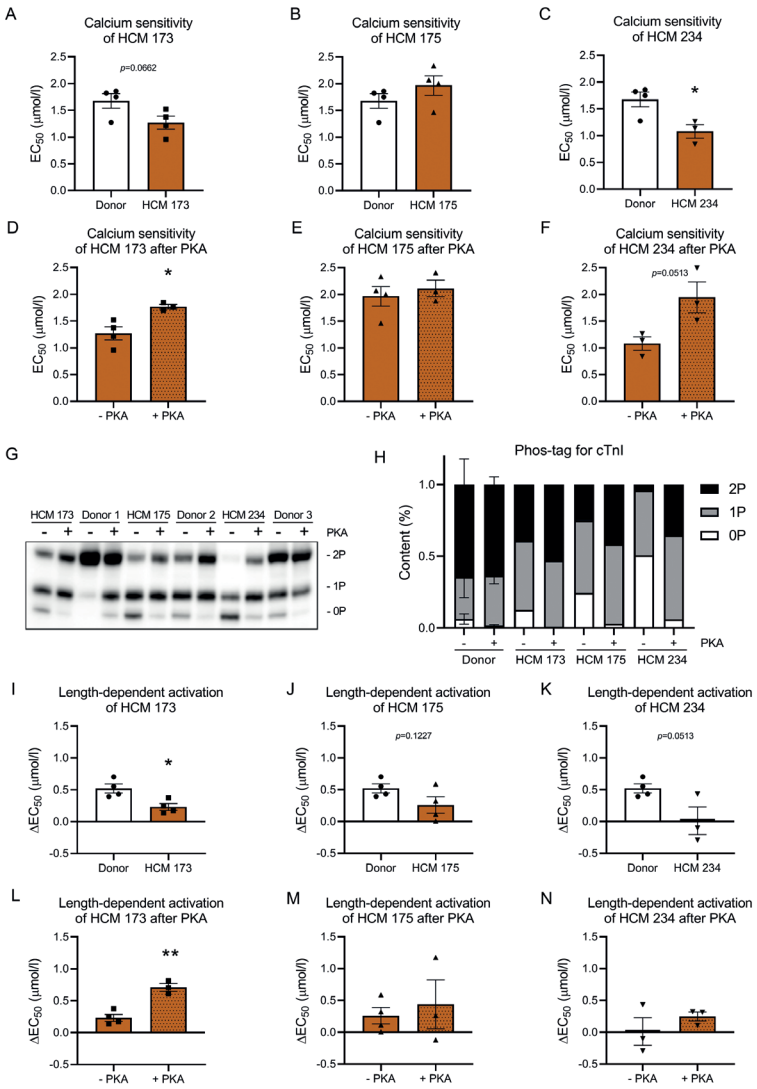

FIGURE 6. (A-C) show myofilament Ca^{2+}-sensitivity measured as EC_{50} for the human samples HCM 173, HCM 175 and HCM 234 carrying the *TNNT2* R278C mutation compared to donor tissue. (D-F) show Ca^{2+}-sensitivity measured as EC_{50} for the human samples HCM 173, HCM 175 and HCM 234 carrying the *TNNT2* R278C mutation before and after normalizing cTnI phosphorylation by incubation with protein kinase A (PKA). (G) and (H) display the phosphorylation status of cardiac troponin I determined by phos-tag gel analysis before and after incubation with PKA. 0P represents non-phosphorylated cTnI, 1P single-phosphorylated cTnI and 2P double-phosphorylated cTnI. (G) shows the phos-tag gel image for the quantified data in (H). (I-K) Length-dependent activation of the human samples HCM 173, HCM 175 and HCM 234 compared to donor. (L-N) Length-dependent activation of the human samples HCM 173, HCM 175 and HCM 234 before and after PKA treatment. *$p < 0.05$, **$p < 0.01$, unpaired *t*-test. n(Donor) = 4, n(HCM 173) = 4/3, n(HCM 175) = 4/3, n(HCM 234) = 3/3 for with/without PKA, respectively.

Mutant protein dose effect is mutation-specific

HCM mutations in thin filament proteins such as cTnT have been associated with an increase in myofilament Ca^{2+}-sensitivity [28,29] and blunted length-dependent myofilament activation [28]. Impaired LDA was normalized to values in non-failing donor cardiomyocytes by reducing the percentage of mutant cTnT to 22% [28]. In the present study, we show that a relatively low dose of mutant cTnT protein is sufficient to increase myofilament Ca^{2+}-sensitivity, which was significant for R94C, though the magnitude is dependent on mutation location (Fig. 2). At low, intermediate and high dose of mutant protein we did not observe differences in LDA (Fig. 3). R94C led to an increase in myofilament Ca^{2+}-sensitivity independent of dose and also I79N showed a strong trend to increased dose-independent myofilament Ca^{2+}-sensitivity, with R94C having an even stronger effect than I79N. The Ca^{2+}- sensitizing effect of I79N has been described previously [12,29,30], and also for R94C a Ca^{2+}-sensitizing effect and hypercontractility has been predicted [31].

In our study, a very low dose of mutant protein results already in the maximal shift in myofilament Ca^{2+}-sensitivity (Fig. 2I). In contrast to our study in human cardiomyocytes, the R92Q mutation showed a dose-dependent effect on atrial mass, hypertrophic markers and structural abnormalities in a Tg mouse model [10]. Unlike the direct mutation effects that we studied in single permeabilized cardiomyocyte, the dose-dependent changes in cardiac remodeling described in the Tg-mice may represent secondary changes and may not be solely due to the direct mutation dose effect. Several studies in animal models and patients have also described that individuals with two disease-causing mutations show earlier disease onset, more severe hypertrophy and a higher risk of sudden cardiac death [32–34]. Double mutations in the same gene, dependent on their location, might have an additive effect as described for two *MYBPC3* mutations [35]. Compound heterozygous or homozygous *MYBPC3* mutations have also been shown to cause severe cardiomyopathy which was lethal in the first few weeks after birth [36,37]. An additive mutation dose effect has also been shown for double heterozygous mutations in two different genes like *MYH7* and *CSRP3* [38]. These studies indicate that the mutation dose effect might not always be in the dose of one gene, but rather in the combination of mutations in different genes that increase the cellular burden resulting in a more severe clinical outcome. In contrast to the findings with the I79N and R94C mutations, R278C shows a trend to increased Ca^{2+}-sensitivity at low and a significant increase at intermediate dose, while a high dose significantly decreased Ca^{2+}-sensitivity (Fig. 2C, F, I). Conflicting results regarding this mutation have been reported in literature, showing either a Ca^{2+}-sensitization or no effect on Ca^{2+}-sensitivity [13,29]. Considering the findings of our study, the different reported effects on myofilament function could be explained by differences in mutant protein dose. The different behavior of the N-terminal *TNNT2* mutations (I79N and R94C) and the C-terminal mutation R278C may also be explained by their interactions with other thin filament proteins, e.g. tropomyosin and cTnC as calcium

binding to cTnC triggers conformational changes in troponin and tropomyosin that subsequently allow interactions between actin and myosin heads. The stoichiometry of 7:1:1 for actin, tropomyosin and troponin underlies the tight regulation of calcium-induced cross-bridge formation and myofilament force development. Molecular models based on crystal structures showed that the N-terminal region of cTnT (residues 87–150) is extremely elongated and interacts with both tropomyosin and 3 out of 7 actin subunits [39], and stabilizes tropomyosin-troponin binding to actin. As the cTnT N-terminus bridges over two tropomyosin strands [39], small amounts of mutant *TNNT2* in this region may already exert a maximal effect on myofilament Ca^{2+}-sensitivity via propagation of the calcium-binding signal over the thin actin-filament. Furthermore, it has recently been shown that the C-terminus of cTnT, at which the R278C mutation is located, can directly interact with cTnC [19]. This cTnT-cTnC interaction may be altered by the presence of mutant R278C in a dose-dependent manner, and thereby differentially alter cTnC sensitivity to calcium. Interestingly, a divergent effect of a *TNNT2* mutation has been reported before. The introduction of the dilated cardiomyopathy (DCM)- causing *TNNT2* mutation ΔK210 in reconstituted thin filaments led to decreased Ca^{2+}-sensitivity when using WT and ΔK210 cTnT in a 50:50 ratio, whereas it resulted in increased Ca^{2+}-sensitivity when using 100% ΔK210 [40]. These findings indicate that dose-dependency of the functional defect might not be a common disease mechanism for all *TNNT2* mutations but might depend on mutation location. Moreover, based on the elegant work by Davis and colleagues, who build proof for tension-mediated cardiomyocyte remodeling [41], the R278C mutation may trigger concentric remodeling (i.e. HCM phenotype) at low dose, and eccentric remodeling (i.e. DCM phenotype) at high protein dose.

Mutation location determines myofilament alterations

The differences between the mutations in this study could be due to mutation-specific changes in protein properties like structure or charge, that have differential effects on protein function by e.g. influencing their interaction with binding partners. In a study with *MYH7* mutations, differences in disease severity have been proposed to depend on the mutation location due to their effect on different protein domains that might be of more or less importance for proper protein function [42]. Some of these mutations could be associated with either mild or severe disease phenotype [43,44]. Also for *ACTC1* it has been described that the subdomain location of the mutation determines the alterations in protein properties. Mutations in one subdomain predominantly affected protein stability or polymerization, whereas mutations in other subdomains caused alterations in protein-protein interactions [45]. Vang et al. have shown in in vitro experiments that different HCM- and DCM-causing mutations in *ACTC1* impair protein folding by the TRiC chaperonin complex resulting in inefficient incorporation into the myofilament and aggregation of actin [46]. A similar mechanism could potentially explain the lower thin filament binding affinity of the *TNNT2* mutant complexes compared to WT (Fig. 1D). Pavadai et al. describe that the R94

residue, together with other charged residues, forms stable salt bridges that border hydrophobic patches leading to a very tight interaction of the cTnT fragment with residues 89–151 and tropomyosin [47]. Having an uncharged cysteine (C) instead of the positively charged arginine (R) at residue 94 may weaken the interaction of cTnT with tropomyosin and explain the reduced binding affinity of R94C to the thin filament. A similar mechanism may be true for the R278C mutation, which shows the same amino acid change. Accordingly, also the change from a non-polar isoleucine (I) to a polar asparagine (N) for the I79N mutation may potentially alter the interaction of cTnT with tropomyosin. Differences in exchangeability into porcine skinned fibers of different mutant cTnT proteins was shown in a previous study, in which R92W, R94L or R130C showed reduced exchangeability compared to WT and other cTnT mutant proteins (A104V, E163R, S179F, E244D) [15]. This is in line with findings by Palm et al., who have shown that mutations within the residues 92–110 alter the interaction of cTnT with tropomyosin [48]. Furthermore, studies in Tg mice showed less efficient incorporation of mutant compared to WT cTnT. Tg-I79N lines expressed 52% and 35% Tg-cTnT compared to 71% Tg-cTnT in the Tg-WT line [12]. Similar results have been reported for the Tg-cTnI mouse lines R145G and R145W that only showed 36% and 11% of mutant Tg-cTnI compared to 66% of Tg-cTnI in the Tg-WT line [49,50]. Overall, our study strengthens the notion that the degree of myofilament dysfunction depends on mutation location, and that mutant cTnT protein reduces thin filament binding affinity of the troponin complex.

Altered antibody binding affinity to cTnT-R278C

Troponins function as part of a complex, which is closely linked with tropomyosin. It has been shown that mutations in one of the troponin units can affect the composition of the entire troponin complex. In a study of different DCM-causing troponin mutations it has been shown for a truncating mutation in *TNNI3* and an amino acid deletion in *TNNT2* that the stoichiometry of the troponin complex was altered. In these DCM patient samples the mutation also affected the protein levels of its binding partners [51]. Although part of our western blot data suggests elevated cTnT levels in the *TNNT2*-R278C samples, we have shown in Fig. S2 that all cTnT antibodies show increased binding specifically to the mutant R278C compared to WT protein. Although the cTnT antibody epitope is more than 100 amino acids away from the mutation site, the amino acid change in the mutant protein is influencing antibody binding in western blot analysis. This, in combination with the ab8295 western blot and IF results, which did not show higher cTnT protein levels compared to donor (Fig. 5), suggest that there is no change in troponin stoichiometry in the HCM patient samples carrying the *TNNT2*-R278C mutation. This study shows that special care has to be taken when analyzing mutant proteins as antibody binding can be affected even under denaturing conditions. Our RNA analyses showed a ~50/50% ratio of WT and mutant mRNA in the *TNNT2* R278C cardiac patient samples, while mass spectrometry revealed that the amount of mutant protein was less than 50%. This finding is in line with our in vitro

data that show reduced binding of the mutant protein to the thin filament compared to WT and may explain the lower percentage of mutant protein in the human tissue. The predicted mRNA structures for WT and R278C mRNA differ, suggesting that R278C mRNA may indeed have different characteristics than WT mRNA (Fig. S4), which may affect its translation efficiency, resulting in lower protein levels of cTnT-R278C. Alternatively, it may be speculated that the turnover of WT cTnT protein is reduced, a mechanism which was recently proposed for *MYBPC3* truncating mutations to maintain normal cMyBP-C levels and prevent haploinsufficiency [52]. Future research is warranted to investigate mechanisms underlying protein translation and turnover in order to define the role of both WT and mutant proteins in sarcomere homeostasis.

Differences in myofilament function between human TNNT2 R278C samples do not correspond with mutant protein dose

Interestingly, our human samples with the R278C mutation showed differences in myofilament Ca^{2+}-sensitivity, while their clinical characteristics were very similar (Table 1) and samples were all collected at the time of myectomy. HCM 173 showed a strong trend to increased myofilament Ca^{2+}-sensitivity and HCM 234 showed a significant increase in myofilament Ca^{2+}-sensitivity compared to donor, whereas HCM 175 was not different. Based on the dose-dependent effect observed for the R278C mutation in our exchange experiments, i.e. high myofilament Ca^{2+}-sensitivity at low dose, and low myofilament Ca^{2+}- sensitivity at high mutant dose, mutant protein levels should be higher in the HCM 175 than in the HCM 173 sample. However, our mass spectrometry data showed a slightly lower mutant protein level in HCM 175 (28%) than in HCM 173 (36%). A well-known modifier of Ca^{2+}-sensitivity is PKA-mediated phosphorylation of cTnI [16]. While the level of cTnI phosphorylation was lower in all three samples compared to non-failing donor tissue, only HCM 173 and HCM 234 displayed increased Ca^{2+}-sensitivity. Restoring phosphorylation of cTnI indeed decreased Ca^{2+}-sensitivity significantly in HCM 173 and with a strong trend in HCM 234. Although PKA phosphorylation of cTnI is a major regulatory mechanism of myofilament Ca^{2+}-sensitivity, there are many more post-translational protein modifications that could potentially alter myofilament function. Also protein kinase C (PKC)-mediated phosphorylation can influence myofilament Ca^{2+}-sensitivity and has been shown to decrease it [53]. Therefore, enhanced PKC activity may explain why Ca^{2+}-sensitivity is not reduced in HCM 175 while the sample does show reduced phosphorylation of cTnI. Additionally, myofilament Ca^{2+}-sensitivity could be influenced by a range of other factors, that are beyond the scope of this study. We can speculate that the extent of fibrosis, medication and the presence of comorbidities can influence myofilament function by altering post-translational modifications of myofilament proteins. Overall, our data illustrate that myofilament Ca^{2+}-sensitivity measured at the time of myectomy in HCM samples harboring *TNNT2* mutations is highly diverse, and most likely reflect a complicated mix of translational and post-translational protein modifications. The latter is in line with our previous observations in HCM and DCM samples with thin

filament gene mutations [28,51], and also matches previously reported conflicting results on the R278C mutation. One study showed dramatically increased Ca^{2+}-sensitivity [29], whereas another one described R278C as a rather benign mutation with no effect on Ca^{2+}- sensitivity [13].

STUDY LIMITATIONS

This study gives new insight into the effect of mutant protein dose and location of *TNNT2* mutations on human myofilament function. It is a limitation of the study that we only assessed two N-terminal mutations and one C-terminal mutation, which all show differences on a functional level. To make a more general statement on the effect of mutations in certain cTnT domains, additional mutation locations have to be investigated. Furthermore, our study shows that isolated mutation effects are not directly translatable to the human situation, since several other disease modifying factors can influence the impact of the mutant protein on the cell and lead to differences in the functional state of the cardiomyocytes between patients with the same mutation.

CONCLUSION

From our exchange experiments we can conclude that mutant protein dose-dependency may be relevant only for certain *TNNT2* mutations. Based on our experiments, this may be true for mutations located in the C-terminal domain that interacts with other troponin subunits. Our studies show that a relatively small dose of mutant protein is sufficient to exert the maximal effect on myofilament Ca^{2+}-sensitivity for the I79N and R94C mutation, while the mutation location determines the magnitude of this effect. This could be explained by the interaction of troponin with tropomyosin which is involved in the regulation of cooperativity of thin filament activation. Our study emphasizes that care has to be taken when analyzing mutant proteins as single amino acid changes can alter antibody binding even under denaturing conditions. The 'classical' view of the HCM-related myofilament Ca^{2+}-sensitization clearly is too simplified, as our study shows that thin filament-based HCM pathology involves additional levels of complexity including sarcomere homeostasis and mutation-specific effects.

AUTHOR CONTRIBUTIONS

MS, JJ, JP, MH and HH performed experiments and analyzed the data. RH, MM and CP acquired patient material and data. MS, JJ, DK, JRP and JV interpreted data. MS, DK and JV wrote the manuscript. All authors reviewed the manuscript and gave valuable input.

DECLARATION OF COMPETING INTEREST

The authors declare no competing interest.

ACKNOWLEDGEMENTS

We would like to thank Ruud Zaremba for technical assistance in protein analysis assays and Pedro Espinosa for performing immunofluorescence stainings. We thank Cris G. dos Remedios from the University of Sydney and the Sydney Heart Bank for the control samples and TNNT2 K280N sample used in this study. We acknowledge the support from the Netherlands Cardiovascular Research Initiative: An initiative with support of the Dutch Heart Foundation, CVON2014-40 DOSIS. JRP acknowledges the support from the National Institute of Health grant HL128683.

REFERENCES

1. Maron BJ, Gardin JM, Flack JM, Gidding SS, Kurosaki TT, Bild DE. Prevalence of hypertrophic cardiomyopathy in a general population of young adults. Echocardiographic analysis of 4111 subjects in the CARDIA Study. Coronary Artery Risk Development in (Young) Adults. Circulation. 1995;92(4):785-9.
2. Semsarian C, Ingles J, Maron MS, Maron BJ. New Perspectives on the Prevalence of Hypertrophic Cardiomyopathy. Journal of the American College of Cardiology. 2015;65(12):1249-54.
3. Ho CY, Charron P, Richard P, Girolami F, Van Spaendonck-Zwarts KY, Pinto Y. Genetic advances in sarcomeric cardiomyopathies: state of the art. Cardiovasc Res. 2015;105(4):397-408.
4. Page SP, Kounas S, Syrris P, Christiansen M, Frank-Hansen R, Andersen PS, et al. Cardiac myosin binding protein-C mutations in families with hypertrophic cardiomyopathy: disease expression in relation to age, gender, and long term outcome. Circ Cardiovasc Genet. 2012;5(2):156-66.
5. Kraft T, Montag J, Radocaj A, Brenner B. Hypertrophic Cardiomyopathy: Cell-to-Cell Imbalance in Gene Expression and Contraction Force as Trigger for Disease Phenotype Development. Circ Res. 2016;119(9):992-5.
6. Parbhudayal RY, Garra AR, Gotte MJW, Michels M, Pei J, Harakalova M, et al. Variable cardiac myosin binding protein-C expression in the myofilaments due to MYBPC3 mutations in hypertrophic cardiomyopathy. J Mol Cell Cardiol. 2018;123:59-63.
7. Wang L, Kim K, Parikh S, Cadar AG, Bersell KR, He H, et al. Hypertrophic cardiomyopathy-linked mutation in troponin T causes myofibrillar disarray and pro-arrhythmic action potential changes in human iPSC cardiomyocytes. J Mol Cell Cardiol. 2018;114:320-7.
8. Martins AS, Parvatiyar MS, Feng HZ, Bos JM, Gonzalez-Martinez D, Vukmirovic M, et al. In Vivo Analysis of Troponin C Knock-In (A8V) Mice: Evidence that TNNC1 Is a Hypertrophic Cardiomyopathy Susceptibility Gene. Circ Cardiovasc Genet. 2015;8(5):653-64.
9. Michele DE, Gomez CA, Hong KE, Westfall MV, Metzger JM. Cardiac dysfunction in hypertrophic cardiomyopathy mutant tropomyosin mice is transgene-dependent, hypertrophy-independent, and improved by beta-blockade. Circ Res. 2002;91(3):255-62.
10. Tardiff JC, Hewett TE, Palmer BM, Olsson C, Factor SM, Moore RL, et al. Cardiac troponin T mutations result in allele-specific phenotypes in a mouse model for hypertrophic cardiomyopathy. J Clin Invest. 1999;104(4):469-81.
11. Maass AH, Ikeda K, Oberdorf-Maass S, Maier SK, Leinwand LA. Hypertrophy, fibrosis, and sudden cardiac death in response to pathological stimuli in mice with mutations in cardiac troponin T. Circulation. 2004;110(15):2102-9.
12. Miller T, Szczesna D, Housmans PR, Zhao J, de Freitas F, Gomes AV, et al. Abnormal contractile function in transgenic mice expressing a familial hypertrophic cardiomyopathy-linked troponin T (I79N) mutation. J Biol Chem. 2001;276(6):3743-55.
13. Hernandez OM, Szczesna-Cordary D, Knollmann BC, Miller T, Bell M, Zhao J, et al. F110I and R278C troponin T mutations that cause familial hypertrophic cardiomyopathy affect muscle contraction in transgenic mice and reconstituted human cardiac fibers. J Biol Chem. 2005;280(44):37183-94.

14. Baudenbacher F, Schober T, Pinto JR, Sidorov VY, Hilliard F, Solaro RJ, et al. Myofilament Ca2+ sensitization causes susceptibility to cardiac arrhythmia in mice. J Clin Invest. 2008;118(12):3893-903.
15. Harada K, Potter JD. Familial hypertrophic cardiomyopathy mutations from different functional regions of troponin T result in different effects on the pH and Ca2+ sensitivity of cardiac muscle contraction. J Biol Chem. 2004;279(15):14488-95.
16. van der Velden J, Papp Z, Zaremba R, Boontje NM, de Jong JW, Owen VJ, et al. Increased Ca2+-sensitivity of the contractile apparatus in end-stage human heart failure results from altered phosphorylation of contractile proteins. Cardiovasc Res. 2003;57(1):37-47.
17. Wijnker PJ, Foster DB, Tsao AL, Frazier AH, dos Remedios CG, Murphy AM, et al. Impact of site-specific phosphorylation of protein kinase A sites Ser23 and Ser24 of cardiac troponin I in human cardiomyocytes. Am J Physiol Heart Circ Physiol. 2013;304(2):H260-8.
18. Pinto JR, Parvatiyar MS, Jones MA, Liang J, Potter JD. A troponin T mutation that causes infantile restrictive cardiomyopathy increases Ca2+ sensitivity of force development and impairs the inhibitory properties of troponin. J Biol Chem. 2008;283(4):2156-66.
19. Johnston JR, Landim-Vieira M, Marques MA, de Oliveira GAP, Gonzalez-Martinez D, Moraes AH, et al. The intrinsically disordered C terminus of troponin T binds to troponin C to modulate myocardial force generation. J Biol Chem. 2019;294(52):20054-69.
20. Pinto JR, Parvatiyar MS, Jones MA, Liang J, Ackerman MJ, Potter JD. A functional and structural study of troponin C mutations related to hypertrophic cardiomyopathy. J Biol Chem. 2009;284(28):19090-100.
21. Urbancikova M, Hitchcock-DeGregori SE. Requirement of amino-terminal modification for striated muscle alpha-tropomyosin function. J Biol Chem. 1994;269(39):24310-5.
22. Najafi A, Schlossarek S, van Deel ED, van den Heuvel N, Guclu A, Goebel M, et al. Sexual dimorphic response to exercise in hypertrophic cardiomyopathy-associated MYBPC3-targeted knock-in mice. Pflugers Arch. 2015;467(6):1303-17.
23. Dobin A, Davis CA, Schlesinger F, Drenkow J, Zaleski C, Jha S, et al. STAR: ultrafast universal RNA-seq aligner. Bioinformatics. 2013;29(1):15-21.
24. Tarasov A, Vilella AJ, Cuppen E, Nijman IJ, Prins P. Sambamba: fast processing of NGS alignment formats. Bioinformatics. 2015;31(12):2032-4.
25. Aransay AM, Lavín Trueba JL. Field guidelines for genetic experimental designs in high-throughput sequencing. Switzerland: Springer; 2016.
26. Robinson MD, McCarthy DJ, Smyth GK. edgeR: a Bioconductor package for differential expression analysis of digital gene expression data. Bioinformatics. 2010;26(1):139-40.
27. Gruber AR, Lorenz R, Bernhart SH, Neubock R, Hofacker IL. The Vienna RNA websuite. Nucleic Acids Res. 2008;36(Web Server issue):W70-4.
28. Sequeira V, Wijnker PJ, Nijenkamp LL, Kuster DW, Najafi A, Witjas-Paalberends ER, et al. Perturbed length-dependent activation in human hypertrophic cardiomyopathy with missense sarcomeric gene mutations. Circ Res. 2013;112(11):1491-505.
29. Szczesna D, Zhang R, Zhao J, Jones M, Guzman G, Potter JD. Altered regulation of cardiac muscle contraction by troponin T mutations that cause familial hypertrophic cardiomyopathy. J Biol Chem. 2000;275(1):624-30.

30. Sirenko SG, Potter JD, Knollmann BC. Differential effect of troponin T mutations on the inotropic responsiveness of mouse hearts--role of myofilament Ca2+ sensitivity increase. J Physiol. 2006;575(Pt 1):201-13.
31. Ezekian JE, Clippinger SR, Garcia JM, Yang Q, Denfield S, Jeewa A, et al. Variant R94C in TNNT2-Encoded Troponin T Predisposes to Pediatric Restrictive Cardiomyopathy and Sudden Death Through Impaired Thin Filament Relaxation Resulting in Myocardial Diastolic Dysfunction. J Am Heart Assoc. 2020;9(5):e015111.
32. Tsoutsman T, Kelly M, Ng DC, Tan JE, Tu E, Lam L, et al. Severe heart failure and early mortality in a double-mutation mouse model of familial hypertrophic cardiomyopathy. Circulation. 2008;117(14):1820-31.
33. Ingles J. Compound and double mutations in patients with hypertrophic cardiomyopathy: implications for genetic testing and counselling. Journal of Medical Genetics. 2005;42(10):e59-e.
34. Pervunina T, Vershinina T, Kiselev A, Nikitina I, Grekhov E, Mitrofanova L, et al. Neonatal hypertrophic cardiomyopathy caused by double mutation in RAS pathway genes. Int J Cardiol. 2015;184:272-3.
35. Gajendrarao P, Krishnamoorthy N, Selvaraj S, Girolami F, Cecchi F, Olivotto I, et al. An Investigation of the Molecular Mechanism of Double cMyBP-C Mutation in a Patient with End-Stage Hypertrophic Cardiomyopathy. J Cardiovasc Transl Res. 2015;8(4):232-43.
36. Wessels MW, Herkert JC, Frohn-Mulder IM, Dalinghaus M, van den Wijngaard A, de Krijger RR, et al. Compound heterozygous or homozygous truncating MYBPC3 mutations cause lethal cardiomyopathy with features of noncompaction and septal defects. Eur J Hum Genet. 2015;23(7):922-8.
37. Van Driest SL, Vasile VC, Ommen SR, Will ML, Tajik AJ, Gersh BJ, et al. Myosin binding protein C mutations and compound heterozygosity in hypertrophic cardiomyopathy. J Am Coll Cardiol. 2004;44(9):1903-10.
38. van Rijsingen IA, Hermans-van Ast JF, Arens YH, Schalla SM, de Die-Smulders CE, van den Wijngaard A, et al. Hypertrophic cardiomyopathy family with double-heterozygous mutations; does disease severity suggest doubleheterozygosity? Neth Heart J. 2009;17(12):458-63.
39. Yamada Y, Namba K, Fujii T. Cardiac muscle thin filament structures reveal calcium regulatory mechanism. Nat Commun. 2020;11(1):153.
40. Robinson P, Mirza M, Knott A, Abdulrazzak H, Willott R, Marston S, et al. Alterations in thin filament regulation induced by a human cardiac troponin T mutant that causes dilated cardiomyopathy are distinct from those induced by troponin T mutants that cause hypertrophic cardiomyopathy. J Biol Chem. 2002;277(43):40710-6.
41. Davis J, Davis LC, Correll RN, Makarewich CA, Schwanekamp JA, Moussavi-Harami F, et al. A Tension-Based Model Distinguishes Hypertrophic versus Dilated Cardiomyopathy. Cell. 2016;165(5):1147-59.
42. Capek P, Vondrasek J, Skvor J, Brdicka R. Hypertrophic cardiomyopathy: from mutation to functional analysis of defective protein. Croat Med J. 2011;52(3):384-91.
43. Rai TS, Ahmad S, Bahl A, Ahuja M, Ahluwalia TS, Singh B, et al. Genotype phenotype correlations of cardiac beta-myosin heavy chain mutations in Indian patients with hypertrophic and dilated cardiomyopathy. Mol Cell Biochem. 2009;321(1-2):189-96.

44. Tanjore RR, Sikindlapuram AD, Calambur N, Thakkar B, Kerkar PG, Nallari P. Genotype-phenotype correlation of R870H mutation in hypertrophic cardiomyopathy. Clin Genet. 2006;69(5):434-6.
45. Mundia MM, Demers RW, Chow ML, Perieteanu AA, Dawson JF. Subdomain location of mutations in cardiac actin correlate with type of functional change. PLoS One. 2012;7(5):e36821.
46. Vang S, Corydon TJ, Borglum AD, Scott MD, Frydman J, Mogensen J, et al. Actin mutations in hypertrophic and dilated cardiomyopathy cause inefficient protein folding and perturbed filament formation. FEBS J. 2005;272(8):2037-49.
47. Pavadai E, Rynkiewicz MJ, Ghosh A, Lehman W. Docking Troponin T onto the Tropomyosin Overlapping Domain of Thin Filaments. Biophys J. 2020;118(2):325-36.
48. Palm T, Graboski S, Hitchcock-DeGregori SE, Greenfield NJ. Disease-causing mutations in cardiac troponin T: identification of a critical tropomyosin-binding region. Biophys J. 2001;81(5):2827-37.
49. Wen Y, Pinto JR, Gomes AV, Xu Y, Wang Y, Wang Y, et al. Functional consequences of the human cardiac troponin I hypertrophic cardiomyopathy mutation R145G in transgenic mice. J Biol Chem. 2008;283(29):20484-94.
50. Wen Y, Xu Y, Wang Y, Pinto JR, Potter JD, Kerrick WG. Functional effects of a restrictive-cardiomyopathy-linked cardiac troponin I mutation (R145W) in transgenic mice. J Mol Biol. 2009;392(5):1158-67.
51. Bollen IAE, Schuldt M, Harakalova M, Vink A, Asselbergs FW, Pinto JR, et al. Genotype-specific pathogenic effects in human dilated cardiomyopathy. J Physiol. 2017;595(14):4677-93.
52. Helms AS, Tang VT, O'Leary TS, Friedline S, Wauchope M, Arora A, et al. Effects of MYBPC3 loss-of-function mutations preceding hypertrophic cardiomyopathy. JCI Insight. 2020;5(2).
53. van der Velden J, Narolska NA, Lamberts RR, Boontje NM, Borbely A, Zaremba R, et al. Functional effects of protein kinase C-mediated myofilament phosphorylation in human myocardium. Cardiovasc Res. 2006;69(4):876-87.

THE SUPPLEMENTARY DATA IS AVAILABLE ONLINE:

https://ars.els-cdn.com/content/image/1-s2.0-S0022282820303011-mmc1.pdf

UNTYING THE KNOT: PROTEIN QUALITY CONTROL IN INHERITED CARDIOMYOPATHIES

Larissa M. Dorsch*, **Maike Schuldt***, Dora Knežević, Marit Wiersma, Diederik WD. Kuster, Jolanda van der Velden, Bianca JJM. Brundel

*contributed equally

Pflügers Archiv – European Journal of Physiology, 2018.

3

ABSTRACT

Mutations in genes encoding sarcomeric proteins are the most important cause of inherited cardiomyopathies, which are a major cause of mortality and morbidity worldwide. Although genetic screening procedures for early disease detection have been improved significantly, treatment to prevent or delay mutation-induced cardiac disease onset is lacking.

Recent findings indicate that loss of protein quality control (PQC) is a central factor in the disease pathology leading to derailment of cellular protein homeostasis. Loss of PQC includes impairment of heat shock proteins, the ubiquitin-proteasome system and autophagy. This may result in accumulation of misfolded and aggregation-prone mutant proteins, loss of sarcomeric and cytoskeletal proteins, and, ultimately, loss of cardiac function. PQC derailment can be a direct effect of the mutation-induced activation, a compensatory mechanism due to mutation-induced cellular dysfunction or a consequence of the simultaneous occurrence of the mutation and a secondary hit. In this review, we discuss recent mechanistic findings on the role of proteostasis derailment in inherited cardiomyopathies, with special focus on sarcomeric gene mutations and possible therapeutic applications.

CLASSIFICATION OF CARDIOMYOPATHIES

Cardiomyopathies (CM) constitute one of the most common causes of sudden cardiac death in young adults and represent major causes for cardiac transplantation [88]. Disease onset generally ranges between 20-50 years of age. CMs are defined by abnormal myocardial structure and function in the absence of any other diseases sufficient to cause these abnormalities [24]. These can be sub-classified based on their functional phenotype and their specific morphological changes. The most common types are hypertrophic CM (HCM), characterized by increased left ventricular (LV) wall thickness often occurring asymmetrically, and dilated CM (DCM), in which the presence of LV dilatation is accompanied by contractile dysfunction [24]. Besides HCM and DCM, there are less frequent forms such as restrictive CM (RCM) and desmin-related cardiomyopathy [24]. All these cardiomyopathies can be familial and are typically inherited in an autosomal dominant manner. Mutations in genes encoding sarcomeric proteins are the most common cause of these types of CMs [3]. However, the genotype-phenotype relationship is far from clear. The variations in age of CM onset and disease phenotype suggest that additional factors play a role in CM pathogenesis.

Accumulating evidence indicates the presence of derailed proteostasis in CMs as well as its contribution to CM onset and progression. This derailment could either be caused directly by the mutation or indirectly due to a compensatory mechanism. In the former case, the mutant protein might be instable or improperly folded leading to direct activation of the protein quality control (PQC). In the latter case, the mutation does not interfere with protein folding or stability but causes functional impairment which in turn leads to cellular stress and indirect activation of the PQC. Furthermore, the "secondary-hit" model may apply in CMs, in which a primary sarcomere mutation enhances vulnerability to secondary stressors which increases cellular burden resulting in PQC derailment. This review summarizes the current knowledge about perturbations in the different components of the PQC in CMs that are caused by mutations in sarcomeric proteins.

PROTEOSTASIS NETWORK ENSURES CARDIAC HEALTH

The heart has a very limited regenerative capacity and therefore requires surveillance by a system that maintains protein homeostasis to ensure cardiac health [106]. The PQC system sustains proteostasis by refolding misfolded proteins or removing them if refolding is impossible. It is composed of heat shock proteins (HSPs), the ubiquitin-proteasome system (UPS) and autophagy. PQC is only then functional when all three components are operative and interact with each other. This means that derailment of one of the parts might impair the function of the others in a direct or indirect manner. In a physiological state, protein folding and refolding is ensured by HSPs and their regulators. Terminally

misfolded and aggregation-prone proteins are cleared by the two degradation systems, i.e. the UPS and autophagy, that work in collaboration with the HSPs (Fig.1).

First, the different parts of the PQC in normal physiology are described, before addressing their role in CMs.

Heat shock proteins

HSPs, originally identified as heat responsive proteins, are constitutively expressed in the cell to serve as molecular chaperones to ensure correct folding and assembly of proteins. HSPs are classified in two categories: the small HSPs with a low molecular weight (15-30 kDa) and the chaperones with a high molecular weight (>30 kDa).
One functional group of HSPs are chaperonin complexes, which are ATP-dependent chaperones with a barrel-like structure, that provide correct folding of nascent proteins after translation. Besides their folding function during protein translation, HSPs are also induced in response to cellular and environmental stressors to maintain a healthy cellular proteostasis by clearance of misfolded proteins [66, 111].
As reviewed by Garrido et al, small HSPs show an ATP-independent holdase activity. This means that they bind to misfolded proteins, keep them in a state competent for either refolding or degradation, and thereby prevent or attenuate their aggregation. Due to the association of small HSPs with the HSPs that have an ATP-dependent folding activity, the misfolded proteins can be refolded into their native and functional conformation [28]. The binding affinity of HSPs to the misfolded protein is dependent on the chaperone cofactors bound to the HSPs. Furthermore, this binding of chaperone cofactors determines the processing of the misfolded protein for either refolding or degradation. Chaperone cofactors involved in degradation pathways can switch off the refolding activity of HSPs by inhibiting their ATPase activity and assist the HSPs and the UPS or autophagy in the breakdown of misfolded proteins (Fig.2) [13, 25]. The degradation of the thick filament protein myosin-binding protein-C (MyBP-C), for instance, is mediated via the chaperone cofactor HSC70 playing a major role in regulating MyBP-C protein turnover [32]. These degradation pathways are addressed in the following sections.

To maintain the structure and function of the highly dynamic cardiac sarcomeres, HSPs play an important role. The molecular chaperones GimC (Prefoldin), chaperonin TCP-1 Ring Complex (TRiC), αB-crystallin and HSP27 ensure correct folding and assembly of proteins, maturation of actin and prevent aggregate formation [10, 14, 34, 36]. HSP27 is mostly found as high–molecular weight oligomers in the cytosol of unstressed cells [23]. Upon stress, HSP27 deoligomerizes and translocates to F-actin and thereby stabilizes the F-actin network [16]. To assemble the myosin thick filament, the chaperones UNC-45, HSP90 and HSP70 are required, whereas the actin filament is self-assembled [7, 8, 94]. Several members of the small HSPs family are expressed in the heart and associate with cytoskeletal proteins [33, 103]. These HSPBs stabilize cytoskeletal structures and improve coping with stress situations [33, 48, 49].

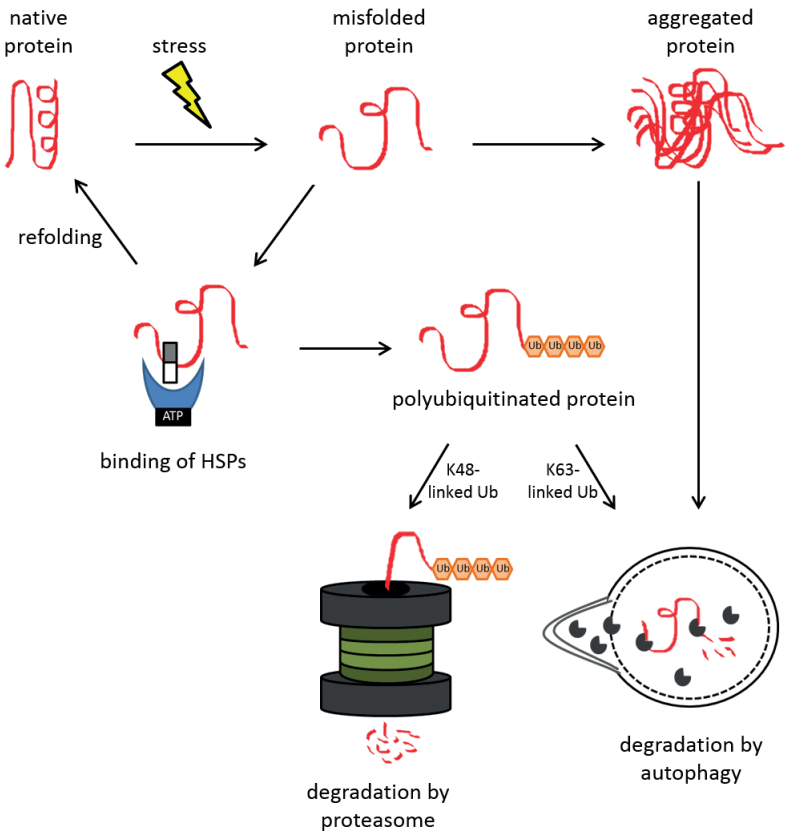

FIGURE 1. Collaboration of the protein quality control components. Stress leads to misfolding of proteins, which may result in abnormal interaction and subsequent aggregation. Small HSPs (white/gray rectangle) and HSPs with ATPase activity (blue moon shape with black rectangle) prevent aggregation formation by binding to the hydrophobic surfaces of misfolded proteins. They either refold the misfolded proteins to its native structure or initiate its polyubiquitination (Ub, orange hexagon). Misfolded proteins with polyubiquitin chains linked to lysine 48 (K48) are mainly degraded by the proteasome. Misfolded proteins carrying K63-linked polyubiquitin chains and aggregated proteins enter the autophagic pathway.

Ubiquitin-proteasome system

In case of terminally misfolded proteins, that failed be refolded, HSPs and their chaperone cofactors recruit enzymes to mediate polyubiquitination of the target substrate and thereby mark them for the appropriate degradation pathway. Short-lived proteins are typically degraded by the UPS, whereas autophagy is mainly used for degrading long-lived proteins and entire organelles [17, 39].

The polyubiquitination of the target substrate requires the sequential action of three enzymes. The ubiquitin-activating enzyme (E1) activates ubiquitin which is

then transferred to a ubiquitin-conjugating enzyme (E2). In the last step, a ubiquitin ligase (E3) links ubiquitin from the E2 enzyme to a lysine residue of the target protein. There are only two E1 enzymes, several E2 enzymes and many E3 ligases, each of which recognizes one or several specific protein motifs. Therefore, the substrate specificity is achieved by the selectivity of the different E3 ligases [26, 80]. Dependent on the combination of E2 enzyme and E3 ligase, polyubiquitin chains are linked to the preceding ubiquitin molecule either via lysine 48 (K48) or via lysine 63 (K63) which marks the protein for degradation. Therefore, the polyubiquitination process determines the degradation pathways: Proteins carrying K48-linked polyubiquitin chains are predominantly targeted to proteasomal degradation, and proteins carrying K63-linked polyubiquitin chains enter the autophagic pathways as discussed in the following paragraph [1].

K48-linked polyubiquitinated proteins are transferred to the proteasome, which is almost exclusively the 26S proteasome in eukaryotic cells. This protein complex consist of one 20S core- and two 19S regulatory subunits forming a barrel-like structure. The regulatory subunits have ubiquitin-binding sites to recognize polyubiquitinated proteins and unfold them using their ATPase activity. The unfolded proteins are transferred to the catalytic core and proteolytically cleaved [104].

Sarcomeric proteins have an average turnover rate of 5-10 days [12, 112]. Therefore, they rely on a proper functioning UPS to regulate their clearance. Once dissociated from the myofibrils, ubiquitin-conjugating enzymes mark the proteins for proteasomal degradation by adding K48-linked polyubiquitin chains [91, 112]. In cardiomyocytes, this step is mediated by the MuRF family of E3 ligases [59, 93].

Autophagy

Autophagy cleans up aggregates or proteins via lysosomal breakdown that cannot be refolded by chaperones or processed by the UPS [46]. During macroautophagy, herein referred to as autophagy, membrane enclosed vesicles are formed containing the targeted cellular components. First, an isolation membrane is formed engulfing the cytoplasmic material. The membrane expands until the edges fuse to form the autophagosome [118]. Fusion of the autophagosome with a lysosome leads to an autolysosome which breaks down the cargo [5]. During selective autophagy, proteins carrying a K63-linked polyubiquitin chain are degraded. In the case the proteasome is overwhelmed with proteins carrying a K48-linked ubiquitin chain, such as aggregated proteins, they can also be cleared via autophagy. Their polyubiquitin chain docks to the adaptor protein p62/SQSTM1 which enables the translocation into the autophagosome [45]. Acidic lysosomal hydrolases degrade the captured material together with the inner membrane and the resulting macromolecules are recycled into ATP, amino acids and fatty acids.

Autophagy is found to be upregulated in response to starvation, growth factor withdrawal or high bioenergetic demands [50, 56, 65, 86]. The ability to sequester

and break down entire organelles, such as mitochondria, peroxisomes, endoplasmic reticulum and intact intracellular microorganisms, makes autophagy a unique and essential process in the cell. Especially in post-mitotic cells like cardiomyocytes, basal activation of autophagy is important to maintain a balanced proteostasis by degradation of long-lived proteins, lipid droplets and dysfunctional organelles [17]. Cardiomyocytes have a low basal autophagic activity under normal conditions. Upon stress, the formation of protein aggregates is facilitated and triggers activation of autophagy [96]. Furthermore, cardiac autophagy is initiated in response to energy stress during periods of nutrient deprivation or high metabolic demand [35].

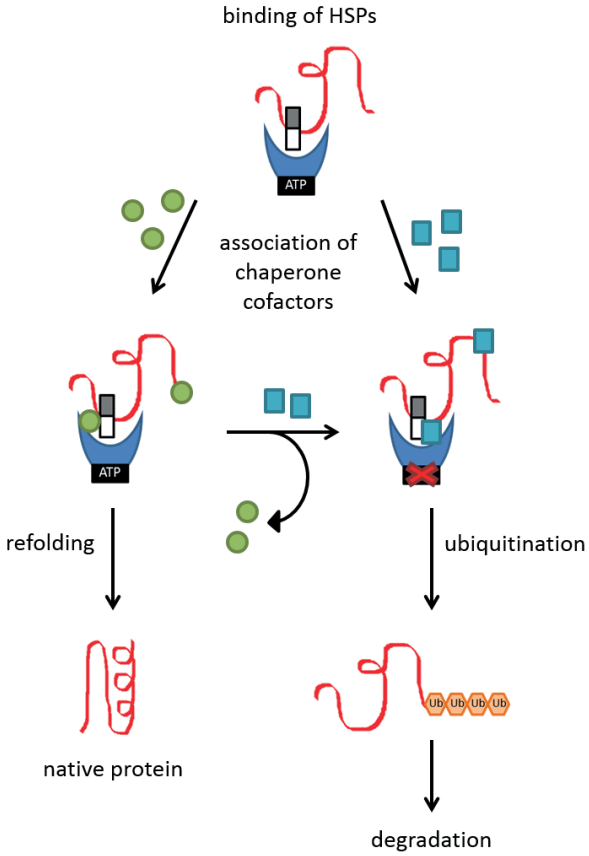

FIGURE 2. Chaperone cofactor binding determines the heat shock protein (HSP) function. Small HSPs (white/gray rectangle) and HSPs with ATPase activity (blue moon shape with black rectangle) bind to the misfolded protein to stabilize it. Dependent on the chaperone cofactors (green circles or turquoise squares), the misfolded protein gets either refolded or ubiquitinated for subsequent degradation. If refolding is impossible, the chaperone cofactors can be exchanged to promote degradation. In case of ubiquitination, the chaperone cofactors can switch off the HSP refolding activity by blocking the ATPase activity and, together with HSPs, assist in clearance of the misfolded protein via the degradation pathways

PROTEOSTASIS DERAILMENT IN INHERITED CARDIOMYOPATHIES

The PQC is of great importance in many cardiac diseases caused by 'wear and tear', including cardiac amyloidosis, myocardial infarction and atrial fibrillation [37, 60, 73, 115]. The activation of PQC in a variety of cardiac stress conditions can be considered as a positive compensatory response to maintain proteostasis. This might be especially true in the case of inherited CMs, where mutant protein expression is the disease-causing mechanism. Recent studies provide evidence for a causative role of the PQC in CM. On one hand, mutations in components of the PQC itself can cause CM. This has been described for the R120G mutation in *CRYAB* encoding for the chaperone αB-crystallin, causing desmin-related CM, and the P209L mutation in the chaperone cofactor *BAG3*, leading to juvenile DCM [87, 105]. Mutations in PQC components as causes of inherited CM are rare, but PQC impairment can also occur as a result of CM-causing sarcomeric mutations. In this case, mutant sarcomeric proteins may impair the function of the PQC through overload of its components including HSPs, UPS and autophagy. This could lead to increased levels of mutant protein, exacerbating CM disease progression.

So far, the role of PQC has been investigated only in a limited number of studies on CM caused by sarcomeric gene mutations. *In vitro* information is available for HCM- and DCM-causing mutations in *ACTC1*. Furthermore, it has been studied *in vivo* with HCM-causing mutations in *MYBPC3*, *MYH7* and *MYOZ2*, DCM-causing *NEBL* mutations and RCM-causing *TNNI3* mutations (Table 1). In the following sections, the interaction between CM and derailments of the different parts of the PQC are described in detail.

Diverse abnormalities in heat shock protein function

HSP impairment or activation contribute to disease pathology in CMs. Desmin-related CM displays HSP impairment and is either caused by mutant desmin itself or mutant chaperone αB-crystallin. In a normal state, αB-crystallin binds to desmin and thereby prevents its aggregation [10]. Mutant desmin, however, impairs the interaction with αB-crystallin leading to desmin accumulation and cardiomyocyte dysfunction [54]. This suggests aberrant protein aggregation can cause CM. Correspondingly, the R120G mutation in *CRYAB* results in desmin-related-CM as well and also presents with aggregates containing desmin and mutant αB-crystallin [105]. Sanbe et al. showed that upregulation of HSPB8 due to geranylgeranylacetone treatment reduces the amount of mutant αB-crystallin-containing aggregates [83]. This implies that other HSPs can compensate for the loss of function to remove aggregates. Furthermore, *in vitro* experiments have shown that HCM- or DCM-causing mutations in *ACTC1*, encoding cardiac actin, can interfere with its folding by the TRiC chaperonin complex resulting in inefficient incorporation of actin into the myofilament and its subsequent aggregation [102]. Mutations in one specific subdomain of actin affect protein stability or polymerization, making actin more prone for degradation. Whereas mutations in other subdomains of actin cause alterations in protein-protein interactions [67]. A gene co-expression

analysis of human controls and HCM samples identified the TRiC chaperonin complex as the most differential pathway thereby further highlighting its importance in HCM [19].

By contrast, various studies on the role of PQC in CMs report on increased levels of HSPs due to PQC activation. However, it still remains unresolved whether the increased levels of HSPs are a direct effect of the mutant protein or a compensatory secondary effect due to increased cellular stress. Therefore, the direct interaction of mutant protein and HSPs needs to be studied. In mice with a truncating *MYBPC3* mutation and an HCM phenotype, increased levels of αB-crystallin have been found [116]. In other CM mouse models, independent of a sarcomeric mutation, increased levels of HSP70 have been observed [62]. A study in patients with chronic heart failure due to DCM revealed a correlation of serum HSP60 levels with disease severity [69]. Since increased levels of HSP27 and HSP70 are associated with a protective effect in models for atrial fibrillation, by maintaining cardiomyocyte function, one can speculate that increased expression of these HSPs might be part of a compensatory protective mechanism in CM [15, 62].

In general, research findings indicate that HSP impairment is detrimental for cardiomyocyte function due to a higher risk of impaired protein folding and aggregate formation. By contrast, HSP activation in CM is considered as a beneficial effect and is most likely a compensatory mechanism of the cell.

Derailment of the ubiquitin-proteasome system

Derailed UPS function in CM affects the degradation of terminally misfolded proteins. *MYBPC3* mutations often lead to expression of truncated protein, which is not incorporated into the sarcomere because the most C-terminal domain needed for incorporation is missing [64]. Truncated MyBP-C has not been detected in cardiac samples of HCM patients [101]. In addition, very low levels (<4%) of truncated MyBP-C, which were not incorporated into the sarcomeres, were found in engineered heart tissue made of *MYBPC3* knock-out mouse cardiomyocytes transfected with a truncating *MYBPC3* mutation [110]. Therefore, it is likely that either the mutant mRNA is degraded via nonsense-mediated mRNA decay and/or the truncated MyBP-C forms a substrate for immediate degradation by the UPS or autophagy. Since MyBP-C is highly expressed in cardiomyocytes, high levels of truncated protein may lead to an increased UPS burden and competitive inhibition of the proteasome [84, 85]. In this case, the UPS is overwhelmed by the amount of truncated protein that needs to be degraded. In line with this hypothesis are analyses of myectomy samples from HCM patients with sarcomeric mutations which show a decrease in proteolytic activity (Table 1) [77, 85]. Decreased processing through the UPS system is also indicated by the increase in overall levels of protein ubiquitination in HCM patients and animal models which is already detectable at an early postnatal phase prior to any other symptom development [6, 30, 77, 85]. Consistent with the studies in *MYBPC3*-mutant samples, UPS perturbations have also been found in mouse heart tissue with *TNNT2*

mutations [30]. Patient samples with a sarcomeric mutation showed higher levels of polyubiquitination and decreased proteolytic activity compared to healthy controls [77].

In addition to overload of the UPS by mutant protein, increased oxidative stress can also impair the function of the proteasome. In this case, the proteasomal dysfunction would not be a direct effect of the mutant protein but a consequence of secondary cellular changes. In CM samples, an increase in oxidation of cytosolic protein content as well as the 19S proteasome, thereby decreasing the overall proteolytic function of the 26S proteasome subunit, has been identified [21, 30, 77].
In addition to the proteasome itself, the expression of ubiquitin ligases can be altered. In an HCM mouse model with mutant *Mybpc3*, the muscle specific E3 ligase Asb2β showed decreased mRNA levels compared to wild-type mice [99]. Since one of its targets is desmin, accumulation of desmin could contribute to the HCM phenotype, as observed for desmin-related CMs.
A large HCM patient cohort and matched healthy controls were screened for genetic variants in all three members of the MuRF family, since mutations in the gene encoding MuRF1 were reported to cause HCM [18]. In this study, a higher prevalence of rare variants of the cardiac-specific E3 ligases MuRF1 and MuRF2 was found in HCM patients [95]. These were associated with earlier disease onset and higher penetrance implying that disturbances of the UPS might act as a disease modifier contributing to HCM.

In contrast to HCM, in DCM the reported UPS derailments could not yet be linked to sarcomeric mutations. A likely reason for this is that the DCM patient samples did not carry a sarcomeric mutation and/or the underlying disease cause was not known. Tissue analysis from explanted DCM hearts revealed increased expression of both E1 and/or E2 enzymes [47, 108]. Further evidence of increased ubiquitin-conjugating enzyme activity was detected in end-stage DCM. Here, increased levels of MuRF1 and MAFbx were associated with increased UPS degradation activity, which might be the cause of ventricle wall thinning as observed in end-stage DCM patients [9]. In line with the increased ubiquitin-conjugating enzyme levels, increased levels of polyubiquitinated proteins have been detected in DCM samples [11, 47, 72, 108]. This finding is further supported by a 2.3-fold reduced expression of the deubiquitinating enzyme isopeptidase-T in DCM patients [47]. Furthermore, increased proteolytic activity of the 26S proteasome as well as the 20S subunit peptidase activity have been found [9, 11, 72].

In contrast to HSPs, the answer to the question whether UPS activation or inhibition would be beneficial in HCM and DCM, is not as straight forward. In an HCM phenotype, proteasome activation might improve the hypertrophic phenotype due to increased mutant protein degradation. However, in DCM, increased proteasome function might augment wall thinning and therefore DCM might benefit from proteasome inhibition.

TABLE 1. Overview of structural changes and adaptations in the protein quality control system related to cardiomyopathies

Gene	Phenotype	Morphological abnormalities	Chaperones	UPS	Autophagy
ACTC1	HCM	not reported	+ (*in vitro*) [102]	not reported	not reported
	DCM	not reported	+ (*in vitro*) [102]	not reported	not reported
	RCM	not reported	not reported	not reported	not reported
ACTN2	HCM	cytoplasmic vacuolization, perinuclear halo, dysmorphic nuclei (human) [31]	not reported	not reported	not reported
	DCM	not reported	not reported	not reported	not reported
MYBPC3	HCM	large irregular vacuoles (infant) [109]	αB-crystallin ↑ (mice) [116]	↓ (mice) [85]	↑ (human)[92] ↓ (mice) [85]
	DCM	not reported	not reported	not reported	not reported
MYH6	HCM	not reported	not reported	not reported	not reported
	DCM	not reported	not reported	not reported	not reported
MYH7	HCM	not reported	not reported	not reported	↑ (human) [92]
	DCM	not reported	not reported	not reported	not reported
	RCM	not reported	not reported	not reported	not reported
MYL2	HCM	not reported	not reported	not reported	not reported
MYL3	HCM	not reported	not reported	not reported	not reported
	RCM	ultrastructural defects (mice) [119]	not reported	not reported	not reported
MYOZ2	HCM	not reported	not reported	↑ (mice) [41]	not reported
NEBL	HCM	myocyte vacuolization (human) [75]	not reported	not reported	not reported
	DCM	enlarged and deformed mitochondria, lipid accumulation (mice) [78]	not reported	not reported	abnormal lysosomes (mice) [78]

TABLE 1. Continued.

Gene	Phenotype	Morphological abnormalities	Chaperones	UPS	Autophagy
TNNC1	HCM	not reported	not reported	not reported	not reported
	DCM	no evidence of vacuolization (human) [43]	not reported	not reported	not reported
	RCM	degeneration of myocardial fibres (human) [76]	not reported	not reported	not reported
TNNI3	HCM	not reported	not reported	not reported	not reported
	DCM	not reported	not reported	not reported	not reported
	RCM	irregularly shaped megamitochondria (human) [117]	not reported	↓proteasomal activity (mice) [20]	not reported
TNNT2	HCM	myocyte atrophy (mice) [97]	not reported	↓(mice) [30]	not reported
	DCM	not reported	not reported	not reported	not reported
	RCM	abnormal mitochondria (human)* [74]	not reported	not reported	not reported
TPM1	HCM	nuclear gigantism [68]	not reported	not reported	not reported
	DCM	accumulation of TPM1 (mice) [79]	not reported	not reported	not reported
	RCM	not reported	not reported	not reported	not reported

Mixed genotypes are indicated with "*" and a "+" indicates a positive finding.

Unresolved role of the autophagic response in cardiomyopathies

Autophagy is a crucial mechanism in CMs that only fulfills its cytoprotective mechanisms when it is in balance [50]. Moderate activation of autophagy has beneficial effects in CM patients by removing aggregates and supplying the cell with energy.

However, protein degradation due to excessive autophagy has been associated with different types of CM, including HCM, DCM, ischemic CM and chemotherapy-induced CM [22, 44, 55, 58, 71, 89]. This could lead to loss of myofibrils, as observed in end-stage HCM and DCM patients [40, 70]. In a recent study, the expression of vacuolar protein sorting 34 (Vps34), an important autophagy regulator, was shown to be decreased in the myocardium of HCM patients and deletion of Vsp34 resulted in an HCM-like phenotype in mice. Furthermore, decreased expression of Vsp34 impaired the HSP-autophagy axis, as indicated by αB-crystallin-positive aggregates [44]. HCM patients with mutations in *MYBPC3* or *MYH7* revealed an upregulation of autophagic vacuoles and markers, indicating increased autophagic activity [92]. In a homozygous *Mybpc3*-mutant HCM mouse model, levels of autophagy markers were increased at the protein level implying autophagic activation. However, mRNA levels of these markers were not increased. This rather suggests an accumulation of autophagic proteins due to defective autophagic-lysosomal degradation instead of activation on transcriptional level [85]. In explanted hearts from DCM patients, the imbalance of high uibiquitination rate and insufficient degradation may contribute to autophagic cell death [47]. Vacuolization in CMs has been reported with mutations in *ACTN2*, *MYBPC3* and *NEBL* [31, 75, 109]. This observation suggests that the accumulation of autophagic vacuoles implies cardiomyocyte stress. However, the interpretation of vacuole accumulation remains unclear since it could reflect an increase in autophagic activity or an impairment of autophagosome-lysome fusion.

For a correct interpretation of the role of autophagy in CM, autophagic flux in combination with gene and protein expression data have to be studied in the future.

Environmental stressors influencing the proteostasis network

Besides the above mentioned effects of the sarcomeric gene mutations on the PQC, other environmental stressors, including physiological stress, genetic and epigenetic pathways and inflammation, can also impair its function [82, 120]. In CM patients with a sarcomeric mutation, these stressors can act as second hit and thereby determine disease severity. Since most of CM patients become symptomatic only in a later stage of their life, the influence of drugs directed at the PQC system as treatment modality for co-morbidities and the age-related decline of the PQC are discussed below.

Several anti-cancer agents block the PQC to cause a lethal proteotoxicity in cancer cells. Anthracyclines, for example, directly impair its function by enhancing proteasomal degradation due to increased expression of E3 ligases and increased

proteasome activity as well as inhibition of autophagy in cardiomyocytes [2, 27, 51, 63]. Furthermore, they disturb Ca^{2+} homeostasis, leading to endoplasmic reticulum stress, which derails protein folding [27]. In CM patients, dealing already with a sarcomeric mutation, treatment of another non-cardiac disease can trigger the onset of CM or worsen the clinical outcome. Cardiotoxic side effects of anthracyclines can lead to anthracycline-associated cardiomyopathy (AACM) which presents as LV dysfunction and DCM in adults and RCM in children [53, 61]. Treatment with a low dose of anti-cancer agents induced CM in cancer patients without a history of cardiac disease. Genetic screening of these patients revealed truncating titin variants which are known as a genetic cause of DCM. These variants may increase the susceptibility for anti-cancer agents-induced CM [52]. In general, patients having a genetic predisposition for DCM are more prone to develop AACM after anthracycline treatment [100, 107]. It can be speculated that the impairment of the PQC due to the anti-cancer treatment is an additional burden to the cardiomyocyte. The clinical cardiac phenotype is caused by insufficient clearance of the mutant protein via UPS and/or autophagy. Therefore, these findings suggest that PQC impairment by anthracyclines can act as catalysts in the development of CM in patients with underlying sarcomeric gene mutation.

Ageing represents another cellular stressor leading to toxic mutation effects because of the late disease onset and development of symptoms in inherited CMs. Clinical characteristics, such as wall thickness and diastolic function, worsen with increasing age [57]. This could be related to an age-associated decline in proteostatic function, which is supported by the presence of damaged macromolecules and mitochondria in aged cardiomyocytes [98]. Dysfunctional mitochondria generate high levels of reactive oxygen species, which promote proteotoxic stress and accelerate detrimental effects on the cardiomyocyte [90]. Also, the activity of the 26S proteasome is decreased during ageing which is possibly caused by oxidation of its components [21, 29, 30, 42]. The age-dependent decline in proteasome function increases the burden for the autophagic pathway. However, not only the proteasome, but also the autophagy-lysosomal system declines during ageing [81]. As an example, mTOR, a negative regulator of autophagy, was upregulated during ageing in a mouse study which indicates decreased autophagic activity [4]. As a result, the activity of the autophagic response might not be sufficient. However, similar to findings related to the UPS, autophagy was enhanced during ageing in some animal models, suggesting an increased need for autophagy in aged cells [113]. Further research is warranted to investigate whether the age-related decline of the PQC is causative for CM onset and/or progression.

FUTURE THERAPEUTIC IMPLICATIONS

To improve the clinical outcome of CM patients, modulation of PQC components might serve as a novel therapeutic strategy. Figure 3 summarizes the three different ways and illustrates how a sarcomeric gene mutation can lead to PQC derailment. In case of a direct mutation effect on the PQC as well as in combination with secondary hits, targeting of the PQC would be most beneficial and the most direct way to prevent cardiomyocyte dysfunction. In case where the PQC derailment is a consequence of mutation-induced cellular disturbances, it is important to also target the cellular dysfunction to prevent further worsening of the PQC.

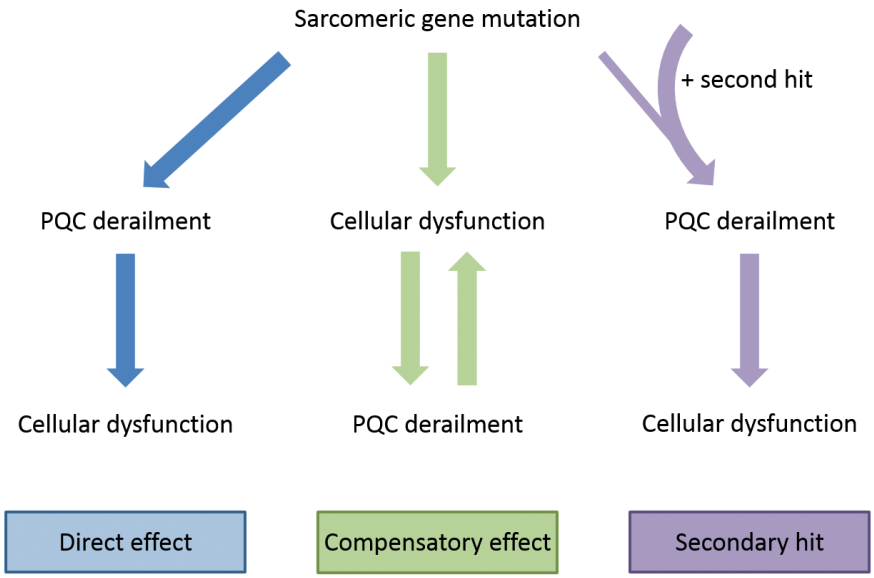

FIGURE 3. Effects of sarcomeric gene mutations on the protein quality control (PQC) system. Sarcomeric gene mutations can directly derail PQC function leading to cardiomyocyte dysfunction. PQC derailments in cardiomyopathies (CMs) can also be a compensatory mechanism to counteract cardiomyocyte dysfunction caused by the sarcomeric gene mutation. The secondary-hit hypothesis suggests that the PQC of cardiomyocytes carrying a sarcomeric gene mutation is more prone to derail in response to additional cellular stressors, thereby resulting in cardiomyocyte dysfunction.

As extensively discussed in this review, PQC alterations in CMs are disease- and mutation-specific leading to either increased or reduced function in one or several of its components. Therefore, personalized treatment strategies are required to restore a balanced proteostasis. Potentially, all three PQC components can be therapeutically targeted with the appropriate compounds.

HSP expression can be induced by the drug geranylgeranylacetone. In animal models of desmin-related CM, the induction of HSP expression by geranylgeranylacetone resulted in a beneficial effect on heart function because desmin-aggregate formation was reduced [83]. This example suggests that activation of HSPs might also be beneficial in other types of inherited CMs since HSPs play a crucial role in coping with the mutant protein.

The derailment of the UPS is context dependent: proteasomal function is decreased in HCM, RCM and desmin-related CM and increased in DCM [9]. Decreased proteasomal function suggest that the misfolded proteins hamper the UPS by overwhelming it due to permanent degradation of misfolded proteins. As a consequence, the activity of the UPS is reduced. Therefore, UPS activation might be a beneficial therapeutic strategy in HCM and desmin-related CM [9]. In line with this, in HCM patients with a *TNNT2* mutation increased proteasomal activity was correlated with a better clinical outcome [30]. In contrast, over-activation of the UPS indicates a direct response of the UPS to the misfolded proteins to ensure optimal clearance. However, excessive activation of the UPS transforms the initially beneficial effects into a detrimental maladaptation that possibly contribute to loss of myofibrils [9]. Nevertheless, complete proteasome inhibition itself triggered cardiac dysfunction and a CM-like phenotype in healthy pigs [38]. Therefore, it is important to achieve a moderate UPS response in DCM to prevent the detrimental effects of complete proteasome inhibition.

The altered autophagic flux in CMs can be caused on the one hand directly by the misfolded protein itself or on the other hand indirectly by compensating for the impaired functionality of the UPS. To optimize the degradation response, the autophagic activity needs to be pharmacologically titrated into its proteostasis promoting range [114].

CONCLUSION

The PQC is crucial for cardiac health and requires the collaboration of all its components to be functional. Key modulators of the PQC are disease- and mutation-specifically altered and derailed in CM. Pharmacological targeting of PQC components represents a novel therapeutic strategy to treat CMs. Since most of the described findings are retrieved from single CM patients or experimental animal models, systematic studies in larger CM patient populations are warranted to untie the knot of disease- and mutation-specific derailments of the PQC.

CONFLICT OF INTEREST

The authors declare that they have no conflict of interest.

ACKNOWLEDGEMENTS

We acknowledge support from the Netherlands Cardiovascular Research Initiative — an initiative with support of the Dutch Heart Foundation, CVON: The Netherlands CardioVascular Research Committee, CVON2014-40 DOSIS. Furthermore, this research has been supported by LSH-TKI (40-43100-98-008), the Dutch Heart Foundation (2013T096, 2013T144) and the Netherlands Organisation for Scientific Research (NWO), as part of their joint strategic research programme: 'Earlier recognition of cardiovascular diseases' (AFFIP: 14728). Van der Velden is supported by a VICI grant from the Netherlands Organization for Scientific Research (NWO-ZonMW; 91818602).

REFERENCES

1. Amm I, Sommer T, Wolf DH (2014) Protein quality control and elimination of protein waste: the role of the ubiquitin-proteasome system. Biochim Biophys Acta 1843:182-196. https://doi.org/10.1016/j.bbamcr.2013.06.031
2. Arai M, Yoguchi A, Takizawa T et al. (2000) Mechanism of doxorubicin-induced inhibition of sarcoplasmic reticulum Ca(2+)-ATPase gene transcription. Circ Res 86:8-14.
3. Arbustini E, Narula N, Dec GW et al. (2013) The MOGE(S) classification for a phenotype-genotype nomenclature of cardiomyopathy: endorsed by the World Heart Federation. J Am Coll Cardiol 62:2046-2072. https://doi.org/10.1016/j.jacc.2013.08.1644
4. Baar EL, Carbajal KA, Ong IM et al. (2016) Sex- and tissue-specific changes in mTOR signaling with age in C57BL/6J mice. Aging Cell 15:155-166. https://doi.org/10.1111/acel.12425
5. Baba M, Takeshige K, Baba N et al. (1994) Ultrastructural analysis of the autophagic process in yeast: detection of autophagosomes and their characterization. J Cell Biol 124:903-913.
6. Bahrudin U, Morisaki H, Morisaki T et al. (2008) Ubiquitin-proteasome system impairment caused by a missense cardiac myosin-binding protein C mutation and associated with cardiac dysfunction in hypertrophic cardiomyopathy. J Mol Biol 384:896-907. https://doi.org/10.1016/j.jmb.2008.09.070
7. Barral JM, Epstein HF (1999) Protein machines and self assembly in muscle organization. Bioessays 21:813-823. https://doi.org/10.1002/(SICI)1521-1878(199910)21:10<813::AID-BIES3>3.0.CO;2-0
8. Barral JM, Hutagalung AH, Brinker A et al. (2002) Role of the myosin assembly protein UNC-45 as a molecular chaperone for myosin. Science 295:669-671. https://doi.org/10.1126/science.1066648
9. Baumgarten A, Bang C, Tschirner A et al. (2013) TWIST1 regulates the activity of ubiquitin proteasome system via the miR-199/214 cluster in human end-stage dilated cardiomyopathy. Int J Cardiol 168:1447-1452. https://doi.org/10.1016/j.ijcard.2012.12.094
10. Bennardini F, Wrzosek A, Chiesi M (1992) Alpha B-crystallin in cardiac tissue. Association with actin and desmin filaments. Circ Res 71:288-294.
11. Birks EJ, Latif N, Enesa K et al. (2008) Elevated p53 expression is associated with dysregulation of the ubiquitin-proteasome system in dilated cardiomyopathy. Cardiovasc Res 79:472-480. https://doi.org/10.1093/cvr/cvn083
12. Boateng SY, Goldspink PH (2008) Assembly and maintenance of the sarcomere night and day. Cardiovasc Res 77:667-675. https://doi.org/10.1093/cvr/cvm048
13. Bozaykut P, Ozer NK, Karademir B (2014) Regulation of protein turnover by heat shock proteins. Free Radic Biol Med 77:195-209. https://doi.org/10.1016/j.freeradbiomed.2014.08.012
14. Brown DD, Christine KS, Showell C et al. (2007) Small heat shock protein Hsp27 is required for proper heart tube formation. Genesis 45:667-678. https://doi.org/10.1002/dvg.20340
15. Brundel BJ, Shiroshita-Takeshita A, Qi X et al. (2006) Induction of heat shock response protects the heart against atrial fibrillation. Circ Res 99:1394-1402. https://doi.org/10.1161/01.RES.0000252323.83137.fe
16. Bryantsev AL, Loktionova SA, Ilyinskaya OP et al. (2002) Distribution, phosphorylation, and activities of Hsp25 in heat-stressed H9c2 myoblasts: a functional link to cytoprotection. Cell Stress Chaperones 7:146-155.

17. Cecconi F, Levine B (2008) The role of autophagy in mammalian development: cell makeover rather than cell death. Dev Cell 15:344-357. https://doi.org/10.1016/j.devcel.2008.08.012
18. Chen SN, Czernuszewicz G, Tan Y et al. (2012) Human molecular genetic and functional studies identify TRIM63, encoding Muscle RING Finger Protein 1, as a novel gene for human hypertrophic cardiomyopathy. Circ Res 111:907-919. https://doi.org/10.1161/CIRCRESAHA.112.270207
19. Chen XM, Feng MJ, Shen CJ et al. (2017) A novel approach to select differential pathways associated with hypertrophic cardiomyopathy based on gene coexpression analysis. Mol Med Rep 16:773-777. https://doi.org/10.3892/mmr.2017.6667
20. Cui Z, Venkatraman G, Hwang SM et al. (2013b) Effect of the Troponin I Restrictive Cardiomyopathy Mutation R145W on Protein Expression in Murine Hearts. Biophys J 104:312a.
21. Day SM, Divald A, Wang P et al. (2013) Impaired assembly and post-translational regulation of 26S proteasome in human end-stage heart failure. Circ Heart Fail 6:544-549. https://doi.org/10.1161/CIRCHEARTFAILURE.112.000119
22. Decker RS, Wildenthal K (1980) Lysosomal alterations in hypoxic and reoxygenated hearts. I. Ultrastructural and cytochemical changes. Am J Pathol 98:425-444.
23. Ehrnsperger M, Lilie H, Gaestel M et al. (1999) The dynamics of Hsp25 quaternary structure. Structure and function of different oligomeric species. J Biol Chem 274:14867-14874.
24. Elliott P, Andersson B, Arbustini E et al. (2008) Classification of the cardiomyopathies: a position statement from the European Society Of Cardiology Working Group on Myocardial and Pericardial Diseases. Eur Heart J 29:270-276. https://doi.org/10.1093/eurheartj/ehm342
25. Esser C, Alberti S, Hohfeld J (2004) Cooperation of molecular chaperones with the ubiquitin/proteasome system. Biochim Biophys Acta 1695:171-188. https://doi.org/10.1016/j.bbamcr.2004.09.020
26. Finley D (2009) Recognition and processing of ubiquitin-protein conjugates by the proteasome. Annu Rev Biochem 78:477-513. https://doi.org/10.1146/annurev.biochem.78.081507.101607
27. Fu HY, Sanada S, Matsuzaki T et al. (2016) Chemical Endoplasmic Reticulum Chaperone Alleviates Doxorubicin-Induced Cardiac Dysfunction. Circ Res 118:798-809. https://doi.org/10.1161/CIRCRESAHA.115.307604
28. Garrido C, Paul C, Seigneuric R et al. (2012) The small heat shock proteins family: the long forgotten chaperones. Int J Biochem Cell Biol 44:1588-1592. https://doi.org/10.1016/j.biocel.2012.02.022
29. Gilda JE, Gomes AV (2017) Proteasome dysfunction in cardiomyopathies. J Physiol 595:4051-4071. https://doi.org/10.1113/JP273607
30. Gilda JE, Lai X, Witzmann FA et al. (2016) Delineation of Molecular Pathways Involved in Cardiomyopathies Caused by Troponin T Mutations. Mol Cell Proteomics 15:1962-1981. https://doi.org/10.1074/mcp.M115.057380
31. Girolami F, Iascone M, Tomberli B et al. (2014) Novel alpha-actinin 2 variant associated with familial hypertrophic cardiomyopathy and juvenile atrial arrhythmias: a massively parallel sequencing study. Circ Cardiovasc Genet 7:741-750. https://doi.org/10.1161/CIRCGENETICS.113.000486

32. Glazier AA, Hafeez N, Mellacheruvu D et al. (2018) HSC70 is a chaperone for wild-type and mutant cardiac myosin binding protein C. JCI Insight 3. https://doi.org/10.1172/jci.insight.99319
33. Golenhofen N, Perng MD, Quinlan RA et al. (2004) Comparison of the small heat shock proteins alphaB-crystallin, MKBP, HSP25, HSP20, and cvHSP in heart and skeletal muscle. Histochem Cell Biol 122:415-425. https://doi.org/10.1007/s00418-004-0711-z
34. Grantham J, Ruddock LW, Roobol A et al. (2002) Eukaryotic chaperonin containing T-complex polypeptide 1 interacts with filamentous actin and reduces the initial rate of actin polymerization in vitro. Cell Stress Chaperones 7:235-242.
35. Gustafsson AB, Gottlieb RA (2008) Recycle or die: the role of autophagy in cardioprotection. J Mol Cell Cardiol 44:654-661. https://doi.org/10.1016/j.yjmcc.2008.01.010
36. Hansen WJ, Cowan NJ, Welch WJ (1999) Prefoldin-nascent chain complexes in the folding of cytoskeletal proteins. J Cell Biol 145:265-277.
37. Henning RH, Brundel B (2017) Proteostasis in cardiac health and disease. Nat Rev Cardiol 14:637-653. https://doi.org/10.1038/nrcardio.2017.89
38. Herrmann J, Wohlert C, Saguner AM et al. (2013) Primary proteasome inhibition results in cardiac dysfunction. Eur J Heart Fail 15:614-623. https://doi.org/10.1093/eurjhf/hft034
39. Hershko A, Ciechanover A (1998) The ubiquitin system. Annu Rev Biochem 67:425-479. https://doi.org/10.1146/annurev.biochem.67.1.425
40. Hoorntje ET, Bollen IA, Barge-Schaapveld DQ et al. (2017) Lamin A/C-Related Cardiac Disease: Late Onset With a Variable and Mild Phenotype in a Large Cohort of Patients With the Lamin A/C p.(Arg331Gln) Founder Mutation. Circ Cardiovasc Genet 10. https://doi.org/10.1161/CIRCGENETICS.116.001631
41. Ivandic BT, Mastitsky SE, Schonsiegel F et al. (2012) Whole-genome analysis of gene expression associates the ubiquitin-proteasome system with the cardiomyopathy phenotype in disease-sensitized congenic mouse strains. Cardiovasc Res 94:87-95. https://doi.org/10.1093/cvr/cvs080
42. Jana NR (2012) Protein homeostasis and aging: role of ubiquitin protein ligases. Neurochem Int 60:443-447. https://doi.org/10.1016/j.neuint.2012.02.009
43. Kaski JP, Burch M, Elliott PM (2007) Mutations in the cardiac Troponin C gene are a cause of idiopathic dilated cardiomyopathy in childhood. Cardiol Young 17:675-677. https://doi.org/10.1017/S1047951107001291
44. Kimura H, Eguchi S, Sasaki J et al. (2017) Vps34 regulates myofibril proteostasis to prevent hypertrophic cardiomyopathy. JCI Insight 2:e89462. https://doi.org/10.1172/jci.insight.89462
45. Kirkin V, Mcewan DG, Novak I et al. (2009) A role for ubiquitin in selective autophagy. Mol Cell 34:259-269. https://doi.org/10.1016/j.molcel.2009.04.026
46. Klionsky DJ (2007) Autophagy: from phenomenology to molecular understanding in less than a decade. Nat Rev Mol Cell Biol 8:931-937. https://doi.org/10.1038/nrm2245
47. Kostin S, Pool L, Elsasser A et al. (2003) Myocytes die by multiple mechanisms in failing human hearts. Circ Res 92:715-724. https://doi.org/10.1161/01.RES.0000067471.95890.5C
48. Landry J, Huot J (1995) Modulation of actin dynamics during stress and physiological stimulation by a signaling pathway involving p38 MAP kinase and heat-shock protein 27. Biochem Cell Biol 73:703-707.
49. Lavoie JN, Lambert H, Hickey E et al. (1995) Modulation of cellular thermoresistance and actin filament stability accompanies phosphorylation-induced changes in the oligomeric structure of heat shock protein 27. Mol Cell Biol 15:505-516.

50. Levine B, Kroemer G (2008) Autophagy in the pathogenesis of disease. Cell 132:27-42. https://doi.org/10.1016/j.cell.2007.12.018
51. Ling YH, Priebe W, Perez-Soler R (1993) Apoptosis induced by anthracycline antibiotics in P388 parent and multidrug-resistant cells. Cancer Res 53:1845-1852.
52. Linschoten M, Teske AJ, Baas AF et al. (2017) Truncating Titin (TTN) Variants in Chemotherapy-Induced Cardiomyopathy. J Card Fail 23:476-479. https://doi.org/10.1016/j.cardfail.2017.03.003
53. Lipshultz SE, Lipsitz SR, Sallan SE et al. (2005) Chronic progressive cardiac dysfunction years after doxorubicin therapy for childhood acute lymphoblastic leukemia. J Clin Oncol 23:2629-2636. https://doi.org/10.1200/JCO.2005.12.121
54. Liu J, Tang M, Mestril R et al. (2006) Aberrant protein aggregation is essential for a mutant desmin to impair the proteolytic function of the ubiquitin-proteasome system in cardiomyocytes. J Mol Cell Cardiol 40:451-454. https://doi.org/10.1016/j.yjmcc.2005.12.011
55. Lu L, Wu W, Yan J et al. (2009) Adriamycin-induced autophagic cardiomyocyte death plays a pathogenic role in a rat model of heart failure. Int J Cardiol 134:82-90. https://doi.org/10.1016/j.ijcard.2008.01.043
56. Lum JJ, Bauer DE, Kong M et al. (2005) Growth factor regulation of autophagy and cell survival in the absence of apoptosis. Cell 120:237-248. https://doi.org/10.1016/j.cell.2004.11.046
57. Luo HC, Pozios I, Vakrou S et al. (2014) Age-related changes in familial hypertrophic cardiomyopathy phenotype in transgenic mice and humans. J Huazhong Univ Sci Technolog Med Sci 34:634-639. https://doi.org/10.1007/s11596-014-1329-6
58. Matsui Y, Takagi H, Qu X et al. (2007) Distinct roles of autophagy in the heart during ischemia and reperfusion: roles of AMP-activated protein kinase and Beclin 1 in mediating autophagy. Circ Res 100:914-922. https://doi.org/10.1161/01.RES.0000261924.76669.36
59. Mcelhinny AS, Perry CN, Witt CC et al. (2004) Muscle-specific RING finger-2 (MURF-2) is important for microtubule, intermediate filament and sarcomeric M-line maintenance in striated muscle development. J Cell Sci 117:3175-3188. https://doi.org/10.1242/jcs.01158
60. Meijering RA, Zhang D, Hoogstra-Berends F et al. (2012) Loss of proteostatic control as a substrate for atrial fibrillation: a novel target for upstream therapy by heat shock proteins. Front Physiol 3:36. https://doi.org/10.3389/fphys.2012.00036
61. Meinardi MT, Van Der Graaf WT, Van Veldhuisen DJ et al. (1999) Detection of anthracycline-induced cardiotoxicity. Cancer Treat Rev 25:237-247. https://doi.org/10.1053/ctrv.1999.0128
62. Min TJ, Jo WM, Shin SY et al. (2015) The protective effect of heat shock protein 70 (Hsp70) in atrial fibrillation in various cardiomyopathy conditions. Heart Vessels 30:379-385. https://doi.org/10.1007/s00380-014-0521-8
63. Minotti G, Licata S, Saponiero A et al. (2000) Anthracycline metabolism and toxicity in human myocardium: comparisons between doxorubicin, epirubicin, and a novel disaccharide analogue with a reduced level of formation and [4Fe-4S] reactivity of its secondary alcohol metabolite. Chem Res Toxicol 13:1336-1341.
64. Miyamoto CA, Fischman DA, Reinach FC (1999) The interface between MyBP-C and myosin: site-directed mutagenesis of the CX myosin-binding domain of MyBP-C. J Muscle Res Cell Motil 20:703-715.
65. Mizushima N, Yamamoto A, Matsui M et al. (2004) In vivo analysis of autophagy in response to nutrient starvation using transgenic mice expressing a fluorescent autophagosome marker. Mol Biol Cell 15:1101-1111. https://doi.org/10.1091/mbc.E03-09-0704

66. Morimoto RI (2008) Proteotoxic stress and inducible chaperone networks in neurodegenerative disease and aging. Genes Dev 22:1427-1438. https://doi.org/10.1101/gad.1657108
67. Mundia MM, Demers RW, Chow ML et al. (2012) Subdomain location of mutations in cardiac actin correlate with type of functional change. PLoS One 7:e36821. https://doi.org/10.1371/journal.pone.0036821
68. Muthuchamy M, Pieples K, Rethinasamy P et al. (1999) Mouse model of a familial hypertrophic cardiomyopathy mutation in alpha-tropomyosin manifests cardiac dysfunction. Circ Res 85:47-56.
69. Niizeki T, Takeishi Y, Watanabe T et al. (2008) Relation of serum heat shock protein 60 level to severity and prognosis in chronic heart failure secondary to ischemic or idiopathic dilated cardiomyopathy. Am J Cardiol 102:606-610. https://doi.org/10.1016/j.amjcard.2008.04.030
70. Nijenkamp L, Bollen IaE, Van Velzen HG et al. (2018) Sex Differences at the Time of Myectomy in Hypertrophic Cardiomyopathy. Circ Heart Fail 11:e004133. https://doi.org/10.1161/CIRCHEARTFAILURE.117.004133
71. Nowis D, Maczewski M, Mackiewicz U et al. (2010) Cardiotoxicity of the anticancer therapeutic agent bortezomib. Am J Pathol 176:2658-2668. https://doi.org/10.2353/ajpath.2010.090690
72. Otsuka K, Terasaki F, Shimomura H et al. (2010) Enhanced expression of the ubiquitin-proteasome system in the myocardium from patients with dilated cardiomyopathy referred for left ventriculoplasty: an immunohistochemical study with special reference to oxidative stress. Heart Vessels 25:474-484. https://doi.org/10.1007/s00380-010-0006-3
73. Patterson C, Ike C, Willis PWT et al. (2007) The bitter end: the ubiquitin-proteasome system and cardiac dysfunction. Circulation 115:1456-1463. https://doi.org/10.1161/CIRCULATIONAHA.106.649863
74. Peddy SB, Vricella LA, Crosson JE et al. (2006) Infantile restrictive cardiomyopathy resulting from a mutation in the cardiac troponin T gene. Pediatrics 117:1830-1833. https://doi.org/10.1542/peds.2005-2301
75. Perrot A, Tomasov P, Villard E et al. (2016) Mutations in NEBL encoding the cardiac Z-disk protein nebulette are associated with various cardiomyopathies. Arch Med Sci 12:263-278. https://doi.org/10.5114/aoms.2016.59250
76. Ploski R, Rydzanicz M, Ksiazczyk TM et al. (2016) Evidence for troponin C (TNNC1) as a gene for autosomal recessive restrictive cardiomyopathy with fatal outcome in infancy. Am J Med Genet A 170:3241-3248. https://doi.org/10.1002/ajmg.a.37860
77. Predmore JM, Wang P, Davis F et al. (2010) Ubiquitin proteasome dysfunction in human hypertrophic and dilated cardiomyopathies. Circulation 121:997-1004. https://doi.org/10.1161/CIRCULATIONAHA.109.904557
78. Purevjav E, Varela J, Morgado M et al. (2010) Nebulette mutations are associated with dilated cardiomyopathy and endocardial fibroelastosis. J Am Coll Cardiol 56:1493-1502. https://doi.org/10.1016/j.jacc.2010.05.045
79. Rajan S, Ahmed RP, Jagatheesan G et al. (2007) Dilated cardiomyopathy mutant tropomyosin mice develop cardiac dysfunction with significantly decreased fractional shortening and myofilament calcium sensitivity. Circ Res 101:205-214. https://doi.org/10.1161/CIRCRESAHA.107.148379
80. Ravid T, Hochstrasser M (2008) Diversity of degradation signals in the ubiquitin-proteasome system. Nat Rev Mol Cell Biol 9:679-690. https://doi.org/10.1038/nrm2468

81. Rubinsztein DC, Marino G, Kroemer G (2011) Autophagy and aging. Cell 146:682-695. https://doi.org/10.1016/j.cell.2011.07.030
82. Sadoul K, Boyault C, Pabion M et al. (2008) Regulation of protein turnover by acetyltransferases and deacetylases. Biochimie 90:306-312. https://doi.org/10.1016/j.biochi.2007.06.009
83. Sanbe A, Daicho T, Mizutani R et al. (2009) Protective effect of geranylgeranylacetone via enhancement of HSPB8 induction in desmin-related cardiomyopathy. PLoS One 4:e5351. https://doi.org/10.1371/journal.pone.0005351
84. Sarikas A, Carrier L, Schenke C et al. (2005) Impairment of the ubiquitin-proteasome system by truncated cardiac myosin binding protein C mutants. Cardiovasc Res 66:33-44. https://doi.org/10.1016/j.cardiores.2005.01.004
85. Schlossarek S, Englmann DR, Sultan KR et al. (2012) Defective proteolytic systems in Mybpc3-targeted mice with cardiac hypertrophy. Basic Res Cardiol 107:235. https://doi.org/10.1007/s00395-011-0235-3
86. Scott RC, Schuldiner O, Neufeld TP (2004) Role and regulation of starvation-induced autophagy in the Drosophila fat body. Dev Cell 7:167-178. https://doi.org/10.1016/j.devcel.2004.07.009
87. Selcen D, Muntoni F, Burton BK et al. (2009) Mutation in BAG3 causes severe dominant childhood muscular dystrophy. Ann Neurol 65:83-89. https://doi.org/10.1002/ana.21553
88. Semsarian C, Ingles J, Wilde AA (2015) Sudden cardiac death in the young: the molecular autopsy and a practical approach to surviving relatives. Eur Heart J 36:1290-1296. https://doi.org/10.1093/eurheartj/ehv063
89. Shimomura H, Terasaki F, Hayashi T et al. (2001) Autophagic degeneration as a possible mechanism of myocardial cell death in dilated cardiomyopathy. Jpn Circ J 65:965-968.
90. Simonsen A, Cumming RC, Brech A et al. (2008) Promoting basal levels of autophagy in the nervous system enhances longevity and oxidant resistance in adult Drosophila. Autophagy 4:176-184.
91. Solomon V, Goldberg AL (1996) Importance of the ATP-ubiquitin-proteasome pathway in the degradation of soluble and myofibrillar proteins in rabbit muscle extracts. J Biol Chem 271:26690-26697.
92. Song L, Su M, Wang S et al. (2014) MiR-451 is decreased in hypertrophic cardiomyopathy and regulates autophagy by targeting TSC1. J Cell Mol Med 18:2266-2274. https://doi.org/10.1111/jcmm.12380
93. Spencer JA, Eliazer S, Ilaria RL, Jr. et al. (2000) Regulation of microtubule dynamics and myogenic differentiation by MURF, a striated muscle RING-finger protein. J Cell Biol 150:771-784.
94. Srikakulam R, Winkelmann DA (2004) Chaperone-mediated folding and assembly of myosin in striated muscle. J Cell Sci 117:641-652. https://doi.org/10.1242/jcs.00899
95. Su M, Wang J, Kang L et al. (2014) Rare variants in genes encoding MuRF1 and MuRF2 are modifiers of hypertrophic cardiomyopathy. Int J Mol Sci 15:9302-9313. https://doi.org/10.3390/ijms15069302
96. Tannous P, Zhu H, Nemchenko A et al. (2008) Intracellular protein aggregation is a proximal trigger of cardiomyocyte autophagy. Circulation 117:3070-3078. https://doi.org/10.1161/CIRCULATIONAHA.107.763870

97. Tardiff JC, Factor SM, Tompkins BD et al. (1998) A truncated cardiac troponin T molecule in transgenic mice suggests multiple cellular mechanisms for familial hypertrophic cardiomyopathy. J Clin Invest 101:2800-2811. https://doi.org/10.1172/JCI2389
98. Terman A, Dalen H, Eaton JW et al. (2003) Mitochondrial recycling and aging of cardiac myocytes: the role of autophagocytosis. Exp Gerontol 38:863-876.
99. Thottakara T, Friedrich FW, Reischmann S et al. (2015) The E3 ubiquitin ligase Asb2beta is downregulated in a mouse model of hypertrophic cardiomyopathy and targets desmin for proteasomal degradation. J Mol Cell Cardiol 87:214-224. https://doi.org/10.1016/j.yjmcc.2015.08.020
100. Van Den Berg MP, Van Spaendonck-Zwarts KY, Van Veldhuisen DJ et al. (2010) Familial dilated cardiomyopathy: another risk factor for anthracycline-induced cardiotoxicity? Eur J Heart Fail 12:1297-1299. https://doi.org/10.1093/eurjhf/hfq175
101. Van Dijk SJ, Dooijes D, Dos Remedios C et al. (2009) Cardiac myosin-binding protein C mutations and hypertrophic cardiomyopathy: haploinsufficiency, deranged phosphorylation, and cardiomyocyte dysfunction. Circulation 119:1473-1483. https://doi.org/10.1161/CIRCULATIONAHA.108.838672
102. Vang S, Corydon TJ, Borglum AD et al. (2005) Actin mutations in hypertrophic and dilated cardiomyopathy cause inefficient protein folding and perturbed filament formation. FEBS J 272:2037-2049. https://doi.org/10.1111/j.1742-4658.2005.04630.x
103. Vos MJ, Kanon B, Kampinga HH (2009) HSPB7 is a SC35 speckle resident small heat shock protein. Biochim Biophys Acta 1793:1343-1353. https://doi.org/10.1016/j.bbamcr.2009.05.005
104. Wang J, Maldonado MA (2006) The ubiquitin-proteasome system and its role in inflammatory and autoimmune diseases. Cell Mol Immunol 3:255-261.
105. Wang X, Osinska H, Klevitsky R et al. (2001) Expression of R120G-alphaB-crystallin causes aberrant desmin and alphaB-crystallin aggregation and cardiomyopathy in mice. Circ Res 89:84-91.
106. Wang X, Su H, Ranek MJ (2008) Protein quality control and degradation in cardiomyocytes. J Mol Cell Cardiol 45:11-27. https://doi.org/10.1016/j.yjmcc.2008.03.025
107. Wasielewski M, Van Spaendonck-Zwarts KY, Westerink ND et al. (2014) Potential genetic predisposition for anthracycline-associated cardiomyopathy in families with dilated cardiomyopathy. Open Heart 1:e000116. https://doi.org/10.1136/openhrt-2014-000116
108. Weekes J, Morrison K, Mullen A et al. (2003) Hyperubiquitination of proteins in dilated cardiomyopathy. Proteomics 3:208-216. https://doi.org/10.1002/pmic.200390029
109. Wessels MW, Herkert JC, Frohn-Mulder IM et al. (2015) Compound heterozygous or homozygous truncating MYBPC3 mutations cause lethal cardiomyopathy with features of noncompaction and septal defects. Eur J Hum Genet 23:922-928. https://doi.org/10.1038/ejhg.2014.211
110. Wijnker PJ, Friedrich FW, Dutsch A et al. (2016) Comparison of the effects of a truncating and a missense MYBPC3 mutation on contractile parameters of engineered heart tissue. J Mol Cell Cardiol 97:82-92. https://doi.org/10.1016/j.yjmcc.2016.03.003
111. Willis MS, Patterson C (2010) Hold me tight: Role of the heat shock protein family of chaperones in cardiac disease. Circulation 122:1740-1751. https://doi.org/10.1161/CIRCULATIONAHA.110.942250
112. Willis MS, Schisler JC, Portbury AL et al. (2009) Build it up-Tear it down: protein quality control in the cardiac sarcomere. Cardiovasc Res 81:439-448. https://doi.org/10.1093/cvr/cvn289

113. Wohlgemuth SE, Julian D, Akin DE et al. (2007) Autophagy in the heart and liver during normal aging and calorie restriction. Rejuvenation Res 10:281-292. https://doi.org/10.1089/rej.2006.0535
114. Xie M, Morales CR, Lavandero S et al. (2011) Tuning flux: autophagy as a target of heart disease therapy. Curr Opin Cardiol 26:216-222. https://doi.org/10.1097/HCO.0b013e328345980a
115. Yan L, Vatner DE, Kim SJ et al. (2005) Autophagy in chronically ischemic myocardium. Proc Natl Acad Sci U S A 102:13807-13812. https://doi.org/10.1073/pnas.0506843102
116. Yang Q, Osinska H, Klevitsky R et al. (2001) Phenotypic deficits in mice expressing a myosin binding protein C lacking the titin and myosin binding domains. J Mol Cell Cardiol 33:1649-1658. https://doi.org/10.1006/jmcc.2001.1417
117. Yang SW, Hitz MP, Andelfinger G (2010) Ventricular septal defect and restrictive cardiomyopathy in a paediatric TNNI3 mutation carrier. Cardiol Young 20:574-576. https://doi.org/10.1017/S1047951110000715
118. Yorimitsu T, Klionsky DJ (2005) Autophagy: molecular machinery for self-eating. Cell Death Differ 12 Suppl 2:1542-1552. https://doi.org/10.1038/sj.cdd.4401765
119. Yuan CC, Kazmierczak K, Liang J et al. (2017) Hypercontractile mutant of ventricular myosin essential light chain leads to disruption of sarcomeric structure and function and results in restrictive cardiomyopathy in mice. Cardiovasc Res 113:1124-1136. https://doi.org/10.1093/cvr/cvx060
120. Zhang K, Kaufman RJ (2008) From endoplasmic-reticulum stress to the inflammatory response. Nature 454:455-462. https://doi.org/10.1038/nature07203

PROTEIN QUALITY CONTROL ACTIVATION AND MICROTUBULE REMODELING IN HYPERTROPHIC CARDIOMYOPATHY

Larissa M. Dorsch, **Maike Schuldt**, Cristobal G. dos Remedios, Arend F.L. Schinkel, Peter L. de Jong, Michelle Michels, Diederik W.D. Kuster, Bianca J.J.M. Brundel and Jolanda van der Velden

Cells, 2019. 8(7).

4

ABSTRACT

Hypertrophic cardiomyopathy (HCM) is the most common inherited cardiac disorder. It is mainly caused by mutations in genes encoding sarcomere proteins. Mutant forms of these highly abundant proteins likely stress the protein quality control (PQC) system of cardiomyocytes. The PQC system, together with a functional microtubule network, maintains proteostasis. We compared left ventricular (LV) tissue of nine donors (controls) with 38 sarcomere mutation-positive (HCMSMP) and 14 sarcomere mutation-negative (HCMSMN) patients to define HCM and mutation-specific changes in PQC. Mutations in HCMSMP result in poison polypeptides or reduced protein levels (haploinsufficiency, HI). The main findings were 1) several key PQC players were more abundant in HCM compared to controls, 2) after correction for sex and age, stabilizing heat shock protein (HSP)B1, and refolding, HSPD1 and HSPA2 were increased in HCMSMP compared to controls, 3) α-tubulin and acetylated α-tubulin levels were higher in HCM compared to controls, especially in HCMHI, 4) myosin-binding protein-C (cMyBP-C) levels were inversely correlated with α-tubulin, and 5) α-tubulin levels correlated with acetylated α-tubulin and HSPs. Overall, carrying a mutation affects PQC and α-tubulin acetylation. The haploinsufficiency of cMyBP-C may trigger HSPs and α-tubulin acetylation. Our study indicates that proliferation of the microtubular network may represent a novel pathomechanism in cMyBP-C haploinsufficiency-mediated HCM.

INTRODUCTION

Hypertrophic cardiomyopathy (HCM) is a common familial cardiac disease with an estimated prevalence of 1:200 [1]. It is characterized by an asymmetrically hypertrophied, non-dilated left ventricle and an impaired diastolic function [2]. More than 1500 pathogenic mutations that most frequently encode proteins in the sarcomere have been identified. Previous studies have shown that sarcomere mutations alter myofilament function (reviewed recently in [3]). However, while the same sarcomere mutation is present in members of one family, the age of onset and disease severity vary greatly between patients, spanning from asymptomatic mutation carriers to symptomatic patients with severe cardiac remodeling [4]. This large clinical heterogeneity implies that HCM pathophysiology is more complex than the functional defects triggered by the gene mutation. Furthermore, pathogenic mutations were only found in ~50% of all HCM patients [4]. Moreover, a recent large international clinical HCM study showed that patients with a mutation in a sarcomere gene had a 2-fold higher risk of adverse outcomes (e.g., heart failure and atrial fibrillation) compared to patients with no known mutations [5]. The exact mechanisms underlying the difference in disease severity between sarcomere mutation-positive (HCM_{SMP}) and mutation-negative (HCM_{SMN}) patients are currently unknown.

A mechanism implicated in HCM progression is perturbed protein quality control (PQC) [6,7]. Cardiomyocytes contain a multilayered PQC system for maintaining proper protein conformation and for reorganizing and removing misfolded or aggregated (mutant) proteins [8]. The PQC system comprises heat shock proteins (HSPs), the ubiquitin-proteasome system (UPS), and autophagy [9]. HSPs are involved at all stages of sustaining protein homeostasis: during protein biosynthesis and maturation, in chaperoning the folding, in protection from environmental stress, in rearrangements of cellular macromolecules during the functional cycles of assembly and disassembly, and finally, in targeting proteins for degradation [10]. Terminally misfolded and aggregation-prone proteins are cleared by the two degradation systems, UPS and autophagy [11]. Furthermore, pathways of PQC are strongly linked to cell architecture, such as the microtubules network [12]. As sarcomere proteins are the most abundant proteins in the heart, maintenance of sarcomere structure and functions depends on functioning PQC mechanisms.

Perturbations in PQC mechanisms may be aggravated by the presence of sarcomere gene mutations that may explain the difference in disease severity between HCM_{SMP} and HCM_{SMN} patient groups. Moreover, the proteotoxic burden on PQC may depend on the type of mutation: in HCM, gene mutations either result in a 'poison polypeptide' (an expressed protein containing a mutated sequence) or haploinsufficiency, where up-regulation of the wild-type protein levels failed to compensate for reduced total protein [13,14].

Here, we identified and quantified key PQC players, such as HSPs and degradation markers (ubiquitinated proteins, p62, LC3BII) and microtubule network markers (for example acetylation of α-tubulin) in a large set of myectomy samples from HCM_{SMP} and HCM_{SMN} patients to define if the presence of a sarcomere mutation differentially affects PQC. In addition, mutation-specific PQC changes were assessed by comparing HCM with missense mutations and *MYBPC3* (cardiac myosin-binding protein-C) mutations, which cause haploinsufficiency.

MATERIALS AND METHODS

Septal Myectomy

Cardiac tissue from the interventricular septum was obtained during myectomy surgery to relieve left ventricular (LV) outflow tract obstruction. Patients were selected for surgery at our HCM center on the basis of the following indications: (1) peak left ventricular outflow tract (LVOT) gradient ≥ 50 mmHg at rest or on provocation and (2) presence of unacceptable symptoms, despite maximally tolerated medications consisting of β-blocking agents and/or calcium channel blockers. The decision to perform surgery was made after the consensus of a heart team consisting of a cardiothoracic surgeon, an interventional cardiologist, and a cardiologist specialized in HCM care [15]. Hypertrophic obstructive cardiomyopathy was evident from the increased septal thickness with a mean (± SD) of 21 (± 6) mm and high LV outflow tract pressure gradient with a mean (± SD) of 66 (± 37) mmHg. Next-generation-sequencing was used to check 48 different HCM-associated genes for variants [16].

This study included 52 septal myectomy patients, as summarized in Table 1. A total of 38 HCM patients were tested positive for carrying a gene variant in one of the genes encoding for the sarcomeric protein. The ages of all 38 HCM_{SMP} patients ranged between 15 and 72, with a mean (± SD) of 49 (± 16) years, and 68% of these were males. Depending on the reported pathomechanism, this group was subdivided into haploinsufficiency (HI) and poison polypeptide (PP) subgroups.

Seven patients of the HCM_{HI} group were identified as carrying the Dutch founder mutation (c.2373dupG) in *MYBPC3*, the gene encoding the A band protein, cardiac myosin-binding protein-C (cMyBP-C) and twelve patients carried other mutations in *MYBPC3*, of which three were missense and the remainder were truncations. Patient ages ranged between 21 and 71 years, with a mean (± SD) of 43 (± 15) years, and 79% of these were males. We collected 19 myectomy samples from HCM_{PP} patients carrying a missense mutation. Nine patients presented with mutations in the gene for the cardiac myosin heavy chain (*MYH7*), the second most commonly mutated gene in HCM patients. Four patients carried mutations in the gene for troponin I (*TNNI3*), three patients carried troponin T (*TNNT2*) mutations and two patients carried myosin light

chain 2 (*MYL2*) mutations. The HCM_{PP} patients were aged between 15 and 72 years, with a mean (± SD) of 55 (± 15) years, and 58% of these were males.

Our study included 14 patients with no known sarcomere gene mutation. HCM_{SMN} patient ages ranged between 22 to 74, with a mean (± SD) of age 57 (± 14), and 64% of these were males. Not all the myectomy samples were sufficiently large to perform all the analyses.

Finally, the 52 HCM samples were compared with nine samples of healthy donor hearts that were not used for heart transplantation, mostly because of poor tissue matching against patients in the heart failure clinic of St Vincent's Hospital. While these controls had no history of cardiac disease, their validity as "controls" was based on their extensive use as such in publications from a wide range of other laboratories. We therefore assumed that these donors are representative of the diverse human population. Consistent with the HCM patients, these donors were 67% male, with a mean age (± SD) of 43 (± 14) years, ranging from 19 to 65. All donor hearts were perfused with ice-cold cardioplegia and transported on ice to the Sydney Heart Bank where ~1 g samples were snap frozen and stored in liquid nitrogen. The average values of the control cardiac samples (n = 9) are indicated by the dotted lines in Figures 1 to 4 and Figure 6. The distribution of the controls is shown in the Supplementary Materials (Figure S1), as well as uncropped full-width images of the membranes (Figure S2). The patients study protocol was approved by the local ethics committees and the donor hearts were approved by the University of Sydney (HREC #7326). All the collections were made with written informed consent obtained from each patient prior to surgery and from the donors' next of kin.

Whole Protein Isolation

Frozen tissue was dissected on dry ice and homogenized with RIPA buffer (0.05 M $C_4H_{11}NO_3$·HCl pH 8.0, 0.15 M NaCl, 1% IGEPAL CA-630, 0.5% sodium deoxycholate, 1% sodium dodecyl sulfate) using a Tissuelyser II (Qiagen). The lysates were centrifuged and the supernatant was collected and passed through an insulin syringe (Becton Dickinson Microlance needle, 25 gauge). Whole protein lysate was mixed with the 4× Laemmli sample buffer (8% sodium dodecyl sulfate, 40% glycerol, 0.04% bromophenol blue, 0.240 M $C_4H_{11}NO_3$·HCl pH 6.8, 10 mM β-mercaptoethanol, 0.01 M NaF, 0.001 M Na_3VO_4, cOmplete mini protease inhibitor cocktail (Roche)), boiled for 5 min and stored at −80 °C.

TABLE 1. Characteristics of controls and manifest HCM patients.

Number	Code	Reported Pathomechanism	Affected Gene	Gene/Protein Variant	Type of Mutation	Sex (F/M)	Age	ST (mm)	LVOT (mmHg)
1	HCM 42 [17–20]	HI	MYBPC3	c.2373dupG	truncation	M	32	23	64
2	HCM 43 [18–22]	HI	MYBPC3	c.2373dupG	truncation	M	60	23	77
3	HCM 103 [20]	HI	MYBPC3	c.2373dupG	truncation	M	26	20	13
4	HCM 104 [20]	HI	MYBPC3	c.2373dupG	truncation	M	33	24	31
5	HCM 120 [20]	HI	MYBPC3	c.2373dupG	truncation	M	27	24	61
6	HCM 123 [20]	HI	MYBPC3	c.2373dupG	truncation	F	59	12	64
7	HCM 169 [20]	HI	MYBPC3	c.2373dupG	truncation	M	52	-	-
8	HCM 34 [18,20,23]	HI	MYBPC3	c.1790G > A; p.Arg597Gln	missense	F	47	20	38
9	HCM 36 [17,18,20–25]	HI	MYBPC3	c.927-2A > G	truncation	M	22	30	71
10	HCM 47 [19,20,23,25]	HI	MYBPC3	c.3407_3409delACT	truncation	M	55	25	96
11	HCM 52 [18–20]	HI	MYBPC3	c.2827C > T	truncation	F	24	24	34
12	HCM 62 [17,18,20,23]	HI	MYBPC3	c.772G > A; p.Glu258Lys	missense	M	35	27	3
13	HCM 63 [20,23]	HI	MYBPC3	c.2827C > T	truncation	M	33	21	25
14	HCM 71 [20]	HI	MYBPC3	c.2827C > T	truncation	M	49	16	9
15	HCM 82 [20]	HI	MYBPC3	c.2783C > T; p.Ser928Leu	missense	M	71	20	64
16	HCM 113 [17,20]	HI	MYBPC3	c.2827C > T	truncation	M	21	45	27
17	HCM 116 [20]	HI	MYBPC3	c.2827C > T	truncation	F	53	-	-
18	HCM 124 [20]	HI	MYBPC3	c.2827C > T	truncation	M	53	21	41
19	HCM 133 [20]	HI	MYBPC3	c.442G > A	truncation	M	58	-	-

TABLE 1. Continued.

Number	Code	Reported Pathomechanism	Affected Gene	Gene/Protein Variant	Type of Mutation	Sex (F/M)	Age	ST (mm)	LVOT (mmHg)
1	HCM 27 [18–20,25]	PP	MYH7	c.4130C > T; p.Thr1377Met	missense	F	58	20	100
2	HCM 42B [18–20,23,25]	PP	MYH7	c.1816G > A; p.Val606Met	missense	F	46	20	77
3	HCM 80 [20]	PP	MYH7	c.1291G > C and c.4327G > A; p.Val431Leu and p.Asp1443Asn	missense	M	34	17	85
4	HCM 92 [20]	PP	MYH7	c.2685A > C; p.Glen895His	missense	M	66	-	-
5	HCM 106 [20]	PP	MYH7	c.2783A > T; p.Asp928Val	missense	M	35	16	16
6	HCM 114 [20]	PP	MYH7	c.976G > C; p.Ala326Pro	missense	M	69	19	71
7	HCM 119 [20]	PP	MYH7	c.3367G > A; p.Glu1123Gln	missense	M	41	20	81
8	HCM 130 [20]	PP	MYH7	c.976G > C; p.Ala326Pro	missense	M	72	18	27
9	HCM 131	PP	MYH7	c.1987C > T; p.Arg663Cys	missense	F	52	21	41
10	HCM 166 [20]	PP	MYH7	c.2080C > T; p.Arg694Cys	missense	F	66	-	-
11	HCM 55 [18,23,25]	PP	TNNI3	c.433C > T; p.Arg145Trp	missense	M	46	23	100

TABLE 1. Continued.

Number	Code	Reported Pathomechanism	Affected Gene	Gene/Protein Variant	Type of Mutation	Sex (F/M)	Age	ST (mm)	LVOT (mmHg)
12	HCM 59 [18,25]	PP	TNNI3	c.433C > T; p.Arg145Trp	missense	M	66	16	67
13	HCM 163	PP	TNNI3	c.433C > T; p.Arg145Trp	missense	F	64	-	-
14	HCM 170	PP	TNNI3	c.433C > T; p.Arg145Trp	missense	F	69	-	-
15	HCM 132	PP	TNNT2	c. 814C > T; p.Arg272Cys	missense	F	15	-	-
16	HCM 173	PP	TNNT2	c.832C > T; p.Arg278Cys	missense	M	58	-	-
17	HCM 175	PP	TNNT2	c.832C > T; p.Arg278Cys	missense	M	61	-	-
18	HCM 135	PP	MYL2	c.64G > A; p.Glu22Lys	missense	M	68	-	-
19	HCM 88	PP	MYL2	c.401A > C; p.Glu134Ala	missense	F	57	-	-
1	HCM 30 [18,19,26]	SMN			-	F	72	24	88
2	HCM 40	SMN			-	M	22	15	100
3	HCM 90	SMN			-	M	53	17	61
4	HCM 96	SMN			-	M	74	17	81
5	HCM 100	SMN			-	F	41	-	81
6	HCM 105	SMN			-	M	65	16	49
7	HCM 109	SMN			-	F	71	20	130

TABLE 1. Continued.

Number	Code	Reported Pathomechanism	Affected Gene	Gene/Protein Variant	Type of Mutation	Sex (F/M)	Age	ST (mm)	LVOT (mmHg)
8	HCM 117 [17]	SMN			-	F	50	16	159
9	HCM 125 [17]	SMN			-	M	66	18	132
10	HCM 126	SMN			-	F	64	15	104
11	HCM 156	SMN			-	F	54	-	-
12	HCM 168	SMN			-	M	46	-	-
13	HCM 172	SMN			-	M	57	-	-
14	HCM 174	SMN			-	M	66	-	-
1	3145 [27–39]	Ctrl			-	M	39	-	-
2	4021 [33–45]	Ctrl			-	F	53	-	-
3	4049 [33–42,46–51]	Ctrl			-	M	65	-	-
4	5126 [46–49,52]	Ctrl			-	F	55	-	-
5	6008 [42,53–55]	Ctrl			-	M	40	-	-
6	7012 [27–32,56,57]	Ctrl			-	M	19	-	-
7	7040 [33–36,55,58]	Ctrl			-	M	37	-	-
8	7054 [55,59]	Ctrl			-	M	33	-	-
9	8004 [55]	Ctrl			-	F	50	-	-

HI: haploinsufficiency; PP: poison polypeptide; SMN: sarcomere mutation-negative; Ctrl: healthy donor hearts; F: female; M: male; Age at time of surgery; ST: septal thickness; LVOT: left outflow tract pressure gradient at rest. Patients without significant obstruction (LVOT gradient < 20 mmHg), but with severe heart failure symptoms, received an extended myectomy in order to increase LV filling.

Electrophoresis and Western Blots

Equal amounts of protein (10 µg) were separated on pre-cast SDS-PAGE 4–12% criterion gels (Bio-Rad) and transferred onto nitrocellulose membranes (Bio-Rad). The membranes were blocked in 5% skim milk/1× TBST for 1 h at room temperature and incubated overnight at 4 °C with the following primary antibodies in 3% BSA/1× TBST: mouse anti-acetylated α-tubulin (T7451, Sigma-Aldrich, Saint Louis, MO, USA, mouse anti-α-actinin (A7811, Merck KGaA, Darmstadt, Germany), mouse anti-HSPA1 (ADI-SPA-810, Enzo Life Sciences, Zandhoven, Belgium), mouse anti-HSPA2 (66291-1, Proteintech Group, Rosemont, IL, USA), mouse anti-HSPB1 (ADI-SPA-800, Enzo Life Sciences, Zandhoven, Belgium), rabbit anti-HSPB5 (ADI-SPA-223, Enzo Life Sciences, Zandhoven, Belgium), rabbit anti-HSPB7 (ab150390, Abcam, Cambridge, UK), rabbit anti-HSPD1 (ADI-SPA-805, Enzo Life Sciences, Zandhoven, Belgium), mouse anti-GAPDH (10R-G109a, Fitzgerald Industries International, Acton, MA, USA), mouse anti-LC3B (#2775, Cell Signaling Technology, Danvers, MA, USA), rabbit anti-p62 (#5114, Cell Signaling Technology), mouse anti-α-tubulin (T9026, Sigma-Aldrich), and rabbit anti-ubiquitin (#3933, Cell Signaling Technology). The membranes were incubated for 1 h at room temperature with horseradish peroxidase-conjugated secondary antibody (DakoCytomation, Santa Clara, CA, USA), raised in goat, in 3% BSA/1x TBST. Signals were detected by Amersham Imager 600 (GE Healthcare, Chicago, IL, USA) and quantified by densitometry (ImageQuant TL, GE Healthcare). To correct for loading differences, protein amounts were expressed relative to GAPDH.

Statistical Analyses

Data were analyzed with SPSS Statistics version 22.0 for Windows (IBM Corporation, Armonk, NY, United States of America) and GraphPad Prism version 7.0 (GraphPad Software Inc., San Diego, CA., United States of America). Data in figures are presented as means ± standard errors of the mean (SEM) per group and in the text, data are presented as means ± standard deviations (SD). The distribution of each data set was determined by Q-Q plots and then double checked by Kolmogorov-Smirnov and Shapiro Wilk tests after data collection was completed. Normally distributed data were analyzed with unpaired t-test (comparing 2 groups) and ordinary one-way ANOVA (comparing > 2 groups) with Tukey's multiple comparisons post-hoc test (comparing ≤ 3 groups) and Dunnett's multiple comparisons post-hoc test (comparing > 3 groups). To analyze non-parametric data, the Mann-Whitney U test (comparing 2 groups) and the Kruskal-Wallis test with Dunn's multiple comparisons post-hoc test (comparing > 2 groups) were used. A two-sided $p < 0.05$ was considered to indicate statistical significance. Multivariate generalized linear model testing (detailed description in the Supplementary Materials) was performed to study the main effects of different mutation groupings, sex, and age at operation on PQC proteins, which were used as dependent variables.

RESULTS

Changes of Protein Quality Control in HCM_{SMP} and HCM_{SMN}

We investigated the expression levels of key PQC proteins to determine if they were altered in patients with HCM at the time of myectomy compared with the levels in LV samples from healthy controls. As the mutant sarcomere proteins may directly affect PQC, we used Western blots to compare myectomy samples from 38 HCM_{SMP} and 14 HCM_{SMN} patients with LV tissue from nine healthy controls that were age- and sex-matched to the HCM samples (Table 1).

HSPs that Stabilize Target Proteins

Dependent on their function, HSPs were classified in two categories: stabilizing HSPs and HSPs with refolding capacity. Stabilizing HSPs (HSPB1 (also known as HSP27), HSPB5 (αB-crystallin), HSPB7 (cardiovascular HSP)) have relatively low molecular weights (15–30 kDa). They stabilize misfolded proteins using an ATP-independent holdase activity, thereby preventing their aggregation (Figure 1A). Compared to controls, the HCM_{SMP} samples expressed significantly higher levels of HSPB1 and HSPB7, while HSPB5 appeared to be unaltered (Figure 1C; Table 2).

We then quantified the protein levels of these stabilizing HSPs (HSPB1, HSPB5 and HSPB7) in HCM_{SMN} samples. Only HSPB7 was significantly higher in HCM_{SMN} compared to controls (Figure 1C; Table 2). Despite this, there were no significant differences in stabilizing HSPs levels between HCM_{SMP} and HCM_{SMN}.

TABLE 2. Overview of results on statistical testing for differences between controls, HCM_{SMP} and HCM_{SMN}

			Adjusted p Value after Post-Hoc Testing		
Proteins	**Statistical Test**	**p Value**	**Controls vs. HCM_{SMP}**	**Controls vs. HCM_{SMN}**	**HCM_{SMP} vs. HCM_{SMN}**
Stabilizing HSPs					
HSPB1	Kruskal-Wallis	0.0019	0.0018	0.2113	0.3302
HSPB5	Ordinary one-way ANOVA	0.1297	0.1090	0.3807	0.8174
HSPB7	Kruskal-Wallis	0.0060	0.0048	0.0341	>0.9999
Refolding HSPs					
HSPD1	Ordinary one-way ANOVA	0.0004	0.0003	0.0530	0.2123
HSPA1	Kruskal-Wallis	0.3636	0.6382	>0.9999	>0.9999
HSPA2	Ordinary one-way ANOVA	0.0101	0.0071	0.1008	0.7334
Protein degradation					
Ubiquitin	Kruskal-Wallis	0.2159	0.3094	>0.9999	0.9890
p62	Ordinary one-way ANOVA	0.1087	0.5822	0.7531	0.1046
LC3BII	Kruskal-Wallis	0.0451	0.0384	0.2455	>0.9999
Tubulin network					
α-tubulin	Ordinary one-way ANOVA	<0.0001	<0.0001	0.0119	0.0019
Acetylated α-tubulin	Kruskal-Wallis	<0.0001	<0.0001	0.0451	0.0516

$p < 0.05$ is considered to be significant.

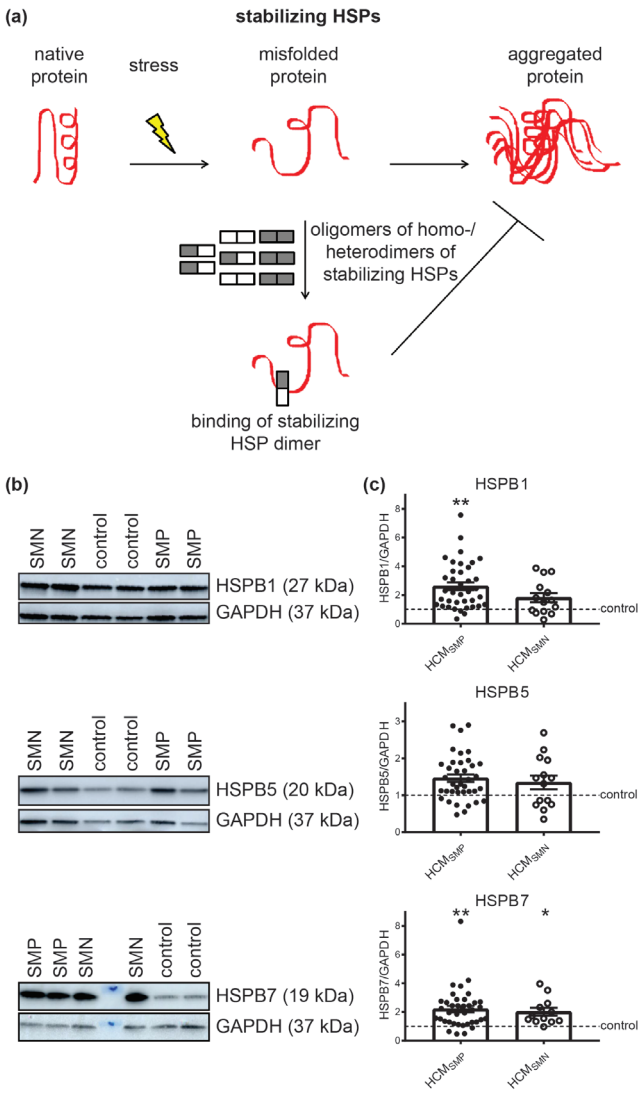

FIGURE 1. Stabilizing HSPs. (**a**) Under stress conditions when native proteins are destabilized and begin to unfold, stabilizing HSPs dissociate from homo- and/or heterogeneous oligomeric complexes into dimers to bind these partially misfolded proteins. Thereby, stabilizing HSPs prevent the aggregation of misfolded proteins. Figure reproduced and adapted with permission from Dorsch, L.M. et al., Pflügers Archiv–European Journal of Physiology; published by Springer Berlin Heidelberg, 2018. (**b**) Representative blot images for HSPB1, HSPB5, and HSPB7 expression. (**c**) Higher levels of HSPB1 and HSPB7 in HCM_{SMP} (n = 38) compared to controls. Higher HSPB7 levels in HCM_{SMN} (n = 12) compared to controls (n = 9; average is shown as dotted line). HSPB1 and HSPB5 protein levels were not different in HCM_{SMP} (n = 14) compared to controls. There were no significant differences between HCM_{SMP} and HCM_{SMN}. Each dot in the scatter plots represents an individual sample. *$p < 0.05$ and **$p < 0.01$ versus controls.

HSPs that Refold Target Proteins

Next we investigated the expression levels of HSPD1 (HSP60), HSPA1 (HSP70 and HSP72) and HSPA2 (HSP70-2) that have an ATP-dependent folding activity. These HSPs have molecular weights >30 kDa and either refold misfolded proteins or assist in their degradation. HSPD1 is mainly located in mitochondria while HSPA1 and HSPA2 are cytosolic, but when they are exposed to heat stress, both translocate to the nucleus [60,61]. Compared to controls, significantly higher levels of HSPD1 and HSPA2 were observed in HCM_{SMP} samples, while HSPA1 levels were not significantly changed. Levels of HSPs with a refolding capacity were not significantly different in HCM_{SMN} compared to controls, although HSPD1 and HSPA2 showed a trend to higher levels. There were no significant differences in HSPs with a refolding capacity between the two HCM groups (Figure 2; Table 2).

Degradation of Proteins

PQC is also involved in the degradation of proteins and therefore levels of ubiquitination, p62 and LC3BII were assessed. The antibody used for ubiquitin recognizes polyubiquitinated proteins without distinguishing between K48-linked polyubiquitin chains (predominantly targeted by proteasomal degradation) and K63-linked polyubiquitin chains (targeted by autophagic degradation) [62]. Levels of ubiquitin and the ubiquitin-binding autophagic adaptor protein p62 were unaltered in both HCM groups compared to controls. Levels of the autophagosome marker LC3BII were significantly higher in HCM_{SMP} compared to controls, while only some samples of the HCM_{SMN} group had higher levels of LC3BII (Figure 3, Table 2).

To ensure that the significant differences detected by ANOVA testing were not related to differences in age and/or sex of the myectomy patients, we performed multivariate testing (Wilks' Lambda test). This test uses age, sex and the HCM grouping (controls, HCM_{SMP} and HCM_{SMN}) as the effects and the HSPs, ubiquitination, p62, and LC3BII as dependent variables. We found an overall significant difference in the levels of key PQC players based on the different mutation groups (Table 3), while sex and age at operation had no significant effect on levels of key PQC players. To determine which of the individual key PQC players differed among groups when taking into account sex and age, we performed tests for between-subjects effects. This test revealed statistically significant differences among groups for HSPB1 and HSPD1 (Table 4).

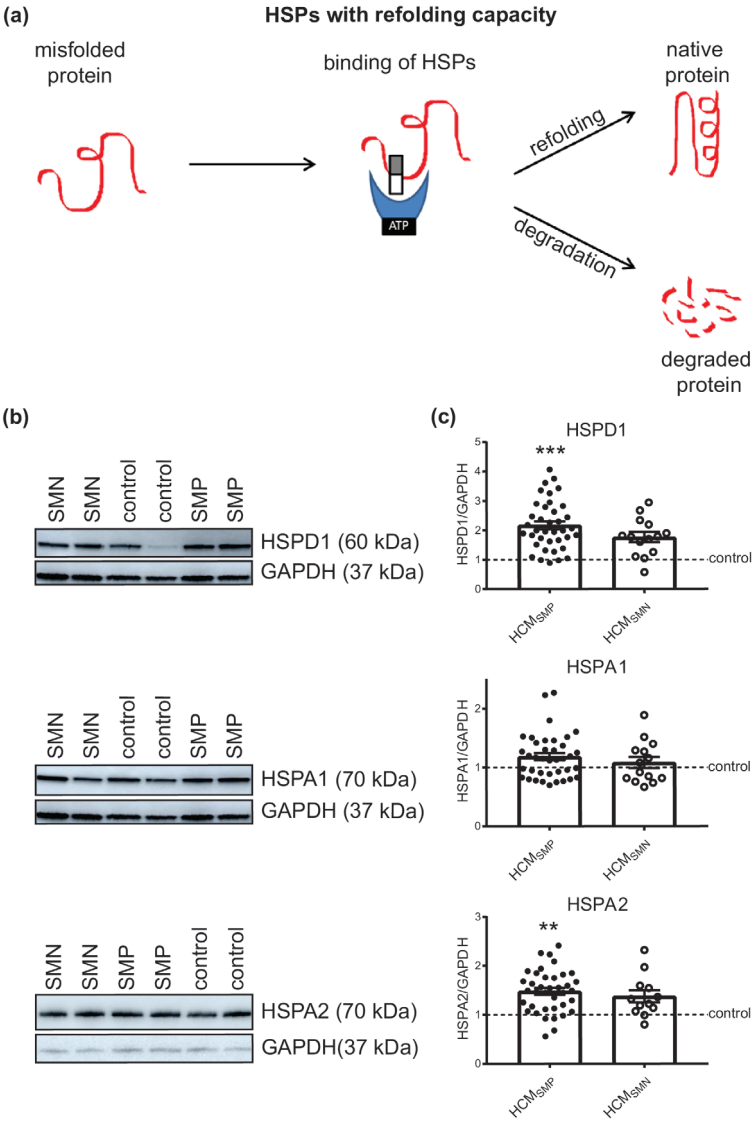

FIGURE 2. HSPs with a refolding capacity. (**a**) HSPs with ATPase activity and stabilizing HSPs bind to the misfolded protein to stabilize and further process it. HSPs with a refolding capacity either refold the misfolded protein to its native structure or, if refolding is impossible, the HSPs assist in the degradation pathways to degrade the misfolded protein. Figure reproduced and adapted with permission from Dorsch, L.M. et al., Pflügers Archiv—European Journal of Physiology, published by Springer Berlin Heidelberg, 2018. (**b**) Representative blot images for HSPD1, HSPA1, and HSPA2 expression. (**c**) Higher levels of HSPD1 and HSPA2 in HCM_{SMP} ($n = 38$) compared to controls. HSPs with refolding capacity were unaltered in HCM_{SMN} (HSPD1, HSPA1: $n = 14$; HSPA2: $n = 12$) compared to controls. There were no significant differences between HCM_{SMP} and HCM_{SMN}. Each dot in the scatter plots represents an individual sample. $^{**}p < 0.01$ and $^{***}p < 0.001$ versus controls.

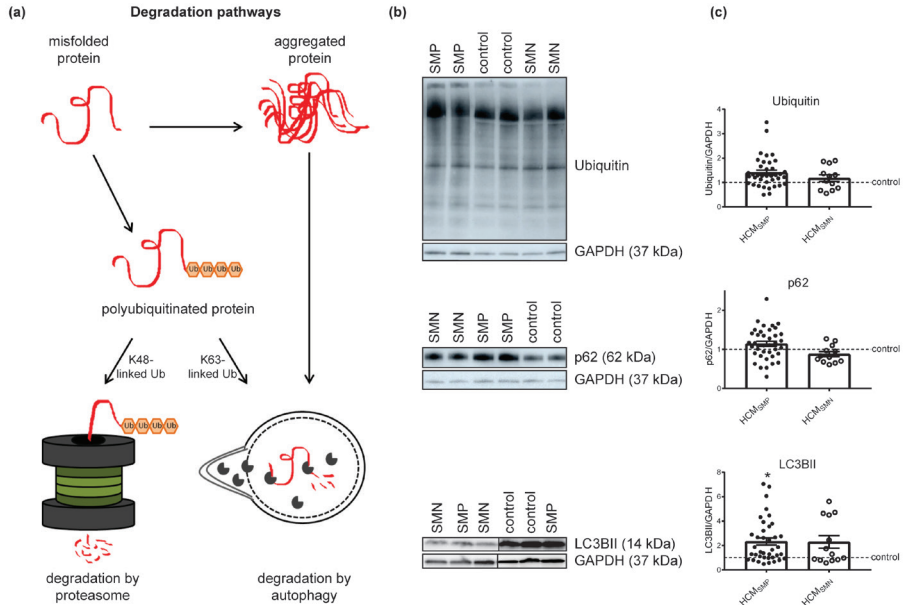

FIGURE 3. Degradation pathways. (**a)** Misfolded proteins with polyubiquitin chains linked via lysine 48 (K48) are mainly degraded by the proteasome. Misfolded proteins carrying K63-linked polyubiquitin chains and aggregated proteins enter the autophagic pathway. Figure reproduced and adapted with permission from Dorsch, L.M. et al., Pflügers Archiv–European Journal of Physiology; published by Springer Berlin Heidelberg, 2018. (**b**) Representative blot images for ubiquitin, p62, and LC3BII expression. (**c**) Protein levels of ubiquitin and p62 did not differ between HCM and controls samples. Higher levels of LC3BII in HCM_{SMP} (n = 38) compared to controls. There were no significant differences between HCM_{SMP} and HCM_{SMN} (ubiquitin, p62: n = 12; LC3BII: n = 13). Each dot in the scatter plots represents an individual sample. *$p < 0.05$ versus controls.

TABLE 3. Multivariate Tests [a]: HCM grouping (controls, HCM_{SMP}, and $HCMS_{MN}$), sex and age at operation.

Effect	Value	F	Hypothesis df	Error df	Significance	Partial eta Squared
Intercept	0.260	14.561 [b]	9.000	46.000	<0.001	0.740
HCM grouping	0.479	2.278 [b]	18.000	92.000	0.006	0.308
Sex	0.754	1.664 [b]	9.000	46.000	0.126	0.246
Age at operation	0.717	2.016 [b]	9.000	46.000	0.059	0.283

[a] Design: Intercept and HCM grouping and sex and age at operation; [b] exact statistic; F: F statistic for the given effect and test statistic; Hypothesis df: Number of degrees of freedom in the model; Error df: Number of degrees of freedom associated with the model errors; Partial eta squared: estimate of effect size; $p < 0.05$ is considered to be significant.

TABLE 4. Tests for between-subjects: HCM grouping (controls, HCM_{SMP}, HCM_{SMN}) as an effect and correction for differences in sex and age at operation.

	Type III Sum of Squares	df	Mean Square	F	Significance	Partial eta Squared	R squared
Stabilizing HSPs							
HSPB1	23.286	2	11.643	6.0313	0.004	0.182	0.261
HSPB5	1.777	2	0.889	2.495	0.092	0.085	0.088
HSPB7	9.725	2	4.863	3.319	0.044	0.109	0.162
Refolding HSPs							
HSPD1	11.104	2	5.552	10.543	<0.001	0.281	0.323
HSPA1	0.258	2	0.129	0.981	0.381	0.035	0.055
HSPA2	1.724	2	0.862	5.114	0.009	0.159	0.171
Protein degradation							
Ubiquitin	1.433	2	0.716	2.101	0.132	0.072	0.097
p62	0.733	2	0.367	2.498	0.092	0.085	0.122
LC3BII	12.839	2	6.420	2.276	0.112	0.078	0.111

df: Number of degrees of freedom in the model; F: F statistic for the given effect and test statistic; Partial eta squared: estimate of effect size; R squared: proportion of the variance in the dependent variable that is predictable from the independent variable; Bonferroni correction: statistical significance at $p < 0.0056$ ($\alpha/9 = 0.05/9 = 0.0056$).

TABLE 5. Simple Contrast Results (K Matrix) for HCM grouping (controls, HCM_{SMP}, HCM_{SMN}) as an effect and correction for differences in age at operation and sex.

			Dependent Variable								
			Stabilizing HSPs			Refolding HSPs			Protein degradation		
			HSPB1	HSPB5	HSPB7	HSPD1	HSPA1	HSPA2	Ubiquitin	p62	LC3BII
HCM_{SMP} vs. controls	Contrast Estimate		1.804	0.447	1.164	1.242	0.177	0.491	0.441	0.128	1.319
	Standard error		0.520	0.223	0.453	0.271	0.136	0.154	0.218	0.143	0.628
	Significance		0.001	0.050	0.013	<0.001	0.198	0.002	0.049	0.375	0.040
	95% Confidence Interval for	Lower Bound	0.761	-0.00002	0.257	0.698	-0.095	0.183	0.003	-0.159	0.060
		Upper Bound	2.848	0.895	2.072	1.786	0.449	0.799	0.878	0.415	2.578
HCM_{SMN} vs. controls	Contrast Estimate		1.522	0.178	0.929	0.961	0.086	0.452	0.301	-0.160	1.335
	Standard error		0.650	0.279	0.565	0.339	0.169	0.192	0.273	0.179	0.784
	Significance		0.023	0.524	0.106	0.006	0.613	0.031	0.274	0.374	0.094
	95% Confidence Interval for	Lower Bound	0.220	-0.380	-0.204	0.282	-0.253	0.041	-0.245	-0.519	-0.236
		Upper Bound	2.825	0.737	2.062	1.641	0.426	0.810	0.848	0.198	2.907

Bonferroni correction: statistical significance at $p < 0.0028$ ($\alpha/18 = 0.05/18 = 0.0028$).

Since we found between-subjects main effects, we performed a contrast analysis to determine significant pairwise differences between controls and the two HCM patient groups corrected for age and sex. A simple main effects analysis revealed significantly higher levels of HSPB1, HSPD1 and HSPA2 in HCM_{SMP} compared to controls (Table 5), while a trend to higher levels of HSPD1 was observed in HCM_{SMN}.

Overall, our analyses showed increased levels of several HSPs in HCM_{SMP} and HCM_{SMN} compared to controls, while no significant differences between HCM_{SMP} and HCM_{SMN} were observed.

Changes of Protein Quality Control: HCM Disease Mechanism

All the studied HCM_{SMP} patients were heterozygous for the mutation, implying the potential to produce either or both the mutant and wild-type protein [14]. Either the expression of the mutant protein, which above a threshold (the 'poison polypeptide' mechanism) level might become toxic or have an inability to upregulate the haplotype protein levels to meet the needs of the heart (the 'haploinsufficiency' mechanism) might underlie HCM [14]. Truncation and missense *MYBPC3* mutations usually involve haploinsufficiency as the disease mechanism since total cMyBP-C protein level is lower and the mutant protein has not been detected in human myectomy samples [13,63].

We determined whether key PQC players were differently changed in samples with haploinsufficiency (HI) and poison polypeptide (PP) by comparing 19 *MYBPC3* mutation samples (HCM_{HI}) with 19 HCM_{SMP} samples carrying a missense mutation (HCM_{PP}). Proteomics analysis using mass spectrometry revealed significantly lower cMyBP-C protein levels in the HCM_{HI} samples compared to the HCM_{PP} patients, consistent with a protein haploinsufficiency mechanism (Figure 4) [64]. No significant differences in PQC components were observed between HCM_{HI} and HCM_{PP} (Figure 5, Table 6).

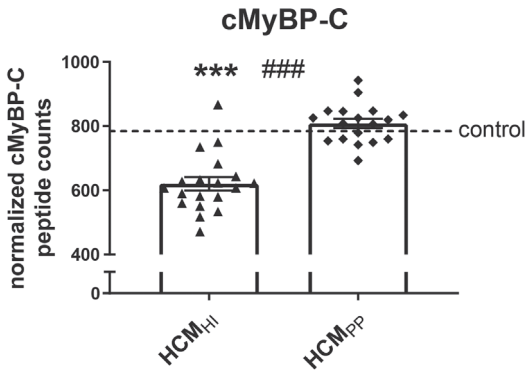

FIGURE 4. cMyBP-C haploinsufficiency. Mass spectrometry-based proteomics analysis revealed lower levels of cMyBP-C in HCM_{HI} (n = 19) compared to controls (n = 5) and HCM_{PP} (n = 18). Each dot on the scatter plot represents an individual sample. ***$p < 0.001$ versus controls and $^{###}p < 0.001$ versus HCM_{PP}.

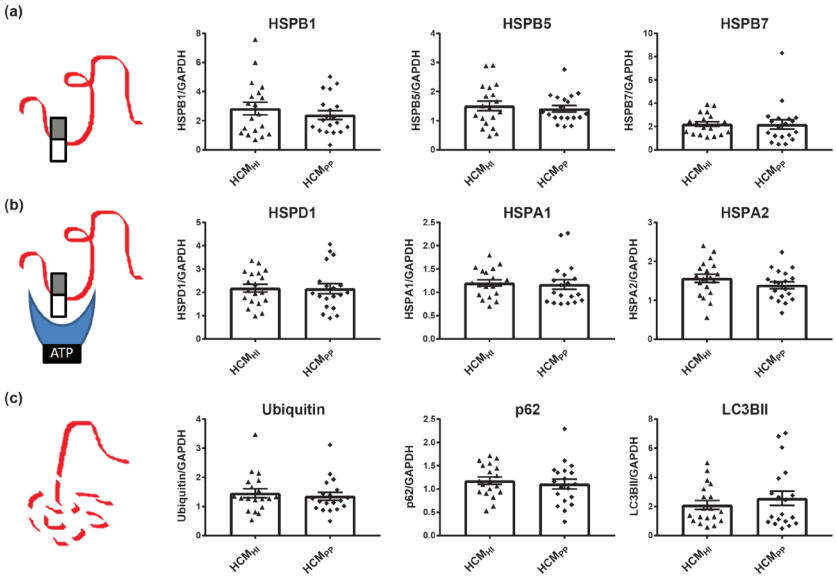

FIGURE 5. Pathomechanism of HCM and key PQC players. (**a**) Stabilizing HSPs (HSPB1, HSPB5, HSPB7), (**b**) HSPs with refolding capacity (HSPD1, HSPA1 HSPA2) and (**c**) degradation markers (ubiquitin, p62, LC3BII) were not significantly different between HCM_{HI} (n = 19) and HCM_{PP} (n = 19). Each dot in the scatter plots represents an individual sample. Figure reproduced and adapted with permission from Dorsch, L.M. et al., Pflügers Archiv–European Journal of Physiology; published by Springer Berlin Heidelberg, 2018.

Microtubule Network

Microtubule-based transport of proteins is required for autophagy and is thus an essential part of PQC. Acetylation of α-tubulin is associated with stable microtubules and is used as a marker of their stability [65,66]. Mouse models of familial HCM showed higher levels of acetylated α-tubulin [67]. Compared to controls, α-tubulin expression levels were significantly higher in both HCM_{SMP} and HCM_{SMN} (Figure 6A,B; Table 2). In addition, acetylation of α-tubulin was significantly higher in both HCM patient groups compared to controls (Figure 6A,B). The increases in the levels of α-tubulin and acetylated α-tubulin were significantly higher in HCM_{SMP} compared to HCM_{SMN}.

When comparing mutation types, significantly higher levels of α-tubulin and acetylated α-tubulin were observed in HCM_{HI} compared to HCM_{PP} (Figure 6C, Table 6). The levels of acetylated α-tubulin significantly correlated with α-tubulin (Figure 6D), which is in line with the observation that acetylation of α-tubulin compartmentalized on the stable microtubules. Moreover, a significant inverse linear correlation was present between the cMyBP-C protein level and α-tubulin in HCM with a sarcomere gene mutation (Figure 6E). Overall, these data show that the presence of a sarcomere mutation coincides with a more extensive and stabilized microtubule network in HCM.

TABLE 6. Overview of results on statistical testing for differences between HCM_{HI} and HCM_{PP}.

Proteins	Statistical Test	p Value
Stabilizing HSPs		
HSPB1	Unpaired t-test	0.4040
HSPB5	Unpaired t-test	0.6236
HSPB7	Mann-Whitney U test	0.4181
Refolding HSPs		
HSPD1	Unpaired t-test	0.1712
HSPA1	Unpaired t-test	0.8044
HSPA2	Unpaired t-test	0.2096
Protein degradation		
Ubiquitin	Unpaired t-test	0.6099
p62	Unpaired t-test	0.5868
LC3BII	Unpaired t-test	0.4297
Tubulin network		
α-tubulin	Unpaired t-test	0.0074
Acetylated α-tubulin	Unpaired t-test	0.0079
Acetylated α-tubulin/α-tubulin	Mann-Whitney U test	0.1629

$p < 0.05$ is considered to be significant.

Strong Correlation of HSPs with α-tubulin

Since the PQC is strongly linked to the microtubules network, we performed multivariate testing (Wilks' Lambda test) using levels of α-tubulin, sex, and age at operation as effects and the HSPs, ubiquitination, p62, and LC3BII as dependent variables. There was an overall statistically significant difference in the levels of key PQC players based on the α-tubulin levels (Table 7).

To determine which of the key PQC players differed when α-tubulin levels changed, we performed tests for between-subjects effects. This test revealed that α-tubulin had a significant effect on all the measured HSPs, but not on the degradation markers (Table 8). The correlation of HSPs and α-tubulin levels is visualized in Figure S3.

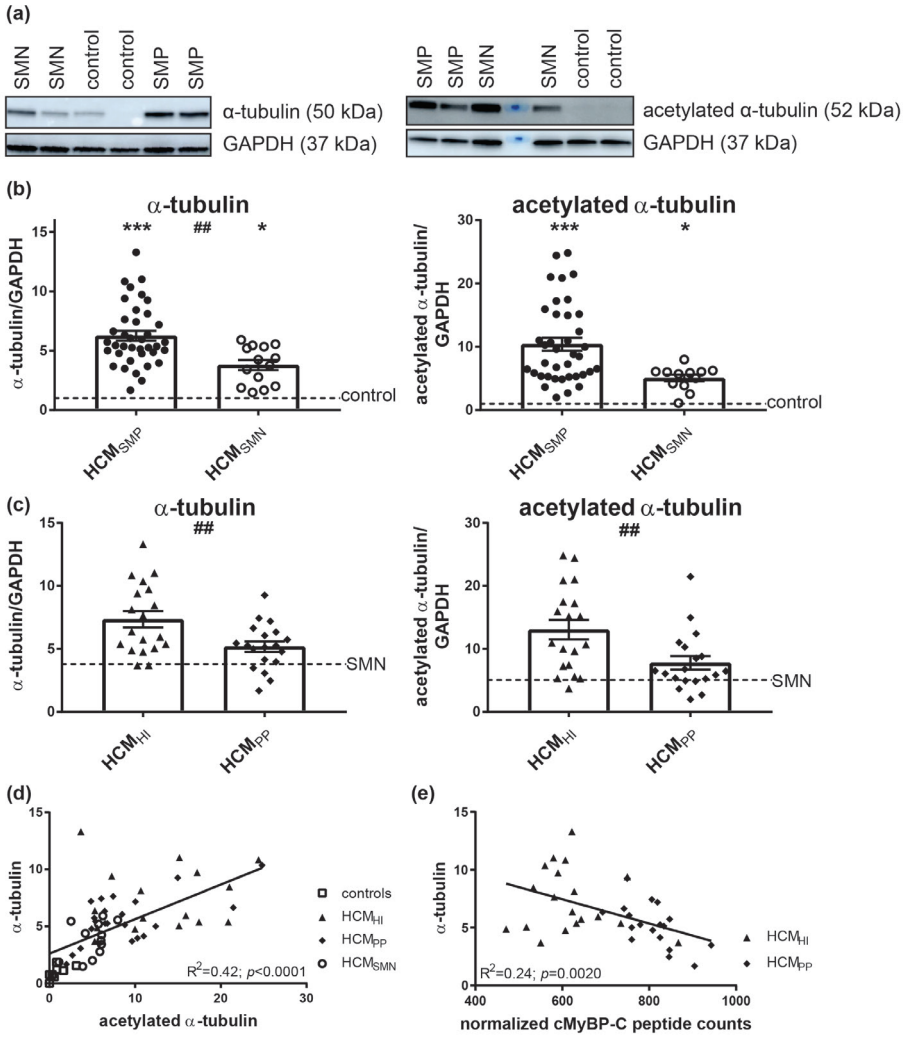

FIGURE 6. Pathomechanism of HCM and acetylation of α-tubulin. (a) Representative blot images for α-tubulin and acetylated α-tubulin. (b) Higher levels of α-tubulin and acetylated α-tubulin in HCM_{SMP} (n = 38) and HCM_{SMN} (α-tubulin: n = 14; acetylated α-tubulin: n = 12) compared to controls. Significant difference of α-tubulin levels between HCM_{SMP} and HCM_{SMN} (##p < 0.01). (c) Higher levels of α-tubulin and acetylated α-tubulin in HCM_{HI} (n = 19) than HCM_{PP} (n = 19). (d) The levels of α-tubulin correlated well with acetylated α-tubulin (e) Significant inverse linear correlation of α-tubulin with cMyBP-C. Controls = open squares, HCM_{SMP} = filled circles, HCM_{SMN} = open circles, HCM_{HI} = filled triangles, HCM_{PP} = filled rhomboids. Each dot in the scatter plots and the correlation analyses represents an individual sample. *$p < 0.05$ and ***$p < 0.001$ versus controls and $^{\#\#}p < 0.01$ and $^{\#\#\#}p < 0.001$ versus HCM_{PP}.

TABLE 7. Multivariate Tests [a]: α-tubulin (all samples), sex, and age at operation.

Effect	Value	F	Hypothesis df	Error df	Significance	Partial eta Squared
Intercept	0.389	8.186 [b]	9.000	47.000	<0.001	0.611
α-tubulin	0.427	7.009 [b]	9.000	47.000	<0.001	0.573
Sex	0.774	1.523 [b]	9.000	47.000	0.168	0.226
Age at operation	0.791	1.384 [b]	9.000	47.000	0.223	0.209

[a] Design: Intercept and α-tubulin and sex and age at operation; [b] exact statistic; F: F statistic for the given effect and test statistic; Hypothesis df: Number of degrees of freedom in the model; Error df: Number of degrees of freedom associated with the model errors; Partial eta squared: estimate of effect size; $p < 0.05$ is considered to be significant.

TABLE 8. Tests for between-subjects: α-tubulin as an effect and correction for differences in sex and age at operation.

	Type III Sum of Squares	df	Mean Square	F	Significance	Partial eta Squared	R Squared
Stabilizing HSPs							
HSPB1	38.460	1	38.460	23.663	>0.001	0.301	0.368
HSPB5	3.630	1	3.630	11.485	0.001	0.173	0.176
HSPB7	14.246	1	14.246	10.504	0.002	0.160	0.209
Refolding HSPs							
HSPD1	10.273	1	10.273	19.305	>0.001	0.260	0.303
HSPA1	1.370	1	1.370	12.580	0.001	0.186	0.203
HSPA2	1.723	1	1.723	10.410	0.002	0.159	0.171
Protein degradation							
Ubiquitin	0.419	1	0.419	1.187	0.281	0.021	0.047
p62	0.418	1	0.418	2.792	0.100	0.048	0.087
LC3BII	3.849	1	3.849	1.312	0.257	0.023	0.058

df: Number of degrees of freedom in the model; F: F statistic for the given effect and test statistic; Partial eta squared: estimate of effect size; R squared: proportion of the variance in the dependent variable that is predictable from the independent variable; Bonferroni correction: statistical significance at $p < 0.0056$ ($\alpha/9 = 0.05/9 = 0.0056$).

DISCUSSION

The incomplete penetrance, age-related onset and the large clinical variability in disease severity imply a complex HCM pathophysiology mechanism. Patients with a sarcomere mutation have a particularly higher risk for adverse outcomes. The underlying causes for the difference in disease between HCM_{SMP} and HCM_{SMN} remain unclear.

Here, we determined the protein levels of key PQC players, including HSPs and degradation markers, and the acetylation of α-tubulin by Western blot analysis in a large set of cardiac samples from HCM_{SMP} and HCM_{SMN} patients to define PQC changes in HCM at the time of myectomy, and identified if the presence of a sarcomere mutation mediates changes in PQC mechanisms and tubulin network. One of the limitations of the current study was that patients had a severe phenotype with LVOT obstruction. Therefore, this group may not be representative for all patients with HCM.

The main findings of our PQC assessment were that: 1) several HSPs and autophagy markers were higher in HCM compared to controls, but there are no major differences between HCM_{SMP} and HCM_{SMN} or mutation type (haploinsufficiency versus poison polypeptide) at the time of myectomy, 2) after correction for sex and age at operation, the major increases in HCM_{SMP} compared to controls were observed in the stabilizing HSPB1 and the refolding HSPD1 and HSPA2, 3) the most significant increase compared to control samples was observed in the levels of α-tubulin and acetylated α-tubulin, with significant differences between the mutation groups: $HCM_{HI} > HCM_{PP} > HCM_{SMN}$, and 4) the levels of α-tubulin significantly correlated with the levels of acetylated α-tubulin and all the HSPs (Figure 7).

Overall, our analyses indicate that carrying a HCM-causing mutation affects PQC and α-tubulin acetylation. We propose that reduced levels of cMyBP-C caused by *MYBPC3* mutations trigger HSPs and α-tubulin acetylation, and may present a pathomechanism in cMyBP-C haploinsufficiency-mediated HCM. The possible impact of the observed PQC changes is discussed below.

Elevated Levels of HSPs in Human HCM

We identified higher levels of HSPB1, HSPD1, and HSPA2 in HCM_{SMP} compared to controls, which could not be explained by differences in sex and age at operation (Table 5). Our findings are in line with studies in human end-stage heart failure studies samples, which showed increases in HSPD1 and HSPB1 compared to controls [68].

HSPB1 is implicated in different cardio-protective processes involving interception of misfolded proteins, cytoskeletal organization, anti-apoptotic and anti-oxidant properties [69]. Therefore, its expression may improve the resistance of tissue exposed to stress and injuries [70]. While moderate cardiac expression of HSPB1 protects against doxorubicin-induced cardiac dysfunction through anti-oxidative stress, reports on the effects of HSPB1 overexpression have been inconsistent [71]. Overexpression of HSPB1 conferred protection against myocardial ischemia-reperfusion injury [72], whereas overexpression of HSPB1 caused reductive stress and cardiomyopathy in another study [73]. Further experiments are needed to clarify if the observed increase in HSPB1 is actually beneficial and may be a response to stress exposure.

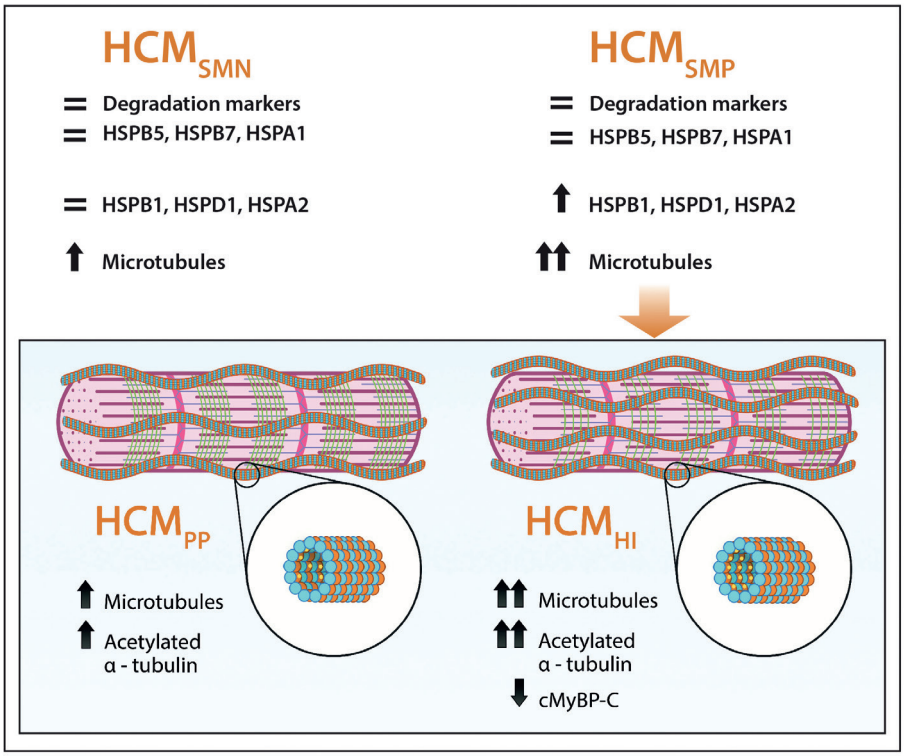

FIGURE 7. Schematic representation of PQC and microtubular system assessment in HCM. Our analyses show that HSPB1, HSPD1 HSPA2, α-tubulin and acetylated α-tubulin were increased in HCM, especially when a sarcomere mutation is present, while HSPB5, HSPB7, HSPA1 and degradation markers are not changed in HCM compared to controls. Levels of α-tubulin (orange balls) and acetylated α-tubulin (small yellow balls attached to α-tubulin in the lumen of polymerized microtubules (blue and orange balls)) were more increased when haploinsufficiency (HI), characterized by lower levels of cardiac myosin-binding protein-C (green lines), was the underlying pathomechanism instead of poison polypeptides (PP). =: similar to controls; ↑: significantly increased compared to controls; ↑↑: highly significantly increased compared to controls; ↓: significantly decreased compared to controls.

HSPD1 fulfills multiple tasks in a cell by refolding key proteins after their import into the mitochondria, transporting proteins between the mitochondrial matrix and the cytoplasm of the cell, and binding to cytosolic pro-apoptotic proteins to sequester them [74]. Upregulation of HSPD1 due to mitochondrial impairment is suggested to be an indicator of mitochondrial stress [75]. A total of 15–20% of HSPD1 is located at extra-mitochondrial sites, suggesting important physiological roles at other locations [61]. In human end-stage heart failure, HSPD1 localizes to the plasma membrane, thereby losing anti-apoptotic and protective effects and becoming detrimental to the cell [76]. Impairment of HSPD1-mediated anti-stress response has been reported in dilated cardiomyopathy (DCM) which progressed to end stage heart failure [77].

Here, we identified higher levels of HSPD1, which may indicate mitochondrial stress, as has been reported in HCM [78].

The Western blot analysis showed higher levels of HSPA2 in HCM_{SMP} compared to controls. In our mass-spectrometry-based proteomics study, HSPA2 was highly upregulated in cardiac disease (Figure 8A) [64]. HSPA2 has been reported in heart tissue and low expression was identified in fibroblasts [60,79]. Recently, HSPA-family chaperones have been suggested to interact with cMyBP-C to regulate its turnover [80]. Moreover, a significant inverse linear correlation was present between cMyBP-C protein levels and HSPA2 (Figure 8B). Therefore, HSPA2 may be an additional regulator of cMyBP-C. Further experiments are warranted to explain the role of HSPA2 in haploinsufficiency for cMyBP-C.

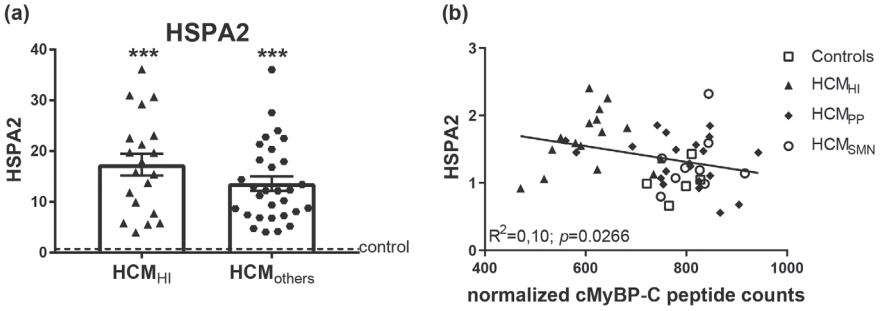

FIGURE 8. Upregulated HSPA2 in HCM in proteomics screen. (a) In a mass-spectrometry based proteomics study, HSPA2 levels were higher in HCM_{HI} (n = 20) and HCM_{others} (n = 30) samples, including HCM_{PP} and HCM_{SMN}, compared to controls (n = 8). (b) Significant inverse correlation of HSPA2 levels, determined by Western blot analysis with cMyBP-C. Controls = open squares, HCM_{HI} = filled triangles, HCM_{PP} = filled rhomboids, HCM_{SMN} = open circles, HCM_{others} = hexagons. Each dot in the scatter plots and correlation analysis represents an individual sample. ***p < 0.001 versus controls.

In contrast, the levels of the HSPB5 and HSPA1 in HCM samples were not different compared to controls after adjusting for sex and age differences. Several studies have shown that HSPB5 and HSPA1 are both increased early in response to acute hypertrophic signaling, but with opposite functions. While HSPB5 is involved in counteracting acute cardiac remodeling by suppressing hypertrophic signaling pathways, HSPA1 supports pro-hypertrophic signaling pathways [81,82]. The increase of HSPA1 was transient and attenuated 14 days after isoproterenol-infusion in a mouse model for cardiac hypertrophy [82]. Consistent with our findings in myectomy samples from patient with advanced disease, HSPA1 levels were not changed in septal myectomy samples of HCM patients and end-stage heart failure patients compared to controls [68,80]. Increased HSPA1 in the heart protects against acute cardiac stress, but not against chronic cardiac stress [83].

Based on these studies, we propose that HSPB5 and HSPA1 levels were not changed in the HCM myectomy samples because of persistent chronic hypertrophic stimuli leading to their blunted response. Further research is warranted to investigate if the failure to increase HSPB5 implies a loss of responsiveness at advanced disease stage because HSPB5 seems to play a beneficial role in hypertrophic signaling.

Protein Degradation in HCM

Defects in the turnover of key sarcomere proteins may account for both hypertrophic and functional defects [9]. UPS dysfunction is characterized by the accumulation of ubiquitinated proteins, altered proteasome activity, and changes in expression of UPS proteins or E2 and E3 enzymes [84]. Upon correction for sex and age, no significant changes were observed in the levels of degradation-associated markers in HCM, such as HSPB7, ubiquitin, p62 and LC3BII. Compared to the protein folding-supportive HSPB1 and HSPB5, HSPB7 plays a critical role in preventing protein aggregation [85]. Genetic variants in HSPB7 have been associated with advanced heart failure and systolic dysfunction [86]. In a zebrafish model, HSPB7 was involved in early post-damage processing of large cytoskeletal proteins and the loss of HSPB7 function was accompanied by an increased damaged protein load, protein aggregation and a risk of cardiomyopathy [87]. Due to the use of an antibody recognizing both K48- and K63-linked polyubiquitinated chains, we do not know if the ratio between K48- and K63-linked polyubiquitinated proteins was altered in HCM. Therefore, we cannot draw any conclusion about the functionality of the proteasome, which would be indicated by an increase in K48-linked polyubiquitinated proteins. LC3BII and p62 are both markers for autophagosomes because in selective autophagy, the cargo adapter protein p62 links polyubiquitinated proteins to the autophagic machinery via LC3 [88]. We did not find a change in autophagosome markers, but this finding does not exclude the prospect that the autophagic flux might be impaired. Autophagy has been implicated in the pathogenesis of a wide range of cardiac pathologies [62,88]. Pre-clinical models of pressure overload-induced cardiac hypertrophy showed that the increase of autophagic flux correlated with the degree of hypertrophy and therapeutic inhibition of autophagy was accompanied by reduced amount of fibrosis [89].

Our analysis of protein degradation markers indicates that there is no enhancement of protein degradation pathways at the time of myectomy. This may indicate that boosting protein degradation may actually represent a treatment option to prevent cardiac dysfunction and remodeling.

Increased Mutation-dependent Proliferation and Acetylation of α-tubulin

Our protein analyses revealed significantly increased levels of α-tubulin in both HCM groups (Figure 6A), which correlated with an increase in α-tubulin acetylation and the levels of all HSPs. Changes of microtubules distribution occurred at the onset of hypertrophy [90]. In chronically hypertrophied hearts, the increase of microtubules

has been shown to be a major cause of contractile defects [91]. Two different hypotheses may explain microtubule densification: (1) microtubules may be involved in myofibrillogenesis and an increase in microtubules would be required when new myofibrils are formed in hypertrophied cardiomyocytes, and (2) microtubules may be intracellular compression-bearing elements needed to cope with increased contractile stress on cardiomyocytes [92,93]. In failing human hearts, the accumulation of microtubules impedes sarcomere motion and contributes to a decreased ventricular compliance [94]. Our results are in line with literature, showing an increase in α-tubulin in the HCM myocardial tissue [95]. The underlying pathomechanism seems to have an effect on extent of increase in α-tubulin and acetylated α-tubulin, since we observed the largest increase in samples with haploinsufficiency for cMyBP-C.

An intact microtubule-based cytoskeleton contributes to the stabilization of myofibril structure in the cardiomyocytes and HSPs may preserve this relationship [96]. Post-chaperonin tubulin-folding cofactors, such as HSPs and other tubulin-associated proteins, regulate the synthesis, transport, and storage of α- and β-tubulin [97]. For instance, HSPA1 binds to native tubulin dimers and microtubules to assist in proper tubulin folding [98]. In addition, HSPB5 prevents the aggregation of tubulin and the chaperone activity is accompanied by the formation of large complexes between HSPB5 and tubulin [99]. We identified that α-tubulin level significantly correlates with all the investigated HSPs.

In addition to HSPs, acetylation of α-tubulin was higher in both HCM groups (Figure 6B). Acetylation of α-tubulin directly tunes the compliance and resilience from mechanical breakage to ensure the persistence of long-lived microtubules [100]. Moreover, acetylation of α-tubulin most often compartmentalizes on the stable microtubules and is suggested to increase the assembly of autophagic cargo along microtubules, thereby initiating augmented autophagic degradation in the heart [101,102]. Interestingly, there is a strong linear relation between acetylated and total α-tubulin levels (Figure 6D). This may suggest hyperacetylation of α-tubulin, which is a common response to several cellular stresses. For example, acetyltransferase induction is triggered by the release of mitochondrial reactive oxygen species (ROS) and by AMP kinase [103,104]. Noteworthily, the underlying pathomechanism (HI versus PP) seems to have an effect on the extent of the increase in α-tubulin and the acetylation of α-tubulin, since we observed the largest increase in samples with haploinsufficiency for cMyBP-C. As such, our analyses suggest that proliferation of the microtubular network represents a pathomechanism in HI-mediated HCM. Based on previous studies [100–104], we propose that the increased tubulin network may function to maintain cellular stability and enhance autophagic flux of damaged proteins, while it may impair contractile function [95,105]. Future studies are warranted to establish this link (cause-consequence) between reduced cMyBP-C protein levels, increased α-tubulin acetylation and cardiomyocyte contractile function and hypertrophy that may underlie initiation and progression of cardiac disease in MYBPC3 mutation carriers.

Inter-individual Differences

We observed large inter-individual differences in various key PQC players and tubulin networks, especially in the presence of a sarcomere mutation. This variability may be explained by the large variability among HCM-causing mutations, which may all have a distinct effect on cellular PQC. Most of the mutation sites of proteins affect stability and aggregation but rarely its function [106]. This concept is supported by the fact that HCM_{HI} mutations cause a rather heterogeneous cMyBP-C haploinsufficiency, with some samples having relatively low cMyBP-C, and others having still relatively high protein level. The loss of cMyBP-C levels correlates very well with α-tubulin, thereby supporting the diverse response to a change in sarcomere protein composition in the case of HCM_{HI}. The microtubule response correlates significantly with the expression level of cMyBP-C, and may represent a direct compensation for the loss of cMyBP-C as cMyBP-C is known to have a central regulatory role in myofibril development and stability [107]. In line with this, reduced myofibril density was detected in septal myectomy samples from HCM_{SMP} patients compared to HCM_{SMN} patients [18]. While the excessive microtubular response to cMyBP-C haploinsufficiency may be an attempt to maintain myofibril stability, it may aggravate cardiac dysfunction by altering cytoskeletal mechanical properties [95,105].

CONCLUSIONS

In summary, our data show that the hypertrophied muscle of HCM patients is characterized by an increased and stabilized tubular network which may be an adaptive response to cardiomyocyte growth. While this compensatory response may aid to stabilize cardiomyocyte architecture, this structural adaption may contribute to a reduced function of the HCM myocardium.

AUTHOR CONTRIBUTIONS

L.M.D., D.W.D.K., B.J.J.M.B and J.v.d.V. conceived, designed and coordinated the study and wrote the manuscript. L.M.D. and M.S. performed and/or analyzed the experiments. C.G.d.R., A.F.L.S., P.L.d.J. and M.M. provided the heart samples and patient data and gave input for the manuscript. All authors reviewed the manuscript.

FUNDING

We acknowledge the support from the Netherlands Cardiovascular Research Initiative: An initiative with support of the Dutch Heart Foundation, CVON2014-40 DOSIS and CVON-STW2016-14728 AFFIP.

ACKNOWLEDGMENTS

We would like to thank Ruud Zaremba for technical assistance with the LC3BII Western blots and Peter van de Ven for statistical analyses.

CONFLICTS OF INTEREST

The authors declare no conflict of interest.

REFERENCES

1. Semsarian, C.; Ingles, J.; Maron, M.S.; Maron, B.J. New perspectives on the prevalence of hypertrophic cardiomyopathy. *J. Am. Coll. Cardiol.* **2015**, *65*, 1249–1254, doi:10.1016/j.jacc.2015.01.019.
2. Michels, M.; Olivotto, I.; Asselbergs, F.W.; van der Velden, J. Life-long tailoring of management for patients with hypertrophic cardiomyopathy: Awareness and decision-making in changing scenarios. *Neth. Heart J.* **2017**, *25*, 186–199, doi:10.1007/s12471-016-0943-2.
3. van der Velden, J.; Stienen, G.J.M. Cardiac disorders and pathophysiology of sarcomeric proteins. *Physiol. Rev.* **2019**, *99*, 381–426, doi: 10.1152/physrev.00040.2017.
4. Maron, B.J.; Olivotto, I.; Spirito, P.; Casey, S.A.; Bellone, P.; Gohman, T.E.; Graham, K.J.; Burton, D.A.; Cecchi, F. Epidemiology of hypertrophic cardiomyopathy-related death: Revisited in a large non-referral-based patient population. *Circulation* **2000**, *102*, 858–864.
5. Ho, C.Y.; Day, S.M.; Ashley, E.A.; Michels, M.; Pereira, A.C.; Jacoby, D.; Cirino, A.L.; Fox, J.C.; Lakdawala, N.K.; Ware, J.S.; et al. Genotype and lifetime burden of disease in hypertrophic cardiomyopathy: Insights from the sarcomeric human cardiomyopathy registry (share). *Circulation* **2018**, *138*, 1387–1398, doi:10.1161/CIRCULATIONAHA.117.033200.
6. Willis, M.S.; Patterson, C. Proteotoxicity and cardiac dysfunction--alzheimer's disease of the heart? *N. Engl. J. Med.* **2013**, *368*, 455–464, doi:10.1056/NEJMra1106180.
7. Henning, R.H.; Brundel, B. Proteostasis in cardiac health and disease. *Nat. Rev. Cardiol.* **2017**, *14*, 637–653, doi:10.1038/nrcardio.2017.89.
8. Wang, X.; Robbins, J. Heart failure and protein quality control. *Circ Res* **2006**, *99*, 1315–1328, 10.1161/01.RES.0000252342.61447.a2.
9. Wang, X.; Su, H.; Ranek, M.J. Protein quality control and degradation in cardiomyocytes. *J. Mol. Cell Cardiol.* **2008**, *45*, 11–27, doi:10.1016/j.yjmcc.2008.03.025.
10. Latchman, D.S. Heat shock proteins and cardiac protection. *Cardiovasc Res.* **2001**, *51*, 637–646.
11. Tannous, P.; Zhu, H.; Nemchenko, A.; Berry, J.M.; Johnstone, J.L.; Shelton, J.M.; Miller, F.J., Jr.; Rothermel, B.A.; Hill, J.A. Intracellular protein aggregation is a proximal trigger of cardiomyocyte autophagy. *Circulation* **2008**, *117*, 3070–3078, doi:10.1161/CIRCULATIONAHA.107.763870.
12. Sontag, E.M.; Vonk, W.I.M.; Frydman, J. Sorting out the trash: The spatial nature of eukaryotic protein quality control. *Curr. Opin. Cell Biol.* **2014**, *26*, 139–146, doi: 10.1016/j.ceb.2013.12.006.
13. Marston, S.; Copeland, O.; Jacques, A.; Livesey, K.; Tsang, V.; McKenna, W.J.; Jalilzadeh, S.; Carballo, S.; Redwood, C.; Watkins, H. Evidence from human myectomy samples that mybpc3 mutations cause hypertrophic cardiomyopathy through haploinsufficiency. *Circ. Res.* **2009**, *105*, 219–222, doi:10.1161/CIRCRESAHA.109.202440.
14. Seidman, J.G.; Seidman, C. The genetic basis for cardiomyopathy: From mutation identification to mechanistic paradigms. *Cell* **2001**, *104*, 557–567.
15. Vriesendorp, P.A.; Schinkel, A.F.; Soliman, O.I.; Kofflard, M.J.; de Jong, P.L.; van Herwerden, L.A.; Ten Cate, F.J.; Michels, M. Long-term benefit of myectomy and anterior mitral leaflet extension in obstructive hypertrophic cardiomyopathy. *Am. J. Cardiol.* **2015**, *115*, 670–675, doi:10.1016/j.amjcard.2014.12.017.

16. van Velzen, H.G.; Vriesendorp, P.A.; Oldenburg, R.A.; van Slegtenhorst, M.A.; van der Velden, J.; Schinkel, A.F.L.; Michels, M. Value of genetic testing for the prediction of long-term outcome in patients with hypertrophic cardiomyopathy. *Am. J. Cardiol.* **2016**, *118*, 881–887, doi:10.1016/j.amjcard.2016.06.038.
17. Parbhudayal, R.Y.; Garra, A.R.; Gotte, M.J.W.; Michels, M.; Pei, J.; Harakalova, M.; Asselbergs, F.W.; van Rossum, A.C.; van der Velden, J.; Kuster, D.W.D. Variable cardiac myosin binding protein-c expression in the myofilaments due to mybpc3 mutations in hypertrophic cardiomyopathy. *J. Mol. Cell Cardiol.* **2018**, *123*, 59–63, doi:10.1016/j.yjmcc.2018.08.023.
18. Witjas-Paalberends, E.R.; Piroddi, N.; Stam, K.; van Dijk, S.J.; Oliviera, V.S.; Ferrara, C.; Scellini, B.; Hazebroek, M.; ten Cate, F.J.; van Slegtenhorst, M. et al. Mutations in myh7 reduce the force generating capacity of sarcomeres in human familial hypertrophic cardiomyopathy. *Cardiovasc Res.* **2013**, *99*, 432–441, doi:10.1093/cvr/cvt119.
19. Witjas-Paalberends, E.R.; Guclu, A.; Germans, T.; Knaapen, P.; Harms, H.J.; Vermeer, A.M.; Christiaans, I.; Wilde, A.A.; Dos Remedios, C.; Lammertsma, A.A. et al. Gene-specific increase in the energetic cost of contraction in hypertrophic cardiomyopathy caused by thick filament mutations. *Cardiovasc Res.* **2014**, *103*, 248–257, doi:10.1093/cvr/cvu127.
20. Nijenkamp, L.; Bollen, I.A.E.; van Velzen, H.G.; Regan, J.A.; van Slegtenhorst, M.; Niessen, H.W.M.; Schinkel, A.F.L.; Kruger, M.; Poggesi, C.; Ho, C.Y. et al. Sex differences at the time of myectomy in hypertrophic cardiomyopathy. *Circ. Heart Fail.* **2018**, *11*, e004133, doi:10.1161/CIRCHEARTFAILURE.117.004133.
21. van Dijk, S.J.; Paalberends, E.R.; Najafi, A.; Michels, M.; Sadayappan, S.; Carrier, L.; Boontje, N.M.; Kuster, D.W.; van Slegtenhorst, M.; Dooijes, D. et al. Contractile dysfunction irrespective of the mutant protein in human hypertrophic cardiomyopathy with normal systolic function. *Circ. Heart Fail.* **2012**, *5*, 36–46, doi:10.1161/CIRCHEARTFAILURE.111.963702.
22. Kuster, D.W.; Mulders, J.; Ten Cate, F.J.; Michels, M.; Dos Remedios, C.G.; da Costa Martins, P.A.; van der Velden, J.; Oudejans, C.B. Microrna transcriptome profiling in cardiac tissue of hypertrophic cardiomyopathy patients with mybpc3 mutations. *J. Mol. Cell Cardiol.* **2013**, *65*, 59–66, doi:10.1016/j.yjmcc.2013.09.012.
23. Sequeira, V.; Najafi, A.; Wijnker, P.J.; Dos Remedios, C.G.; Michels, M.; Kuster, D.W.; van der Velden, J. Adp-stimulated contraction: A predictor of thin-filament activation in cardiac disease. *Proc. Natl. Acad. Sci. USA* **2015**, *112*, E7003-7012, doi:10.1073/pnas.1513843112.
24. van Dijk, S.J.; Boontje, N.M.; Heymans, M.W.; Ten Cate, F.J.; Michels, M.; Dos Remedios, C.; Dooijes, D.; van Slegtenhorst, M.A.; van der Velden, J.; Stienen, G.J. Preserved cross-bridge kinetics in human hypertrophic cardiomyopathy patients with mybpc3 mutations. *Pflug. Arch.* **2014**, *466*, 1619–1633, doi:10.1007/s00424-013-1391-0.
25. Sequeira, V.; Wijnker, P.J.; Nijenkamp, L.L.; Kuster, D.W.; Najafi, A.; Witjas-Paalberends, E.R.; Regan, J.A.; Boontje, N.; Ten Cate, F.J.; Germans, T. et al. Perturbed length-dependent activation in human hypertrophic cardiomyopathy with missense sarcomeric gene mutations. *Circ. Res.* **2013**, *112*, 1491–1505, doi:10.1161/CIRCRESAHA.111.300436.
26. Witjas-Paalberends, E.R.; Ferrara, C.; Scellini, B.; Piroddi, N.; Montag, J.; Tesi, C.; Stienen, G.J.; Michels, M.; Ho, C.Y.; Kraft, T., et al. Faster cross-bridge detachment and increased tension cost in human hypertrophic cardiomyopathy with the r403q myh7 mutation. *J. Physiol.* **2014**, *592*, 3257–3272, doi:10.1113/jphysiol.2014.274571.

27. Robinson, A.A.; Dunn, M.J.; McCormack, A.; dos Remedios, C.; Rose, M.L. Protective effect of phosphorylated hsp27 in coronary arteries through actin stabilization. *J. Mol. Cell Cardiol.* **2010**, *49*, 370–379, doi:10.1016/j.yjmcc.2010.06.004.
28. Polden, J.; McManus, C.A.; Dos Remedios, C.; Dunn, M.J. A 2-d gel reference map of the basic human heart proteome. *Proteomics* **2011**, *11*, 3582–3586, doi:10.1002/pmic.201000182.
29. Narolska, N.A.; Piroddi, N.; Belus, A.; Boontje, N.M.; Scellini, B.; Deppermann, S.; Zaremba, R.; Musters, R.J.; dos Remedios, C.; Jaquet, K., et al. Impaired diastolic function after exchange of endogenous troponin i with c-terminal truncated troponin i in human cardiac muscle. *Circ. Res.* **2006**, *99*, 1012–1020, doi:10.1161/01.RES.0000248753.30340.af.
30. Zhang, P.; Kirk, J.A.; Ji, W.; dos Remedios, C.G.; Kass, D.A.; Van Eyk, J.E.; Murphy, A.M. Multiple reaction monitoring to identify site-specific troponin i phosphorylated residues in the failing human heart. *Circulation* **2012**, *126*, 1828–1837, doi:10.1161/CIRCULATIONAHA.112.096388.
31. Kooij, V.; Zhang, P.; Piersma, S.R.; Sequeira, V.; Boontje, N.M.; Wijnker, P.J.; Jimenez, C.R.; Jaquet, K.E.; dos Remedios, C.; Murphy, A.M., et al. Pkcalpha-specific phosphorylation of the troponin complex in human myocardium: A functional and proteomics analysis. *Plos One* **2013**, *8*, e74847, doi:10.1371/journal.pone.0074847.
32. Wijnker, P.J.; Li, Y.; Zhang, P.; Foster, D.B.; dos Remedios, C.; Van Eyk, J.E.; Stienen, G.J.; Murphy, A.M.; van der Velden, J. A novel phosphorylation site, serine 199, in the c-terminus of cardiac troponin i regulates calcium sensitivity and susceptibility to calpain-induced proteolysis. *J. Mol. Cell Cardiol.* **2015**, *82*, 93–103, doi:10.1016/j.yjmcc.2015.03.006.
33. Krysiak, J.; Unger, A.; Beckendorf, L.; Hamdani, N.; von Frieling-Salewsky, M.; Redfield, M.M.; Dos Remedios, C.G.; Sheikh, F.; Gergs, U.; Boknik, P., et al. Protein phosphatase 5 regulates titin phosphorylation and function at a sarcomere-associated mechanosensor complex in cardiomyocytes. *Nat. Commun.* **2018**, *9*, 262, doi:10.1038/s41467-017-02483-3.
34. Gotzmann, M.; Grabbe, S.; Schone, D.; von Frieling-Salewsky, M.; Dos Remedios, C.G.; Strauch, J.; Bechtel, M.; Dietrich, J.W.; Tannapfel, A.; Mugge, A., et al. Alterations in titin properties and myocardial fibrosis correlate with clinical phenotypes in hemodynamic subgroups of severe aortic stenosis. *Jacc. Basic Transl. Sci.* **2018**, *3*, 335–346, doi:10.1016/j.jacbts.2018.02.002.
35. Kruger, M.; Kotter, S.; Grutzner, A.; Lang, P.; Andresen, C.; Redfield, M.M.; Butt, E.; dos Remedios, C.G.; Linke, W.A. Protein kinase g modulates human myocardial passive stiffness by phosphorylation of the titin springs. *Circ. Res.* **2009**, *104*, 87–94, doi:10.1161/CIRCRESAHA.108.184408.
36. Kotter, S.; Gout, L.; Von Frieling-Salewsky, M.; Muller, A.E.; Helling, S.; Marcus, K.; Dos Remedios, C.; Linke, W.A.; Kruger, M. Differential changes in titin domain phosphorylation increase myofilament stiffness in failing human hearts. *Cardiovasc Res.* **2013**, *99*, 648–656, doi:10.1093/cvr/cvt144.
37. Huang, Z.P.; Ding, Y.; Chen, J.; Wu, G.; Kataoka, M.; Hu, Y.; Yang, J.H.; Liu, J.; Drakos, S.G.; Selzman, C.H. et al. Long non-coding rnas link extracellular matrix gene expression to ischemic cardiomyopathy. *Cardiovasc Res.* **2016**, *112*, 543–554, doi:10.1093/cvr/cvw201.
38. Lin, Z.; Guo, H.; Cao, Y.; Zohrabian, S.; Zhou, P.; Ma, Q.; VanDusen, N.; Guo, Y.; Zhang, J.; Stevens, S.M. et al. Acetylation of vgll4 regulates hippo-yap signaling and postnatal cardiac growth. *Dev. Cell* **2016**, *39*, 466–479, doi:10.1016/j.devcel.2016.09.005.
39. Kong, S.W.; Hu, Y.W.; Ho, J.W.; Ikeda, S.; Polster, S.; John, R.; Hall, J.L.; Bisping, E.; Pieske, B.; dos Remedios, C.G. et al. Heart failure-associated changes in rna splicing of sarcomere genes. *Circ. Cardiovasc. Genet.* **2010**, *3*, 138–146, doi:10.1161/CIRCGENETICS.109.904698.

40. Lu, Z.; Xu, X.; Hu, X.; Lee, S.; Traverse, J.H.; Zhu, G.; Fassett, J.; Tao, Y.; Zhang, P.; dos Remedios, C. et al. Oxidative stress regulates left ventricular pde5 expression in the failing heart. *Circulation* **2010**, *121*, 1474–1483, doi:10.1161/CIRCULATIONAHA.109.906818.
41. Fermin, D.R.; Barac, A.; Lee, S.; Polster, S.P.; Hannenhalli, S.; Bergemann, T.L.; Grindle, S.; Dyke, D.B.; Pagani, F.; Miller, L.W. et al. Sex and age dimorphism of myocardial gene expression in nonischemic human heart failure. *Circ. Cardiovasc. Genet.* **2008**, *1*, 117–125, doi:10.1161/CIRCGENETICS.108.802652.
42. McNamara, J.W.; Li, A.; Lal, S.; Bos, J.M.; Harris, S.P.; van der Velden, J.; Ackerman, M.J.; Cooke, R.; Dos Remedios, C.G. Mybpc3 mutations are associated with a reduced super-relaxed state in patients with hypertrophic cardiomyopathy. *Plos One* **2017**, *12*, e0180064, doi:10.1371/journal.pone.0180064.
43. Montag, J.; Syring, M.; Rose, J.; Weber, A.L.; Ernstberger, P.; Mayer, A.K.; Becker, E.; Keyser, B.; Dos Remedios, C.; Perrot, A. et al. Intrinsic myh7 expression regulation contributes to tissue level allelic imbalance in hypertrophic cardiomyopathy. *J. Muscle Res. Cell Motil.* **2017**, *38*, 291–302, doi:10.1007/s10974-017-9486-4.
44. Montag, J.; Kowalski, K.; Makul, M.; Ernstberger, P.; Radocaj, A.; Beck, J.; Becker, E.; Tripathi, S.; Keyser, B.; Muhlfeld, C. et al. Burst-like transcription of mutant and wildtype myh7-alleles as possible origin of cell-to-cell contractile imbalance in hypertrophic cardiomyopathy. *Front Physiol.* **2018**, *9*, 359, doi:10.3389/fphys.2018.00359.
45. Iorga, B.; Schwanke, K.; Weber, N.; Wendland, M.; Greten, S.; Piep, B.; Dos Remedios, C.G.; Martin, U.; Zweigerdt, R.; Kraft, T. et al. Differences in contractile function of myofibrils within human embryonic stem cell-derived cardiomyocytes vs. Adult ventricular myofibrils are related to distinct sarcomeric protein isoforms. *Front Physiol.* **2017**, *8*, 1111, doi:10.3389/fphys.2017.01111.
46. Messer, A.E.; Gallon, C.E.; McKenna, W.J.; Dos Remedios, C.G.; Marston, S.B. The use of phosphate-affinity sds-page to measure the cardiac troponin i phosphorylation site distribution in human heart muscle. *Proteom. Clin. Appl.* **2009**, *3*, 1371–1382, doi:10.1002/prca.200900071.
47. Hoskins, A.C.; Jacques, A.; Bardswell, S.C.; McKenna, W.J.; Tsang, V.; dos Remedios, C.G.; Ehler, E.; Adams, K.; Jalilzadeh, S.; Avkiran, M., et al. Normal passive viscoelasticity but abnormal myofibrillar force generation in human hypertrophic cardiomyopathy. *J. Mol. Cell Cardiol.* **2010**, *49*, 737–745, doi:10.1016/j.yjmcc.2010.06.006.
48. Bayliss, C.R.; Jacques, A.M.; Leung, M.C.; Ward, D.G.; Redwood, C.S.; Gallon, C.E.; Copeland, O.; McKenna, W.J.; Dos Remedios, C.; Marston, S.B. et al. Myofibrillar ca(2+) sensitivity is uncoupled from troponin i phosphorylation in hypertrophic obstructive cardiomyopathy due to abnormal troponin t. *Cardiovasc. Res.* **2013**, *97*, 500–508, doi:10.1093/cvr/cvs322.
49. Messer, A.E.; Bayliss, C.R.; El-Mezgueldi, M.; Redwood, C.S.; Ward, D.G.; Leung, M.C.; Papadaki, M.; Dos Remedios, C.; Marston, S.B. Mutations in troponin t associated with hypertrophic cardiomyopathy increase ca(2+)-sensitivity and suppress the modulation of ca(2+)-sensitivity by troponin i phosphorylation. *Arch. Biochem. Biophys.* **2016**, *601*, 113–120, doi:10.1016/j.abb.2016.03.027.
50. Mamidi, R.; Gresham, K.S.; Li, A.; dos Remedios, C.G.; Stelzer, J.E. Molecular effects of the myosin activator omecamtiv mecarbil on contractile properties of skinned myocardium lacking cardiac myosin binding protein-c. *J. Mol. Cell Cardiol.* **2015**, *85*, 262–272, doi:10.1016/j.yjmcc.2015.06.011.

51. Mamidi, R.; Li, J.; Gresham, K.S.; Verma, S.; Doh, C.Y.; Li, A.; Lal, S.; Dos Remedios, C.G.; Stelzer, J.E. Dose-dependent effects of the myosin activator omecamtiv mecarbil on cross-bridge behavior and force generation in failing human myocardium. *Circ. Heart Fail.* **2017**, *10*, doi:10.1161/CIRCHEARTFAILURE.117.004257.
52. Coats, C.J.; Heywood, W.E.; Virasami, A.; Ashrafi, N.; Syrris, P.; Dos Remedios, C.; Treibel, T.A.; Moon, J.C.; Lopes, L.R.; McGregor, C.G.A. et al. Proteomic analysis of the myocardium in hypertrophic obstructive cardiomyopathy. *Circ. Genom. Precis Med.* **2018**, *11*, e001974, doi:10.1161/CIRCGEN.117.001974.
53. Mollova, M.; Bersell, K.; Walsh, S.; Savla, J.; Das, L.T.; Park, S.Y.; Silberstein, L.E.; Dos Remedios, C.G.; Graham, D.; Colan, S., et al. Cardiomyocyte proliferation contributes to heart growth in young humans. *Proc. Natl. Acad. Sci. USA* **2013**, *110*, 1446–1451, doi:10.1073/pnas.1214608110.
54. Polizzotti, B.D.; Ganapathy, B.; Walsh, S.; Choudhury, S.; Ammanamanchi, N.; Bennett, D.G.; dos Remedios, C.G.; Haubner, B.J.; Penninger, J.M.; Kuhn, B. Neuregulin stimulation of cardiomyocyte regeneration in mice and human myocardium reveals a therapeutic window. *Sci. Transl. Med.* **2015**, *7*, 281ra245, doi:10.1126/scitranslmed.aaa5171.
55. Bollen, I.A.E.; Ehler, E.; Fleischanderl, K.; Bouwman, F.; Kempers, L.; Ricke-Hoch, M.; Hilfiker-Kleiner, D.; Dos Remedios, C.G.; Kruger, M.; Vink, A., et al. Myofilament remodeling and function is more impaired in peripartum cardiomyopathy compared with dilated cardiomyopathy and ischemic heart disease. *Am. J. Pathol.* **2017**, *187*, 2645–2658, doi:10.1016/j.ajpath.2017.08.022.
56. Bergmann, O.; Zdunek, S.; Felker, A.; Salehpour, M.; Alkass, K.; Bernard, S.; Sjostrom, S.L.; Szewczykowska, M.; Jackowska, T.; Dos Remedios, C., et al. Dynamics of cell generation and turnover in the human heart. *Cell* **2015**, *161*, 1566–1575, doi:10.1016/j.cell.2015.05.026.
57. Gomez-Arroyo, J.; Mizuno, S.; Szczepanek, K.; Van Tassell, B.; Natarajan, R.; dos Remedios, C.G.; Drake, J.I.; Farkas, L.; Kraskauskas, D.; Wijesinghe, D.S., et al. Metabolic gene remodeling and mitochondrial dysfunction in failing right ventricular hypertrophy secondary to pulmonary arterial hypertension. *Circ. Heart Fail.* **2013**, *6*, 136–144, doi:10.1161/CIRCHEARTFAILURE.111.966127.
58. Martin-Garrido, A.; Biesiadecki, B.J.; Salhi, H.E.; Shaifta, Y.; Dos Remedios, C.G.; Ayaz-Guner, S.; Cai, W.; Ge, Y.; Avkiran, M.; Kentish, J.C. Monophosphorylation of cardiac troponin-i at ser-23/24 is sufficient to regulate cardiac myofibrillar ca(2+) sensitivity and calpain-induced proteolysis. *J. Biol. Chem.* **2018**, *293*, 8588–8599, doi:10.1074/jbc.RA117.001292.
59. Piroddi, N.; Witjas-Paalberends, E.R.; Ferrara, C.; Ferrantini, C.; Vitale, G.; Scellini, B.; Wijnker, P.J.M.; Sequiera, V.; Dooijes, D.; Dos Remedios, C. et al. The homozygous k280n troponin t mutation alters cross-bridge kinetics and energetics in human hcm. *J. Gen. Physiol.* **2019**, *151*, 18–29, 10.1085/jgp.201812160.
60. Brocchieri, L.; Conway de Macario, E.; Macario, A.J. Hsp70 genes in the human genome: Conservation and differentiation patterns predict a wide array of overlapping and specialized functions. *Bmc. Evol. Biol.* **2008**, *8*, 19, doi:10.1186/1471-2148-8-19.
61. Soltys, B.J.; Gupta, R.S. Immunoelectron microscopic localization of the 60-kda heat shock chaperonin protein (hsp60) in mammalian cells. *Exp. Cell Res.* **1996**, *222*, 16–27, doi:10.1006/excr.1996.0003.
62. Dorsch, L.M.; Schuldt, M.; Knezevic, D.; Wiersma, M.; Kuster, D.W.D.; van der Velden, J.; Brundel, B. Untying the knot: Protein quality control in inherited cardiomyopathies. *Pflug. Arch.* **2018**, doi:10.1007/s00424-018-2194-0.

63. van Dijk, S.J.; Dooijes, D.; dos Remedios, C.; Michels, M.; Lamers, J.M.; Winegrad, S.; Schlossarek, S.; Carrier, L.; ten Cate, F.J.; Stienen, G.J., et al. Cardiac myosin-binding protein c mutations and hypertrophic cardiomyopathy: Haploinsufficiency, deranged phosphorylation, and cardiomyocyte dysfunction. *Circulation* **2009**, *119*, 1473–1483, doi:10.1161/CIRCULATIONAHA.108.838672.
64. Schuldt, M.; Pei, J.; Harakalova, M.; Dorsch, L.M.; Mokry, M.; Knol, J.C.; Pham, T.V.; Schelfhorst, T.; Piersma, S.R.; dos Remedios, C. et al. Detyrosinated tubulin as treatment target in genetic heart disease: Proteomic and functional studies in hypertrophic cardiomyopathy. Status: Manuscript in preparation.
65. Matsuyama, A.; Shimazu, T.; Sumida, Y.; Saito, A.; Yoshimatsu, Y.; Seigneurin-Berny, D.; Osada, H.; Komatsu, Y.; Nishino, N.; Khochbin, S. et al. In vivo destabilization of dynamic microtubules by hdac6-mediated deacetylation. *Embo J.* **2002**, *21*, 6820–6831.
66. Hubbert, C.; Guardiola, A.; Shao, R.; Kawaguchi, Y.; Ito, A.; Nixon, A.; Yoshida, M.; Wang, X.F.; Yao, T.P. Hdac6 is a microtubule-associated deacetylase. *Nature* **2002**, *417*, 455–458, doi:10.1038/417455a.
67. Ng, D.C.; Ng, I.H.; Yeap, Y.Y.; Badrian, B.; Tsoutsman, T.; McMullen, J.R.; Semsarian, C.; Bogoyevitch, M.A. Opposing actions of extracellular signal-regulated kinase (erk) and signal transducer and activator of transcription 3 (stat3) in regulating microtubule stabilization during cardiac hypertrophy. *J. Biol. Chem.* **2011**, *286*, 1576–1587, doi:10.1074/jbc.M110.128157.
68. Knowlton, A.A.; Kapadia, S.; Torre-Amione, G.; Durand, J.B.; Bies, R.; Young, J.; Mann, D.L. Differential expression of heat shock proteins in normal and failing human hearts. *J. Mol. Cell Cardiol.* **1998**, *30*, 811–818, doi:10.1006/jmcc.1998.0646.
69. Benjamin, I.J.; McMillan, D.R. Stress (heat shock) proteins: Molecular chaperones in cardiovascular biology and disease. *Circ. Res.* **1998**, *83*, 117–132.
70. Arrigo, A.P. Mammalian hspb1 (hsp27) is a molecular sensor linked to the physiology and environment of the cell. *Cell Stress Chaperones* **2017**, *22*, 517–529, doi:10.1007/s12192-017-0765-1.
71. Liu, L.; Zhang, X.; Qian, B.; Min, X.; Gao, X.; Li, C.; Cheng, Y.; Huang, J. Over-expression of heat shock protein 27 attenuates doxorubicin-induced cardiac dysfunction in mice. *Eur. J. Heart Fail.* **2007**, *9*, 762–769, doi:10.1016/j.ejheart.2007.03.007.
72. Efthymiou, C.A.; Mocanu, M.M.; de Belleroche, J.; Wells, D.J.; Latchmann, D.S.; Yellon, D.M. Heat shock protein 27 protects the heart against myocardial infarction. *Basic Res. Cardiol.* **2004**, *99*, 392–394, doi:10.1007/s00395-004-0483-6.
73. Zhang, X.; Min, X.; Li, C.; Benjamin, I.J.; Qian, B.; Zhang, X.; Ding, Z.; Gao, X.; Yao, Y.; Ma, Y., et al. Involvement of reductive stress in the cardiomyopathy in transgenic mice with cardiac-specific overexpression of heat shock protein 27. *Hypertension* **2010**, *55*, 1412–1417, doi:10.1161/HYPERTENSIONAHA.109.147066.
74. Knowlton, A.A.; Srivatsa, U. Heat-shock protein 60 and cardiovascular disease: A paradoxical role. *Future Cardiol.* **2008**, *4*, 151–161, doi:10.2217/14796678.4.2.151.
75. Pellegrino, M.W.; Nargund, A.M.; Haynes, C.M. Signaling the mitochondrial unfolded protein response. *Biochim. Biophys. Acta* **2013**, *1833*, 410–416, doi:10.1016/j.bbamcr.2012.02.019.
76. Lin, L.; Kim, S.C.; Wang, Y.; Gupta, S.; Davis, B.; Simon, S.I.; Torre-Amione, G.; Knowlton, A.A. Hsp60 in heart failure: Abnormal distribution and role in cardiac myocyte apoptosis. *Am. J. Physiol. Heart Circ. Physiol.* **2007**, *293*, H2238-2247, doi:10.1152/ajpheart.00740.2007.
77. Sidorik, L.; Kyyamova, R.; Bobyk, V.; Kapustian, L.; Rozhko, O.; Vigontina, O.; Ryabenko, D.; Danko, I.; Maksymchuk, O.; Kovalenko, V.N. et al. Molecular chaperone, hsp60, and cytochrome p450 2e1 co-expression in dilated cardiomyopathy. *Cell Biol. Int.* **2005**, *29*, 51–55, doi:10.1016/j.cellbi.2004.11.011.

78. Unno, K.; Isobe, S.; Izawa, H.; Cheng, X.W.; Kobayashi, M.; Hirashiki, A.; Yamada, T.; Harada, K.; Ohshima, S.; Noda, A. et al. Relation of functional and morphological changes in mitochondria to myocardial contractile and relaxation reserves in asymptomatic to mildly symptomatic patients with hypertrophic cardiomyopathy. *Eur. Heart J.* **2009**, *30*, 1853–1862, doi:10.1093/eurheartj/ehp184.
79. Roux, A.F.; Nguyen, V.T.; Squire, J.A.; Cox, D.W. A heat shock gene at 14q22: Mapping and expression. *Hum. Mol. Genet.* **1994**, *3*, 1819–1822.
80. Glazier, A.A.; Hafeez, N.; Mellacheruvu, D.; Basrur, V.; Nesvizhskii, A.I.; Lee, L.M.; Shao, H.; Tang, V.; Yob, J.M.; Gestwicki, J.E. et al. Hsc70 is a chaperone for wild-type and mutant cardiac myosin binding protein c. *JCI Insight* **2018**, *3*, doi:10.1172/jci.insight.99319.
81. Kumarapeli, A.R.; Su, H.; Huang, W.; Tang, M.; Zheng, H.; Horak, K.M.; Li, M.; Wang, X. Alpha b-crystallin suppresses pressure overload cardiac hypertrophy. *Circ. Res.* **2008**, *103*, 1473–1482, doi:10.1161/CIRCRESAHA.108.180117.
82. Kee, H.J.; Eom, G.H.; Joung, H.; Shin, S.; Kim, J.R.; Cho, Y.K.; Choe, N.; Sim, B.W.; Jo, D.; Jeong, M.H. et al. Activation of histone deacetylase 2 by inducible heat shock protein 70 in cardiac hypertrophy. *Circ. Res.* **2008**, *103*, 1259–1269, 10.1161/01.RES.0000338570.27156.84.
83. Bernardo, B.C.; Weeks, K.L.; Patterson, N.L.; McMullen, J.R. Hsp70: Therapeutic potential in acute and chronic cardiac disease settings. *Future Med. Chem.* **2016**, *8*, 2177–2183, doi:10.4155/fmc-2016-0192.
84. Day, S.M. The ubiquitin proteasome system in human cardiomyopathies and heart failure. *Am. J. Physiol. Heart Circ. Physiol.* **2013**, *304*, H1283-1293, doi:10.1152/ajpheart.00249.2012.
85. Vos, M.J.; Zijlstra, M.P.; Kanon, B.; van Waarde-Verhagen, M.A.; Brunt, E.R.; Oosterveld-Hut, H.M.; Carra, S.; Sibon, O.C.; Kampinga, H.H. Hspb7 is the most potent polyq aggregation suppressor within the hspb family of molecular chaperones. *Hum. Mol. Genet.* **2010**, *19*, 4677–4693, doi:10.1093/hmg/ddq398.
86. Villard, E.; Perret, C.; Gary, F.; Proust, C.; Dilanian, G.; Hengstenberg, C.; Ruppert, V.; Arbustini, E.; Wichter, T.; Germain, M., et al. A genome-wide association study identifies two loci associated with heart failure due to dilated cardiomyopathy. *Eur. Heart J.* **2011**, *32*, 1065–1076, doi:10.1093/eurheartj/ehr105.
87. Mercer, E.J.; Lin, Y.F.; Cohen-Gould, L.; Evans, T. Hspb7 is a cardioprotective chaperone facilitating sarcomeric proteostasis. *Dev. Biol.* **2018**, *435*, 41–55, doi:10.1016/j.ydbio.2018.01.005.
88. Lavandero, S.; Troncoso, R.; Rothermel, B.A.; Martinet, W.; Sadoshima, J.; Hill, J.A. Cardiovascular autophagy: Concepts, controversies, and perspectives. *Autophagy* **2013**, *9*, 1455–1466, doi:10.4161/auto.25969.
89. Weng, L.Q.; Zhang, W.B.; Ye, Y.; Yin, P.P.; Yuan, J.; Wang, X.X.; Kang, L.; Jiang, S.S.; You, J.Y.; Wu, J. et al. Aliskiren ameliorates pressure overload-induced heart hypertrophy and fibrosis in mice. *Acta Pharm. Sin.* **2014**, *35*, 1005–1014, doi:10.1038/aps.2014.45.
90. Samuel, J.L.; Bertier, B.; Bugaisky, L.; Marotte, F.; Swynghedauw, B.; Schwartz, K.; Rappaport, L. Different distributions of microtubules, desmin filaments and isomyosins during the onset of cardiac hypertrophy in the rat. *Eur. J. Cell Biol.* **1984**, *34*, 300–306.
91. Tagawa, H.; Rozich, J.D.; Tsutsui, H.; Narishige, T.; Kuppuswamy, D.; Sato, H.; McDermott, P.J.; Koide, M.; Cooper, G.t. Basis for increased microtubules in pressure-hypertrophied cardiocytes. *Circulation* **1996**, *93*, 1230–1243.
92. Stamenovic, D.; Mijailovich, S.M.; Tolic-Norrelykke, I.M.; Chen, J.; Wang, N. Cell prestress. Ii. Contribution of microtubules. *Am. J. Physiol. Cell Physiol.* **2002**, *282*, C617-624, doi:10.1152/ajpcell.00271.2001.

93. Watkins, S.C.; Samuel, J.L.; Marotte, F.; Bertier-Savalle, B.; Rappaport, L. Microtubules and desmin filaments during onset of heart hypertrophy in rat: A double immunoelectron microscope study. *Circ. Res.* **1987**, *60*, 327–336.
94. Heling, A.; Zimmermann, R.; Kostin, S.; Maeno, Y.; Hein, S.; Devaux, B.; Bauer, E.; Klovekorn, W.P.; Schlepper, M.; Schaper, W. et al. Increased expression of cytoskeletal, linkage, and extracellular proteins in failing human myocardium. *Circ. Res.* **2000**, *86*, 846–853.
95. Robison, P.; Caporizzo, M.A.; Ahmadzadeh, H.; Bogush, A.I.; Chen, C.Y.; Margulies, K.B.; Shenoy, V.B.; Prosser, B.L. Detyrosinated microtubules buckle and bear load in contracting cardiomyocytes. *Science* **2016**, *352*, aaf0659, doi:10.1126/science.aaf0659.
96. Decker, R.S.; Decker, M.L.; Nakamura, S.; Zhao, Y.S.; Hedjbeli, S.; Harris, K.R.; Klocke, F.J. Hsc73-tubulin complex formation during low-flow ischemia in the canine myocardium. *Am. J. Physiol. Heart Circ. Physiol.* **2002**, *283*, H1322-1333, doi:10.1152/ajpheart.00062.2002.
97. Lopez-Fanarraga, M.; Avila, J.; Guasch, A.; Coll, M.; Zabala, J.C. Review: Postchaperonin tubulin folding cofactors and their role in microtubule dynamics. *J. Struct Biol.* **2001**, *135*, 219–229, doi:10.1006/jsbi.2001.4386.
98. Sanchez, C.; Padilla, R.; Paciucci, R.; Zabala, J.C.; Avila, J. Binding of heat-shock protein 70 (hsp70) to tubulin. *Arch Biochem. Biophys.* **1994**, *310*, 428–432, doi:10.1006/abbi.1994.1188.
99. Ohto-Fujita, E.; Fujita, Y.; Atomi, Y. Analysis of the alphab-crystallin domain responsible for inhibiting tubulin aggregation. *Cell Stress Chaperones* **2007**, *12*, 163–171.
100. Xu, Z.; Schaedel, L.; Portran, D.; Aguilar, A.; Gaillard, J.; Marinkovich, M.P.; Thery, M.; Nachury, M.V. Microtubules acquire resistance from mechanical breakage through intralumenal acetylation. *Science* **2017**, *356*, 328–332, doi:10.1126/science.aai8764.
101. Geeraert, C.; Ratier, A.; Pfisterer, S.G.; Perdiz, D.; Cantaloube, I.; Rouault, A.; Pattingre, S.; Proikas-Cezanne, T.; Codogno, P.; Pous, C. Starvation-induced hyperacetylation of tubulin is required for the stimulation of autophagy by nutrient deprivation. *J. Biol. Chem.* **2010**, *285*, 24184–24194, doi:10.1074/jbc.M109.091553.
102. McLendon, P.M.; Ferguson, B.S.; Osinska, H.; Bhuiyan, M.S.; James, J.; McKinsey, T.A.; Robbins, J. Tubulin hyperacetylation is adaptive in cardiac proteotoxicity by promoting autophagy. *Proc. Natl. Acad. Sci. USA* **2014**, *111*, E5178-5186, doi:10.1073/pnas.1415589111.
103. Mackeh, R.; Lorin, S.; Ratier, A.; Mejdoubi-Charef, N.; Baillet, A.; Bruneel, A.; Hamai, A.; Codogno, P.; Pous, C.; Perdiz, D. Reactive oxygen species, amp-activated protein kinase, and the transcription cofactor p300 regulate alpha-tubulin acetyltransferase-1 (alphatat-1/mec-17)-dependent microtubule hyperacetylation during cell stress. *J. Biol. Chem.* **2014**, *289*, 11816–11828, doi:10.1074/jbc.M113.507400.
104. Li, L.; Yang, X.J. Tubulin acetylation: Responsible enzymes, biological functions and human diseases. *Cell Mol. Life Sci.* **2015**, *72*, 4237–4255, doi:10.1007/s00018-015-2000-5.
105. Caporizzo, M.A.; Chen, C.Y.; Salomon, A.K.; Margulies, K.B.; Prosser, B.L. Microtubules provide a viscoelastic resistance to myocyte motion. *Biophys. J.* **2018**, *115*, 1796–1807, doi:10.1016/j.bpj.2018.09.019.
106. DePristo, M.A.; Weinreich, D.M.; Hartl, D.L. Missense meanderings in sequence space: A biophysical view of protein evolution. *Nat. Rev. Genet.* **2005**, *6*, 678–687, doi:10.1038/nrg1672.
107. Ehler, E.; Gautel, M. The sarcomere and sarcomerogenesis. *Adv. Exp. Med. Biol.* **2008**, *642*, 1–14.

THE SUPPLEMENTARY DATA IS AVAILABLE ONLINE:

https://www.mdpi.com/2073-4409/8/7/741#supplementary

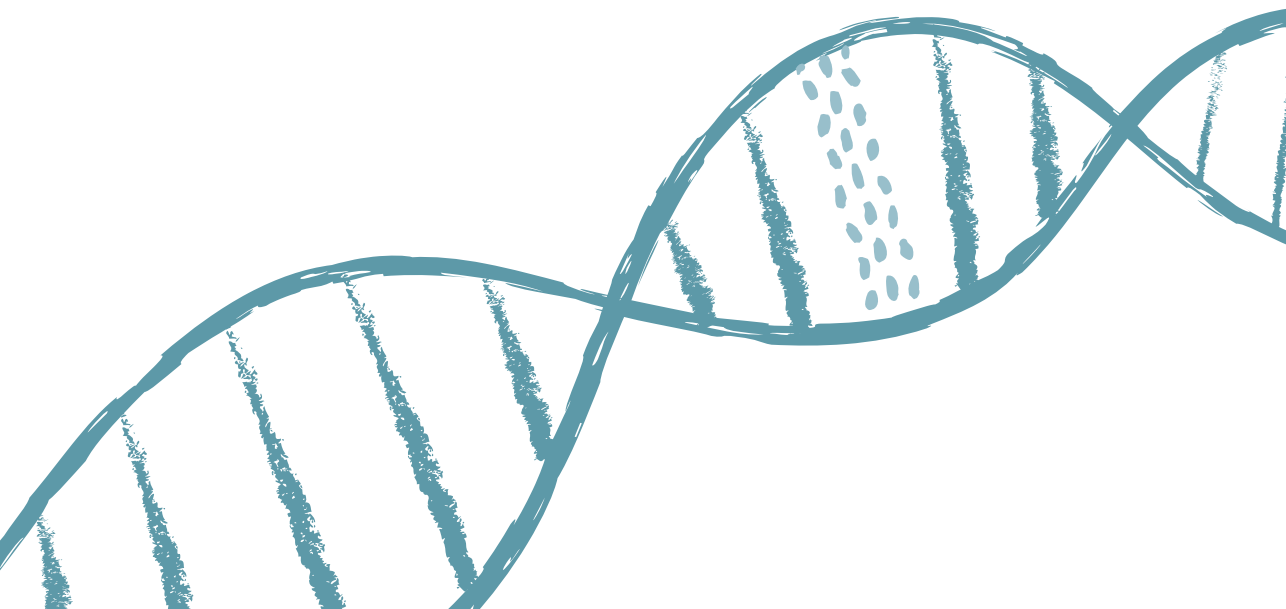

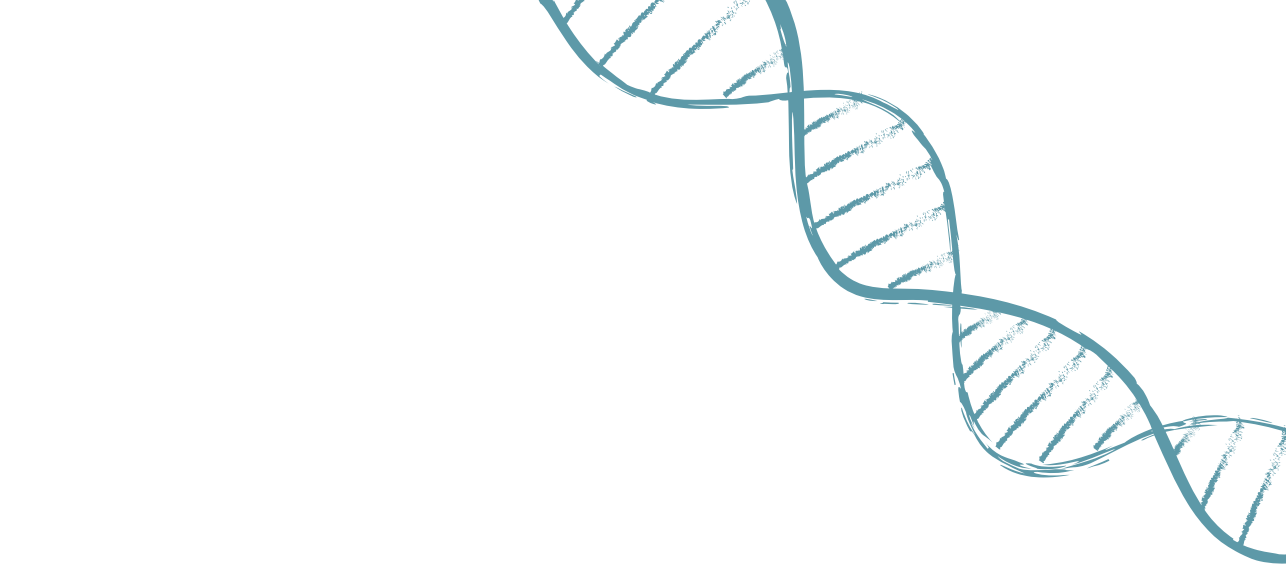

PART 2
OMICS-STUDIES TO IDENTIFY NOVEL DISEASE MODIFIERS

PROTEOMIC AND FUNCTIONAL STUDIES REVEAL DETYROSINATED TUBULIN AS TREATMENT TARGET IN SARCOMERE MUTATION-INDUCED HYPERTROPHIC CARDIOMYOPATHY

Maike Schuldt, Jiayi Pei, Magdalena Harakalova, Larissa M. Dorsch, Saskia Schlossarek, Michal Mokry, Jaco C. Knol, Thang V. Pham, Tim Schelfhorst, Sander R. Piersma, Cris dos Remedios, Michiel Dalinghaus, Michelle Michels, Folkert W. Asselbergs, Marie-Jo Moutin, Lucie Carrier, Connie R. Jimenez, Jolanda van der Velden‡, Diederik W.D. Kuster‡

‡shared last author

Circulation: Heart Failure, 2021: p. CIRCHEARTFAILURE120007022.

(with Editorial)

5

ABSTRACT

Background: Hypertrophic cardiomyopathy (HCM) is the most common genetic heart disease. While ~50% of HCM patients carry a sarcomere gene mutation (HCM_{SMP}), the genetic background is unknown in the other half of the patients (sarcomere mutation-negative, HCM_{SMN}). Genotype-specific differences have been reported in cardiac function. Moreover, HCM_{SMN} patients have later disease onset and better prognosis than HCM_{SMP} patients. To define if genotype-specific derailments at the protein level may explain the heterogeneity in disease development, we performed a proteomic analysis in cardiac tissue from a clinically well-phenotyped HCM patient group.

Methods: A proteomics screen was performed in cardiac tissue from 39 HCM_{SMP}, 11 HCM_{SMN} patients and 8 non-failing controls. HCM patients had obstructive cardiomyopathy with left ventricular outflow tract obstruction and diastolic dysfunction. A novel *MYBPC3*$_{2373insG}$ mouse model was used to confirm functional relevance of our proteomic findings.

Results: In all HCM patient samples we found lower levels of metabolic pathway proteins and higher levels of extracellular matrix proteins. Levels of total and detyrosinated α-tubulin were markedly higher in HCM_{SMP} than in HCM_{SMN} and controls. Higher tubulin detyrosination was also found in two unrelated *MYBPC3* mouse models and its inhibition with parthenolide normalized contraction and relaxation time of isolated cardiomyocytes.

Conclusion: Our findings indicate that microtubules and especially its detyrosination contribute to the pathomechanism of HCM_{SMP} patients. This is of clinical importance since it represents a potential treatment target to improve cardiac function in HCM_{SMP} patients, whereas a beneficial effect may be limited in HCM_{SMN} patients.

CLINICAL PERSPECTIVE

What is new?

This study shows that the most prominent derailment at the protein level in cardiac tissue obtained during myectomy of HCM patients in an advanced disease stage is reduced levels of proteins involved in metabolic pathways. This is common for all genotypes.

The study further demonstrates that increased levels of detyrosinated tubulin are specific for sarcomere mutation-positive HCM patients.

The increase in tubulin detyrosination is resembled in a mouse model with the Dutch founder mutation *MYBPC3*$_{2373insG}$. Pharmacological inhibition of tubulin detyrosination normalizes contractile function in isolated cardiomyocytes.

What are the clinical implications?

Recent and ongoing clinical trials investigate the therapeutic effect of targeting the energy metabolism in HCM patients which is supported by our proteomic data showing metabolic derailment.

Lowering tubulin detyrosination presents a potential novel treatment strategy that may improve contractile function in sarcomere-mutation positive HCM patients. Since HCM is characterized by diastolic dysfunction, enhancing cardiomyocyte relaxation by lowering detyrosination of microtubules is considered to be beneficial for HCM patients.

This study provides evidence that there is a need for genotype-specific treatment in HCM. Due to differences in pathomechanism, not every therapeutic strategy may be beneficial in all patient groups.

INTRODUCTION

Hypertrophic cardiomyopathy (HCM) is characterized by diastolic dysfunction and asymmetric left ventricular (LV) hypertrophy, which lead to LV outflow tract obstruction (LVOTO) in the majority of cases[1]. Mutations in genes encoding sarcomere proteins cause HCM and are identified in more than half of the patients (sarcomere mutation-positive, HCM_{SMP}). The heterogeneity in genetic background of HCM is large with more than 1500 identified HCM-causing mutations[2]. Approximately 80% of mutations are located in *MYH7* and *MYBPC3*. Less frequent are mutations in *TNNT2* and *TNNI3*[3, 4]. Previous research in HCM mouse models and humans showed genotype-specific differences in cellular characteristics and cardiac remodeling and function. Gene-specific differences in cellular redox and mitochondrial function were reported in mice harboring a *MYH7* or *TNNT2* mutation[5]. In accordance with studies in HCM mouse models, studies on patient myectomy samples reported gene-specific differences in the response to calcium, ADP, protein kinase A, and length-dependent activation of myofilaments compared to non-failing cardiomyocytes[6, 7]. Also, a comparison of two different patient-specific induced pluripotent stem cell-derived cardiomyocyte cell lines, carrying either a mutation in *MYBPC3* or *TPM1*, showed differences in calcium handling and electrophysiological properties[8]. These in vitro studies are strengthened by clinical patient studies which revealed a more severe decline in myocardial efficiency in *MYH7* than in *MYBPC3* mutation carriers[9], accompanied by a different response to therapy[10]. Notably, there is also a large patient population in which a disease-causing mutation cannot be identified, the so-called sarcomere mutation-negative patients (HCM_{SMN}). While the cause of the disease in these patients is unknown, they present with the same clinical phenotype as HCM_{SMP} patients albeit at older age[3]. Moreover, recent data from the SHaRe registry indicate that HCM_{SMP} have a 2-fold greater risk of adverse outcomes than HCM_{SMN}[11]. Whereas LVOTO can be invasively corrected by surgical myectomy, other symptoms can only be managed by pharmacological therapies, which do not halt or reverse cardiac disease[1]. Knowledge about the cellular changes that cause cardiac dysfunction and hypertrophy in HCM patients is needed to design new therapies.

The main goal of this study was to define HCM- and genotype-specific derailments at the protein level, which may explain the heterogeneity in cardiac characteristics and disease initiation and progression. Therefore, we used an unbiased proteomics approach in a large number of myectomy samples from a clinically well-characterized HCM patient group with (HCM_{SMP}) and without (HCM_{SMN}) sarcomere mutations. We show that lower levels of metabolic pathway proteins and higher levels of extracellular matrix (ECM) proteins are the most prominent genotype-independent HCM-specific disease characteristics at the time of myectomy. However, abundance and detyrosination of α-tubulin was significantly higher in HCM_{SMP} than in non-failing (NF) controls, with intermediate levels in HCM_{SMN}. Recent studies in human heart failure identified a

central role for detyrosinated microtubules in regulating cardiomyocyte function and demonstrated the functional benefit upon reversal of this modification[12, 13]. Our study in a European HCM patient cohort and genetic HCM mouse models strengthens the concept that targeting the microtubule network represents a therapeutic strategy to correct impaired function, and extends it to HCM caused by sarcomere mutations.

METHODS

The proteomics data have been deposited to the ProteomeXchange Consortium via the PRIDE partner repository with the dataset identifier PXD012467 and are publicly available (http://proteomecentral.proteomexchange.org/cgi/GetDataset?ID=PXD012467).

Human cardiac samples

Tissue of the IVS of 50 HCM patients was obtained during myectomy surgery to relieve LVOTO or after heart transplantation (1 sample, HCM 164). Samples of IVS from 8 healthy NF donors (5 males, 3 females; mean age 45.9 ± 9.7 years) with no history of cardiac abnormalities was obtained from the Sydney Heart Bank (HREC Univ Sydney 2012/030) and served as controls. The parameters of all HCM and NF individuals are summarized in *Table I*. In this table we organized HCM patients based on their genotype into 5 sub-groups: Patients with the Dutch *MYBPC3* founder mutation (2373insG), where the truncating mutation resulted in MYBPC3 haploinsufficiency[14]; Patients with *MYBPC3* mutations other than the 2373insG mutation of which 81.8% were truncating mutations as well; Patients with *MYH7* mutations; Patients with mutations in less frequently affected sarcomere genes (*TNNT2*, *TNNI3* and *MYL2*); and HCM_{SMN} patients. In line with studies in other cohorts[15], almost all mutations in *MYBPC3* were truncating mutations, whereas mutations in other sarcomeric proteins were missense except the truncating mutation c.814C>T in *TNNT2*.

Proteomics analysis

Tissue homogenization

Pulverized frozen tissue was homogenized in 40 µl/mg tissue 1x reducing sample buffer (106 mM Tris-HCl, 141 mM Tris-base, 2% lithium dodecyl sulfate (LDS), 10% glycerol, 0.51 mM EDTA, 0.22 mM SERVA Blue G250, 0.18 mM Phenol Red, 100 mM DTT) using a glass tissue grinder. Proteins were denatured by heating to 99°C for 5 min, after which samples were sonicated and heated again. Debris was removed by centrifugation at maximum speed for 10 min in a microcentrifuge (Sigma, 1-15K).

Protein fractionation

Proteins were separated using 1D SDS-PAGE. Samples from each group were loaded alternating on the gels to avoid bias. Equal volumes of sample (30 µl protein homogenate per sample, containing approximately 20-30 µg of protein) were loaded on a precast 4-12% NuPAGE Novex Bis-Tris 1.5 mm mini gel (Invitrogen). Electrophoresis was performed at 200V in NuPAGE MES SDS running buffer until the dye front reached the bottom of the gel. Gels were fixed in a solution of 50% ethanol and 3% phosphoric acid, and stained with 0.1% Coomassie brilliant blue G-250 solution (containing 34% methanol, 3% phosphoric acid and 15% ammonium sulfate). Images of all gels are provided in *Figure I*.

In-gel digestion and nano-LC-MS/MS

Each gel lane was cut into 5 pieces and in-gel digestion was performed as described previously[16]. Samples were measured by LC-MS per gel band starting at the high molecular weight (MW) fraction for all samples, before continuing with the next gel band until the last (low MW fraction) band. Injections alternated between all different group samples to minimize experimental bias between groups. Analysis of the experiment was performed as described in Piersma et al[17]. Peptides were separated using an Ultimate 3000 Nano LC-MS/MS system (Dionex LC-Packings, Amsterdam, The Netherlands) equipped with a 40 cm x 75 µm ID fused silica column custom packed with 1.9 µm ,120 Å ReproSil Pur C18 aqua (Dr Maisch GMBH, Ammerbuch-Entringen, Germany). Eluting peptides were ionized at a potential of + 2 kV into a Q Exactive mass spectrometer (Thermo Fisher, Bremen, Germany). MS/MS spectra were acquired at resolution 17,500 (at m/z 200) in the orbitrap using an AGC target value of $1x10^6$ charges, a maxIT of 60 ms and an underfill ratio of 0.1%. Dynamic exclusion was applied with a repeat count of 1 and an exclusion time of 30 s (additional details to in-gel-digestion and nano-LC-MS/MS are provided in the Supplemental Methods).

Data analysis

MS/MS spectra were searched against a Uniprot human reference proteome FASTA file (Swissprot_2017_03_human_canonical_and_isoform.fasta, 42161 entries) using MaxQuant version 1.5.4.1 (details to search settings are provided in the Supplemental Methods). The mass spectrometry proteomics data are provided in *Table V* and the raw data have been deposited to the ProteomeXchange Consortium via the PRIDE[18] partner repository with the dataset identifier PXD012467. Beta-binominal statistics were used to assess differential protein expression between groups, after normalization on the sum of the counts for each sample[19]. Proteins with a *p* value below 0.05 were considered significantly differentially expressed. Proteins which were present in less than 25% of the samples or had an average normalized count of less than 1.4 were excluded from further functional analysis. Principal component analysis was performed in R. Therefore quantile normalization and log2 transformation was performed on the normalized counts. The 95th Percentile was taken, the data median centered and the principal components calculated. Hierarchical clustering was performed after a statistical multi-

group comparison. Proteins with a raw p-value <0.05 were selected for the pathway analysis. Protein networks were generated utilizing the STRING database (Search Tool for the Retrieval of Interacting Genes/Proteins) and visualized with Cytoscape software[20]. Protein interaction networks were generated with ClusterONE and gene ontology (GO) analysis was performed using the BiNGO application in cytoscape[21, 22]. Heatmaps for a specific GOs were created with ToppGene Suite[23] and Graphpad Prism v7 software. Venn diagrams were created with InteractiVenn tool[24] and the layout modified if needed.

Animal experiments

The *MYBPC3*$_{2373insG}$ mouse model was engineered using CRISPR/Cas9 (details are provided in the Supplemental Methods). Echocardiographic phenotyping (Vevo 2100, Visualsonics) was performed on 7 homozygous *MYBPC3*$_{2373insG}$ mice (3 females, 4 males) and 8 WT littermates (3 females, 5 males). The age of the mice ranged from 20-28 weeks. Group size of 7 was determined by a power calculation to achieve a power of 0.8 and an alpha of 0.05 and to detect an effect size of 20% in echocardiography.

The *MYBPC3*$_{772G>A}$ mice were developed previously[25] and maintained on a blackswiss genetic background. Western blot analysis was performed of the cytosolic fraction of LV tissue in 6 homozygous *MYBPC3*$_{772G>A}$ mice (2 females, 4 males) and 6 WT littermates (2 females, 4 males). The age of these mice was 55-59 weeks.

Intact cardiomyocyte isolation and measurements

Intact adult cardiomyocytes were isolated from 4 WT and 6 homozygous *MYBPC3*$_{2373insG}$ mice as described previously[26]. Cells were suspended in plating medium composed of Medium 199 (Lonza), 1% penicillin/streptomycin and 5% bovine serum and plated on a laminin coated dish (10 µg/ml, Sigma-Aldrich). The cells were incubated for 1 hour at 37°C in humidified air with 5% CO_2 to let them attach to the coated dish. Afterwards, non-attached cells were removed by washing cells with pre-heated culture medium (Medium 199 (Lonza), 1% penicillin/streptomycin, 1x ITS supplement (Sigma-Aldrich) and 0.5 µM cytochalasin D (Life technologies)). Cells were incubated with DMSO (0.1% v/v) or 10 µM parthenolide (Sigma) for 2 hours. Contractility measurements were performed in tyrode solution (HEPES 10 mM, NaCl 133.5 mM, KCl 5 mM, NaH_2PO_4 1.2 mM, $MgSO_4$ 1.2 mM, glucose 11.1 mM, sodium pyruvate 5mM; pH 7.4 at 37°C) at 37°C using the MultiCell system (CytoCypher, the Netherlands). The dish was field-stimulated at 2 Hz, 25 V and a 4 ms pulse duration. Changes in sarcomere length were recorded with a high-speed camera and Ionoptix software (Ionoptix, Westwood MA, USA). The contractility profiles were analyzed with the automated batch analysis software CytoSolver (CytoCypher, Amsterdam, NL). An R^2 for peak and recovery fit >0.95 was selected as inclusion criteria for contraction data.

For protein analysis, cells were incubated with DMSO (0.1% v/v) or 10 µM parthenolide (Sigma) for 2 hours, washed with PBS and directly lysed in loading buffer.

Study approval

The study protocol for the human tissue samples was approved by the local medical ethics review committees and written informed consent was obtained from each patient prior to surgery.

Animal experiments were performed in accordance with the Guide for the Animal Care and Use Committee of the VU University Medical Center (VUmc) and with approval of the Animal Care Committee of the VUmc (CCD-number AVD114002016700) and conform the guidelines from Directive 2010/63/EU of the European Parliament on the protection of animals used for scientific purposes.

Extended methods section in the supplementary materials.

RESULTS

No major genotype-specific protein changes

We performed an unbiased proteomics approach to compare the protein expression profile of 50 interventricular septum (IVS) samples from HCM patients at the time of myectomy with 8 NF_{IVS} samples (*Table 1*, *Table I*; patient characteristics). Patient characteristics are shown in Table 1. Echochardiographic parameters were assessed as described previously[27]. All HCM patients had obstructive HCM and showed impaired diastolic function evident from increased LV filling pressure indicated by an E/e' ratio >15 and atrial dilation indicated by increased left atrial diameter (LAD) compared to reference values[28, 29]. IVS thickness was higher in HCM_{SMP} compared to HCM_{SMN}. We identified 3,811 proteins of which we included 2,127 into our analysis after applying our inclusion criteria of an average normalized count of >1.4 and the protein being detected in >25% of samples. This filtered out low-level proteins that could not be reliably quantified.

Samples were grouped based on their genotype and protein expression changes were analyzed in different group-wise comparisons. *Table II* lists all group-wise comparisons and the corresponding number of significantly deregulated proteins that contributed to the subsequent cluster and gene ontology (GO) analysis. An unbiased principal component analysis (PCA) of the protein expression data revealed separate clustering of the NF_{IVS} and HCM samples, indicating different protein expression profiles between controls and patients (*Figure 1A*). Supervised hierarchical clustering of a multi-group comparison revealed separate clusters for NF_{IVS} and HCM samples (*Figure 1B*). However, in both analysis the HCM samples did not cluster according to their genotypes, indicating that the protein profile at the time of myectomy surgery is relatively homogeneous with differences between genotypes that are not sufficiently large to distinguish them with cluster analysis.

TABLE 1. Clinical Characteristics of the HCM_{SMP} and HCM_{SMN} Patient Group.

	HCM_{SMP} (n=38)	**HCM_{SMN} (n=11)**	***P* value**
Sex, male	65.8% (25)	63.6% (7)	>0.9999
Age at myectomy (years)	46.2 ± 17.4	53.6 ± 13.9	0.2084
Dimensions			
IVS (mm)	21.0 [18.8-23.3]	16.0 [15.0-18.0]	<0.0001*
LAD (mm)	46.0 ± 6.5	48.1 ± 5.4	0.3861
EDD (mm)	42.5 ± 5.2	44.3 ± 6.4	0.4466
ESD (mm)	21.7 ± 5.0	26.0 ± 2.8	0.2595
Diastolic parameters			
E/A ratio	1.16 [0.81-1.54]	0.92 [0.67-1.15]	0.1795
E/e' ratio	16.2 [13.1-20.1]	21.7 [16.0-33.4]	0.0226*
TR velocity (cm/s)	2.3 ± 0.5	*NA*	
Stadium of diastolic dysfunction			
1	46.9% (15)	40.0% (4)	>0.9999
2	31.3% (10)	40.0% (4)	0.7071
3	21.9% (7)	20.0% (2)	>0.9999
Systolic parameter			
FS (%)	47.4 ± 11.7	47.5 ± 0.7	0.9942
LVOTg (mmHg)	54.9 ± 31.9	91.7 ± 40.9	0.0034*
Medication			
beta blocker	79.5% (31)	63.6% (7)	0.4240
calcium channel blocker	33.3% (13)	45.5% (5)	0.4945
Statins	12.8% (5)	18.2% (2)	0.6407

Displayed are the mean±SD or the median with interquartile range when appropriate. EDD indicates end-diastolic diameter; ESD, end-systolic diameter; FS, fractional shortening; HCM, hypertrophic cardiomyopathy; IVS, interventricular septum; LAD, left atrial diameter; LVOTg, left ventricular outflow tract gradient; SMN, sarcomere mutation-negative; SMP, sarcomere mutation-positive; and TR, tricuspid regurgitation.

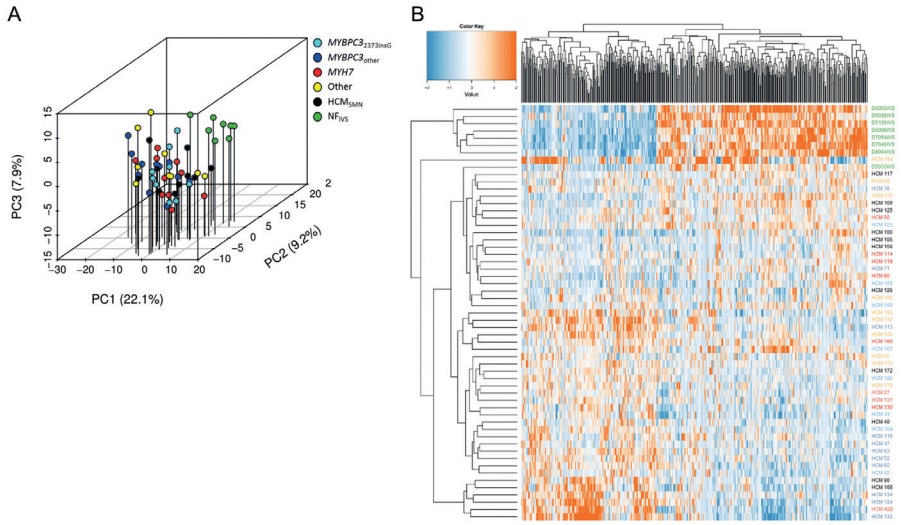

FIGURE 1. Clustering of proteome of controls and patient samples. A, Principal component (PC) analysis of the filtered protein expression data reveals separate clustering of the nonfailing interventricular septum (NF_{IVS}) samples (n=8) and the hypertrophic cardiomyopathy (HCM) samples (n=50) showing that the overall protein expression profile between NFIVS and HCM samples differs. HCM samples did not form separate clusters based on genotypes, indicating that genotype does not lead to major changes in protein expression profile. Also sarcomere mutation-positive (HCM_{SMP}) and sarcomere mutation-negative (HCM_{SMN}) samples do not show major differences at the overall protein expression profile as they cluster together. B, Hierarchical clustering of a multigroup comparison of all proteins that are differently expressed at $P<0.05$ when comparing all HCM (HCM_{all}) with NF_{IVS}. Hierarchical clustering of all significantly different proteins between HCM_{all} and NF_{IVS} shows that the NF_{IVS} samples cluster together and are most different from the HCM samples. Also among this selection of proteins, the HCM samples do not cluster based on genotype or based on presence or absence of mutation (HCM_{SMP} and HCM_{SMN}).

Sample HCM 83 did not cluster with any of the other HCM or NF_{IVS} samples and turned out to have a very high serum albumin content. This implicated contamination with blood and therefore we excluded this sample from all further analyses. Sample HCM 164 also showed a unique protein expression pattern. It may reflect the infant proteome due to the young age (2 months), or the very severe disease stage since this is the only sample obtained from a heart transplantation. Since the variation in this sample is due to a biological reason, we did not exclude it.

To validate our experimental approach, we checked the expression of proteins involved in pathways that are known to be altered in HCM (*Figure II, Table III*). Fibrosis, characterized by an increase in ECM components, is a well-established feature of HCM as shown by data from myectomy biopsies and cardiac magnetic resonance imaging of patients[27, 30]. In line with the presence of fibrosis in patients, we found increased levels of fibronectin, thrombospondin 4 and periostin (*Figures IIA-C*). Since

hypertrophy is a morphological hallmark of HCM, we checked FHL2 expression as a negative regulator of hypertrophy[31]. In line with pro-hypertrophic signaling, reduced FHL2 protein expression was observed (*Figure IID*). The hypertrophic phenotype was also evident from reduced α-MHC encoded by *MYH6*, and increased CSRP3 expression in HCM samples (*Figures IIE-F*)[32, 33]. Finally, MYBPC3 haploinsufficiency was confirmed in samples with a mutation in *MYBPC3* irrespective of whether the mutation is a truncation or missense mutation (*Figures IIG-H, Table IV*)[14, 34].

Additionally, we performed RNA sequencing in a subset of samples. Similar to the proteomics data, the PCA plot of the RNA data did not show clustering based on genotype (*Figure IIIA*). The MA-plot depicts all genes with the differentially expressed genes in red (*Figure IIIB*).Gene set enrichment analysis of the proteomics and transcriptomics data revealed a significant correlation of upregulated proteins with genes that showed higher expression levels in HCM compared to NF_{IVS} (FDR<0.001), while less expressed proteins are positively correlated with genes that showed lower expression levels in HCM (FDR=0.008). This observation suggested that protein expression changes were well correlated with the mRNA expression changes between HCM and NF_{IVS} (*Figure IIIC-D*).

5

HCM-specific protein changes

To identify HCM disease-specific protein expression patterns at the time of myectomy we grouped all HCM samples (HCM_{all}) and compared them to NF_{IVS}. We identified clusters of interacting proteins for higher and lower expressed proteins separately.

Analysis of all significantly lower expressed proteins of HCM_{all} compared to NF_{IVS} uncovered the highest enrichment in oxidative phosphorylation, generation of precursor metabolites and energy, NAD metabolic process, translation, fatty acid catabolic process, regulated exocytosis and neutrophil degranulation (*Figure 2A*, more extensive list in *Figure IV*). This shows that the major changes in tissue of HCM patients are in metabolic pathways related to energy metabolism including both glucose and fatty acid metabolism. We selected all significantly lower expressed proteins annotated to the pathways and created a heatmap displaying the log2-fold change for a detailed visualization of protein changes in the pathway. We included RNA expression data of the corresponding genes to check if the protein changes coincide with changes at the RNA level. Strikingly, most of these proteins are not changed on RNA level (*Figure V*).

The top clusters of the higher expressed proteins are associated with the GO terms ECM organization, actin filament-based process, myofibril assembly, muscle contraction, post-translational protein modification, protein folding and microtubule cytoskeleton organization (*Figure 2B*, more extensive list in *Figure VI*). The biggest cluster of more abundant proteins is ECM organization representing different

collagens that are components of fibrotic tissue. Interestingly, many of these genes showed unaltered RNA levels compared to NF_{IVS}. The same was observed for the other top clusters of higher expressed proteins, namely actin filament-based process, myofibril assembly and muscle contraction, where RNA levels were unaltered or even lower than in NF_{IVS} (*Figure VII*).

Since HCM at the time of myectomy is characterized by pronounced hypertrophy of the myocardium, we expected a protein cluster related to hypertrophy among the significantly increased proteins. Surprisingly, we did not find this. This could be because the myocardium is not in a state of active hypertrophic growth at the time of sample collection, or because we did not detect low abundant hypertrophy promoting signaling proteins. It is also known that several signaling proteins are regulated by post-translational modifications rather than by abundance on which our proteomics screen was based. Western blot analysis of the expression and phosphorylation of AKT and ERK, two well-known inducers of hypertrophy[35, 36], showed higher AKT and ERK phosphorylation in HCM_{all} samples, indicating activation of hypertrophic signaling (*Figure VIII*).

Subsequently, we repeated the cluster and GO analysis restricted to proteins that are higher and lower expressed if all 5 genotype HCM groups are compared individually to NF_{IVS} to extract the most consistent and robust changes. Venn diagrams (*Figure IX and X*) were made to identify overlapping protein changes (76 higher and 92 lower expressed), which were subsequently used as analysis input.

The results confirmed the findings from the initial analysis showing that the major HCM-specific protein changes include reduced metabolism, increased ECM remodeling, and pathways including muscle related processes.

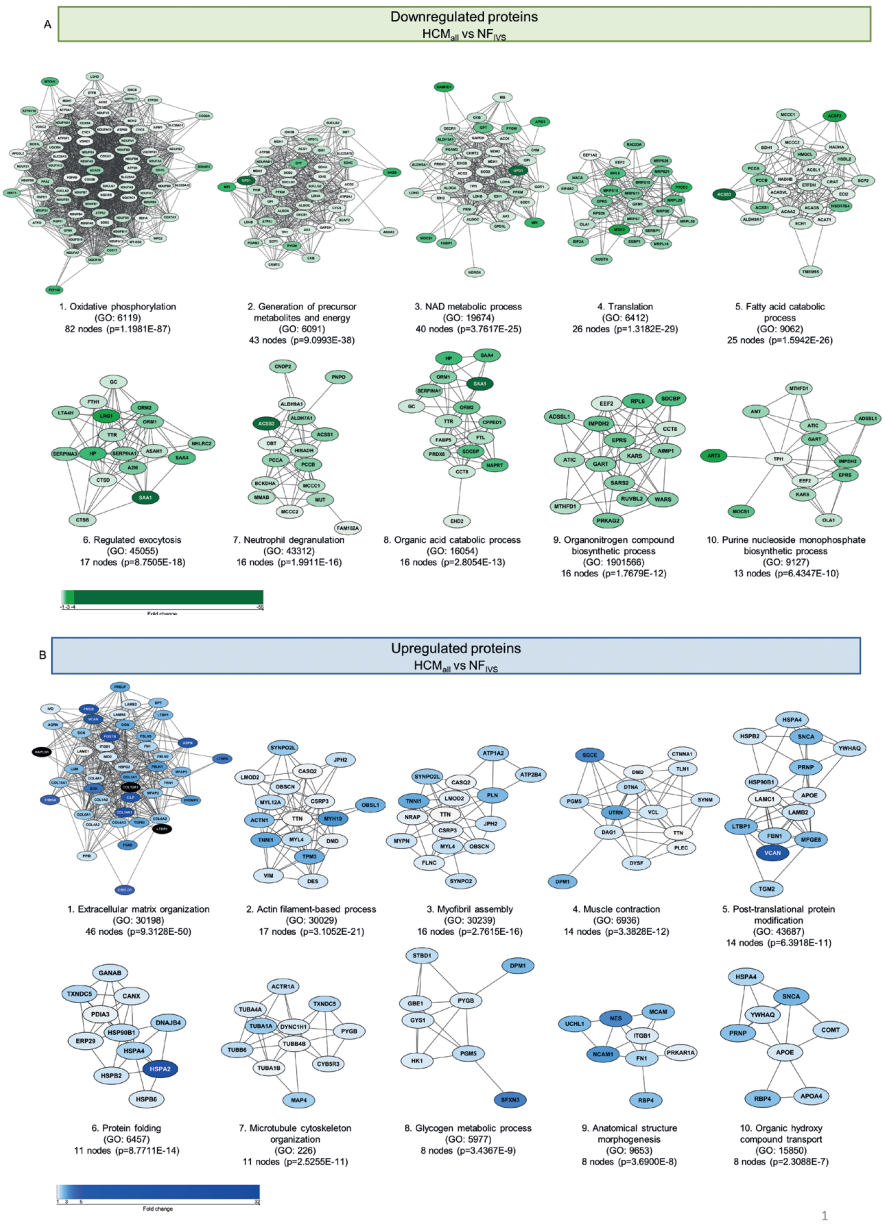

FIGURE 2. Hypertrophic cardiomyopathy (HCM)-specific changes in biological processes. Protein interaction cluster of significantly different proteins between all HCM (HCM_{all}) and nonfailing interventricular septum (NF_{IVS}) were identified and are displayed with the most significant corresponding gene ontology (GO) term. A, Top 10 downregulated protein interaction cluster based on cluster size with the most significant biological process related to this cluster. B, Top 10 upregulated protein interaction cluster based on cluster size with the most significant biological process related to this cluster. The color gradient from light to dark indicates an increase in fold change.

Specific changes for HCM_{SMP} and HCM_{SMN}

To study the pathways that are characteristic for HCM_{SMP} or HCM_{SMN} and might explain sarcomere mutation-specific changes in cardiac function, we created a Venn diagram of significantly different proteins in HCM_{SMP} and HCM_{SMN} compared to NF_{IVS}. The Venn diagrams (*Figures 3 and XI*) illustrate that the majority of significantly different proteins are similar in HCM_{SMP} and HCM_{SMN} (191 lower and 121 higher expressed proteins). However, a substantial number of proteins is only changed in either HCM_{SMP} or HCM_{SMN}, when compared to NF_{IVS}.

The 130 proteins that are specifically less abundant in HCM_{SMP} overlap to a large degree with the biological processes of the 194 proteins that are significantly less abundant in both HCM_{SMP} and HCM_{SMN} when compared to NF_{IVS} (*Figure XII*). Analysis of the 62 proteins that are specifically less expressed in HCM_{SMN} results in clusters related to stress granule assembly, translational initiation and protein folding (*Figure XI*).

The majority of the shared higher expressed proteins involve ECM organization (*Figure XIII*). GO analysis of the 68 proteins that are specifically more abundant in HCM_{SMP} identified amongst others a protein clusters related to microtubule cytoskeleton organization (*Figure 3*).

This cluster representing tubulin subunits is solely more abundant in HCM_{SMP} when compared to NF_{IVS}, and is also among the functional protein cluster of proteins that are significantly upregulated in HCM_{SMP} when directly compared to HCM_{SMN} (*Figure XIV*). Since the tubulin network is highly regulated by post-translational modifications, we determined the levels of total α-tubulin, tyrosinated and detyrosinated tubulin by western blot (*Figure 4, Figure XVA*). In line with the proteomics data we found an increase in total α-tubulin which is more prominent in HCM_{SMP} than in HCM_{SMN} (*Figure 4A*). We validated this with another primary antibody and obtained very comparable results (*Figure XVA*). A post-translational modification of tubulin that leads to increased stiffness of cardiomyocytes is detyrosination of α-tubulin[12]. We found markedly elevated detyrosinated tubulin only in HCM_{SMP} samples (*Figure 4C*), while levels of tyrosinated tubulin were slightly increased in both HCM_{SMP} and HCM_{SMN} (*Figure 4B*). Within the HCM_{SMP} group, levels of α-tubulin tend to be highest in the $MYBPC3_{other}$ group and lowest in the *MYH7* group, whereas desmin levels tend to be highest in *MYH7*. Levels of tyrosinated and detyrosinated tubulin do not show any genotype-specific differences. Levels of tyrosinated and detyrosinated tubulin normalized to total α-tubulin are depicted in *Figure XVB-C*. Our data show that high levels of tubulin in HCM_{SMP} represent mostly the detyrosinated form. We also determined desmin protein levels by Western blot since this protein is associated with microtubules in cardiomyocytes. Accordingly, desmin levels were elevated in HCM with the largest increase in HCM_{SMP} (*Figure 4D*).

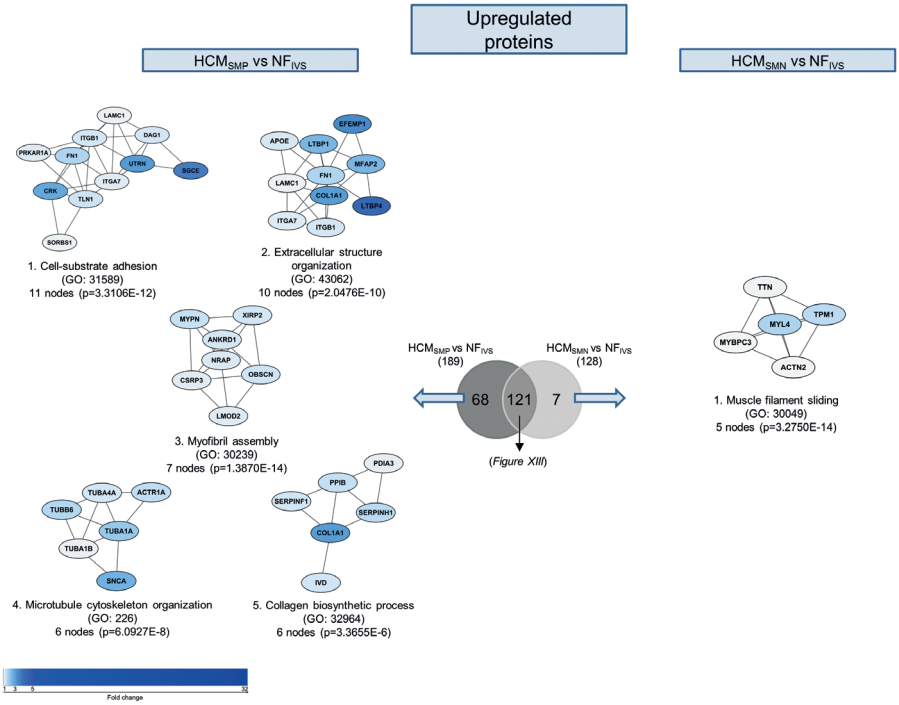

FIGURE 3. Differences in upregulated proteins between patients with hypertrophic cardiomyopathy sarcomere mutation-positive (HCM_{SMP}) and sarcomere mutation-negative (HCM_{SMN}). Protein interaction cluster of proteins that are only significantly upregulated for the HCM_{SMP} vs nonfailing interventricular septum (NF_{IVS}) or the HCM_{SMN} vs NF_{IVS} comparison were identified and are displayed with the most significant corresponding gene ontology (GO) term. The top 5 protein interaction clusters of upregulated proteins are displayed The color gradient from light to dark indicates an increase in fold change.

Inhibition of tubulin detyrosination corrects cardiomyocyte dysfunction in $MYBPC3_{2373insG}$ mice

Based on previous studies in human heart failure[13], our data in human myectomy samples indicate that microtubules may represent a treatment target to correct cardiac dysfunction in HCM. To provide proof for a role of tubulin in modulating cardiomyocyte function in HCM caused by a sarcomere gene mutation, we generated a HCM knock-in (KI) mouse model of the Dutch founder mutation c.2373insG in *MYBPC3* (*Figures XVIA-B*). This mutation introduces a new splice donor site in exon 25 leading to a frameshift and premature stop codon resulting in an expected truncated protein of 95 kDa[37]. As no truncated protein is found in HCM patients carrying this mutation at the heterozygous state[14], degradation of mutant mRNA and/or protein is likely. Accordingly, Western blot analysis did not reveal any truncated MYBPC3 protein in homozygous $MYBPC3_{2373insG}$ mice (*Figure XVIC*).

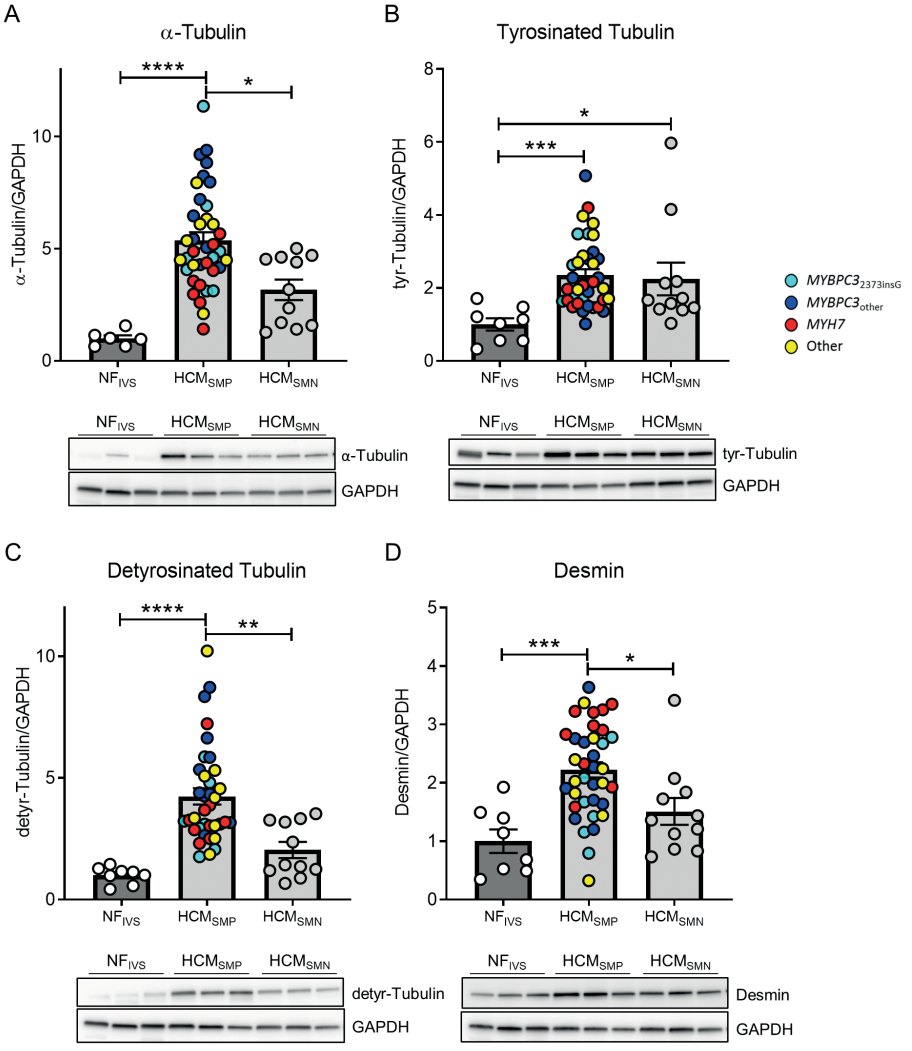

FIGURE 4. Tubulin expression and post-translational modifications in patients with hypertrophic cardiomyopathy (HCM). Protein levels of α-tubulin (A), its tyrosinated (B) and detyrosinated forms (C) and desmin (D), all normalized to GAPDH, in tissue of patients with HCM. Kruskal-Wallis test with Dunn multiple comparisons test, ****P<0.0001, ***P=0.0003 in (B), ***P=0.0009 in (D), **P=0.0074, *P=0.0437 in (A), *P=0.0499 in (B) and *P=0.0357 in (D). Average of the control group is set to 1. n(nonfailing interventricular septum [NF_{IVS}]/HCM_{SMP}/HCM_{SMN})=6/38/11 for (A), 8/36/11 for (B and C), 8/37/11 for (D). SMN indicates sarcomere mutation-negative; and SMP, sarcomere mutation-positive.

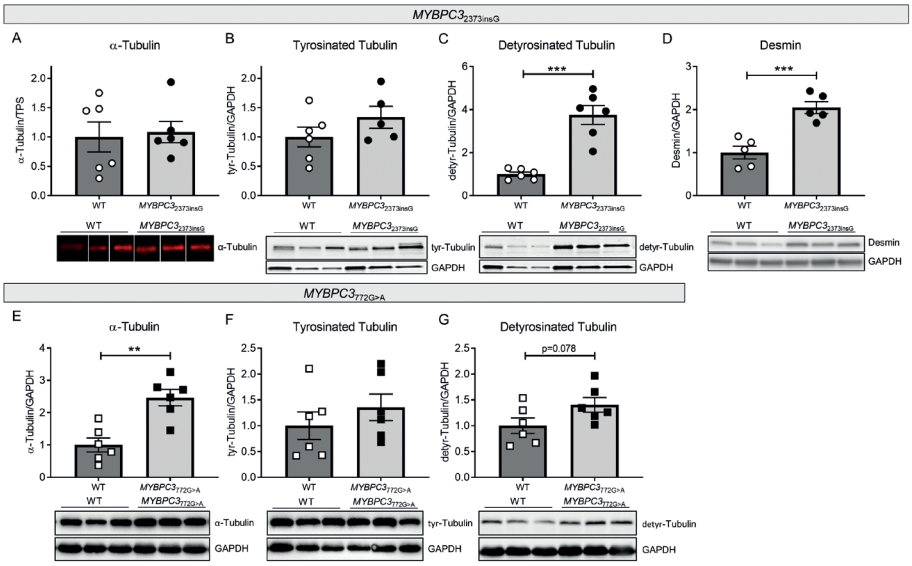

FIGURE 5. Tubulin composition in *MYBPC3*$_{2373insG}$ and *MYBPC3*$_{772G>A}$ mouse models. Quantification and representative western blot images of (A) α-tubulin, (B) tyrosinated tubulin, (C) detyrosinated tubulin and (D) desmin in *MYBPC3*$_{2373insG}$ mice and (E) α-tubulin, (F) tyrosinated tubulin and (G) detyrosinated tubulin in *MYBPC3*$_{772G>A}$ mice, respectively. (A) is normalized to total protein stain (TPS, image provided in Figure XVD), (B-G) are normalized to GAPDH. Lanes in (A) were run on the same gel but were noncontiguous. n(WT/*MYBPC3*$_{2373insG/772G>A}$)=6/6 (4 females, 2 males/3 females, 3 males of 20-27 weeks for *MYBPC3*$_{2373insG}$ and the corresponding WT; 2 females, 4 males for of 55-59 weeks for *MYBPC3*$_{772G>A}$ and the corresponding WT) for (A, C, E-G), 6/5 (4 females, 2 males/3 females, 2 males; 20-27 weeks) for (B) and 5/5 (3 females, 2 males/2 females, 3 males; 20-27 weeks) for (D), unpaired two-tailed t-test, *** p=0.0001 in (C) and p=0.009 in (D), ** p=0.0014.

Levels of total and tyrosinated α-tubulin did not differ between the groups, whereas the detyrosinated tubulin and desmin levels were markedly higher in *MYBPC3*$_{2373insG}$ than in wildtype (WT) mice (*Figures 5A-D*, loading control to panel A shown in *Figure XVD)*. To evaluate whether these findings were specific to this model, we assessed the levels of total and detyrosinated tubulin in a second HCM mouse model carrying a different *MYBPC3* mutation[25]. Homozygous *MYBPC3*$_{772G>A}$ mice showed a strong accumulation of α-tubulin and no difference in tyrosinated tubulin compared to their WT littermates. In addition, a trend to higher levels of detyrosinated tubulin was observed (*Figures 5E-G)*. Overall, these mouse models consistently show tubulin changes in cardiomyopathy caused by *MYBPC3* gene mutations.

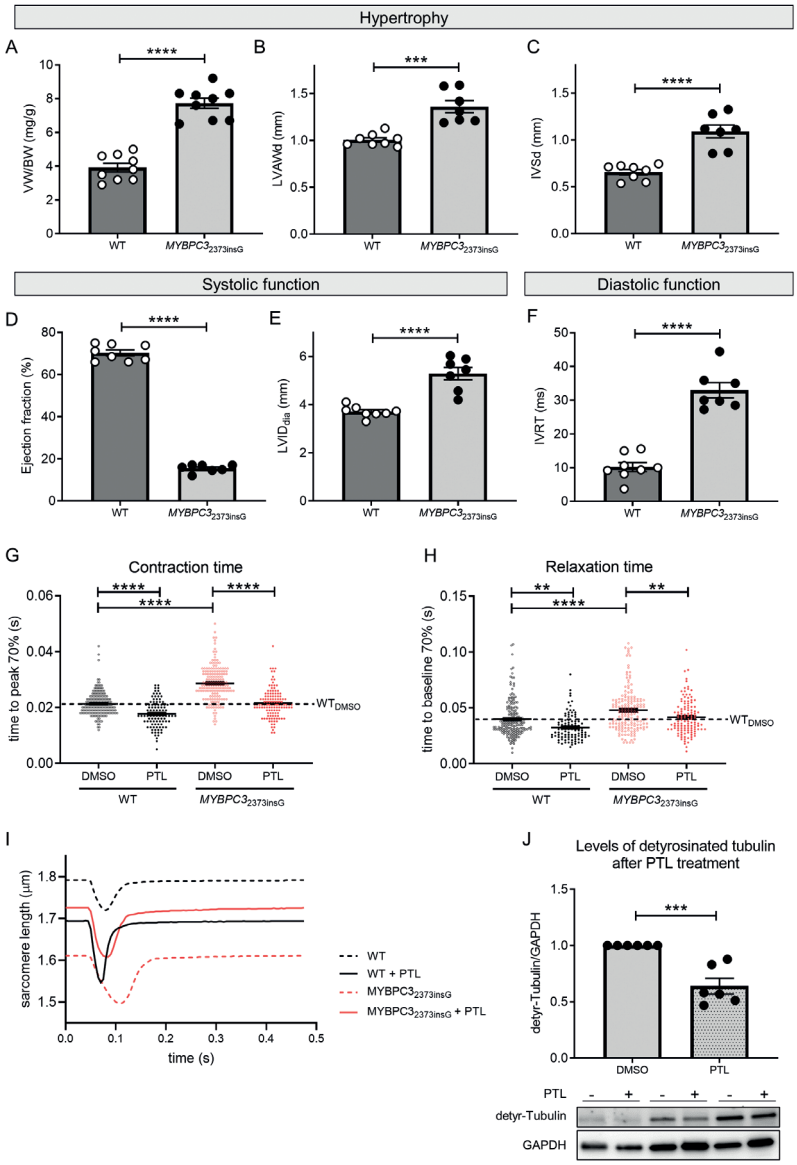

FIGURE 6. Morphometric and phenotypic analysis of *MYBPC3*$_{2373insG}$ mice and contractile function of isolated *MYBPC3*$_{2373insG}$ cardiomyocytes upon inhibition of tubulin detyrosination. Quantification of the hypertrophy parameters (A) ventricle weight (VW)/body weight (BW) ratio and (B) anterior wall thickness in diastole (LWADd) and (C) interventricular septum thickness in diastole (IVSd) measured by echocardiography. (D) and (E) show parameters of systolic function measured by ejection fraction and left ventricular internal diameter (LVID) and (F) displays diastolic function assessed by isovolumetric relaxation time (IVRT). n(WT/*MYBPC3*$_{2373insG}$)=9/9 (4 females, 5 males; 20-27 weeks) for (A) and 8/7 (3 females, 5 resp. 4 males; 25-27 weeks) for (B-F), unpaired two-tailed t-test, **** p<0.0001, *** p=0.0001.

(G) displays the effect of tubulin detyrosination inhibition by PTL on the contractile parameter time to peak 70% and (H) on the diastolic parameter time to baseline 70%. The dotted line visualizes the WT baseline level. (I) shows example force transients for each condition of the single cell measurements. For (G-H) N(WT mice)=4 (2 females and 2 males, 13-33 weeks) with total n(cells DMSO/PTL)=191/99 and N(*MYBPC3*$_{2373insG}$ mice)=6 (2 females and 4 males, 13-35 weeks) with total n(cells DMSO/PTL)=169/123. (G) and (H) were analyzed by 2way-ANOVA, ** p<0.01, **** p<0.0001. (J) Levels of detyrosinated tubulin normalized to GAPDH in isolated *MYBPC3*$_{2373insG}$ cardiomyocytes upon inhibition of tubulin detyrosination by PTL. Every PTL treated sample was normalized to the DMSO control condition from the same animal. N(*MYBPC3*$_{2373insG}$ mice)=6 (2 females, 4 males, 13-19 weeks); (J) was analyzed with an unpaired two-tailed t-test, *** p=0.0004.

MYBPC3$_{2373insG}$ mice had a severe cardiac phenotype characterized by higher ventricular weight to body weight ratio, increased LV anterior wall diameter and interventricular septum thickness, lower ejection fraction, increased left ventricular internal diameter and longer isovolumetric relaxation time than WT mice (*Figures 6A-F*). Single cardiomyocytes from *MYBPC3*$_{2373insG}$ hearts showed contractile deficits compared to WT as shown by an increase in time to peak of contraction and an impaired relaxation shown by an increase in time to baseline (*Figures 6G-H*). Inhibition of detyrosination by treatment with parthenolide (PTL) reduced levels of detyrosinated tubulin by 36% (*Figure 6J*) and normalized the contraction and relaxation times in *MYBPC3*$_{2373insG}$ mice to baseline WT levels (*Figures 6G-H*), whereas it had no effect on calcium release and reuptake time in *MYBPC3*$_{2373insG}$ mice (*Figure XVIIA-B*), indicating a direct effect on myofilament function.

DISCUSSION

In this study we compared the protein profile of cardiac tissue from HCM patients with different disease-causing gene mutations to identify common HCM disease changes as well as genotype-specific protein changes at the time of myectomy. The majority of detected protein changes were common for all HCM samples and independent of the underlying gene mutation. Our approach revealed different protein profiles in the presence or absence of a sarcomere gene mutation. While hypertrophic remodeling in HCM$_{SMP}$ is characterized by an increase in the levels of proteins involved in microtubule cytoskeleton organization, HCM$_{SMN}$ samples show reduced levels of proteins involved in protein translation.

Deregulated energy metabolism proteome

Our analysis revealed that the majority of deregulated proteins are related to energy metabolism and show a consistent lower expression of proteins involved in oxidative phosphorylation, glycolysis and fatty acid oxidation. Especially subunits of mitochondrial respiratory chain complex I, that are part of cluster 1 in *Figure 2A*, are consistently lower expressed. This is in line with another recent proteomics study of HCM tissue samples in which reduced levels of energy metabolism proteins was one of the main findings[38]. It also matches observations of energy deficiency in animal

models[39] and human studies[40, 41]. Energy deficiency has been proposed as the primary mutation-induced pathomechanism leading to compensatory hypertrophy[42], which is supported by the fact that even asymptomatic mutation carriers without hypertrophy display reduced cardiac energetic status[9, 41]. The reduced cardiac efficiency was larger in *MYH7* mutation carriers compared to *MYBPC3* mutation carriers pointing towards genotype-specific functional differences[9]. Our proteomic analyses did not show gene-dependent differences in proteins involved in cardiac energy metabolism. This indicates that the deregulated energy metabolism proteome is a secondary consequence due to cellular stress that is similar in patients with advanced HCM.

Protein homeostasis differs between HCM_{SMP} and HCM_{SMN}

Interestingly, proteins involved in protein translation are less abundant, particularly in HCM_{SMN} patient tissue when compared to NF_{IVS}, implying that the protein translation system is either more impaired or differently regulated in HCM_{SMN}. Among the more abundant proteins, we observed a protein cluster related to protein folding. Protein folding proteins (chaperones) are needed for correct folding of de novo synthesized proteins as well as for refolding of misfolded mutant or damaged proteins. Since our data show downregulation of protein translation, it is unlikely that protein folding proteins are upregulated for folding of newly synthesized proteins. Instead, we speculate that their expression is upregulated to repair or remove misfolded (mutant) proteins[43]. This is in line with recent data describing an upregulation of protein folding proteins specifically in HCM_{SMP} samples[44]. Protein folding proteins represent potential treatment targets since boosting their expression has already shown beneficial effects in animal models of other cardiac diseases and in cardiomyopathies[45-47].

Impact of increased tubulin network on cardiomyocyte function in HCM

A striking observation was the specific upregulation of microtubule subunits and post-translational modification detyrosination in HCM_{SMP} compared to HCM_{SMN}, when comparing both to NF_{IVS}. Previous studies indicated important regulatory roles of microtubules in cardiomyocyte function[48]. Recent reports showed that the translation of the sarcomere proteins is localized to the myofilaments which points to a role of microtubules in the transportation of mRNA to the myofilament[49, 50]. Increased expression of tubulin subunits strengthens the microtubule network and facilitates the transportation of mRNAs to the sarcomere and concomitant increasing cardiomyocyte stability. In addition to tubulins, desmin protein level was significantly higher in HCM_{SMP} than in HCM_{SMN}. In the healthy heart, desmin is localized at the Z-discs forming a striated pattern and playing a central role in cardiomyocyte mechanical stability[51]. Overall, these protein changes suggest a compensatory mechanism of the cell to ensure sarcomere stability in the presence of a sarcomere gene mutation.

Furthermore, microtubules and their post-translational modifications play an important role in cardiomyocyte mechanics, especially in regulating cardiomyocyte stiffness[52, 53].

Detyrosinated tubulin stabilizes microtubules by inhibiting disassembly[54] and can anchor microtubules to the Z-discs of the sarcomere, most likely via desmin, and enhance stability and stiffness of the myofilaments and the microtubular network[52]. The *TUBA4A* transcript is directly synthesized in it is detyrosinated form and an upregulation could at least partly explain the increase in detyrosinated tubulin. In our RNA sequencing data, the *TUBA4A* transcript is however significantly downregulated when comparing HCM with NF_{IVS} and it is not differentially expressed in the direct comparison of HCM_{SMP} and HCM_{SMN}.

Tubulin detyrosination is enzymatically regulated by the tubulin tyrosine ligase (TTL) and tubulin carboxypeptidases (TCPs) that have detyrosinating activity and also the *TUBA4A* transcript can undergo these reactions[55]. Recently, vasohibins have been identified as the first tubulin detyrosinating enzymes[56, 57], and act in complex with small vasohibin-binding protein (SVBP). In accordance with findings by Robison et al. in explanted hearts of heart failure and cardiomyopathy patients[12], we observed a specific upregulation of tubulins and enhanced detyrosination in our genetically well-characterized HCM myectomy samples. Notably, we found the increase in tubulin detyrosination specific for HCM_{SMP} samples. Although levels of detyrosinated tubulin are equal between HCM_{SMP} and HCM_{SMN} when normalized to total levels of α-tubulin, the absolute levels of α-tubulin and detyrosinated tubulin are much higher in HCM_{SMP} and thereby have a much greater impact on contractile function in these patients. Chen et al. have already demonstrated the reversibility of tubulin detyrosination in isolated cardiomyocytes from explanted HCM hearts associated with an improvement of contractile function[13, 58]. Here we performed proof-of-concept studies in HCM mouse models to define the impact of tubulin detyrosination in the presence of a sarcomere mutation. Homozygous $MYBPC3_{2373insG}$ mice replicated the tubulin detyrosination without an increase in total α-tubulin levels, whereas homozygous $MYBPC3_{772G>A}$ mice display an increase in total α-tubulin with a trend to increased tubulin detyrosination. Considering the age difference of the mice with the $MYBPC3_{772G>A}$ mice being much older than the $MYBPC3_{2373insG}$ mice at the time of analysis, we speculate that the increase in tubulin detyrosination is an early disease change together with an increase in desmin protein levels, which is followed by an increase of total α-tubulin during disease progression and ageing. In $MYBPC3_{2373insG}$ mice we showed that the increase in tubulin detyrosination is accompanied by reduced contraction and relaxation kinetics in isolated intact cardiomyocytes. Inhibition of tubulin detyrosination by PTL restored contraction and relaxation kinetics to WT levels in $MYBPC3_{2373insG}$ cardiomyocytes. The used concentration of PTL has already been proven to be sufficient to reduce detyrosination of tubulin[12, 59] and Chen et al. and Robison et al. have demonstrated that the PTL-induced effects on kinetics of contraction are the same as obtained by overexpression of TTL[12, 13], which specifically lowers tubulin detyrosination. The positive effect of PTL on cardiomyocyte function of $MYBPC3_{2373insG}$ cardiomyocytes is therefore explained by a decrease in cardiomyocyte stiffness due to lower levels of detyrosinated tubulin.

Overall, our findings in a European HCM patient cohort strengthens the evidence that increased detyrosination of microtubules contributes to cardiomyocyte stiffness and dysfunction in HCM. Importantly, we show that this is especially true in the presence of a sarcomere mutation.

STUDY LIMITATIONS AND CLINICAL IMPLICATIONS

We sex- and age-matched our experimental groups as good as the availability of human samples allowed us. As seen in Table 1, sex and age, as well as most clinical parameters, are not statistically different between groups. We cannot exclude that differences in disease progression, as displayed by the difference in IVS thickness, E/e' ratio and LVOTg between HCM_{SMP} and HCM_{SMN}, may influence the results. However, collection of patient heart tissue is only possible at the time of myectomy. Therefore, all our samples have the same clinical endpoint, i.e. time of myectomy. This is likely the cause for the low number of genotype-specific protein changes and we cannot exclude that genotype-specific differences might have occurred at earlier disease stages. Due to unavailability of myocardial biopsies from asymptomatic mutation carriers, animal models and human-derived cardiomyocyte muscle models should provide insight into gene-specific pathomechanisms at early disease stages.

Most of the patients in this study have been on drug therapy, therefore we cannot exclude that some of the proteomic changes are caused by medication. However, some of the main findings, e.g. energy deficiency, have also been observed in animal models[39], and the number of patients on the most commonly used drugs does not differ between HCM_{SMP} and HCM_{SMN} (*Table 1)*. Therefore it is more likely that the observed changes are driven by disease rather than medication.

Although we detected and quantified a large number of proteins in this study, we do not reach full coverage of the proteome as this method only reliably quantifies the more abundant proteins. Therefore, our list of differentially expressed proteins is not comprehensive. Also, we did not assess post-translational modifications in the proteomics study which have important regulatory functions. The changes at the protein level reflect whole tissue alterations and cannot be solely assigned to the mutation-carrying cardiomyocytes but might also arise from other cell types. However, cardiomyocytes are responsible for most of the tissue volume and therefore drive most of the protein changes.

Homozygous $MYBPC3_{2373insG}$ mice do not fully resemble human HCM patients, since patients typically carry heterozygous mutations. Whilst both patients and the homozygous $MYBPC3_{2373insG}$ mouse model show hypertrophy and diastolic dysfunction, the prominent LV systolic dysfunction as observed in the homozygous $MYBPC3_{2373insG}$

mice is not seen in most HCM patients. But due to the lack of phenotype in heterozygous mice they provide a suitable genetic model of loss of MYBPC3 protein levels.

In our proteomic screen in a large set of human HCM samples we identified reduced levels of proteins involved in metabolic pathways as the most prominent derailment. This finding supports recent and ongoing clinical trials investigating the therapeutic effect of targeting the metabolism in HCM. Based on the proteomic data and functional studies in a novel HCM mouse model, we propose that an increase in detyrosinated tubulin contributes to the clinical and cellular differences that we see between HCM_{SMP} and HCM_{SMN} samples (*Figure 7*). Detyrosinated microtubules may represent a target for therapeutic intervention in genetic heart disease because reducing detyrosination improves contractile function in isolated cardiomyocytes. Since the increase in detyrosinated tubulin is largest in HCM_{SMP}, this treatment strategy is proposed to be most beneficial in mutation-positive HCM patients. A specific inhibitor of detyrosination needs to be developed due to the known off-target effects of PTL. As sarcomere mutation carriers are identified before disease onset, targeting the microtubules may represent a preventive treatment option.

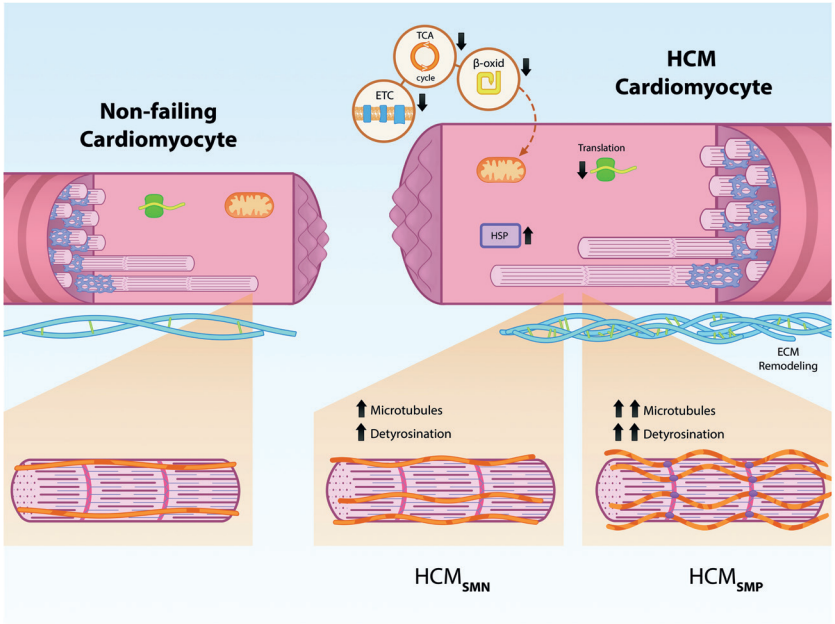

FIGURE 7. Schematic representation of genotype-independent changes in HCM and genotype-specific differences in the microtubular system. Our analysis shows that all HCM patients display downregulation of metabolic pathways (electron transport chain (ETC), tricarboxylic acid (TCA) cycle, β-oxidation (β-oxid)) and ribosomal proteins (Translation), as well as an upregulation of protein folding proteins (heat shock proteins, HSPs) and extracellular matrix (ECM) proteins. HCM_{SMP} patients have a large increase in microtubules and levels of its detyrosinated form, whereas HCM_{SMN} patients only have a slight increase compared to non-failing controls.

ACKNOWLEDGEMENTS

We would like to thank Ruud Zaremba, Valentijn Jansen and Max Goebel for technical assistance. We thank Feng Zhang for providing the Addgene plasmid #42230.

SOURCES OF FUNDING

We acknowledge the support from the Netherlands Cardiovascular Research Initiative: An initiative with support of the Dutch Heart Foundation, CVON2014-40 DOSIS and NWO (NWO-ZonMW; 91818602 VICI grant to Jolanda van der Velden). Folkert Asselbergs is supported by UCL Hospitals NIHR Biomedical Research Centre. Magdalena Harakalova is supported by NWO VENI grant (no. 016.176.136). Lucie Carrier and Saskia Schlossarek are supported by the German Centre for Cardiovascular Research (DZHK), the German Ministry of Research Education (BMBF), the Deutsche Herzstiftung and the Helmut und Charlotte Kassau Stiftung.

DISCLOSURES

None.

REFERENCES

1. Michels M, Olivotto I, Asselbergs FW and van der Velden J. Life-long tailoring of management for patients with hypertrophic cardiomyopathy : Awareness and decision-making in changing scenarios. *Neth Heart J*. 2017;25:186-199. doi: 10.1007/s12471-016-0943-2
2. Ingles J, Burns C, Barratt A and Semsarian C. Application of Genetic Testing in Hypertrophic Cardiomyopathy for Preclinical Disease Detection. *Circ Cardiovasc Genet*. 2015;8:852-9. doi: 10.1161/CIRCGENETICS.115.001093
3. Authors/Task Force, Elliott PM, Anastasakis A, Borger MA, Borggrefe M, Cecchi F, Charron P, Hagege AA, Lafont A, Limongelli G, et al. 2014 ESC Guidelines on diagnosis and management of hypertrophic cardiomyopathy: the Task Force for the Diagnosis and Management of Hypertrophic Cardiomyopathy of the European Society of Cardiology (ESC). *Eur Heart J*. 2014;35:2733-79. doi: 10.1093/eurheartj/ehu284
4. Richard P, Charron P, Carrier L, Ledeuil C, Cheav T, Pichereau C, Benaiche A, Isnard R, Dubourg O, Burban M, et al. Hypertrophic cardiomyopathy: distribution of disease genes, spectrum of mutations, and implications for a molecular diagnosis strategy. *Circulation*. 2003;107:2227-32. doi: 10.1161/01.CIR.0000066323.15244.54
5. Vakrou S, Fukunaga R, Foster DB, Sorensen L, Liu Y, Guan Y, Woldemichael K, Pineda-Reyes R, Liu T, Tardiff JC, et al. Allele-specific differences in transcriptome, miRNome, and mitochondrial function in two hypertrophic cardiomyopathy mouse models. *JCI Insight*. 2018;3. doi: 10.1172/jci.insight.94493
6. Sequeira V, Wijnker PJM, Nijenkamp LLaM, Kuster DWD, Najafi A, Witjas-Paalberends ER, Regan Ja, Boontje N, Ten Cate FJ, Germans T, et al. Perturbed length-dependent activation in human hypertrophic cardiomyopathy with missense sarcomeric gene mutations. *Circulation research*. 2013;112:1491-505. doi: 10.1161/CIRCRESAHA.111.300436
7. Sequeira V, Najafi A, Wijnker PJ, Dos Remedios CG, Michels M, Kuster DW and van der Velden J. ADP-stimulated contraction: A predictor of thin-filament activation in cardiac disease. *Proc Natl Acad Sci U S A*. 2015;112:E7003-12. doi: 10.1073/pnas.1513843112
8. Ojala M, Prajapati C, Polonen RP, Rajala K, Pekkanen-Mattila M, Rasku J, Larsson K and Aalto-Setala K. Mutation-Specific Phenotypes in hiPSC-Derived Cardiomyocytes Carrying Either Myosin-Binding Protein C Or alpha-Tropomyosin Mutation for Hypertrophic Cardiomyopathy. *Stem Cells Int*. 2016;2016:1684792. doi: 10.1155/2016/1684792
9. Witjas-Paalberends ER, Guclu A, Germans T, Knaapen P, Harms HJ, Vermeer AM, Christiaans I, Wilde AA, Dos Remedios C, Lammertsma AA, et al. Gene-specific increase in the energetic cost of contraction in hypertrophic cardiomyopathy caused by thick filament mutations. *Cardiovasc Res*. 2014;103:248-57. doi: 10.1093/cvr/cvu127
10. Ho CY, Lakdawala NK, Cirino AL, Lipshultz SE, Sparks E, Abbasi SA, Kwong RY, Antman EM, Semsarian C, Gonzalez A, et al. Diltiazem treatment for pre-clinical hypertrophic cardiomyopathy sarcomere mutation carriers: a pilot randomized trial to modify disease expression. *JACC Heart Fail*. 2015;3:180-8. doi: 10.1016/j.jchf.2014.08.003
11. Ho CY, Day SM, Ashley EA, Michels M, Pereira AC, Jacoby D, Cirino AL, Fox JC, Lakdawala NK, Ware JS, et al. Genotype and Lifetime Burden of Disease in Hypertrophic Cardiomyopathy: Insights from the Sarcomeric Human Cardiomyopathy Registry (SHaRe). *Circulation*. 2018;138:1387-1398. doi: 10.1161/CIRCULATIONAHA.117.033200

12. Robison P, Caporizzo MA, Ahmadzadeh H, Bogush AI, Chen CY, Margulies KB, Shenoy VB and Prosser BL. Detyrosinated microtubules buckle and bear load in contracting cardiomyocytes. *Science*. 2016;352:aaf0659. doi: 10.1126/science.aaf0659
13. Chen CY, Caporizzo MA, Bedi K, Vite A, Bogush AI, Robison P, Heffler JG, Salomon AK, Kelly NA, Babu A, et al. Suppression of detyrosinated microtubules improves cardiomyocyte function in human heart failure. *Nat Med*. 2018;24:1225-1233. doi: 10.1038/s41591-018-0046-2
14. van Dijk SJ, Dooijes D, dos Remedios C, Michels M, Lamers JM, Winegrad S, Schlossarek S, Carrier L, ten Cate FJ, Stienen GJ, et al. Cardiac myosin-binding protein C mutations and hypertrophic cardiomyopathy: haploinsufficiency, deranged phosphorylation, and cardiomyocyte dysfunction. *Circulation*. 2009;119:1473-83. doi: 10.1161/CIRCULATIONAHA.108.838672
15. Alfares AA, Kelly MA, McDermott G, Funke BH, Lebo MS, Baxter SB, Shen J, McLaughlin HM, Clark EH, Babb LJ, et al. Results of clinical genetic testing of 2,912 probands with hypertrophic cardiomyopathy: expanded panels offer limited additional sensitivity. *Genetics In Medicine*. 2015;17:880. doi: 10.1038/gim.2014.205
16. Warmoes M, Jaspers JE, Pham TV, Piersma SR, Oudgenoeg G, Massink MP, Waisfisz Q, Rottenberg S, Boven E, Jonkers J, et al. Proteomics of mouse BRCA1-deficient mammary tumors identifies DNA repair proteins with potential diagnostic and prognostic value in human breast cancer. *Mol Cell Proteomics*. 2012;11:M111 013334. doi: 10.1074/mcp.M111.013334
17. Piersma SR, Broxterman HJ, Kapci M, de Haas RR, Hoekman K, Verheul HM and Jimenez CR. Proteomics of the TRAP-induced platelet releasate. *J Proteomics*. 2009;72:91-109. doi: 10.1016/j.jprot.2008.10.009
18. Perez-Riverol Y, Csordas A, Bai J, Bernal-Llinares M, Hewapathirana S, Kundu DJ, Inuganti A, Griss J, Mayer G, Eisenacher M, et al. The PRIDE database and related tools and resources in 2019: improving support for quantification data. *Nucleic Acids Res*. 2019;47:D442-D450. doi: 10.1093/nar/gky1106
19. Pham TV, Piersma SR, Warmoes M and Jimenez CR. On the beta-binomial model for analysis of spectral count data in label-free tandem mass spectrometry-based proteomics. *Bioinformatics*. 2010;26:363-9. doi: 10.1093/bioinformatics/btp677
20. Shannon P, Markiel A, Ozier O, Baliga NS, Wang JT, Ramage D, Amin N, Schwikowski B and Ideker T. Cytoscape: a software environment for integrated models of biomolecular interaction networks. *Genome Res*. 2003;13:2498-504. doi: 10.1101/gr.1239303
21. Maere S, Heymans K and Kuiper M. BiNGO: a Cytoscape plugin to assess overrepresentation of gene ontology categories in biological networks. *Bioinformatics*. 2005;21:3448-9. doi: 10.1093/bioinformatics/bti551
22. Nepusz T, Yu H and Paccanaro A. Detecting overlapping protein complexes in protein-protein interaction networks. *Nat Methods*. 2012;9:471-2. doi: 10.1038/nmeth.1938
23. Chen J, Bardes EE, Aronow BJ and Jegga AG. ToppGene Suite for gene list enrichment analysis and candidate gene prioritization. *Nucleic Acids Res*. 2009;37:W305-11. doi: 10.1093/nar/gkp427
24. Heberle H, Meirelles GV, da Silva FR, Telles GP and Minghim R. InteractiVenn: a web-based tool for the analysis of sets through Venn diagrams. *BMC Bioinformatics*. 2015;16:169. doi: 10.1186/s12859-015-0611-3

25. Vignier N, Schlossarek S, Fraysse B, Mearini G, Kramer E, Pointu H, Mougenot N, Guiard J, Reimer R, Hohenberg H, et al. Nonsense-mediated mRNA decay and ubiquitin-proteasome system regulate cardiac myosin-binding protein C mutant levels in cardiomyopathic mice. *Circ Res*. 2009;105:239-48. doi: 10.1161/CIRCRESAHA.109.201251
26. Najafi A, Schlossarek S, van Deel ED, van den Heuvel N, Guclu A, Goebel M, Kuster DW, Carrier L and van der Velden J. Sexual dimorphic response to exercise in hypertrophic cardiomyopathy-associated MYBPC3-targeted knock-in mice. *Pflugers Arch*. 2015;467:1303-17. doi: 10.1007/s00424-014-1570-7
27. Nijenkamp L, Bollen IAE, van Velzen HG, Regan JA, van Slegtenhorst M, Niessen HWM, Schinkel AFL, Kruger M, Poggesi C, Ho CY, et al. Sex Differences at the Time of Myectomy in Hypertrophic Cardiomyopathy. *Circ Heart Fail*. 2018;11:e004133. doi: 10.1161/CIRCHEARTFAILURE.117.004133
28. Nagueh SF, Appleton CP, Gillebert TC, Marino PN, Oh JK, Smiseth OA, Waggoner AD, Flachskampf FA, Pellikka PA and Evangelista A. Recommendations for the evaluation of left ventricular diastolic function by echocardiography. *J Am Soc Echocardiogr*. 2009;22:107-33. doi: 10.1016/j.echo.2008.11.023
29. Lang RM, Bierig M, Devereux RB, Flachskampf FA, Foster E, Pellikka PA, Picard MH, Roman MJ, Seward J, Shanewise JS, et al. Recommendations for chamber quantification: a report from the American Society of Echocardiography's Guidelines and Standards Committee and the Chamber Quantification Writing Group, developed in conjunction with the European Association of Echocardiography, a branch of the European Society of Cardiology. *J Am Soc Echocardiogr*. 2005;18:1440-63. doi: 10.1016/j.echo.2005.10.005
30. Maron MS, Appelbaum E, Harrigan CJ, Buros J, Gibson CM, Hanna C, Lesser JR, Udelson JE, Manning WJ and Maron BJ. Clinical profile and significance of delayed enhancement in hypertrophic cardiomyopathy. *Circ Heart Fail*. 2008;1:184-91. doi: 10.1161/CIRCHEARTFAILURE.108.768119
31. Purcell NH, Darwis D, Bueno OF, Muller JM, Schule R and Molkentin JD. Extracellular signal-regulated kinase 2 interacts with and is negatively regulated by the LIM-only protein FHL2 in cardiomyocytes. *Mol Cell Biol*. 2004;24:1081-95. doi: 10.1128/mcb.24.3.1081-1095.2004
32. Lowes BD, Minobe W, Abraham WT, Rizeq MN, Bohlmeyer TJ, Quaife RA, Roden RL, Dutcher DL, Robertson AD, Voelkel NF, et al. Changes in gene expression in the intact human heart. Downregulation of alpha-myosin heavy chain in hypertrophied, failing ventricular myocardium. *J Clin Invest*. 1997;100:2315-24. doi: 10.1172/JCI119770
33. Nakao K, Minobe W, Roden R, Bristow MR and Leinwand LA. Myosin heavy chain gene expression in human heart failure. *J Clin Invest*. 1997;100:2362-70. doi: 10.1172/JCI119776
34. Marston S, Copeland O, Gehmlich K, Schlossarek S and Carrier L. How do MYBPC3 mutations cause hypertrophic cardiomyopathy? *J Muscle Res Cell Motil*. 2012;33:75-80. doi: 10.1007/s10974-011-9268-3
35. Heineke J and Molkentin JD. Regulation of cardiac hypertrophy by intracellular signalling pathways. *Nat Rev Mol Cell Biol*. 2006;7:589-600. doi: 10.1038/nrm1983
36. Matsui T, Nagoshi T and Rosenzweig A. Akt and PI 3-kinase signaling in cardiomyocyte hypertrophy and survival. *Cell Cycle*. 2003;2:220-3. doi:
37. Moolman Ja, Reith S, Uhl K, Bailey S, Gautel M, Jeschke B, Fischer C, Ochs J, McKenna WJ, Klues H, et al. A newly created splice donor site in exon 25 of the MyBP-C gene is responsible for inherited hypertrophic cardiomyopathy with incomplete disease penetrance. *Circulation*. 2000;101:1396-1402. doi: 10.1161/01.CIR.101.12.1396

38. Coats CJ, Heywood WE, Virasami A, Ashrafi N, Syrris P, Dos Remedios C, Treibel TA, Moon JC, Lopes LR, McGregor CGA, et al. Proteomic Analysis of the Myocardium in Hypertrophic Obstructive Cardiomyopathy. *Circ Genom Precis Med*. 2018;11:e001974. doi: 10.1161/CIRCGEN.117.001974
39. Luedde M, Flogel U, Knorr M, Grundt C, Hippe HJ, Brors B, Frank D, Haselmann U, Antony C, Voelkers M, et al. Decreased contractility due to energy deprivation in a transgenic rat model of hypertrophic cardiomyopathy. *J Mol Med (Berl)*. 2009;87:411-22. doi: 10.1007/s00109-008-0436-x
40. Guclu A, Knaapen P, Harms HJ, Parbhudayal RY, Michels M, Lammertsma AA, van Rossum AC, Germans T and van der Velden J. Disease Stage-Dependent Changes in Cardiac Contractile Performance and Oxygen Utilization Underlie Reduced Myocardial Efficiency in Human Inherited Hypertrophic Cardiomyopathy. *Circ Cardiovasc Imaging*. 2017;10. doi: 10.1161/CIRCIMAGING.116.005604
41. Crilley JG, Boehm EA, Blair E, Rajagopalan B, Blamire AM, Styles P, McKenna WJ, Ostman-Smith I, Clarke K and Watkins H. Hypertrophic cardiomyopathy due to sarcomeric gene mutations is characterized by impaired energy metabolism irrespective of the degree of hypertrophy. *J Am Coll Cardiol*. 2003;41:1776-82. doi:
42. Ashrafian H, Redwood C, Blair E and Watkins H. Hypertrophic cardiomyopathy:a paradigm for myocardial energy depletion. *Trends Genet*. 2003;19:263-8. doi: 10.1016/S0168-9525(03)00081-7
43. Tarone G and Brancaccio M. Keep your heart in shape: molecular chaperone networks for treating heart disease. *Cardiovasc Res*. 2014;102:346-61. doi: 10.1093/cvr/cvu049
44. Dorsch LM, Schuldt M, dos Remedios CG, Schinkel AFL, de Jong PL, Michels M, Kuster DWD, Brundel B and van der Velden J. Protein Quality Control Activation and Microtubule Remodeling in Hypertrophic Cardiomyopathy. *Cells*. 2019;8. doi: 10.3390/cells8070741
45. Dorsch LM, Schuldt M, Knezevic D, Wiersma M, Kuster DWD, van der Velden J and Brundel B. Untying the knot: protein quality control in inherited cardiomyopathies. *Pflugers Arch*. 2018. doi: 10.1007/s00424-018-2194-0
46. Sanbe A, Daicho T, Mizutani R, Endo T, Miyauchi N, Yamauchi J, Tanonaka K, Glabe C and Tanoue A. Protective effect of geranylgeranylacetone via enhancement of HSPB8 induction in desmin-related cardiomyopathy. *PLoS One*. 2009;4:e5351. doi: 10.1371/journal.pone.0005351
47. Bhuiyan MS, Pattison JS, Osinska H, James J, Gulick J, McLendon PM, Hill JA, Sadoshima J and Robbins J. Enhanced autophagy ameliorates cardiac proteinopathy. *J Clin Invest*. 2013;123:5284-97. doi: 10.1172/JCI70877
48. Grimes KM, Prasad V and McNamara JW. Supporting the heart: Functions of the cardiomyocyte's non-sarcomeric cytoskeleton. *J Mol Cell Cardiol*. 2019;131:187-196. doi: 10.1016/j.yjmcc.2019.04.002
49. Lewis YE, Moskovitz A, Mutlak M, Heineke J, Caspi LH and Kehat I. Localization of transcripts, translation, and degradation for spatiotemporal sarcomere maintenance. *J Mol Cell Cardiol*. 2018;116:16-28. doi: 10.1016/j.yjmcc.2018.01.012
50. Scholz D, Baicu CF, Tuxworth WJ, Xu L, Kasiganesan H, Menick DR and Cooper Gt. Microtubule-dependent distribution of mRNA in adult cardiocytes. *Am J Physiol Heart Circ Physiol*. 2008;294:H1135-44. doi: 10.1152/ajpheart.01275.2007
51. Thottakara T, Friedrich FW, Reischmann S, Braumann S, Schlossarek S, Kramer E, Juhr D, Schluter H, van der Velden J, Munch J, et al. The E3 ubiquitin ligase Asb2beta is downregulated in a mouse model of hypertrophic cardiomyopathy and targets desmin for proteasomal degradation. *J Mol Cell Cardiol*. 2015;87:214-24. doi: 10.1016/j.yjmcc.2015.08.020

52. Robison P and Prosser BL. Microtubule mechanics in the working myocyte. *J Physiol*. 2017;595:3931-3937. doi: 10.1113/JP273046
53. Zile MR, Koide M, Sato H, Ishiguro Y, Conrad CH, Buckley JM, Morgan JP and Cooper Gt. Role of microtubules in the contractile dysfunction of hypertrophied myocardium. *J Am Coll Cardiol*. 1999;33:250-60. doi:
54. Infante AS, Stein MS, Zhai Y, Borisy GG and Gundersen GG. Detyrosinated (Glu) microtubules are stabilized by an ATP-sensitive plus-end cap. *J Cell Sci*. 2000;113 (Pt 22):3907-19. doi:
55. Nieuwenhuis J and Brummelkamp TR. The Tubulin Detyrosination Cycle: Function and Enzymes. *Trends Cell Biol*. 2019;29:80-92. doi: 10.1016/j.tcb.2018.08.003
56. Aillaud C, Bosc C, Peris L, Bosson A, Heemeryck P, Van Dijk J, Le Friec J, Boulan B, Vossier F, Sanman LE, et al. Vasohibins/SVBP are tubulin carboxypeptidases (TCPs) that regulate neuron differentiation. *Science*. 2017;358:1448-1453. doi: 10.1126/science.aao4165
57. Nieuwenhuis J, Adamopoulos A, Bleijerveld OB, Mazouzi A, Stickel E, Celie P, Altelaar M, Knipscheer P, Perrakis A, Blomen VA, et al. Vasohibins encode tubulin detyrosinating activity. *Science*. 2017;358:1453-1456. doi: 10.1126/science.aao5676
58. Kerr JP, Robison P, Shi G, Bogush AI, Kempema AM, Hexum JK, Becerra N, Harki DA, Martin SS, Raiteri R, et al. Detyrosinated microtubules modulate mechanotransduction in heart and skeletal muscle. *Nat Commun*. 2015;6:8526. doi: 10.1038/ncomms9526
59. Swiatlowska P, Sanchez-Alonso JL, Wright PT, Novak P and Gorelik J. Microtubules regulate cardiomyocyte transversal Young's modulus. *Proc Natl Acad Sci U S A*. 2020;117:2764-2766. doi: 10.1073/pnas.1917171117
60. Dobin A, Davis CA, Schlesinger F, Drenkow J, Zaleski C, Jha S, Batut P, Chaisson M and Gingeras TR. STAR: ultrafast universal RNA-seq aligner. *Bioinformatics*. 2013;29:15-21. doi: 10.1093/bioinformatics/bts635
61. Tarasov A, Vilella AJ, Cuppen E, Nijman IJ and Prins P. Sambamba: fast processing of NGS alignment formats. *Bioinformatics*. 2015;31:2032-4. doi: 10.1093/bioinformatics/btv098
62. Aransay AM and Lavín Trueba JL. Field guidelines for genetic experimental designs in high-throughput sequencing. 2016. http://link.springer.com/book/10.1007/978-3-319-31350-4
63. Robinson MD, McCarthy DJ and Smyth GK. edgeR: a Bioconductor package for differential expression analysis of digital gene expression data. *Bioinformatics*. 2010;26:139-40. doi: 10.1093/bioinformatics/btp616
64. Love MI, Huber W and Anders S. Moderated estimation of fold change and dispersion for RNA-seq data with DESeq2. *Genome Biol*. 2014;15:550. doi: 10.1186/s13059-014-0550-8
65. Afgan E, Baker D, Batut B, van den Beek M, Bouvier D, Cech M, Chilton J, Clements D, Coraor N, Gruning BA, et al. The Galaxy platform for accessible, reproducible and collaborative biomedical analyses: 2018 update. *Nucleic Acids Res*. 2018;46:W537-W544. doi: 10.1093/nar/gky379
66. Subramanian A, Tamayo P, Mootha VK, Mukherjee S, Ebert BL, Gillette MA, Paulovich A, Pomeroy SL, Golub TR, Lander ES, et al. Gene set enrichment analysis: a knowledge-based approach for interpreting genome-wide expression profiles. *Proc Natl Acad Sci U S A*. 2005;102:15545-50. doi: 10.1073/pnas.0506580102
67. Cong L, Ran FA, Cox D, Lin S, Barretto R, Habib N, Hsu PD, Wu X, Jiang W, Marraffini LA, et al. Multiplex genome engineering using CRISPR/Cas systems. *Science*. 2013;339:819-23. doi: 10.1126/science.1231143

THE SUPPLEMENTARY DATA IS AVAILABLE ONLINE:

https://www.ahajournals.org/doi/suppl/10.1161/CIRCHEARTFAILURE.120.007022

EDITORIAL

TUBULIN DETYROSINATION: AN EMERGING THERAPEUTIC TARGET IN HYPERTROPHIC CARDIOMYOPATHY

Kenneth B. Margulies, Benjamin L. Prosser

Circulation: Heart Failure, 2021;14(1):e008006.

Since the first reported series of patients with cardiac hypertrophy of unknown cause in 1944,[1] insights into the primary pathogenesis and secondary consequences of hypertrophic cardiomyopathy (HCM) have advanced considerably. Beyond recognition that HCM is the most common genetic heart disease, there has been progress in elucidating the genetic origins of HCM, including a predominance of sarcomere protein mutations and typical autosomal dominant inheritance with variable penetrance. In a sizable subset of patients with HCM, there has been recognition that hypercontractility, due to increased myofilament calcium sensitivity, conspires with anatomic remodeling to produce dynamic left ventricular outflow tract obstruction (LVOTO). These insights inspired effective utilization of negative inotropic agents (β-blockers, calcium-channel blockers, and disopyramide) that often provide significant symptomatic relief in patients with LVOTO. When the anatomic features of HCM and LVOTO prove refractory to negative inotropes, alcohol septal ablation and surgical myectomy are highly effective at improving symptoms.[2] Recently, more sophisticated targeting of the subcellular basis for hypercontractility has allowed development of direct myosin inhibitors that are highly effective at mitigating hypercontractility and LVOTO with a more favorable tolerability profile than previously used agents. These recent successes, coupled with the ability to identify the specific pathogenic mutation in about half of patients with HCM, have inspired consideration of even more precise disease targeting and perhaps even genotype-specific therapeutics.

In this context, the article by Schuldt et al[3] in this issue of *Circulation: Heart Failure* reports the results of a proteomic analysis of myocardial tissue from a cohort of patients with HCM who had undergone septal myectomy for symptomatic LVOTO. The full cohort of patients with HCM was subdivided into 39 subjects who had an identified pathogenic sarcomere protein mutation and 11 in whom no pathogenic mutation was identified. The proteomic profiling revealed that many of the abnormalities in myocardial expression of metabolic, extracellular matrix, and muscle-related proteins in patients with HCM are similar among those with and without an identified sarcomere protein mutation. However, notable exceptions were abnormalities in cytoskeletal proteins and particularly the abundance of detyrosinated α-tubulin, which was much greater among patients with HCM, and a known sarcomere gene mutation than in those without an identified mutation. This particular finding is notable because recent studies have shown that this specific posttranslational modification—detyrosination of α-tubulin—has significant effects on the stability and density of the cardiomyocyte cytoskeleton and cell biomechanics. Specifically, increased detyrosination and associated changes to the cardiomyocyte microtubule network are causally linked to increased stiffness and viscoelasticity that reduce contractility and slow both contraction and relaxation.[4–8] To better define the functional significance of increased tubulin detyrosination in genotype-positive patients, Schuldt et al performed studies using a murine model designed to mimic the most severely affected genotype in the HCM patient cohort: *MYBPC3*$_{2373insG}$. In these studies, mice homozygous for this

mutation exhibited particularly severe hypertrophy, a reduced ejection fraction, and severe relaxation abnormalities. Moreover, hearts from mice with this analogue of the human mutation had markedly increased levels of detyrosinated tubulin compared with wild-type controls, and cardiomyocytes from these mice demonstrated slowed contraction and relaxation. Importantly, administration of parthenolide—an agent known to reduce the proportion of detyrosinated tubulin—normalized the cardiomyocyte contraction and relaxation times, suggesting that increased detyrosination contributes to the contractility and relaxation defects in mice (and humans) carrying the *MYBPC3*$_{2373insG}$ mutation. Compared with a second mouse strain with a different *Mybpc3* mutation, less severe increases in tubulin detyrosination, and slower progression of hypertrophy and contractile defects, the mice carrying the *MYBPC3*$_{2373insG}$ mutation developed severe remodeling at a much earlier age. Though parthenolide has actions that are independent of decreased detyrosination,[9] the authors conclude that increased detyrosination of microtubules contributes to cardiomyocyte stiffness and dysfunction with a greater impact in the presence of a pathogenic sarcomere protein mutation. To a large extent, the findings by Schuldt et al confirm and complement previous reports demonstrating increased tubulin detyrosination in hearts obtained from patients with advanced HCM requiring heart transplantation.[4,5] In those studies, parthenolide or genetic manipulation of the enzymes of the detyrosination/tyrosination cycle improved contractility and relaxation velocities in intact human cardiomyocytes isolated from patients with HCM.[5,6] In this context, the studies by Schuldt et al using myectomy samples suggest that the development of functionally significant tubulin detyrosination in HCM may occur long before end-stage heart disease requiring transplantation. The interpretation of the findings in the smaller subset of HCM patients without a pathogenic mutation, who exhibited more modest increases in tubulin detyrosination, is less clear. While Schuldt et al conclude that the presence or absence of a demonstrable sarcomeric mutation determines the pathogenic contribution of tubulin detyrosination, the significant differences in the absolute degree of hypertrophy in the HCM groups with and without sarcomere protein mutations represents a potential confounding factor because the patients without a sarcomere protein mutation had significantly less hypertrophy than those with an identified mutation. Specifically, among patients without an identified mutation, none had a septal thickness over 20 mm. In contrast, 19 of 39 patients with a pathogenic mutation had a septal thickness >20 mm, and 17 of 18 patients of those with a *MYBPC3* mutation had a septal thickness ≥20 mm. Thus, it could be the degree of pathological hypertrophy that drives the magnitude of α-tubulin detyrosination among patients with HCM, irrespective of mutation status. Indeed, the aforementioned studies using hearts from transplant recipients[4,5] demonstrate that patients with advanced dilated cardiomyopathy also demonstrated substantially increased degrees of tubulin detyrosination, which was not observed in nonfailing hearts with compensated hypertrophy. The temporal progression of this posttranslational modification and its correlative or causative link to the initiation,

establishment, and progression of hypertrophy requires further inquiry in controlled research models. The imperfect modeling of human HCM with mouse models is another shortcoming worth noting. In contrast with the heterozygous *MYBPC3* mutations in the patients classified as genotype positive by Schuldt et al, the murine models used for their longitudinal and isolated myocyte studies are homozygous. This is an important difference that likely exacerbates and accelerates the progression of HCM in mice and could affect the magnitude of downstream changes including tubulin detyrosination. Nevertheless, the current studies further advance the concept that the myocardial adaptations downstream of primary genetic defects may be opportunities for therapeutic targeting. In particular, microtubule-dependent cardiomyocyte stiffening, as a consequence of reversible, post-transcriptional detyrosination of α-tubulin, is a promising therapeutic target that is supported by both the human proteomics and mouse studies in the article by Schuldt et al. In addition to clearer elucidation of the degree to which specific pathogenic mutations drive tubulin detyrosination, independent of hypertrophy magnitude, further studies should examine whether in vivo targeting of tubulin detyrosination improves contractile and relaxation defects at the organ level or alters the progression of HCM and its associated morbidity.

REFERENCES

1. Levy RL, Von Glahn WC. Cardiac hypertrophy of unknown cause: a study of the clinical and pathologic features in ten adults. Am Heart J. 1944;28:714–741. doi: 10.1016/S0002-8703(44)91039-2
2. Dearani JA, Ommen SR, Gersh BJ, Schaff HV, Danielson GK. Surgery insight: septal myectomy for obstructive hypertrophic cardiomyopathy–the Mayo Clinic experience. Nat Clin Pract Cardiovasc Med. 2007;4:503–512. doi: 10.1038/ncpcardio0965
3. Schuldt M, Pei J, Harakalova M, Dorsch LM, Schossarek S, Mokry M, Knol JC, Pham TV, Schelfhorst T, Piersma SR, et al. Proteomic and functional studies reveal detyrosinated tubulin as treatment target in sarcomere mutation-induced hypertrophic cardiomyopathy. Circ Heart Fail. 2021;14:39–55. doi: 10.1161/CIRCHEARTFAILURE.120.007022
4. Robison P, Caporizzo MA, Ahmadzadeh H, Bogush AI, Chen CY, Margulies KB, Shenoy VB, Prosser BL. Detyrosinated microtubules buckle and bear load in contracting cardiomyocytes. Science. 2016;352:aaf0659. doi: 10.1126/science.aaf0659
5. Chen CY, Caporizzo MA, Bedi K, Vite A, Bogush AI, Robison P, Heffler JG, Salomon AK, Kelly NA, Babu A, et al. Suppression of detyrosinated microtubules improves cardiomyocyte function in human heart failure. Nat Med. 2018;24:1225–1233. doi: 10.1038/s41591-018-0046-2
6. Chen CY, Salomon AK, Caporizzo MA, Curry S, Kelly NA, Bedi K, Bogush AI, Krämer E, Schlossarek S, Janiak P, et al. Depletion of vasohibin 1 speeds contraction and relaxation in failing human cardiomyocytes. Circ Res. 2020;127:e14–e27. doi: 10.1161/CIRCRESAHA.119.315947
7. Caporizzo MA, Chen CY, Bedi K, Margulies KB, Prosser BL. Microtubules increase diastolic stiffness in failing human cardiomyocytes and myocardium. Circulation. 2020;141:902–915. doi: 10.1161/CIRCULATIONAHA.119.043930
8. Swiatlowska P, Sanchez-Alonso JL, Wright PT, Novak P, Gorelik J. Microtubules regulate cardiomyocyte transversal Young's modulus. Proc Natl Acad Sci USA. 2020;117:2764–2766. doi: 10.1073/pnas.1917171117
9. Kurdi M, Bowers MC, Dado J, Booz GW. Parthenolide induces a distinct pattern of oxidative stress in cardiac myocytes. Free Radic Biol Med. 2007;42:474–481. doi: 10.1016/j.freeradbiomed.2006.11.012

MULTI-OMICS INTEGRATION IDENTIFIES KEY UPSTREAM REGULATORS OF PATHOMECHANISMS IN HYPERTROPHIC CARDIOMYOPATHY DUE TO TRUNCATING *MYBPC3* MUTATIONS

J. Pei[‡], **M. Schuldt[‡]**, E. Nagyova[‡], Z. Gu, S. el Bouhaddani, L. Yiangou, M. Jansen, J.J.A. Calis, L.M. Dorsch, C. Snijders Blok, N.A.M. van den Dungen, N. Lansu, B.J. Boukens, I.R. Efimov, M. Michels, M.C. Verhaar, R. de Weger, A. Vink, F.G. van Steenbeek, A.F. Baas, R.P. Davis, H.W. Uh, D.W.D Kuster, C. Cheng, M. Mokry, J. van der Velden[*], F.W. Asselbergs[*], M. Harakalova[*]

[‡]Equal contribution of first authors, [*]Equal contribution of last authors

Clinical Epigenetics, 2021. 13(1): p.61.

6

ABSTRACT

Background

Hypertrophic cardiomyopathy (HCM) is the most common genetic disease of the cardiac muscle, frequently caused by mutations in *MYBPC3*. However, little is known about the upstream pathways and key regulators causing the disease. Therefore, we employed a multi-omics approach to study the pathomechanisms underlying HCM comparing patient hearts harboring *MYBPC3* mutations to control hearts.

Results

Using H3K27ac ChIP-seq and RNA-seq we obtained 9,310 differentially acetylated regions and 2,033 differentially expressed genes, respectively, between 13 HCM and 10 control hearts. We obtained 441 differentially expressed proteins between 11 HCM and 8 control hearts using proteomics. By integrating multi-omics datasets, we identified a set of DNA regions and genes that differentiate HCM from control hearts and 53 protein-coding genes as the major contributors. This comprehensive analysis consistently points towards altered extracellular matrix formation, muscle contraction, and metabolism. Therefore, we studied enriched transcription factor (TF) binding motifs and identified 9 motif-encoded TFs, including *KLF15, ETV4, AR, CLOCK, ETS2, GATA5, MEIS1, RXRA,* and *ZFX*. Selected candidates were examined in stem cell derived-cardiomyocytes with and without mutated *MYBPC3*. Furthermore, we observed an abundance of acetylation signals and transcripts derived from cardiomyocytes compared to non-myocyte populations.

Conclusions

By integrating histone acetylome, transcriptome, and proteome profiles, we identified major effector genes and protein networks that drive the pathological changes in HCM with mutated *MYBPC3*. Our work identifies 38 highly affected protein-coding genes as potential plasma HCM biomarkers and 9 TFs as potential upstream regulators of these pathomechanisms that may serve as possible therapeutic targets.

INTRODUCTION

Hypertrophic cardiomyopathy (HCM), characterized by thickening of the myocardium that is not explained by abnormal loading conditions, is the most common inherited cardiac disease [1]. More than 1,500 associated mutations, primarily in genes encoding parts of the sarcomere, such as *MYBPC3*, *MYH7*, and *TNNT2*, have been identified. The remodeled myocardium is characterized by cardiomyocyte hypertrophy and disarray, extensive fibrosis, and reduced capillary density [2]. HCM is a heterogeneous disease as the onset, the disease phenotype, and the severity of the clinical presentations differ greatly among mutation carriers [3]. Additionally, different mutated genes exhibit distinct biological impact on cellular contractility, energy metabolism, and sarcomeric protein expression in HCM hearts [4]. However, the driving pathological mechanisms underlying the heterogenous HCM remains largely unknown.

Next-generation sequencing technologies (NGS) are instrumental in understanding disease etiology, delivering a clinical diagnosis, and discovering new treatment options. Multiple studies employed NGS to reveal the epigenetic modifications in heart failure, including DNA methylation and histone (de-)acetylation, which provided insights and identification of the driving mechanism underlying the disease [5,6]. We previously showed the influence of histone acetylation changes on QRS complex-related GWAS loci in HCM [7,8]. Additionally, studies from our group and others have shown that H3K27ac corresponds to the gene expression in human cardiac tissues as well as human cardiomyocytes [9,10], highlighting it as a promising epigenetic mark for predicting gene expression. Studies also employed RNA sequencing to identify the affected transcription factor-mediated upstream regulatory events and the distinct gene expressions that define heart failure [9,10]. Furthermore, data-piling studies are now connecting proteomics to NGS to get comprehensive information on the disease biology for precision medicine [11].

In this study, we aim to understand the pathomechanisms driving HCM by employing a multi-omics approach, including chromatin immunoprecipitation sequencing (ChIP-seq), RNA sequencing (RNA-seq), and proteomics, using myocardial tissue obtained from clinically well-phenotyped HCM patients with truncating *MYBPC3* mutations and compared these with non-failing donor hearts. We revealed altered histone acetylome, transcriptome, and proteome profiles in HCM versus control hearts and studied affected biological functions. Besides, we identified key factors that may play a critical role in regulating the pathomechanisms underlying HCM. We also evaluated the contribution of histone acetylation and transcription signals in 11 cell types in the heart. Combined, this multi-omics study gives insight into the underlying disease pathways driving HCM and identifies promising candidates for therapeutic strategies.

RESULTS

Pairwise comparison between HCM and control hearts reveals distinct histone acetylome profiles

H3K27ac ChIP-seq was used to capture acetylated DNA regions in each sample and to compare the acetylation levels between 13 HCM (n=13) and 10 control hearts (Figure 1A and Supplementary Table 1) using DESeq2. In total, we identified 4,226 regions presented higher acetylation levels (hyperacetylated regions) and 5,084 regions presented lower acetylation levels (hypoacetylated regions) in HCM versus control hearts (P_{adj}<0.05, Figure 1B, Supplementary Table 2A). Examples of hyper- and hypoacetylated regions are shown in Supplementary Figure 1. Region-to-gene annotation using either a 5kb or 50kb window from the transcription start site (TSS) revealed genes in the hyperacetylated regions are mostly involved in muscle contraction and extracellular matrix (ECM) development-related processes, whereas genes in the hypoacetylated regions are mostly involved in metabolic processes (Supplementary Table 2B-2E).

Pairwise comparison between HCM and control hearts reveals distinct transcriptome profiles

Following RNA-seq of the same biopsies, the transcriptional profiles between 13 HCM (n=13) and 10 control hearts were compared using DESeq2. In total, we identified 936 up-regulated genes and 1,097 down-regulated genes in HCM hearts compared to controls (P_{adj}<0.05, Figure 1C, Supplementary Table 3A). The top biological processes enriched by up-regulated genes are involved in the muscle system process and energy production. The top biological processes enriched by down-regulated genes are involved in lipid metabolism and cell adhesion (Supplementary Table 3B and 3C).

Pairwise comparison between HCM and control hearts reveals distinct proteome profiles

We also performed proteomics in 11 HCM samples and compared their protein expression levels to another control group (n=8) using DESeq2. In total, we identified 216 up-regulated proteins and 225 down-regulated proteins in HCM hearts compared to controls (P<0.05, Figure 1D, Supplementary Table 4A). The top enriched biological processes by up-regulated proteins are involved in muscular and ECM development. The top enriched biological processes by down-regulated proteins are involved in metabolism (Supplementary Figure 2, Supplementary Table 4B, and 4C).

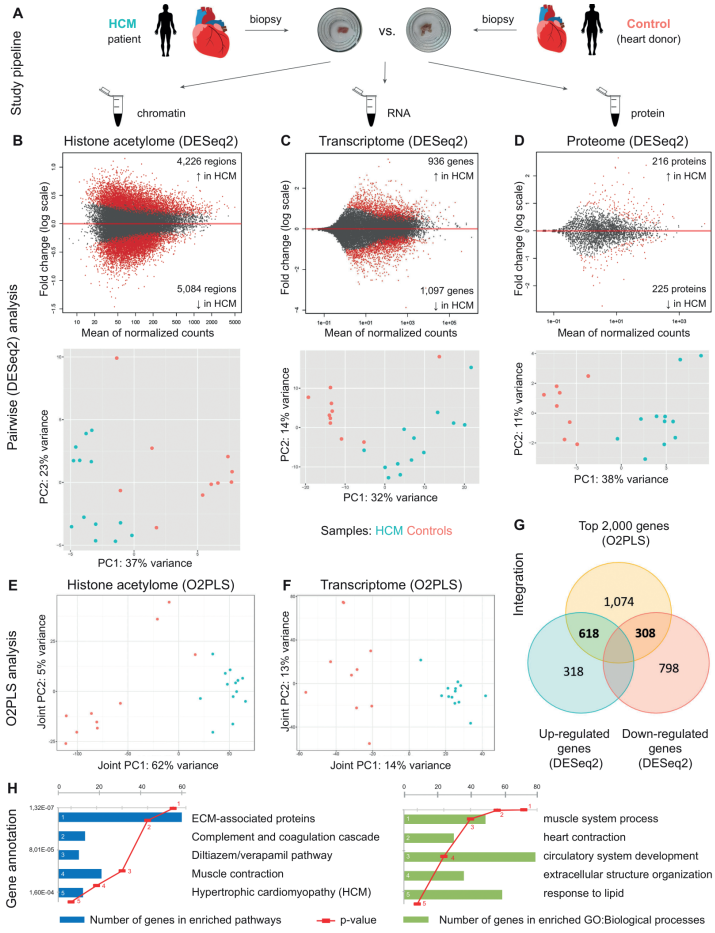

FIGURE 1. Pairwise analyses using DESeq2 and integrative analyses using unsupervised O2PLS in all samples. **(A)** An overview of the study design. **(B)** Upper plot: MA (ratio intensity) plot showing the hyper- and hypoacetylation regions in HCM samples compared to controls using DESeq2; Bottom plot: principal component analysis (PCA) plot showing the separation between HCM and control samples based on the top differentially acetylated regions using DESeq2. Mean values of normalized counts in all samples are depicted on the x-axis and fold changes (log2) on the y-axis. **(C)** Upper plot: PCA plot showing the separation between HCM and control samples based on the top differentially expressed genes using DESeq2; Bottom plot: MA plot showing the up-regulated and down-regulated genes in HCM samples compared to controls using DESeq2. **(D)** Upper plot: PCA plot showing the separation between HCM and control samples based on the top differentially expressed proteins using DESeq2; Bottom plot: MA plot showing the up-regulated and down-regulated proteins in HCM samples compared to controls using DESeq2. **(E)** Score plot of the first joint component of the H3K27ac ChIP-seq data showing the separation of HCM hearts from controls. **(F)** Score plot of the first joint component of the RNA-seq data discriminating HCM hearts from controls. **(G)** Venn diagram showing the overlapping targets between the top 2,000 genes obtained using the integrative approach (O2PLS) and differentially expressed genes obtained using the pairwise comparison (DESeq2). **(H)** Enrichment analyses using the overlapping targets, which included 618 up-regulated genes and 308 down-regulated genes.

Integrating histone acetylome, transcriptome, and proteome changes in HCM

We also integrated H3K27ac ChIP-seq and RNA-seq data in an unsupervised manner using O2PLS. Notably, without predefining the patient and the control groups, the first joint component of both ChIP-seq and RNA-seq plots discriminated HCM from control hearts (Figure 1E and 1F). DNA regions and genes that contributed to the separation between HCM and control hearts are shown in Supplementary Table 5. Next, we aimed to identify key genes that underlie the separation between two groups and show altered expression levels in HCM hearts versus controls. Therefore, we overlapped 2,000 genes that discriminate HCM hearts and controls from the integrative analysis (O2PLS) with the differentially expressed genes from the pairwise comparison with the top and obtained 618 up-regulated genes and 308 down-regulated genes (Figure 1G and Supplementary Table 6A). These overlapping genes are enriched for biological processes in the circulatory system and muscle contraction and pathways involved in the ECM formation and complement system (Figure 1H, Supplementary Table 6B).

Since only 11 out of 13 HCM samples were included in the proteomics experiment and a different set of control samples was used in comparison with the HCM group, we could not apply O2PLS to integrate the proteomic data with either H3K27ac ChIP-seq or RNA-seq data. We, therefore, overlapped differentially expressed genes supported by DESeq2 and O2PLS analyses with proteomic data and identified 36 up-regulated protein-coding genes and 17 down-regulated protein-coding genes in HCM versus control hearts (Table 1). Notably, the protein levels of 38 protein-coding genes are detectable in the plasma and 5 out of them were consistently changed in the same direction in HCM versus control hearts at DNA (5kb from TSS), RNA, and protein levels, including the up-regulation of ASPN, FMOD, MCAM, and NPPA and the down-regulation of AASS, highlighting them as promising candidates for biomarker discovery in HCM (Table 1).

TABLE 1. Promising candidates showing the same changing direction in HCM versus control hearts at multi-omics levels.

Symbol	Known expression level in cardiomyocytes*	Protein level in the plasma/serum‡	Rank in the O2PLS analysis	Transcriptome change (log2FC)	Proteome change (log2FC)	Histone acetylome change in the matched direction (50Kb of TSS)	Transcriptome change in diseased versus control cardiomyocytes† log2(FC)
AASS	Medium	Detected	1046	-1,279808444	-0,773247332	Yes	-0,414920406
ABHD11	Medium	Detected	669	1,137180651	0,640971138	-	-
ACTN2	High	Detected	1597	0,570095367	0,184641682	-	-
ADH1B	Low	Detected	1281	-1,081956134	-0,880289941	-	-
ARHGAP1	Medium	Detected	1512	1,763584	0,597291165	Yes	-
ASPN	Not detected	Detected	454	2,204317	1,77725136	Yes	-
ATP2A2	High	Detected	728	-1,466783433	-0,353968239	-	-
BGN	Medium	Detected	1012	1,832538	1,533815477	-	0,588280947
C6	Not detected	Detected	130	-1,776237721	-0,695516121	-	-
CA3	Not detected	Detected	43	4,518344	1,686864533	-	-
CHCHD6	Medium	Not detected	910	2,003514	0,778880421	-	-
CHDH	Low	Not detected	98	-2,209806815	-1,442995937	Yes	-
CLGN	Not detected	Not detected	1751	-1,088152172	-0,808838009	Yes	-
DDAH1	Not detected	Detected	452	1,764206	1,115473264	Yes	-
EFHD1	Not detected	Not detected	682	1,865517	1,264459654	Yes	0,318203232
FGF12	No data	Not detected	62	-2,353022973	-1,079274106	Yes	-0,30374396
FHL2	High	Not detected	440	-1,255001122	-0,411782639	-	-
FMOD	No data	Detected	395	2,594323	1,414783229	Yes	-
FSCN1	Not detected	Detected	1276	1,759951	0,971207984	Yes	0,456046007
GATM	Not detected	Detected	277	1,545734889	1,002695568	Yes	-
GPD1	Medium	Detected	1708	-1,687472289	-1,343895776	Yes	-0,410181446

TABLE 1. Continued.

Symbol	Known expression level in cardiomyocytes*	Protein level in the plasma/serum‡	Rank in the O2PLS analysis	Transcriptome change (log2FC)	Proteome change (log2FC)	Histone acetylome change in the matched direction (50Kb of TSS)	Transcriptome change in diseased versus control cardiomyocytes† log2(FC)
GPD1L	No data	Not detected	1342	-1,066784553	-0,526757351	-	-
HSPA2	Not detected	Detected	171	3,490234	2,652261545	Yes	-
HSPB6	High	Detected	647	2,253803	0,392977171	-	-3,170003763
LDHA	Not detected	Detected	974	-1,219034333	-0,474108409	Yes	-
LTBP2	Not detected	Detected	829	2,1279	2,317830122	Yes	-
LUM	Not detected	Detected	217	2,135187	0,959297891	-	0,512857369
MAP4	Medium	Detected	717	1,851811	1,003525943	Yes	-0,223635511
MCAM	Low	Detected	1338	1,653115	1,104716402	Yes	-0,264831197
MFAP2	Not detected	Not detected	1303	1,84358	0,70531399	Yes	-0,357062335
MYH6	High	Detected	40	-2,919038787	-1,009056575	-	-
MYL12A	Medium	Detected	64	2,419604	0,578322489	-	-0,14329672
MYLK3	High	Not detected	1904	-1,007764366	-0,747812735	-	0,127033902
NES	Medium	Detected	641	1,806419	1,936943877	-	-
NPPA	Medium	Detected	13	1,549472808	0,747781872	Yes	0,542363796
NUDT4	High	Not detected	1531	-1,093022558	-0,695436878	-	0,207067638
PDK4	High	Not detected	1724	-1,07459529	-0,607585372	Yes	-
RAB24	No data	Not detected	1085	2,211788	1,041018278	-	-
RRAS	High	Detected	1642	1,788982	0,447281909	-	-
S100A6	Not detected	Detected	1486	1,859224	0,794548978	-	-

TABLE 1. Continued.

Symbol	Known expression level in cardiomyocytes*	Protein level in the plasma/serum‡	Rank in the O2PLS analysis	Transcriptome change (log2FC)	Proteome change (log2FC)	Histone acetylome change in the matched direction (50Kb of TSS)	Transcriptome change in diseased versus control cardiomyocytes† log2(FC)
SAA1	No data	Detected	63	-1,173021107	-2,740052623	-	-
SERPINE2	No data	Detected	338	1,002427623	0,652055032	-	0,714236168
SGCG	High	Not detected	1805	0,707480434	0,430185184	Yes	-
SLC25A5	High	Detected	1634	1,811682	0,613247381	-	-
SNCA	Not detected	Detected	274	2,629958	1,02410125	-	-
SORBS2	No data	Detected	1991	1,475585	0,484980733	Yes	-0,241151423
STMN1	Not detected	Detected	1211	0,77170211	0,807423435	-	-
SYNPO2L	High	Not detected	483	2,306538	1,028059491	Yes	-
TANGO2	Low	Detected	1086	1,981163	0,733156318	-	-
THBS4	Low	Detected	618	2,323482	2,106545221	-	-
TPM3	Medium	Detected	981	2,116673	1,224815654	-	0,36243013
TPPP	Not detected	Not detected	1374	-0,898226805	-0,830942802	Yes	-
UCHL1	Not detected	Detected	44	5,052289	0,933127805	-	-

*: The known expression level of each candidate in cardiomyocyte is collected from the Human Protein Atlas (https://www.proteinatlas.org/).
‡: The detectable protein level of each candidate in plasma and serum is collected from the Human Plasma Proteome Project Data Central (http://www.peptideatlas.org/hupo/hppp/).
†: Differentially expressed genes between programmed cardiomyocytes with and without mutated MYBPC3 from a published study was used with a threshold of P value below 0.05 (GSE140965).
FC=fold change, TSS=transcription start site, -: not matching.

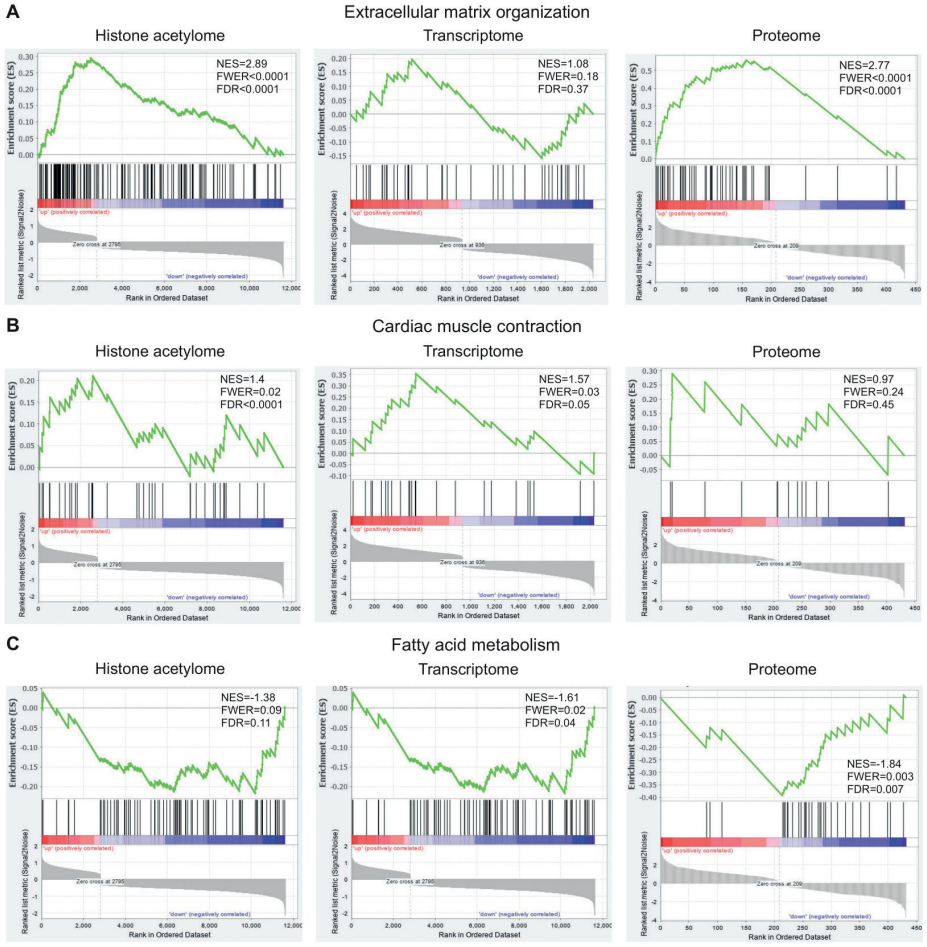

FIGURE 2. Gene set enrichment analysis showing the correlation of the gene set, which are established in extracellular matrix organization **(A)**, cardiac muscle contraction **(B)**, and fatty acid metabolism **(C)**, in annotated genes from differentially acetylated regions (histone acetylome), differentially expressed genes (transcriptome), and genes encoding differentially expressed proteins (proteome), respectively. Differentially expressed genes were ranked by their fold changes and shown on the x-axis. The running correlation throughout the gene set is shown by the curve (green) and the running enrichment score (ES) is shown on the y-axis. Enrichment score normalized for gene set size (NES), Familywise-error rate p-value (FWER), and the false discovery rate (FDR) are shown per enrichment plot.

Combined omics analyses identify ECM, muscle contraction, and metabolism as the main mechanisms altered in HCM

Genes annotated to differentially acetylated regions in the histone acetylome data, differentially expressed genes in the transcriptome data, and differentially expressed proteins in the proteome data consistently pointed to biological functions involved in enhancement of ECM, enhancement of muscle contraction, and suppression of metabolism in HCM versus control hearts. To further evaluate these biological functions, we collected gene sets that are known to regulate ECM remodeling, muscle contraction, and metabolism, and performed GSEA to study whether they are primarily found in the up-regulated or down-regulated data sets in our study or they are randomly distributed. We observed that genes involved in ECM and cardiac muscle contraction were positively correlated with genes annotated to the hyperacetylated regions in the ChIP-seq data, the up-regulated genes in the RNA-seq data, and genes encoding the up-regulated proteins in the proteomics data (Figure 2A and 2B). Genes that are related to fatty acid metabolism were significantly correlated with genes annotated to the hypoacetylated regions in the ChIP-seq data, the down-regulated genes in the RNA-seq data, and genes encoding the down-regulated proteins in the proteomics data (Figure 2C, Supplementary Figure 3). Combined, we confirmed that pathways involved in ECM, muscle contraction, and metabolism were affected in HCM.

Consistently, protein-coding genes (36 up-regulated and 17 down-regulated ones) were enriched for comparable biological processes and pathways as shown in previous analyses, such as ECM and muscle contraction (Supplementary Table 6C). We also studied protein networks among them and observed that ECM and muscle contraction were the most enriched pathways by the up-regulated protein-coding genes and metabolism was the most enriched pathway by the down-regulated protein-coding genes (Figure 3A and 3B).

Enriched transcription factor binding motifs in differentially acetylated regions

To define the actual factors that regulate altered RNA/protein expression in HCM hearts, we studied the putative transcription factors (TFs) encoded by enriched transcription factor binding motifs (TFBMs) in differentially acetylated regions by scanning through the HOCOMOCO motif database of 769 human primary and alternative binding models. We obtained 125 TFBMs in the hyperacetylated regions and 115 TFs were predicted to bind to them. In the hypoacetylated regions, 120 TFBMs were enriched and they encoded for 111 TFs. Out of those, 68 annotated TFs were enriched in both hyper- and hypo-acetylated regions (Supplementary Figure 4).

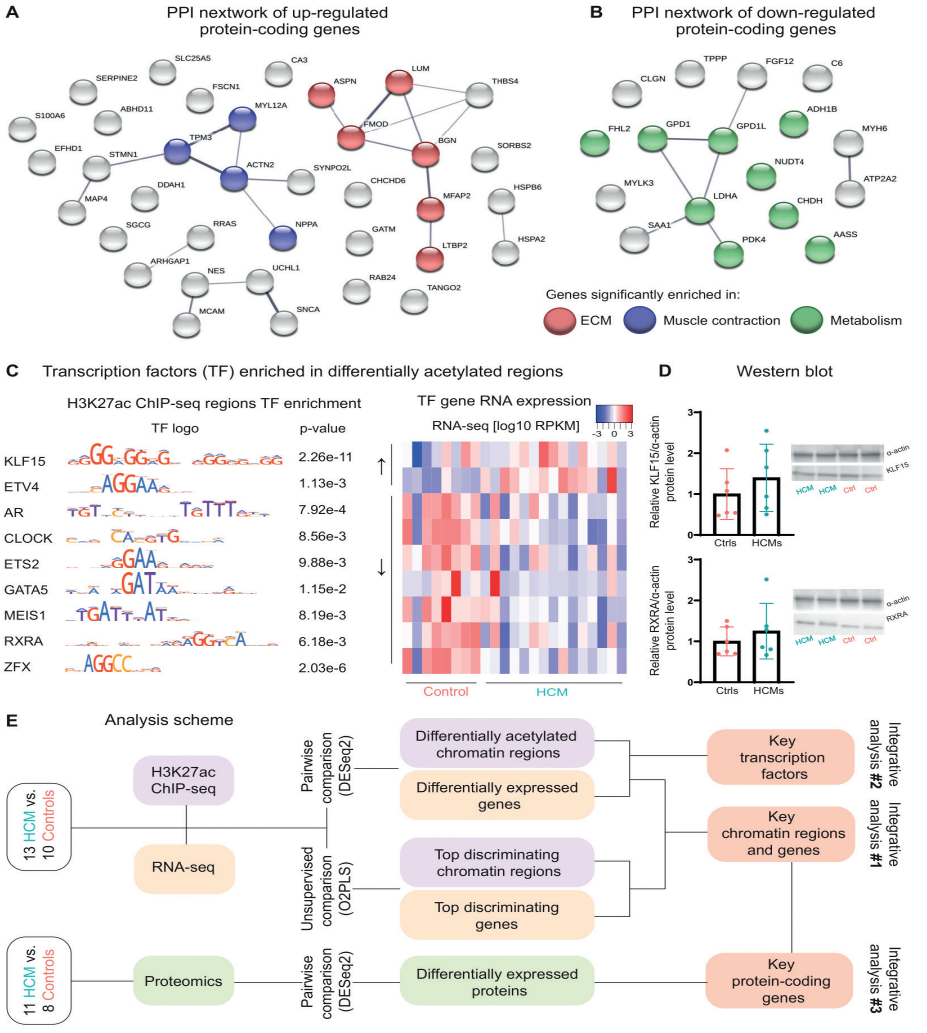

FIGURE 3. (A) An overview of protein-protein interactions of up-regulated proteins in HCM versus control hearts. Each node represents an individual protein. Nodes highlighted in red are involved in the top enriched pathway in extracellular matrix organization (ECM). Nodes highlighted in blue are involved in the top enriched pathway in muscle contraction. **(B)** An overview of protein-protein interactions of down-regulated proteins in HCM versus control hearts. Each node represents an individual protein. Nodes highlighted in green are involved in the top enriched pathway in metabolism. **(C)** Transcription factors enriched in differentially acetylated chromatin regions and their corresponding p-values (Fisher test) are shown on the left, and their mRNA expression levels among all samples are shown in the heatmap on the right. RPKM: reads per kilobase million. **(D)** Western blot data showing the protein levels of KLF15 and RXRA were comparable between HCM and control hearts. **(E)** A schematic overview showing all analysis steps in histone acetylome, transcriptome, and proteome data used in this study.

Notably, 2 TFs (*KLF15* and *ETV4*) that were encoded by enriched TFBMs in the hyperacetylated regions showed higher mRNA levels in HCM hearts than controls, and 7 TFs (*AR*, *CLOCK*, *ETS2*, *GATA5*, *MEIS1*, *RXRA*, and *ZFX*) that were encoded by enriched TFBMs in the hypoacetylated regions showed lower mRNA levels in HCM hearts than controls (Figure 3C). These TFs are enriched for biological functions involved in muscle hypertrophy and lipid metabolism (Supplementary Table 7), suggesting their potential roles in regulating the upstream signaling in HCM. Next, we examined their expressions in cardiomyocytes using the public single-nuclear RNA-seq data from adult human hearts [12]. We observed that they were all expressed in ventricular cardiomyocytes (Supplementary Figure 7). Interestingly, *KLF15*, *AR*, *CLOCK*, *MEIS1*, and *ZFX* were more abundantly expressed than *ETV4*, *ETS2*, *GATA5*, and *RXRA*. We also examined their mRNA expressions in genome-engineered cardiomyocytes with mutated *MYBPC3* compared to the control cardiomyocytes from a published study using RNA-seq (Supplementary Table 10), which provided insights into the early biological changes due to mutated *MYBPC3* in cardiomyocytes [13]. Interestingly, in line with our findings obtained from the bulk level at the severe stage, the mRNA level of *ETV4* was significantly increased (P-value=9.56E-9) in mutant cardiomyocytes compared to the controls, whereas the mRNA level of *RXRA* was significantly decreased (P-value=0.001) in mutant versus control cardiomyocytes. However, they showed comparable expression levels between HCM and control hearts in the proteome data. We further examined their protein expressions using western blot and confirmed that they were not significantly changed in HCM versus control hearts (Figure 3D). We performed additional immunofluorescence staining and examined the expression of KLF15 in human induced pluripotent stem cell-derived cardiomyocytes (hiPSC-cardiomyocytes) with and without mutated *MYBPC3*. We observed the expression of KLF15 in hiPSC-cardiomyocytes (Figure 6A), however, more cell lines derived from different patients and healthy individuals are needed to study whether the KLF15 signal differs between diseased and control cardiomyocytes.

A schematic overview of all analysis steps is shown in Figure 3E.

Genes discriminating HCM from controls show consistent changes on various levels

We further selected an example of one down-regulated and one up-regulated gene and examined them in more detail to demonstrate the strength of our integrative omic analysis. *ATP2A2*, one protein-coding gene from the overlapping candidates, encodes the sarcoplasmic reticulum Ca2+-ATPase pump SERCA2a and plays a critical role in the regulation of calcium handling [14]. We identified *ATP2A2* as one of the major candidates in discriminating HCM hearts from controls in our integrated H3K27ac ChIP-seq and RNA-seq analysis (Figure 4A). Besides, its mRNA and protein levels were significantly lower in HCM versus control hearts in the pairwise comparison, and the suppressed protein level was also validated using western blot (Figure 4B).

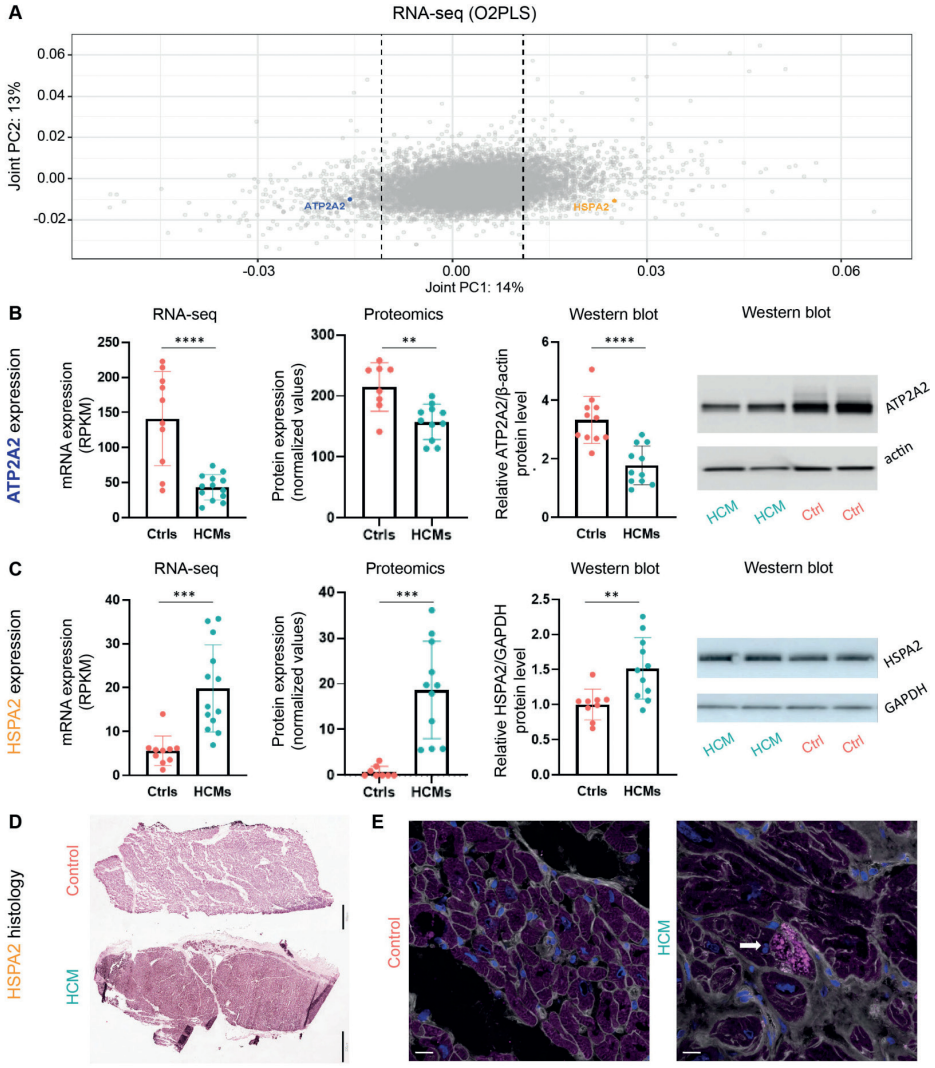

FIGURE 4. Changes of ATP2A/SERCA2a and HSPA2 at the mRNA and protein levels in HCM versus control hearts. **(A)** A plot of the joint component loadings of RNA-seq data showed *ATP2A2* and *HSPA2* were two major players in discriminating HCM hearts from controls. The dashed lines on both positive and negative sides indicate the cutoff threshold, with genes with a large contribution to the joint component falling outside of the dash lines. **(B)** ATP2A2 mRNA and protein levels in HCM and control samples at the mRNA and protein levels. **(C)** HSPA2 mRNA and protein levels expression in HCM and control samples. **: P<0.01, ***: P<0.001, ****: P<0.0001. **(D)** Representative immunohistochemistry staining showing higher HSPA2 staining intensity in HCM heart as compared to control. Scale bar=400μm (control sample) and 800μm (HCM sample). **(E)** Representative immunofluorescence staining showing HSPA2 aggregates in an HCM heart (indicated by the arrow), whereas the control shows diffuse staining of the cytoplasm without aggregates. WGA-AF488 appears in grey to visualize the cell membrane and DAPI appears in blue to visualize the nuclei. Scale bar=16μm.

HSPA2, another protein-coding gene from the overlapping candidates, is involved in protein quality control [15]. We demonstrated that HSPA2 acts as another key player in discriminating HCM hearts from controls (Figure 4A). Its mRNA and protein levels were significantly higher in HCM versus control hearts in the pairwise comparison, and the enhanced protein level was also validated using western blot (Figure 4C). The upstream regulatory region of *HSPA2* also showed a higher acetylation level in HCM versus control hearts (Table 1). Moreover, we showed a profound HSPA2 intensity in HCM compared to the control heart using the immunohistochemistry staining at low magnification (Figure 4D). Next, we employed immunofluorescence staining at high magnification and observed occasional HSPA2 aggregates in cardiomyocytes from the HCM heart, whereas no HSPA2 aggregates were shown in the control heart (Figure 4E).

Allelic imbalance of MYBPC3 in HCM hearts is observed at both DNA and RNA levels

To further explore the potential of the produced data, we investigated the contribution of both *MYBPC3* alleles in the sequencing datasets. In the patient cohort, three heterozygous truncating mutations were present in *MYBPC3*, namely c.2373dupG (n=5), c.2827C>T (n=6), and c.927-2A>G (n=2). We observed that the average acetylation ratio of *MYBPC3* with c.2373dupG, c.2827C>T, and c.927-2A>G mutation to wildtype allele was 50%, 25%, and 66.6% respectively (Supplementary Figure 5A). The average mRNA expression ratio of *MYBPC3* with c.2373dupG, c.2827C>T, and c.927-2A>G mutation to wildtype allele was 6.7%, 19.7%, and 43.4% respectively (Supplementary Figure 5B). The acetylation and mRNA levels of three mutations were not observed in control hearts (Supplementary Figure 5C and 5D). It has to be noted that it is not possible to effectively distinguish between wildtype and mutant alleles in the proteomics data.

Cellular fraction sub-analysis of bulk cardiac tissue transcriptome indicates cardiomyocyte enrichment in a cellular-specific response in HCM

Since there are multiple cell types present in the heart samples, we collected cell-type-specific markers for cardiomyocytes and 11 non-myocyte cell types as revealed by recent single-cell studies in the heart [16,17], ranging from 8 to 19 markers per cell type (Supplementary Table 9), and we examined their expression levels in our bulk sequencing data. Cardiomyocyte-specific markers showed higher histone acetylation and mRNA levels than markers of 11 non-myocyte cell types (Figure 5A and 5B), regardless of health and disease. The mRNA expression of several cell-type-specific markers was significantly different between HCM and control hearts (Figure 5C). The upstream regulatory region of three cardiomyocyte-specific markers and one T-cell-specific marker also showed significantly higher acetylation activities in HCM hearts versus controls (Figure 5D).

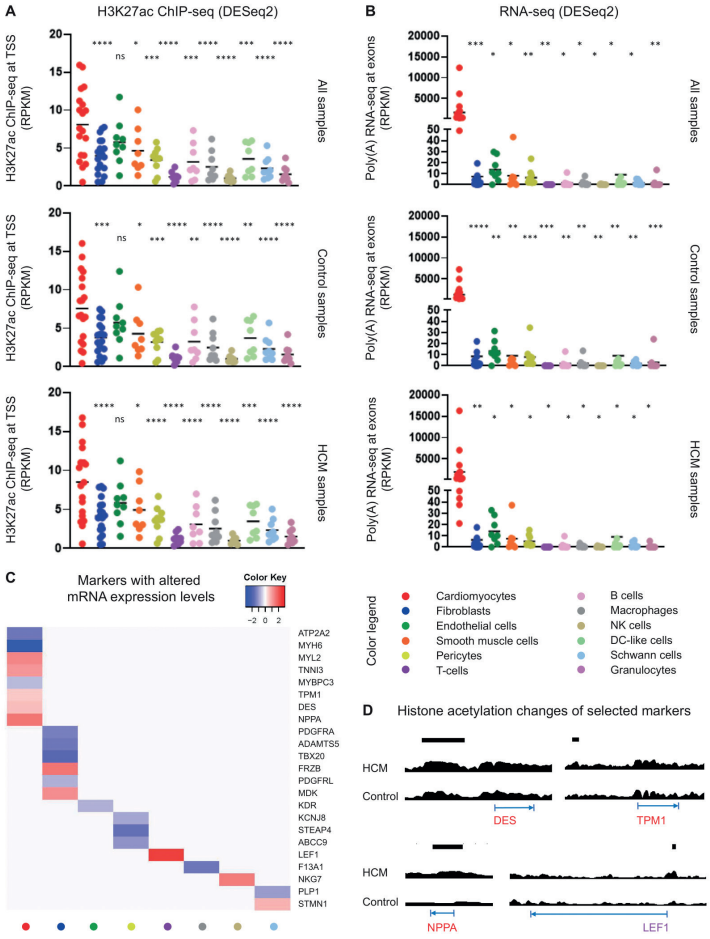

FIGURE 5. The expression of cell-type-specific markers in 12 cell populations. **(A)** The histone acetylation levels of 11 cell-type-specific markers. Each dot represents the average acetylation value of each marker for all samples, or only control or HCM samples. One-way ANOVA was used to compare the mean of cardiomyocyte-specific markers with the mean of non-myocyte markers separately: ns (not significant), *p<0.05, **p<0.01, ***p<0.001, ****p<0.0001. **(B)** The mRNA expression levels of 11 cell-type-specific markers. Each dot represents the average expression value of each marker for all samples, or only control or HCM samples. One-way ANOVA was used to compare the mean of cardiomyocyte-specific markers with the mean of non-myocyte markers separately: ns (not significant), *p<0.05, **p<0.01, ***p<0.001, ****p<0.0001. **(C)** Heat-map showing cell-type-specific markers with significantly changed mRNA expression levels in HCM hearts compared to controls. Fold changes of these markers are depicted. Positive fold changes (red) and negative fold changes (blue) represent up-regulation and down-regulation in HCM versus control hearts respectively. **(D)** Histone acetylation levels at the upstream (50 kb) of three cardiomyocytes-specific markers (red) and one T cells-specific marker (violet) were significantly changed between HCM and control hearts. Tracks of one HCM and one control heart were scaled in the UCSC genome browser (ln(x+1): 0-10). Significantly changed upstream regions are indicated by the black bar above. The transcription start and end site of each marker are indicated by the blue arrow below.

Identified candidates supported by multi-omics data in human induced pluripotent stem cells derived cardiomyocytes (hiPSC-cardiomyocytes)

We further evaluated the presence of obtained candidates, which were supported by the acetylome, transcriptome, and/or proteome data (Table 1), using hiPSC-cardiomyocytes with and without mutated *MYBPC3*. We first employed the transcriptome profile comparing the genome-engineered cardiomyocytes harboring mutated *MYBPC3* with the controls (Supplementary Table 10) from a published study [13]. Out of 53 candidates, 18 protein-coding genes (34%) from our bulk data also showed significantly affected mRNA levels between diseased and control cardiomyocytes (Table 1). Next, we examined the expression levels of several candidates between hiPSC-cardiomyocytes with and without mutated MYBPC3 using immunofluorescence staining, including ACTN2 and ATP2A2. Consistent with the suppressed mRNA and protein levels of ACTN2 in HCM versus control hearts, we observed that unlike the well-aligned cytoskeleton structure in control cardiomyocytes, HCM cardiomyocytes seemed to have a disrupted cytoskeleton as revealed by ACTN2 staining (Figure 6B). Besides, we again observed the inhibited expression of ATP2A2/SERCA2a in HCM cardiomyocytes when compared with the controls (Figure 6C). Combined, we showed that candidates screened by multi-omics approaches from the cardiac tissues also expressed in cardiomyocytes and showed similar changing direction in HCM versus control cardiomyocytes.

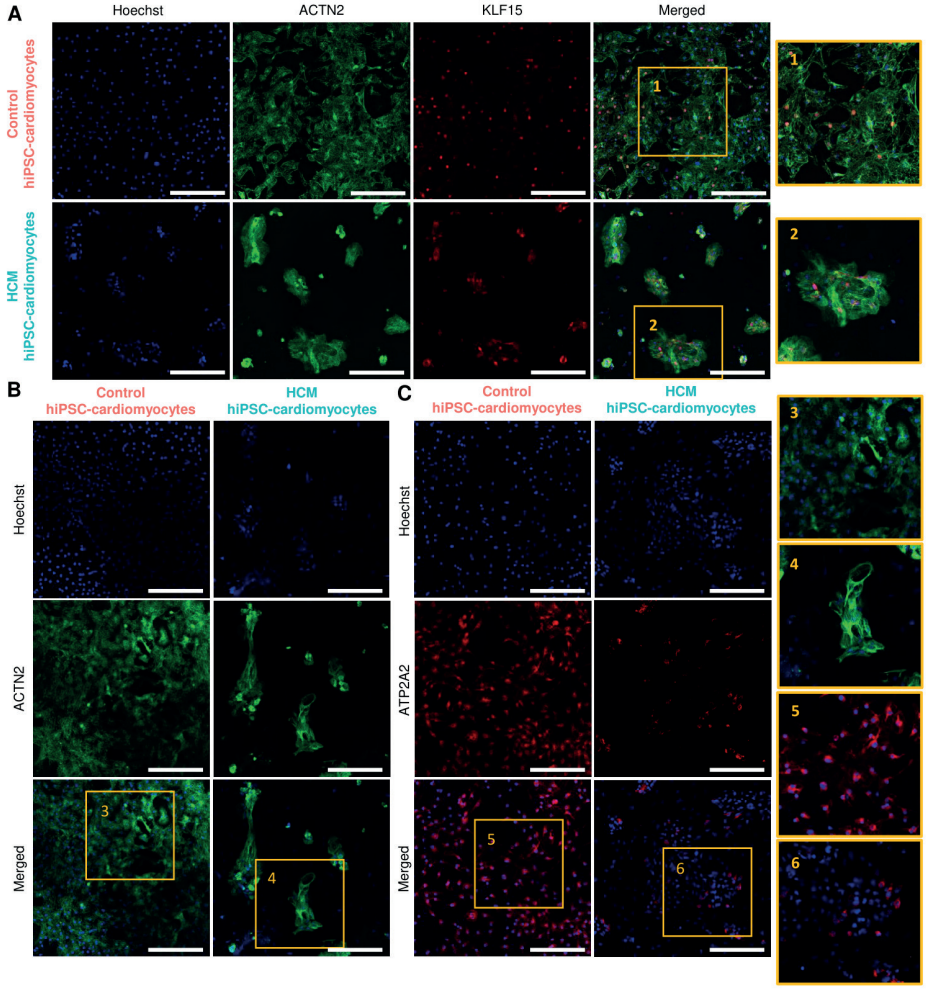

FIGURE 6. Immunofluorescence (IF) staining of selected candidates in control and HCM hiPS-cardiomyocytes. The same amount of control and HCM hiPS-cardiomyocytes (20,000 cells per well) were seeded to the plate and cultured for 27 days prior to the staining. **(A)** Representative IF staining showing the expression of KLF15 in HCM and control cardiomyocytes (KLF15: red; ACTN2: green; blue: cell nuclei). **(B)** Representative IF staining showing disrupted ACTN2 in HCM cardiomyocytes compared to controls (ACTN2: green; blue: cell nuclei). **(C)** Representative IF staining showing suppressed ATP2A2 in HCM cardiomyocytes compared to controls (ATP2A2: red; blue: cell nuclei). Nuclei were stained by Hoechst. All overview images were taken at 20x magnification, scale bar = 100 µm. All zoomed regions were taken under Zoom Factor=1.5.

DISCUSSION

In the present study, we studied changes in histone acetylome, transcriptome, and proteome between HCM and control hearts. Integrating these multi-omics data, we present for the first time a set of DNA regions and genes that differentiate HCM from control hearts and identified 53 protein-coding genes as the major contributors. Since these comprehensive datasets consistently indicated altered biological functions involved in ECM, muscle contraction, and metabolism, we further studied and identified the upstream TFs that could play a critical regulatory role. We also observed an abundance of acetylation signals and transcripts signals from cardiomyocyte-specific markers compared to markers of 11 non-myocyte populations in the heart.

By integrating ChIP-seq, RNA-seq, and proteomics data we identified a list of deciding elements in discriminating HCM hearts from controls. Among these, *ATP2A2*/SERCA2a, the cardiomyocyte-specific marker, transports cytosolic calcium into the sarcoplasmic reticulum and subsequently regulates the contraction and relaxation of cardiomyocytes [18]. Suppressed *ATP2A2*/SERCA2a expression is associated with impaired relaxation in cardiomyocytes and contributes to diastolic dysfunction in HCM [14,19]. Consistent with previous findings, we also showed lower mRNA and protein levels in HCM hearts compared to controls. Additionally, we employed iPSC-derived cardiomyocytes and confirmed the suppressed ATP2A2/SERCA2a in HCM versus control cardiomyocytes.

Another element HSPA2 (heat shock-related 70 kDa protein 2), which protects cardiac integrity by correcting misfolded proteins upon stress [20], showed higher upstream acetylation level, mRNA level, and protein level in HCM hearts versus controls. Up-regulated HSPA2 protein level has been observed at both the initial stage of diseased cardiomyocytes and at the end stage of diseased heart with diastolic dysfunction [21,22]. We previously also showed elevated HSPA2 protein level in HCM with mutations in different sarcomeric proteins when compared to controls and it was negatively correlated with MYBPC3 peptide counts [15]. Here we further demonstrated a cardiomyocyte-specific elevation of HSPA2 accompanied by the occasional HSPA2 aggregates in the HCM heart, which may contribute to the disease progression by hampering the protein quality control system.

Interestingly, both ATP2A2/Serca2a- and HSPA2-mediated activities are ATP-dependent, highlighting the strength of our sequencing data that align with previous observations showing energy deficiency as a key pathomechanism in HCM development. A reduced myocardial external efficiency, the ratio between cardiac work and oxygen consumption, in asymptomatic *MYBPC3* mutation carriers compared to the control hearts [23]. More details on the metabolic changes in HCM hearts are summarized in our review [24]. Isolated cardiomyocytes from HCM hearts with

MYBPC3 mutations showed a reduced super-relax state, which may result in an increased sarcomere energy utilization [25]. Likewise, hiPSC-derived cardiomyocytes with mutated *MYH7*, another sarcomeric gene that is often mutated in HCM patients, also showed a reduced super-relax state, increased contractility, and a greater basal oxygen consumption rate when compared to the controls, suggesting an impaired energetics [26]. Taken together, previous studies show mutation-mediated contractile dysfunction with associated disturbed energetics. Here, besides the enriched metabolism using the ChIP-seq, RNA-seq, and proteomic data, we also identified several TFs as potential key upstream factors in regulating metabolisms in HCM hearts, such as *KLF15*, *AR*, and *RXRA* [27–29]. Furthermore, we confirmed the expression of KLF15, a key regulator in cardiac metabolism [30], in hiPSC-cardiomyocytes using immunofluorescence staining, highlighting the potential involvement of KLF15 in diseased cardiomyocytes. Drugs targeting energy metabolism, such as trimetazidine, have been investigated in the clinical trial in HCM patients [31]. Combined, identified TFs could be potential therapeutic targets in restoring metabolic homeostasis in HCM patients, and future studies in hiPSC-cardiomyocyte models are warranted to define the mutation-mediated sequence in mitochondrial function and cellular metabolism.

Although those identified TFs showed the same changing direction at the acetylation and mRNA levels in HCM versus control hearts, their protein levels were comparable between HCM and control hearts. Similarly, some of those identified key protein-coding genes, which changed in the same direction at the mRNA and protein levels, showed comparable acetylation levels between HCM and control hearts. These findings indicate that the central dogma of cellular information transition from DNA, RNA, to protein is oversimplified [32]. Numerous factors, such as the post-translational modifications on gene expression and TF activity, mRNA degradation, and protein degradation [33–36], could lead to a poor correlation between DNA, mRNA, and protein expressions. Additionally, both H3K27ac ChIP-seq and RNA-seq data were generated from the same 13 HCM and 10 control samples. Whereas, only 11 out of 13 HCM samples were included in the proteomics analysis in comparison with 8 different control samples. Thus, different donor samples and group sizes might obscure the integrative analysis of the multi-omics data. Therefore, it is important to find an optimal way to integrate multi-omics data rather than a simple correlative. The discovery of new types of machinery beyond the central dogma is also needed in future studies.

Previous studies from our group and others showed around a 30% ratio of mutant to wildtype *MYH7*- and *MYBPC3*-alleles in HCM patients at the mRNA and the protein levels, respectively [37,38]. In this study, we present the imbalanced mRNA expression of three truncating mutations in *MYBPC3*. Notably, we showed for the first time the presence of such an imbalance at the DNA level by evaluating allele-specific histone acetylation signals. The mutant/wildtype expression ratio differs between truncating

mutations and between DNA and mRNA levels, suggesting mutation-specific imbalance and additional machinery between DNA and mRNA. It is important to point out that H3K27ac ChIP-seq is sensitive in capturing upstream regulatory regions of a gene and is restored in covering the core gene body [39], the allelic expression based on the histone acetylation level could be limited by the nature of the technique. Nevertheless, this finding highlights another utilization of omics data in detecting allelic imbalance for genetic diseases.

As the cell composition changes in diseased hearts, we investigated cell-type-specific signals from cardiomyocytes and 11 non-myocyte cell types and observed more ChIP-seq signals and transcripts in cardiomyocyte-specific markers than all non-myocyte markers, suggesting a considerable portion of cardiomyocytes-derived signals in the bulk sequencing data. Gene set enrichment analysis showed enriched pathways in ECM, which is in line with previous reports indicating fibrosis as a hallmark of HCM [40]. Apart from fibroblasts, cardiomyocytes also express ECM-related genes, including two fibroblast-specific markers (*DKK3* and *ABI3BP*) [41]. Because cell-type-specific markers might also be expressed by other cell types and the limitation of capturing pure cell populations from snap-frozen tissues without damaging the DNA and RNA integrity, we can only speculate that the majority of the signals were likely obtained from cardiomyocytes and it remains a challenge to separate them in bulk sequencing. Additionally, we used cell-type-specific markers obtained from the murine models [16,17], which may not translate one-to-one across species. Therefore, future studies are required to validate the cellular-specific response in HCM by isolating single-cell populations from human cardiac tissues.

In conclusion, our study presents detailed information in HCM hearts with truncating *MYBPC3* mutations. These data showed altered ECM, muscle contraction, and metabolism in HCM. Integrative analyses further identified a subset of protein-coding genes and upstream TFs that could drive these pathophysiological mechanisms and serve as promising diagnostic and/or therapeutic targets. We also showed a considerable amount of cardiomyocyte-derived signals compared to non-myocyte cell types, providing cardiomyocyte-specific insights to better understand HCM in future studies.

MATERIALS AND METHODS

Human cardiac samples

The study protocol was approved by the local medical ethics review committees, including the Biobank Research Ethics Committee of University Medical Center Utrecht (protocol number 12/387), the local ethics committee of the Erasmus MC (2010-409), the Washington University School of Medicine Ethics Committee (Institutional

Review Board), and the Sydney Heart Bank (HREC Univ. Sydney 2012/030). Since septal thickening is a typical feature of HCM, septal myectomy is commonly performed to relieve left ventricular outflow tract obstruction in HCM patients [2,42,43]. Therefore, we collected cardiac tissue of the interventricular septum of 13 HCM patients. Genetic analyses of all patients revealed three truncating pathogenic heterozygous mutations in *MYBPC3*, namely c.2373dupG in 5 HCM patients, c.2827C>T in 6 patients, and c927-2A>G in 2 HCM patients. Control tissues of 18 non-failing donors were obtained from the Biobank of University Medical Center Utrecht, the Washington University School of Medicine, and the Sydney Heart Bank. Informed consent was obtained from each patient prior to surgery or was waived by the ethics committee when acquiring informed consent was not possible due to the death of the donor. Samples were collected and snap-frozen in liquid nitrogen and stored at -80˚C up until analysis. Detailed clinical characteristics are shown in Supplementary Table 1 and an overview of samples included in the following experiments is shown in Figure 1A.

H3K27ac chromatin immunoprecipitation and sequencing (ChIP-seq)

We performed chromatin immunoprecipitation and sequencing (ChIP-seq) using the H3K27ac mark to study the differences of the histone acetylome between patient and control samples as previously described [10]. To study the differences of the histone acetylome between patient and control samples, we performed chromatin immunoprecipitation and sequencing (ChIP-seq) using the H3K27ac mark. Briefly, all cardiac samples were sectioned at a thickness of 10µm, and chromatin was isolated using the MAGnify™ Chromatin Immunoprecipitation System kit (Life Technologies) according to the manufacturer's instructions. The anti-histone H3K27ac antibody (ab4729, Abcam) was used for immunoprecipitation. Captured DNA was purified using the ChIP DNA Clean & Concentrator kit (Zymo Research). Libraries were prepared using the NEXTflex™ Rapid DNA Sequencing Kit (Bioo Scientific). Samples were PCR amplified, checked for the proper size range and absence of adaptor dimers on a 2% agarose gel, and barcoded libraries were sequenced 75 bp single-end on an Illumina NextSeq500 sequencer. Sequencing reads were mapped against the reference genome (hg19 assembly, NCBI37) using the BWA package (mem –t 7 –c 100 –M –R)1. Multiple reads mapping to the same location and strand were collapsed to a single read and only uniquely placed reads were used for peak-calling. Peaks/regions were called using Cisgenome 2.02 (–e 150 -maxgap 200 –minlen 200). Region coordinates from all samples were stretched to at least 2000 base pairs and collapsed into a single common list. Overlapping regions were merged based on their coordinates. Only regions supported by at least 2 independent datasets were further analyzed. Autosomal sequencing reads from each ChIP-seq library were overlapped back with the common region list to set the H3K27ac occupancy for every region-sample pair. Differentially acetylated regions between HCM and control hearts were identified using DESeq2 under the default setting in the Galaxy environment [44].

Annotating genes in the vicinity of differentially acetylated regions

Region-to-gene annotation was performed to study potentially affected genes in the vicinity of DNA regions with altered acetylation levels in HCM hearts when compared with controls. Differentially acetylated regions located within either +/-5 kb or +/-50 kb window from the transcription start site (TSS) of all genes were obtained, and the nearest genes of these regions were collected.

Predicting transcription factor binding motifs in differentially acetylated regions

To study the putative upstream signaling, we studied the enriched transcription factor binding motifs (TFBMs) by differentially acetylated regions and motifs-encoded transcription factors (TFs). DNAse I hypersensitivity regions in human cardiac samples, which play a key role in transcription factor footprinting [45], were collected from the ENCODE project and overlapped with differentially acetylated regions in this study [46]. Overlapping DNA sequences between differentially acetylated regions and DNAse I hypersensitivity regions were used to studying the enriched transcription factor binding motifs and motifs-encoded TFs using MEME Suite AME tool (HOCOMOCO Human v11 Full, average odds scoring method, and Fisher's exact test) [47].

RNA sequencing

We also performed RNA sequencing (RNA-seq) and obtained the transcriptome landscapes in all samples. Briefly, RNA was isolated using the RNeasy Micro Kit (Qiagen) or ISOLATE II RNA Mini Kit (Bioline) according to the manufacturer's instructions. Sample quality was assessed using the 2100 Bioanalyzer with an RNA 6000 Pico Kit (Agilent), and sample quantity was measured using Qubit Fluorometer with an HS RNA Assay (Thermo Fisher). Afterward, libraries were prepared using the NEXTflexTM Rapid RNA-seq Kit (Bioo Scientific) and sequenced by the Nextseq500 platform (Illumina). Sequenced reads were aligned to the human reference genome GRCh37 using STAR v2.4.2a [48]. Reads per kilobase million reads sequenced (RPKMs) were calculated with edgeR's RPKM function [49]. To identify a list of differentially expressed genes between HCM and control hearts at $P_{adj}<0.05$, we employed d DESeq2 to process all the raw counts per sample per group in the Galaxy environment [44].

Allele-specific expression of MYBPC3 in ChIP-seq and RNA-seq data

RNA-seq and ChIP-seq reads were processed with TrimGalore (version 0.6.5) to detect and clip off adaptor sequences, reads with a remaining length of 20 or more nucleotides, and an average read quality q>20 were selected. The reads were aligned to the human genome (GRCh37) with transcript annotation from Ensembl (version 74) using the STAR aligner (version 2.7.1a). To facilitate the equal alignment of reads from wildtype and mutant alleles, alignments were made without clipping off end sequences (STAR option alignEndsType set to EndToEnd), and only best scoring alignments were selected (STAR option outSAMprimaryFlag set to AllBestScore). Alignments were selected to remove duplicated reads by an in-house HTSeq based

python (version 2.7.10) script [50]. Reads that aligned to the same genomic interval and that aligned with identical bases to the two non-indel *MYBPC3* SNPs (rs397516082 and rs387907267) of interest, were considered duplicates. ChIP-seq reads matching to one of the three SNPs of interest were assigned to the wildtype or mutant allele based on the following rules: for the single base polymorphic SNPs (rs397516082 and rs387907267), based on having the wildtype or mutant nucleotide aligned to the SNP position; for the indel SNP (rs397515963) based on having the exact wildtype or mutant sequence of the SNP with 10 surrounding bases in a read aligned to the SNP. In addition, ChIP-seq reads with wildtype or mutant assignment were required to have >90% of the bases aligned to the genome. For RNA-seq reads, the assignment to be wildtype or mutant allele derived was complicated by changed splice patterns for two of the three SNPs. For rs387907267 (c.2827C>T) that has no changed splice patterns, reads were classified based on having the wildtype or mutant nucleotide aligned to the SNP position. For rs397515963 (c.2373dupG) that disrupts the correct splicing of intron 23, reads covering the splice-junction with the correct intron spliced out were counted as wildtype reads, whereas reads using either the correct intron donor or acceptor site, but not both, were counted as mutant reads. For rs397516082 (c.927-2A>G) that disrupts the correct splicing of intron 11, reads covering the splice-junction with the correct intron spliced out were counted as wildtype reads, whereas reads that were running through the intron 11 - exon 12 splice site and into the SNP position were counted as wildtype or mutant based on having the wildtype or mutant nucleotide aligned to the SNP position.

Integrating ChIP-seq and RNA-seq data with Two-way Orthogonal Partial Least Squares

To find common parts between RNA-seq and ChIP-seq data simultaneously across all genes and regions, a data integration approach is considered using Two-way Orthogonal Partial Least Squares (O2PLS) [51]. O2PLS decomposes both RNA-seq and ChIP-seq datasets into joint, omic-specific, and residual parts. The joint subspaces contain variations that are correlated to one another. The Joint Principal Components (JPCs) that span the joint subspaces are obtained by finding linear combinations of genes and regions that maximize the covariation. Omic-specific subspaces capture variation unrelated to another omics dataset, enabling JPCs to better estimate the underlying system. Here, the rows of the ChIP-seq and RNA-seq data should represent the same samples. Note that O2PLS uses all genes and regions in the datasets, and does not rely on prior information about the position or function of these features. Furthermore, O2PLS is unsupervised, and its algorithm is implemented in the OmicsPLS R package and freely available from CRAN [52]. Prior to the analysis, genes with expression lower than 10 counts in at least 22 samples were removed. Samples in both datasets were matched and 23 overlapping samples were retained. The expression data is normalized. Both datasets were log-transformed, and quantile

normalized across samples. The dimensionality of the preprocessed datasets is 23 by 15,882 (RNA-seq) and 23 by 33,642 (ChIP-seq).

Proteomics

We performed proteomics using cardiac samples from the same patients (n=11) and 8 non-failing donor samples from the Sydney heart bank (Supplementary Table 1). Briefly, proteins were loaded to a 4-12% NuPAGE Novex Bis-Tris 1.5 mm mini gel (Invitrogen) for separation, followed by fixation (50% ethanol and 3% phosphoric acid) and staining using 0.1% Coomassie brilliant blue G-250 solution. In-gel digestion was performed and the samples were concentrated in a vacuum centrifuge as described previously [53]. Nano-LC-MS/MS was performed as described previously [54]. Briefly, separated peptides were separated using an Ultimate 3000 Nano LC-MS/MS system (Dionex LC-Packings, Amsterdam, The Netherlands) and trapped. Eluting peptides were ionized into a Q Exactive mass spectrometer (Thermo Fisher, Bremen, Germany), and intact masses were measured in the orbitrap. Among all, the top 10 peptide signals were selected and analyzed using the MS/MS. MS/MS spectra were searched against a Uniprot human reference proteome FASTA file (Swissprot_2017_03_human_canonical_and_isoform.fasta, 42161 entries) using MaxQuant version 1.5.4.1. Differentially expressed proteins between HCM and control hearts at $P<0.05$ were identified using DESeq2 [44].

Functional enrichment analysis

Gene Ontology (GO) enrichment analysis: To study the enriched biological functions, GO enrichment analysis was performed using the ToppFun ToppGene Suite under the default settings (FDR correction, p-value cutoff of 0.05, and gene limits between 1 and 2,000) [55].

Gene set enrichment analysis (GSEA): Established gene sets involved in the most enriched biological functions in HCM versus control hearts were collected from Molecular Signature Database v7.1 (Supplementary Table 8) [56,57]. Each gene set per biological function was studied for its positive or negative correlation with genes annotated from the altered acetylated levels in the ChIP-seq data, genes with altered mRNA levels in the RNA-seq data, and protein-coding genes with altered protein levels in the proteomic data in this study under the following setting: Number of permutations: 1,000; Phenotype labels: up_versus_down; Collapses dataset to gene symbols: false; Permutation type: gene_set; Enrichment statistics: weighted; Metric for ranking genes: Signal2Noise; Gene list sorting mode: real; Gene list ordering mode: descending; Max size: 500; Min size: 1.

Protein-protein interaction (PPI) networks: Protein networks were performed using the STRING Version 11.0 under the following settings: the meaning of network edges: confident, minimum required interaction score: medium confidence (0.400) [58].

Human induced pluripotent stem cells derived cardiomyocytes (hiPSC-cardiomyocytes)

Clones from one control hiPSC line and one hiPSC line derived from an HCM patient with mutated *MYBPC3* were differentiated to cardiomyocytes as previously described [59]. The contractile function of differentiated control and HCM cardiomyocytes were examined as previously described [60]. Cells were seeded at the density of 20,000 cells per well to the 96-well plate. After culturing for 27 days, cardiomyocytes were fixed and stained for interested proteins.

Western blot

Western blot was performed as described previously [15]. Primary antibodies, including mouse anti-HSPA2 (heat shock-related 70 kDa protein 2, 66291-1, Proteintech Group), mouse anti-GAPDH (10R-G109a, Fitzgerald Industries International), anti-ATP2A2 (sarcoplasmic reticulum Ca2+-ATPase 2, also known as SERCA2), anti-KLF15 (AV32587, Sigma Aldrich), anti-RXRA (ab125001, Abcam), and anti-β-actin, were used.

Immunohistochemistry and immunofluorescence (IF) staining

Tissue sections were thawed and left at RT for 20 min inside a closed box. Then the sections were treated with peroxidase blocking solution (3% H2O2 in MeOH) and blocked with 1% BSA. HSPA2 (Anti-HSPA2 rabbit-Polyclonal antibody Prestige Antibodies HPA000798) primary antibodies were incubated for 1 hour at RT (1:100 for IF and 1:200 for IHC). Sections were washed and incubated with the secondary antibodies for 30 min. Vector Vectastain Universal Elite ABC Kit (PK-6200) was used to enhance the brightfield staining (IHC) and WGA (for cell membranes) and DAPI (nuclei) were added to counterstain fluorescence staining. The brightfield slides were washed, treated with DAB, counterstained with Mayers Hematoxylin, dehydrated, and mounted with DPX. Fluorescence staining was mounted with Mowiol. Images were acquired with the Vectra Polaris Scanner (brightfield/IHC) or Confocal Nikon A1 (IF). The analysis was performed with QuPath, Fiji, and NIS Nikon software.

HiPSC-cardiomyocytes were fixed using 4% paraformaldehyde solution for 10 mins at room temperature and incubated overnight with the primary antibodies, including ACTN2 (A7811, Sigma Aldrich) and ATP2A2 (MA3-910, Thermo Fisher Scientific). Afterward, cells were washed three times with PBS and incubated for 1 hr with Hoechst 33342 and the secondary antibodies (Invitrogen), including Alexa Fluor 488 and Alexa Fluor 568. Images were taken by Leica confocal microscope at 20x magnification.

Availability of data and materials

All relevant data are available within the article and the supplementary files. Because of the sensitive nature of the data collected for this study (13 patient samples and 10 control samples), requests to access the raw sequencing dataset from qualified researchers trained in human subject confidentiality protocols may be sent to the corresponding authors. It is important to note that processed RNA-seq and

H3K27ac ChIP-seq data of 11 patient samples and 7 control samples are published in a GWAS study [7] and available in Supplementary Table 3 and Supplementary Table 5, respectively. Raw proteomics data within the article can be found at the ProteomeXchange Consortium via the PRIDE partner repository with the dataset identifier PXD012467 [61]. Currently, the paper is accepted by Circulation: Heart Failure and will become publicly available soon.

ACKNOWLEDGEMENT

We would like to thank Pedro Espinosa for performing immunohistochemistry and immunofluorescent stainings. Grateful thanks to Cris dos Remedios and the Sydney Heart Bank for providing non-failing donor tissue.

FUNDING

This work was supported by the Netherlands Foundation for Cardiovascular Excellence (to C.C.), the NWO VENI grant (no. 016.176.136 to M.H.), three NWO VIDI grants (no. 91714302 to C.C., no. 016096359 to M.C.V, and no. 91715303 to R.P.D.), ZonMW-NWO VICI grant 91818902 (to J.V.), the Erasmus MC fellowship grant (to C.C.), the RM fellowship grant of the UMC Utrecht (to C.C.), Wilhelmina Children's Hospital research funding (no. OZF/14 to M.H.), the Netherlands Cardiovascular Research Initiative: An initiative with the support of the Dutch Heart Foundation (CVON2014-40 DOSIS to J.V., M.H., F.W.A., CVON2014-11 RECONNECT to C.C., M.C.V., Dekker 2015T041 to A.F.B., and Queen of Heart to C.C. and M.C.V.), UCL Hospitals NIHR Biomedical Research Centre (to F.W.A.), and the Starting Grant (STEMCARDIORISK) from the European Research Council under the European Union's Horizon 2020 Research and Innovation Program (H2020 European Research Council; grant agreement 638030) to R.P.D.

REFERENCES

1. Elliott PM, Anastasakis A, Borger MA, Borggrefe M, Cecchi F, Charron P, et al. 2014 ESC Guidelines on diagnosis and management of hypertrophic cardiomyopathyThe Task Force for the Diagnosis and Management of Hypertrophic Cardiomyopathy of the European Society of Cardiology (ESC). Eur Heart J. Oxford Academic; 2014;35:2733–79.
2. Llam N, Bollen IAE, Niessen HWM, Dos Remedios CG, Michels M, Poggesi C, et al. Sex-specific cardiac remodeling in early and advanced stages of hypertrophic cardiomyopathy. PLoS One. 2020;15:e0232427–e0232427.
3. Sabater-Molina M, Pérez-Sánchez I, Hernández Del Rincón JP, Gimeno JR. Genetics of hypertrophic cardiomyopathy: A review of current state. Clin Genet. 2018;93:3–14.
4. Wijnker PJM, van der Velden J. Mutation-specific pathology and treatment of hypertrophic cardiomyopathy in patients, mouse models and human engineered heart tissue. Biochim Biophys Acta Mol Basis Dis. 2020;165774.
5. Liu C-F, Tang WHW. Epigenetics in Cardiac Hypertrophy and Heart Failure. JACC Basic Transl Sci. 2019;4:976–93.
6. Zhang W, Song M, Qu J, Liu G-H. Epigenetic Modifications in Cardiovascular Aging and Diseases. Circ Res. 2018;123:773–86.
7. Hemerich D, Pei J, Harakalova M, van Setten J, Boymans S, Boukens BJ, et al. Integrative Functional Annotation of 52 Genetic Loci Influencing Myocardial Mass Identifies Candidate Regulatory Variants and Target Genes. Circ Genom Precis Med. 2019;12:e002328.
8. Manduchi E, Hemerich D, Setten J, Tragante V, Harakalova M, Pei J, et al. A comparison of two workflows for regulome and transcriptome-based prioritization of genetic variants associated with myocardial mass [Internet]. Genetic Epidemiology. 2019. Available from: http://dx.doi.org/10.1002/gepi.22215
9. Gilsbach R, Schwaderer M, Preissl S, Grüning BA, Kranzhöfer D, Schneider P, et al. Distinct epigenetic programs regulate cardiac myocyte development and disease in the human heart in vivo. Nat Commun. 2018;9:391.
10. Pei J, Harakalova M, Treibel TA, Thomas Lumbers R, Boukens BJ, Efimov IR, et al. H3K27ac acetylome signatures reveal the epigenomic reorganization in remodeled non-failing human hearts. Clin Epigenetics. BioMed Central; 2020;12:1–18.
11. Low TY, Mohtar MA, Ang MY, Jamal R. Connecting Proteomics to Next-Generation Sequencing: Proteogenomics and Its Current Applications in Biology. Proteomics. 2019;19:e1800235.
12. Litviňuková M, Talavera-López C, Maatz H, Reichart D, Worth CL, Lindberg EL, et al. Cells of the adult human heart. Nature. Nature Publishing Group; 2020;1–7.
13. Helms AS, Tang VT, O'Leary TS, Friedline S, Wauchope M, Arora A, et al. Effects of MYBPC3 loss-of-function mutations preceding hypertrophic cardiomyopathy. JCI insight [Internet]. JCI Insight; 2020 [cited 2020 Dec 28];5. Available from: https://pubmed.ncbi.nlm.nih.gov/31877118/
14. Kresin N, Stücker S, Krämer E, Flenner F, Mearini G, Münch J, et al. Analysis of Contractile Function of Permeabilized Human Hypertrophic Cardiomyopathy Multicellular Heart Tissue. Front Physiol. 2019;10:239.
15. Dorsch LM, Schuldt M, dos Remedios CG, Schinkel AFL, de Jong PL, Michels M, et al. Protein Quality Control Activation and Microtubule Remodeling in Hypertrophic Cardiomyopathy. Cells [Internet]. 2019;8. Available from: http://dx.doi.org/10.3390/cells8070741

16. Skelly DA, Squiers GT, McLellan MA, Bolisetty MT, Robson P, Rosenthal NA, et al. Single-Cell Transcriptional Profiling Reveals Cellular Diversity and Intercommunication in the Mouse Heart. Cell Rep. 2018;22:600–10.
17. Gladka MM, Molenaar B, de Ruiter H, van der Elst S, Tsui H, Versteeg D, et al. Single-Cell Sequencing of the Healthy and Diseased Heart Reveals Cytoskeleton-Associated Protein 4 as a New Modulator of Fibroblasts Activation. Circulation. 2018;138:166–80.
18. New perspectives on the role of SERCA2's Ca2+ affinity in cardiac function. Biochimica et Biophysica Acta (BBA) - Molecular Cell Research. Elsevier; 2006;1763:1216–28.
19. Somura F, Izawa H, Iwase M, Takeichi Y, Ishiki R, Nishizawa T, et al. Reduced Myocardial Sarcoplasmic Reticulum Ca(2+)-ATPase mRNA Expression and Biphasic Force-Frequency Relations in Patients With Hypertrophic Cardiomyopathy. Circulation [Internet]. Circulation; 2001 [cited 2020 Jul 10];104. Available from: https://pubmed.ncbi.nlm.nih.gov/11489771/
20. Ranek MJ, Stachowski MJ, Kirk JA, Willis MS. The role of heat shock proteins and co-chaperones in heart failure. Philos Trans R Soc Lond B Biol Sci [Internet]. The Royal Society; 2018 [cited 2020 Apr 9];373. Available from: https://www.ncbi.nlm.nih.gov/pmc/articles/PMC5717530/
21. Birket MJ, Raibaud S, Lettieri M, Adamson AD, Letang V, Cervello P, et al. A Human Stem Cell Model of Fabry Disease Implicates LIMP-2 Accumulation in Cardiomyocyte Pathology [Internet]. Stem Cell Reports. 2019. p. 380–93. Available from: http://dx.doi.org/10.1016/j.stemcr.2019.07.004
22. Li W, Rong R, Zhao S, Zhu X, Zhang K, Xiong X, et al. Proteomic Analysis of Metabolic, Cytoskeletal and Stress Response Proteins in Human Heart Failure. J Cell Mol Med [Internet]. J Cell Mol Med; 2012 [cited 2020 Jul 10];16. Available from: https://pubmed.ncbi.nlm.nih.gov/21545686/
23. Güçlü A, Knaapen P, Harms HJ, Parbhudayal RY, Michels M, Lammertsma AA, et al. Disease Stage-Dependent Changes in Cardiac Contractile Performance and Oxygen Utilization Underlie Reduced Myocardial Efficiency in Human Inherited Hypertrophic Cardiomyopathy. Circ Cardiovasc Imaging [Internet]. 2017;10. Available from: http://dx.doi.org/10.1161/CIRCIMAGING.116.005604
24. van der Velden J, Tocchetti CG, Varricchi G, Bianco A, Sequeira V, Hilfiker-Kleiner D, et al. Metabolic changes in hypertrophic cardiomyopathies: scientific update from the Working Group of Myocardial Function of the European Society of Cardiology. Cardiovasc Res. Oxford University Press; 2018;114:1273.
25. McNamara JW, Li A, Lal S, Martijn Bos J, Harris SP, van der Velden J, et al. MYBPC3 mutations are associated with a reduced super-relaxed state in patients with hypertrophic cardiomyopathy. PLoS One. Public Library of Science; 2017;12:e0180064.
26. Toepfer CN, Garfinkel AC, Venturini G, Wakimoto H, Repetti G, Alamo L, et al. Myosin Sequestration Regulates Sarcomere Function, Cardiomyocyte Energetics, and Metabolism, Informing the Pathogenesis of Hypertrophic Cardiomyopathy. Circulation. 2020;141:828–42.
27. Gonthier K, Poluri RTK, Audet-Walsh É. Functional Genomic Studies Reveal the Androgen Receptor as a Master Regulator of Cellular Energy Metabolism in Prostate Cancer. J Steroid Biochem Mol Biol [Internet]. J Steroid Biochem Mol Biol; 2019 [cited 2020 Jul 5];191. Available from: https://pubmed.ncbi.nlm.nih.gov/31051242/

28. Subbarayan V, Mark M, Messadeq N, Rustin P, Chambon P, Kastner P. RXRα overexpression in cardiomyocytes causes dilated cardiomyopathy but fails to rescue myocardial hypoplasia in RXRα-null fetuses [Internet]. Journal of Clinical Investigation. 2000. p. 387–94. Available from: http://dx.doi.org/10.1172/jci8150
29. Fisch S, Gray S, Heymans S, Haldar SM, Wang B, Pfister O, et al. Kruppel-like factor 15 is a regulator of cardiomyocyte hypertrophy. Proc Natl Acad Sci U S A. National Academy of Sciences; 2007;104:7074–9.
30. Prosdocimo DA, Anand P, Liao X, Zhu H, Shelkay S, Artero-Calderon P, et al. Kruppel-like factor 15 is a critical regulator of cardiac lipid metabolism. J Biol Chem. 2014;289:5914–24.
31. van Driel BO, van Rossum AC, Michels M, Huurman R, van der Velden J. Extra energy for hearts with a genetic defect: ENERGY trial. Neth Heart J. Springer; 2019;27:200.
32. Franklin S, Vondriska TM. Genomes, proteomes, and the central dogma. Circ Cardiovasc Genet. 2011;4:576.
33. Valencia-Sanchez MA, Liu J, Hannon GJ, Parker R. Control of translation and mRNA degradation by miRNAs and siRNAs. Genes Dev. 2006;20:515–24.
34. Sha Z, Zhao J, Goldberg AL. Measuring the Overall Rate of Protein Breakdown in Cells and the Contributions of the Ubiquitin-Proteasome and Autophagy-Lysosomal Pathways. Methods Mol Biol. 2018;1844:261–76.
35. Teixeira D, Sheth U, Valencia-Sanchez MA, Brengues M, Parker R. Processing bodies require RNA for assembly and contain nontranslating mRNAs. RNA. 2005;11:371–82.
36. Zhang Y, Li S, Xiang Y, Qiu L, Zhao H, Hayes JD. The selective post-translational processing of transcription factor Nrf1 yields distinct isoforms that dictate its ability to differentially regulate gene expression. Sci Rep. Nature Publishing Group; 2015;5:1–30.
37. Montag J, Kowalski K, Makul M, Ernstberger P, Radocaj A, Beck J, et al. Burst-Like Transcription of Mutant and Wildtype -Alleles as Possible Origin of Cell-to-Cell Contractile Imbalance in Hypertrophic Cardiomyopathy. Front Physiol. 2018;9:359.
38. Parbhudayal RY, Garra AR, Götte MJW, Michels M, Pei J, Harakalova M, et al. Variable cardiac myosin binding protein-C expression in the myofilaments due to MYBPC3 mutations in hypertrophic cardiomyopathy. J Mol Cell Cardiol. 2018;123:59–63.
39. Sanchez GJ, Richmond PA, Bunker EN, Karman SS, Azofeifa J, Garnett AT, et al. Genome-wide dose-dependent inhibition of histone deacetylases studies reveal their roles in enhancer remodeling and suppression of oncogenic super-enhancers. Nucleic Acids Res. Oxford University Press; 2018;46:1756.
40. Freitas P, Ferreira AM, Arteaga-Fernández E, de Oliveira Antunes M, Mesquita J, Abecasis J, et al. The amount of late gadolinium enhancement outperforms current guideline-recommended criteria in the identification of patients with hypertrophic cardiomyopathy at risk of sudden cardiac death. J Cardiovasc Magn Reson. BioMed Central; 2019;21:1–10.
41. Cardiomyocytes facing fibrotic conditions re-express extracellular matrix transcripts. Acta Biomater. Elsevier; 2019;89:180–92.
42. Reant P, Captur G, Mirabel M, Nasis A, M Sado D, Maestrini V, et al. Abnormal septal convexity into the left ventricle occurs in subclinical hypertrophic cardiomyopathy. J Cardiovasc Magn Reson. 2015;17:64.
43. Dearani JA, Danielson GK. Septal myectomy for obstructive hypertrophic cardiomyopathy. Semin Thorac Cardiovasc Surg Pediatr Card Surg Annu [Internet]. Semin Thorac Cardiovasc Surg Pediatr Card Surg Annu; 2005 [cited 2020 Dec 14]; Available from: https://pubmed.ncbi.nlm.nih.gov/15818363/
44. Afgan E, Baker D, Batut B, van den Beek M, Bouvier D, Cech M, et al. The Galaxy platform for accessible, reproducible and collaborative biomedical analyses: 2018 update. Nucleic Acids Res. 2018;46:W537–44.

45. Ouyang N, Boyle AP. TRACE: transcription factor footprinting using DNase I hypersensitivity data and DNA sequence [Internet]. bioRxiv. 2019 [cited 2020 Jun 29]. p. 801001. Available from: https://www.biorxiv.org/content/10.1101/801001v1.abstract
46. Rosenbloom KR, Sloan CA, Malladi VS, Dreszer TR, Learned K, Kirkup VM, et al. ENCODE data in the UCSC Genome Browser: year 5 update. Nucleic Acids Res. 2013;41:D56–63.
47. McLeay RC, Bailey TL. Motif Enrichment Analysis: a unified framework and an evaluation on ChIP data [Internet]. BMC Bioinformatics. 2010. Available from: http://dx.doi.org/10.1186/1471-2105-11-165
48. Dobin A, Davis CA, Schlesinger F, Drenkow J, Zaleski C, Jha S, et al. STAR: ultrafast universal RNA-seq aligner. Bioinformatics. 2013;29:15–21.
49. Robinson MD, McCarthy DJ, Smyth GK. edgeR: a Bioconductor package for differential expression analysis of digital gene expression data. Bioinformatics. 2010;26:139–40.
50. Anders S, Pyl PT, Huber W. HTSeq--a Python framework to work with high-throughput sequencing data. Bioinformatics. 2015;31:166–9.
51. Bouhaddani S el, el Bouhaddani S, Houwing-Duistermaat J, Salo P, Perola M, Jongbloed G, et al. Evaluation of O2PLS in Omics data integration [Internet]. BMC Bioinformatics. 2016. Available from: http://dx.doi.org/10.1186/s12859-015-0854-z
52. Bouhaddani S el, el Bouhaddani S, Uh H-W, Jongbloed G, Hayward C, Klarić L, et al. Integrating omics datasets with the OmicsPLS package [Internet]. BMC Bioinformatics. 2018. Available from: http://dx.doi.org/10.1186/s12859-018-2371-3
53. Warmoes M, Jaspers JE, Pham TV, Piersma SR, Oudgenoeg G, Massink MP, et al. Proteomics of Mouse BRCA1-deficient Mammary Tumors Identifies DNA Repair Proteins With Potential Diagnostic and Prognostic Value in Human Breast Cancer. Mol Cell Proteomics [Internet]. Mol Cell Proteomics; 2012 [cited 2020 Jul 10];11. Available from: https://pubmed.ncbi.nlm.nih.gov/22366898/
54. Piersma SR, Broxterman HJ, Kapci M, de Haas RR, Hoekman K, Verheul HM, et al. Proteomics of the TRAP-induced Platelet Releasate. J Proteomics [Internet]. J Proteomics; 2009 [cited 2020 Jul 10];72. Available from: https://pubmed.ncbi.nlm.nih.gov/19049909/
55. Chen J, Bardes EE, Aronow BJ, Jegga AG. ToppGene Suite for gene list enrichment analysis and candidate gene prioritization. Nucleic Acids Res. 2009;37:W305–11.
56. Subramanian A, Tamayo P, Mootha VK, Mukherjee S, Ebert BL, Gillette MA, et al. Gene set enrichment analysis: A knowledge-based approach for interpreting genome-wide expression profiles. Proc Natl Acad Sci U S A. National Academy of Sciences; 2005;102:15545–50.
57. Liberzon A, Birger C, Thorvaldsdóttir H, Ghandi M, Mesirov JP, Tamayo P. The Molecular Signatures Database (MSigDB) hallmark gene set collection. Cell systems. NIH Public Access; 2015;1:417.
58. Snel B. STRING: a web-server to retrieve and display the repeatedly occurring neighbourhood of a gene [Internet]. Nucleic Acids Research. 2000. p. 3442–4. Available from: http://dx.doi.org/10.1093/nar/28.18.3442
59. Cryopreservation of human pluripotent stem cell-derived cardiomyocytes is not detrimental to their molecular and functional properties. Stem Cell Res. Elsevier; 2020;43:101698.
60. Birket MJ, Ribeiro MC, Kosmidis G, Ward D, Leitoguinho AR, van de Pol V, et al. Contractile Defect Caused by Mutation in MYBPC3 Revealed under Conditions Optimized for Human PSC-Cardiomyocyte Function. Cell Rep. 2015;13:733–45.
61. Perez-Riverol Y, Csordas A, Bai J, Bernal-Llinares M, Hewapathirana S, Kundu DJ, et al. The PRIDE database and related tools and resources in 2019: improving support for quantification data. Nucleic Acids Res. 2019;47:D442–50.

THE SUPPLEMENTARY DATA IS AVAILABLE ONLINE:

https://clinicalepigeneticsjournal.biomedcentral.com/articles/10.1186/s13148-021-01043-3#Sec27

SEX-RELATED DIFFERENCES IN PROTEIN EXPRESSION IN SARCOMERE MUTATION-POSITIVE HYPERTROPHIC CARDIOMYOPATHY

Maike Schuldt, Larissa M. Dorsch, Jaco C. Knol, Thang V. Pham, Tim Schelfhorst, Sander R. Piersma, Cris dos Remedios, Michelle Michels, Connie R. Jimenez, Diederik WD. Kuster, Jolanda van der Velden

Frontiers in Cardiovascular Medicine, 2021. 8(129).

7

ABSTRACT

Background

Sex-differences in clinical presentation contribute to the phenotypic heterogeneity of hypertrophic cardiomyopathy (HCM) patients. While disease prevalence is higher in men, women present with more severe diastolic dysfunction and worse survival. Until today, little is known about the cellular differences underlying sex-differences in clinical presentation.

Methods

To define sex-differences at the protein level, we performed a proteomic analysis in cardiac tissue obtained during myectomy surgery to relieve left ventricular outflow tract obstruction of age-matched female and male HCM patients harboring a sarcomere mutation (n=13 in both groups). Furthermore, these samples were compared to 8 non-failing controls. Women presented with more severe diastolic dysfunction.

Results

Out of 2099 quantified proteins, direct comparison of male and female HCM samples revealed only 46 significantly differentially expressed proteins. Increased levels of tubulin and heat shock proteins were observed in female compared to male HCM patients. Western blot analyses confirmed higher levels of tubulin in female HCM samples. In addition, proteins involved in carbohydrate metabolism were significantly lower in female compared to male samples. Furthermore, we found lower levels of translational proteins specifically in male HCM samples. The disease-specificity of these changes were confirmed by a second analysis in which we compared female and male samples separately to non-failing control samples. Transcription factor analysis showed that sex hormone-dependent transcription factors may contribute to differential protein expression, but do not explain the majority of protein changes observed between male and female HCM samples.

Conclusion

In conclusion, based on our proteomics analyses we propose that increased levels of tubulin partly underlie more severe diastolic dysfunction in women compared to men. Since heat shock proteins have cardioprotective effects, elevated levels of heat shock proteins in females may contribute to later disease onset in woman, while reduced protein turnover in men may lead to the accumulation of damaged proteins which in turn affects proper cellular function.

INTRODUCTION

Hypertrophic cardiomyopathy (HCM) is the most prevalent inherited cardiac disease with a prevalence of 1:200-500 (1, 2). Clinically, it is characterized by unexplained asymmetric left ventricular hypertrophy and diastolic dysfunction (3, 4). A pathogenic mutation is identified in about 50–60% of all patients (5). Both genetic and clinical heterogeneity is large, with more than 1,500 identified gene mutations, and mutation carriers who are asymptomatic, die of acute cardiac arrest or show end-stage heart failure (6).

Sex-differences in clinical presentation contribute to the phenotypic heterogeneity of HCM. Several large cohort studies observed a higher disease prevalence in men representing 55–65% of the total HCM population (7–11). At HCM diagnosis, women are on average 9 years older than men (7, 12), and at the time of myectomy surgery women are on average 7 years older than men (13). While women display less ventricular remodeling (14, 15), several studies have demonstrated more severe diastolic dysfunction (13, 16–18) and worse survival compared to men (19). Based on recent studies, our group put forward the hypothesis that disease severity in female patients with HCM is underestimated because females have smaller hearts than men, and the diagnostic criterion of ≥15mm wall thickness does not take into account a correction by body surface area (BSA) (20). Consequently, womenmay be diagnosed at a later disease stage, since it takes more time for them to reach the diagnostic threshold of 15mm wall thickness. This is supported by the observation that differences in wall thickness between genotype-positive men and women, that presented for cardiac screening, aremitigated after correction for BSA (21).

Recently, efforts have been made to understand the sexspecific phenotypical differences on a cellular level. Single cardiomyocyte studies did not observe sex-specific changes in passive stiffness compared to non-failing controls, and the HCMrelated increase in myofilament Ca2+-sensitivity was similar in male and female HCM patients, implying that the sex-difference in diastolic dysfunction is not explained by sarcomere function itself (13). However, women had more fibrosis compared to men, expressed more compliant titin and showed reduced levels of calcium-handling proteins (13). These findings are first indications of differences between males and females on a cellular level. To further investigate cellular alterations that may underlie the sex-differences in HCM, we analyzed protein expression data of males and females in a proteomics data set of septal myocardial tissue that was collected during myectomy surgery.

By direct comparison of male and female samples we found higher levels of tubulin subunits and heat shock proteins in females. The levels of a-tubulin, determined by Western blot analysis, correlate with diastolic function displayed as E/e' and may therefore at least partly underlie the sex-difference in diastolic dysfunction. The increased levels of heat shock proteins in females are proposed to be cardioprotective (22, 23) and may contribute to later disease onset in women.

METHODS

Proteomics Analysis

The proteomics data in this study is a new analysis of a subset of the samples that were included of the study from Schuldt et al. (24), where we identified HCM-specific protein changes compared to non-failing controls. We here focus on sex-specific protein changes in HCM by comparing cardiac samples from age-matched female and male genotype-positive HCM patients. In addition, a comparison was made between the proteomics data from the female and the male group, and the proteomic data from the non-failing control group. HCM patient tissue from the interventricular septum (IVS) of HCM patients was obtained during myectomy surgery to relieve left ventricular outflow tract obstruction (LVOTO). The study protocol for the human tissue samples was approved by the local medical ethics review committees and written informed consent was obtained from each patient prior to surgery.

For the analysis of sex-differences age-matched sarcomere mutation-positive (SMP) female (n = 13) and male (n = 13) samples were compared in a group-wise comparison using the beta binomial test as described previously (24, 25). Furthermore, the male and female SMP samples were compared to 8 nonfailing healthy controls (NFIVS; 5 females and 3 males) obtained fromthe SydneyHeart Bank (HREC Univ Sydney 2012/030). The non-failing controls have no history of cardiac disease and do not take anymedication. The clinical characteristics of the groups are summarized in Table 1, individual patient characteristics are displayed in Supplementary Table 1.

Tissue Homogenization

Pulverized frozen tissue was homogenized in 40 µl/mg tissue 1x reducing sample buffer (106 mM Tris-HCl, 141 mM Tris-base, 2% lithium dodecyl sulfate (LDS), 10% glycerol, 0.51 mM EDTA, 0.22 mM SERVA Blue G250, 0.18 mM Phenol Red, 100 mM DTT) using a glass tissue grinder. Proteins were denatured by heating to 99°C for 5 min, after which samples were sonicated and heated again. Debris was removed by centrifugation at maximum speed for 10 min in a microcentrifuge (Sigma, 1-15K).

Protein Fractionation

Proteins were separated using 1D SDS-PAGE. Samples from each group were loaded alternating on the gels to avoid bias. Equal volumes of sample (30 µl protein homogenate per sample, containing approximately 20-30 µg of protein) were loaded on a precast 4-12% NuPAGE Novex Bis-Tris 1.5 mm mini gel (Invitrogen). Electrophoresis was performed at 200V in NuPAGE MES SDS running buffer until the dye front reached the bottom of the gel. Gels were fixed in a solution of 50% ethanol and 3% phosphoric acid, and stained with 0.1% (w/v) Coomassie brilliant blue G-250 solution (containing 34% (v/v) methanol, 3% (v/v) phosphoric acid and 15% (w/v) ammonium sulfate).

In-Gel-Digestion

In-gel digestion was performed as described previously (26). The proteins were in-gel reduced with 10 mM DTT and alkylated with 54 mM iodoacetamide. Each gel lane was cut into 5 pieces which were subsequently sliced into 1 mm^3 cubes. Proteins were digested in-gel with 6.3 ng/ml trypsin. Peptides were extracted from gel slices with 1% formic acid and 5% formic acid/50% acetonitrile and concentrated in a vacuum centrifuge prior to nano-LC-MS/MS measurement. Samples were measured by LC-MS per gel band starting at the high molecular weight (MW) fraction for all samples, before continuing with the next gel band until the last (low MW fraction) band was measured. Injections alternated between all different group samples to minimize experimental bias between groups.

Nano-LC-MS/MS

Analysis of the experiment was performed as described in Piersma et al (27). Peptides were separated using an Ultimate 3000 Nano LC-MS/MS system (Dionex LC-Packings, Amsterdam, The Netherlands) equipped with a 40 cm x 75 µm ID fused silica column custom packed with 1.9 µm ,120 Å ReproSil Pur C18 aqua (Dr Maisch GMBH, Ammerbuch-Entringen, Germany). After injection, peptides were trapped at 6 µl/min on a 10 mm × 100 µm ID trap column packed with 5 µm, 120 Å ReproSil Pur C18aqua at 2% buffer B (buffer A: 0.5% acetic acid (Fischer Scientific), buffer B: 80% acetonitrile, 0.5% acetic acid) and separated at 300 nl/min in a 10–40% buffer B gradient in 60 minutes (90 min inject-to-inject). Eluting peptides were ionized at a potential of + 2 kV into a Q Exactive mass spectrometer (Thermo Fisher, Bremen, Germany). Intact masses were measured at resolution 70,000 (at m/z 200) in the orbitrap using an automatic gain control (AGC) target value of $3x10^6$ charges. The top 10 peptide signals (charge-states 2+ and higher) were submitted to MS/MS in the HCD (higher-energy collision) cell using 1.6 amu isolation width and 25% normalized collision energy. MS/MS spectra were acquired at resolution 17,500 (at m/z 200) in the orbitrap using an AGC target value of $1x10^6$ charges, a maxIT of 60 ms and an underfill ratio of 0.1%. Dynamic exclusion was applied with a repeat count of 1 and an exclusion time of 30 s.

Data Analysis

MS/MS spectra were searched against a Uniprot human reference proteome FASTA file (Swissprot_2017_03_human_canonical_and_isoform.fasta, 42161 entries) using MaxQuant version 1.5.4.1. Enzyme specificity was set to trypsin and up to two missed cleavages were allowed. Cysteine carboxamidomethylation was treated as fixed modification, and methionine oxidation and N-terminal acetylation as variable modifications. Peptide precursor ions were searched with a maximum mass deviation of 4.5 parts per million (ppm) and fragment ions with a maximum mass deviation of 20 ppm. Peptide and protein identifications were filtered at a false discovery rate (FDR) of 1% using the decoy database strategy. The minimal peptide length was 7 amino acids, the minimum Andromeda score for modified peptides was 40, and the minimum delta score

was 6. Proteins that could not be differentiated based on MS/MS spectra alone were grouped to protein groups (default MaxQuant settings). Searches were performed with the label-free quantification option selected. The mass spectrometry proteomics data have been deposited to the ProteomeXchange Consortium via the PRIDE (28) partner repository with the dataset identifier PXD012467. Beta-binominal statistics were used to assess differential protein expression between groups, after normalization on the sum of the counts for each sample (25). Proteins with a *p* value below 0.05 were considered significantly differentially expressed. Proteins which were present in less than 25% of the samples or had an average normalized count of less than 1.4 were excluded from further functional analysis. Principal component analysis was performed in R. Therefore quantile normalization and log2 transformation was performed on the normalized counts. The 95th Percentile was taken, the data median centered and the principal components calculated. Hierarchical clustering was performed after a statistical multi-group comparison. Protein networks were generated utilizing the STRING database (Search Tool for the Retrieval of Interacting Genes/Proteins) and visualized with Cytoscape software (29). Protein interaction networks were generated with ClusterONE and gene ontology (GO) analysis was performed using the BiNGO application in cytoscape (30, 31). Venn diagrams were created with InteractiVenn tool (32) and the layout modified if needed.

Transcription Factor Analysis

The ToppFun tool from the ToppGene Suite was used to identify transcription factors of significantly different proteins between HCM_{female} and HCM_{male} (33). All significantly different proteins between HCM_{female} and HCM_{male} were used as input.

Western Blot

For analysis of protein levels by Western blot, whole tissue lysates were used from either the proteomic analysis or were prepared as described previously (34). Proteins were separated on precast SDS-PAGE 4-12% criterion gels (Bio-Rad) and transferred to polyvinylidene difluoride or nitrocellulose membranes. Site-specific antibodies directed to acetylated a-tubulin (Sigma, T7451), HSPA1 (Enzo Life Sciences, ADI-SPA-810), HSPA2 (Proteintech group, 66291-1), HSPB1 (Enzo Life Sciences, ADISPA-800), HSPB5 (Enzo Life Sciences, ADI-SPA-223), HSPB7 (abcam, ab150390), HSPD1 (Enzo Life Sciences, ADI-SPA-805), HSPA4 (Cell Signaling, 3303S), HSP90 (Cell Signaling, 4874S), a-tubulin (Sigma, T9026), tyrosinated tubulin (Sigma, T9028), detyrosinated tubulin (abcam, ab48389), and GAPDH (Cell Signaling, 2118S; Fitzgerald, 10R-G109a) were used to detect the proteins which were visualized with an enhanced chemiluminescence detection kit (Amersham) and scanned with Amersham Imager 600. Protein levels were determined by densitometric analysis and normalized to GAPDH.

Statistics

Graphpad Prism v8 software was used for statistical analysis. Normally distributed data (except proteomics data) were statistically analyzed with the Student's *t*-test

when comparing 2 groups and with one-way ANOVA when comparing more than 2 groups. Non-normally distributed data were analyzed with Mann-Whitney test. Linear regression was statistically tested with Pearson correlation. Data are presented as means ± standard errors of the mean, clinical characteristics are presented as mean ± standard deviation or median with interquartile range when appropriate. Categorical data was statistically analyzed using Fisher's exact test and presented as frequencies. A p-value ≤0.05 was considered as significantly different.

RESULTS

To define sex-specific protein changes in HCM, we compared the protein expression profile of male and female HCM samples. We performed a new analysis on a subset of patients from our proteomics data set (24). We compared age-matched samples from 13 male and 13 female sarcomere mutation-positive (SMP) HCM patients. The genotype distribution of both groups is depicted in Figure 1 and shows that the majority of mutations in both groups are located in the thick filament genes *MYBPC3* and *MYH7*. Clinical characteristics of the groups are summarized in Table 1. Both male and female patients had obstructive HCM. While male patients presented with a larger LV end-systolic diameter (ESD), females displayed more severe diastolic dysfunction, indicated by a higher E/e' ratio compared to male patients, and more females with diastolic dysfunction stage 2 (35, 36).

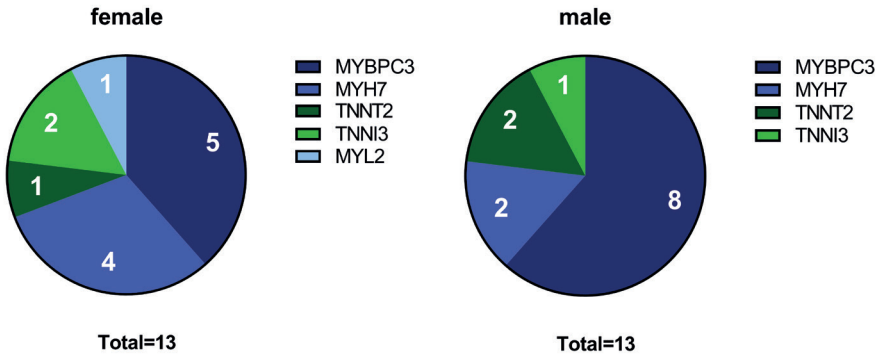

FIGURE 1. Genotypes in female and male HCM patient groups. The pie charts indicate the number of patients with a mutation in *MYBPC3*, *MYH7*, *TNNT2*, *TNNI3* and *MYL2* for the female and male group, respectively.

TABLE 1. Clinical characteristics. Table displays clinical characteristics of female and male HCM patient group with testing for statistical differences. Abbreviations: LVOTg, left ventricular outflow tract gradient; LAD, left atrial diameter; IVS, interventricular septum; IVS_i, indexed interventricular septum thickness corrected for body surface area (BSA); EDD, end-diastolic diameter; ESD, end-systolic diameter; FS, fractional shortening.

	HCM_{female} (n=13)	**HCM_{male} (n=13)**	***P* value**
Age at myectomy (years)	48.5 ± 17.7	49.8 ± 15.5	0.85
LVOTg (mmHg)	60.4 ± 31.8	55.6 ± 32.2	0.72
LV parameters			
LAD (mm)	45.5 ± 4.3	48.4 ± 7.3	0.25
IVS (mm)	21.0 [20.0-23.0]	21.0 [18.3-23.0]	0.80
IVS_i	12.5 [10.0-13.8]	10.0 [8.3-10.8]	0.07
EDD (mm)	41.5 [39.3-42.8]	43.5 [40.0-46.5]	0.39
ESD (mm)	16.7 ± 1.2	24.9 ± 4.7	**0.02*
Systolic parameter			
FS (%)	56.7 ± 2.5	44.4 ± 12.3	0.13
Diastolic parameters			
E/A ratio	1.20 [0.79-2.17]	0.87 [0.74-1.40]	0.34
E/e' ratio	20.3 [17.9-32.7]	13.9 [12.6-16.0]	****0.0003*
TR velocity (cm/s)	2.6 [2.1-2.9]	2.3 [2.2-2.4]	0.20
Grade of diastolic dysfunction			
1	11.1% (1)	75.0% (9)	***0.008*
2	55.6% (5)	8.3% (1)	**0.046*
3	33.3% (3)	16.7% (2)	0.61
Medication			
beta blocker	84.6% (11)	84.6% (11)	>0.9999
calcium channel blocker	46.2% (6)	23.1% (3)	0.41
statins	15.4% (2)	23.1% (3)	>0.9999

Although there is no difference between women and men in absolute IVS thickness, the women included in this study showed a higher IVS thickness when corrected for BSA compared to males (25% increase, p=0.07; Table 1). This is in line with a previous study showing significant differences in IVS thickness between women and men when corrected for BSA (13).

Females Express More Tubulin and Heat Shock Proteins

Out of 2099 quantified proteins, only 46 proteins were significantly differentially expressed in the direct comparison of the female and male group. Two functional protein interaction clusters were identified for both the 14 downregulated and the 32 upregulated proteins in females compared to males. The functional protein clusters that were less expressed in females compared to males were related to muscle filament sliding and carbohydrate catabolic process (Figure 2A). The functional protein clusters

of proteins that are more expressed in females compared to males are chaperone-mediated protein complex assembly and action potential (Figure 2B). Chaperone-mediated complex assembly is, based on the number of proteins in this cluster (18, 39% of the differentially expressed proteins), the dominating protein cluster in the comparison of female and male SMP HCM samples. Interestingly, this cluster contains mainly heat shock proteins (HSPs) and tubulin subunits. HSPs and tubulin have already been investigated before by our group in the context of SMP and sarcomere-mutation negative HCM samples (24, 34). Therefore, we now further determined if there are any sex-differences at the protein levels of tubulin and a selection of HSPs that were assessed by western blot. While we did not observe significant sex-differences in the levels of HSPA1, HSPA2, HSPB5, HSPB7, HSPA4 and HSP90, we found a trend to higher levels of HSPD1 ($p = 0.0957$) and HSPB1 ($p=0.0850$) in female compared to male samples [Figure 3, reanalyzed from the dataset from Dorsch et al. (34)]. Although the HSPs assessed by western blot do not show significant differences between females and males, the data are in line with the small fold changes found in the proteomics data and point toward higher levels of HSPs in female compared to male HCM tissue. Likewise, we analyzed the sex-differences in our tubulin data set (Figure 4), re-analyzed from the datasets from Dorsch et al. and Schuldt et al. (24, 34). In line with the proteomics data, levels of a-tubulin were significantly higher in females compared to males, whereas we did not find any sex-differences in the posttranslational modifications acetylation, tyrosination and detyrosination. To determine if elevated levels of tubulin may correlate with diastolic dysfunction, we plotted levels of a-tubulin with the clinical parameter E/e' for male and female patients separately (Figure 4E). Female patients have higher levels of a-tubulin in combination with more severe diastolic dysfunction, as indicated by increased E/e', compared to male patients who show lower levels of a-tubulin with less severe diastolic dysfunction.

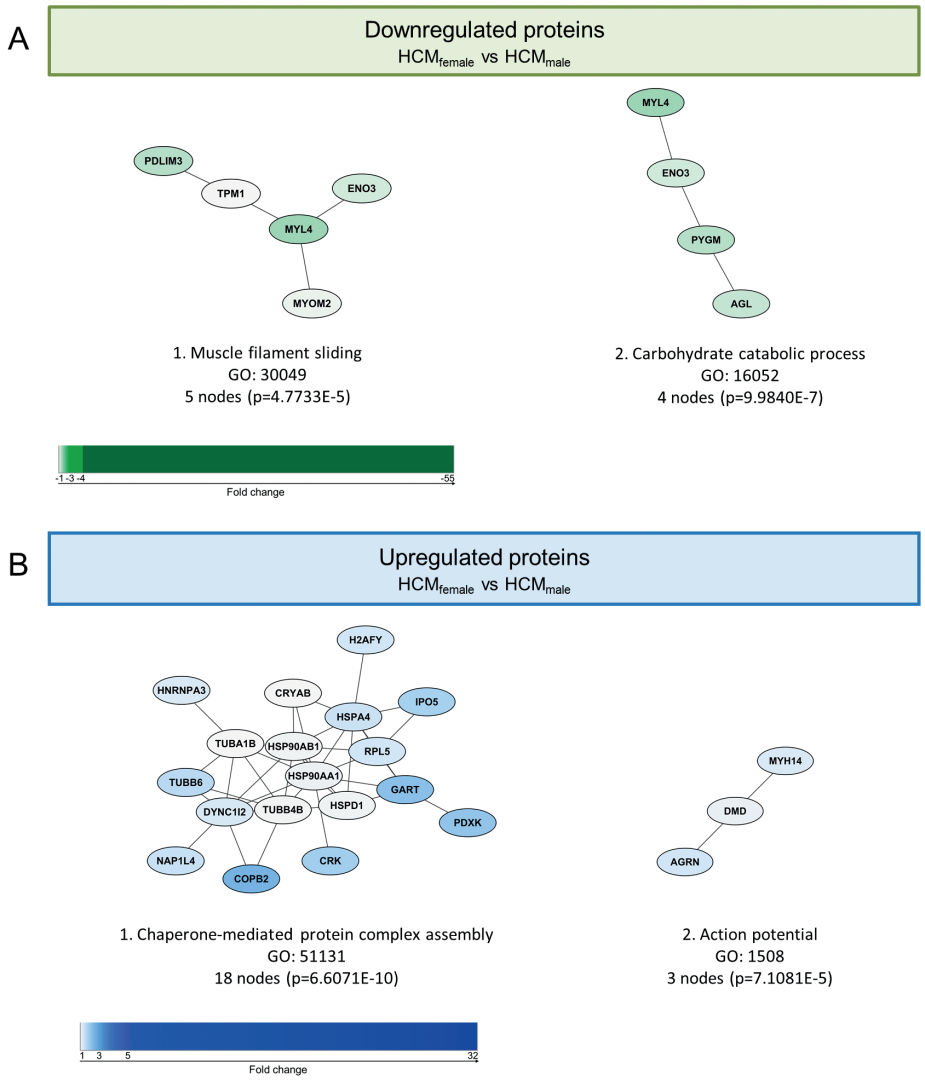

FIGURE 2. Functional protein cluster of the direct comparison of HCM_{female} and HCM_{male}. (A) illustrates the functional protein cluster of the proteins that are significantly lower expressed in females compared to males. (B) shows the functional protein cluster of the proteins that are significantly higher expressed in females compared to males. For each protein cluster the most significant biological process is given. Proteins with a p-value <0.05 were used for the analysis.

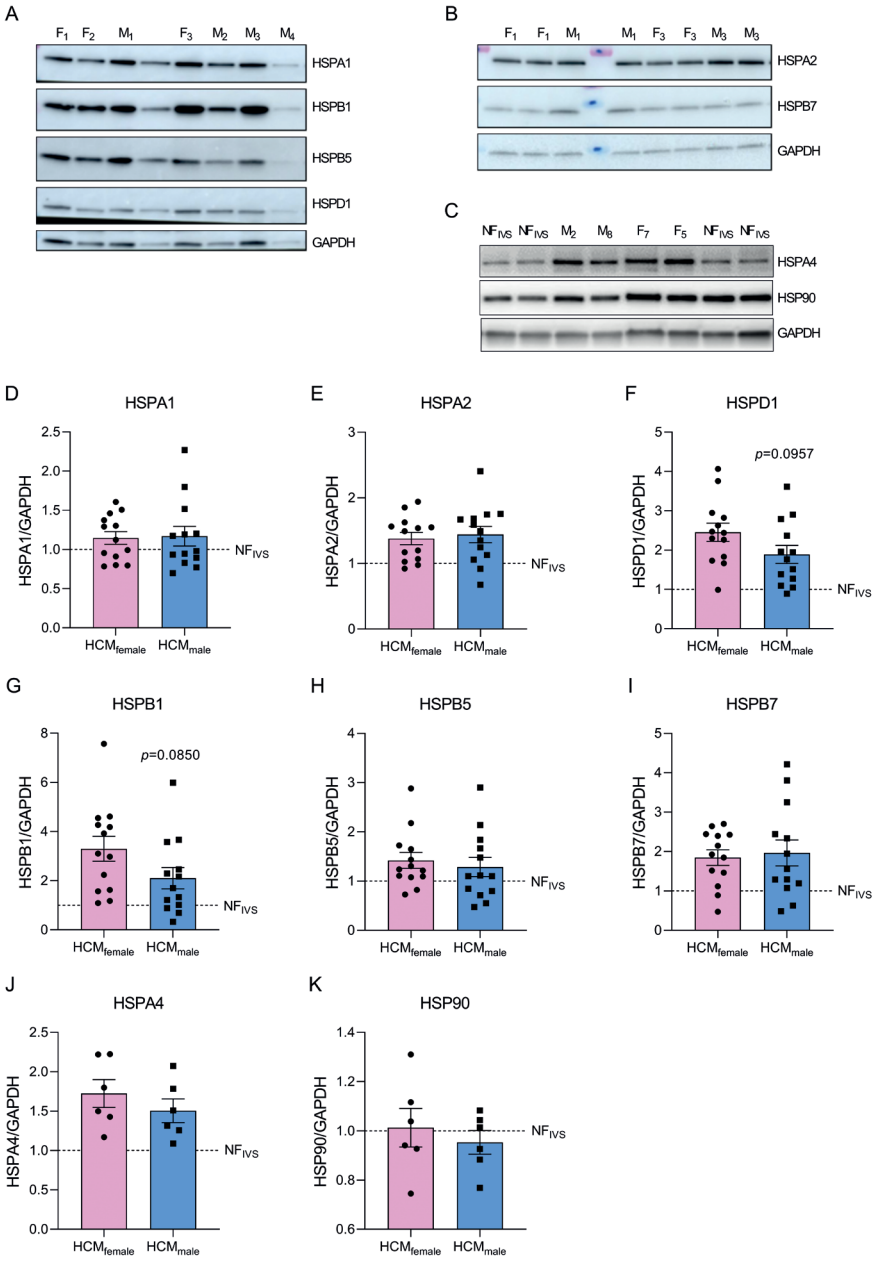

FIGURE 3. Protein levels of heat shock proteins determined by western blot. (A–C) Show representative western blot images. (D–K) Display quantified protein levels for HSPA1, HSPA2, HSPD1, HSPB1, HSPB5, HSPB7, HSPA4, and HSP90, respectively. Data were statistically analyzed by unpaired two-tailed *t*-test. Dashed line indicates protein levels in the NF_{IVS}. Western blot dataset is partly derived from Dorsch et al. and re-analyzed for the age-matched samples included in the current study (34).

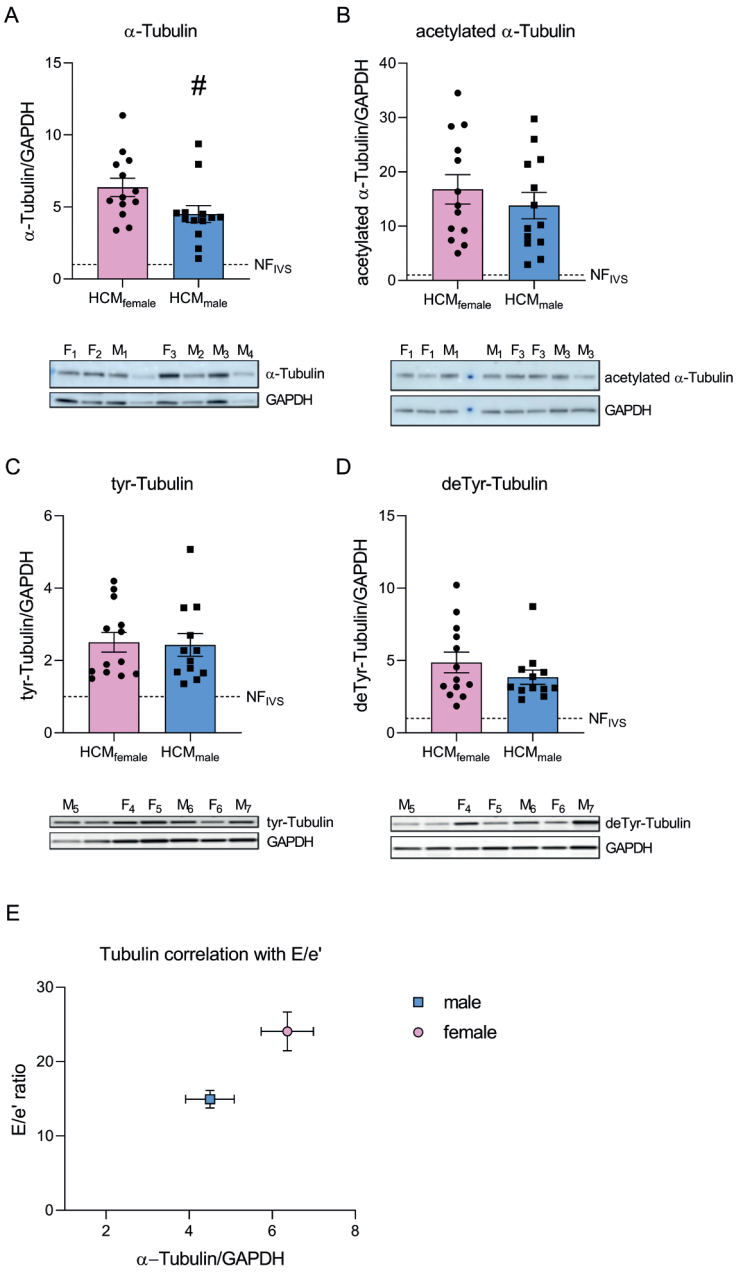

FIGURE 4. Protein levels of α-tubulin and its posttranslational modifications determined by western blot. Panels (A-D) show protein levels of α-tubulin (A), acetylated tubulin (B), tyrosinated tubulin (C) and detyrosinated tubulin (D) with representative images. Data were statistically analyzed by unpaired two-tailed t-test, #p=0.0407. Dashed line indicates protein levels in the NF_{IVS}:Western blot dataset is new analysis of a subset of samples from Dorsch et al. and Schuldt et al. (24, 34). (E) shows correlation of α-tubulin levels with E/e' ratio.

Proteins Involved in Translation Are Specifically Downregulated in Male HCM Patients Compared to Non-failing Control Myocardium

As an additional approach, we compared protein expression of both the male and the female group to NF_{IVS} to look at specific sex-related protein changes compared to non-failing myocardium, thereby identifying proteins that are not only sex but also disease-specific. We have identified 236 proteins that are less expressed and 214 proteins that are more expressed in the female HCM patients versus NF_{IVS}. In the male HCM patients we identified 251 lower expressed proteins and 156 more abundant proteins compared to NF_{IVS}. The top 10 functional protein interaction clusters of the females compared to NF_{IVS} are listed in Table 2 and the top 10 protein clusters of the male samples compared to NF_{IVS} are displayed in Table 3. The complete set of protein interaction clusters resulting from this analysis is shown in Supplementary Figures 1-4. To identify differences between female and male HCM using this analysis approach, we created Venn diagrams of the significantly different proteins from the female vs NF_{IVS} and the male vs NF_{IVS} comparison to look at overlapping proteins that are shared by both comparisons, and proteins that are unique for either males or females compared to NF_{IVS} (Figures 5, 6, Venn diagrams).

Of the proteins that are downregulated compared to NF_{IVS} we identified 181 proteins that are overlapping between males and females. These proteins belong mainly to metabolic pathways (Supplementary Figure 5), and can be considered as general HCM-specific protein changes. Fifty five of the downregulated proteins are only significantly different for the females. The functional protein clusters of these proteins are related to respiratory electron transport chain, cellular lipid catabolic process, response to activity, small molecule catabolic process, neutrophil degranulation, energy deprivation by oxidation of organic compounds and response to aldosterone (Figure 5A). Seventy downregulated proteins are only significantly different in the male group and cluster analysis revealed that the biggest protein cluster is related to the biological process translation. It contains many ribosomal proteins that have a consistently high fold-change compared no NF_{IVS}. Other clusters are related to amide biosynthetic process and several processes related to energy metabolism like ketone body biosynthetic process, electron transport chain and tricarboxylic acid metabolic process. Furthermore, we obtained protein clusters related to pyridoxal phosphate biosynthetic process, cellular water homeostasis, glutathione metabolic process and extracellular matrix disassembly (Figure 5B).

TABLE 2. Top 10 differentially regulated pathways in HCM_{female} vs NF_{IVS}.

Downregulated proteins			Upregulated proteins		
Pathway (GO ID)	**nodes**	**p-value**	**Pathway (GO ID)**	**nodes**	**p-value**
Cellular respiration (45333)	70	6.7945E-73	Extracellular structure organization (43062)	45	8.1156E-43
NAD metabolic process (19674)	28	1.7205E-22	Muscle contraction (6936)	19	1.9361E-16
Monocarboxylic acid metabolic process (32787)	22	2.3313E-25	Post-translational protein modification (43687)	17	1.4103E-11
Organic acid catabolic process (16054)	20	1.0701E-24	Organelle localization (51640)	13	1.6284E-8
Neutrophil degranulation (43312)	15	2.5257E-15	Response to unfolded protein (6986)	12	2.2706E-12
Cellular nitrogen compound biosynthetic process (44271)	12	3.4079E-11	Striated muscle cell development (55002)	12	6.9444E-9
Muscle contraction (6936)	12	5.6834E-9	Myofibril assembly (30239)	10	4.2003E-14
Acute-phase response (6953)	11	5.0201E-14	Regulation of cell migration (30334)	9	1.3513-8
Cellular detoxification (1990748)	9	6.5002E-10	Cellular carbohydrate metabolic process (44262)	8	2.0038E-9
Cardiac muscle tissue development (48738)	8	9.5592E-12	Membrane organization (61024)	8	4.7889E-6

Table lists the top 10 functional protein cluster (based on size) of the down- and upregulated proteins for the comparison of HCM_{female} with NF_{IVS}. Displayed are the most significant biological process (gene ontology), the number of nodes in the cluster and the p-value.

TABLE 3. Top 10 differentially regulated pathways in HCM_{male} vs NF_{IVS}.

Downregulated proteins			Upregulated proteins		
Pathway (GO ID)	**nodes**	**p-value**	**Pathway (GO ID)**	**nodes**	**p-value**
Cellular respiration (45333)	62	9.9733E-62	Extracellular matrix organization (30198)	47	9.0957E-40
Small molecule metabolic process (44281)	29	3.0796E-22	Actin filament-based process (30029)	13	3.2873E-10
Amide biosynthetic process (43604)	27	2.6386E-19	Striated muscle cell development (55002)	12	4.8955E-11
Carboxylic acid catabolic process (46395)	26	3.3911E-26	Platelet aggregation (70527)	11	1.0179E-8
Regulated exocytosis (45055)	15	3.5280E-13	Muscle contraction (6936)	10	1.1585E-7
Translational initiation (6413)	15	6.4097E-8	Calcium-independent cell-matrix adhesion (7161)	8	5.7263E-7
Protein folding (6457)	15	1.9000E-7	Response to muscle inactivity involved in regulation of muscle adaptation (14877)	8	8.5753E-6
Organic acid catabolic process (16054)	13	1.0083E-14	Neutrophil degranulation (43312)	7	3.3963E-7
Acute-phase response (6953)	12	1.0023E-13	Carbohydrate metabolic process (5975)	6	6.4278E-8
Creatine metabolic process (6600)	12	3.2195E-12	Regulation of podosome assembly (71801)	6	9.2900E-6

Table lists the top 10 functional protein cluster (based on size) of the down- and upregulated proteins for the comparison of HCM_{male} with NF_{IVS}. Displayed are the most significant biological process (gene ontology), the number of nodes in the cluster and the p-value.

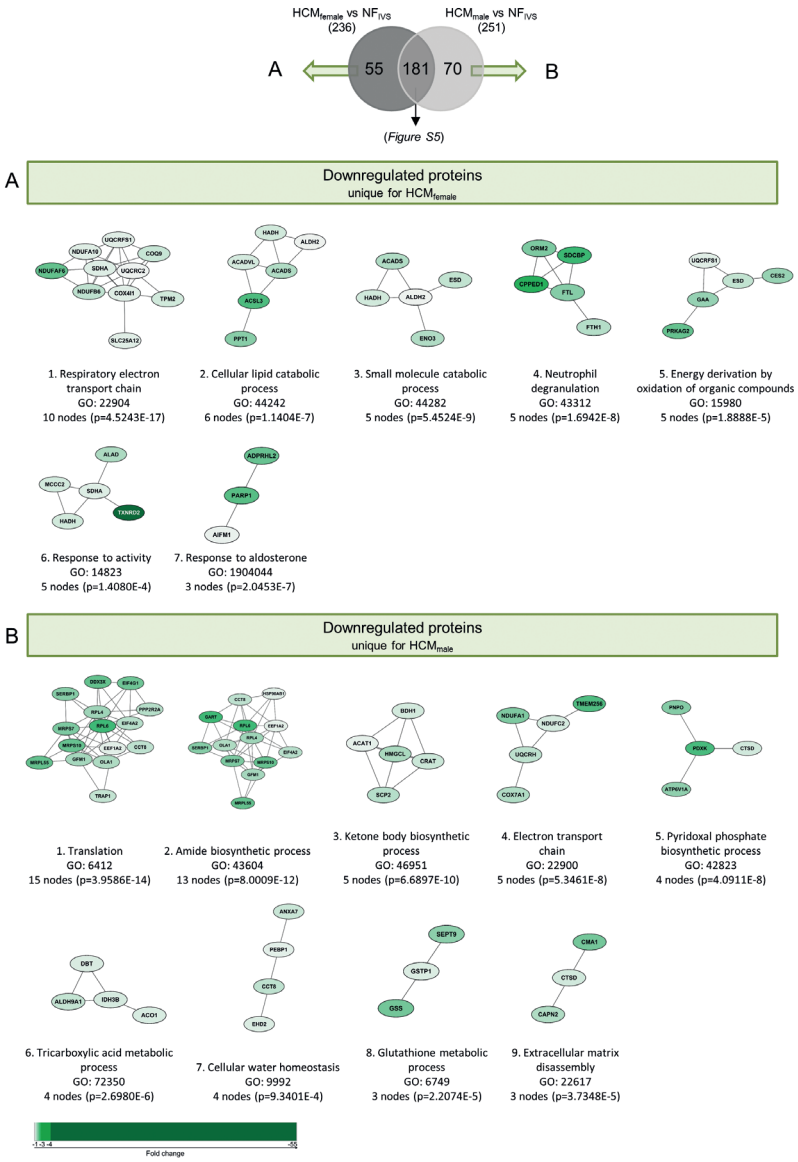

FIGURE 5. Functional protein cluster of the downregulated proteins that are unique for either HCM_{female} or HCM_{male} when compared separately to NF_{IVS}. A Venn diagram was created with the significantly lower expressed proteins between HCM_{female} and NF_{IVS} and HCM_{male} and NF_{IVS}, to identify the downregulated proteins that are unique for either males or females, or shared by both groups. Panel (A) illustrates the functional protein cluster of the proteins that are only significantly lower expressed in females when compared to NF_{IVS}, whereas (B) shows the functional protein cluster of the proteins that are only significantly lower expressed in males when compared to NF_{IVS}. For each protein cluster the most significant biological process is given. Proteins with a p-value <0.05 were used for the analysis.

Microtubular and Heat Shock Proteins Are Specifically Upregulated in Female HCM Patients When Compared to Controls

For the upregulated proteins, 140 proteins are significantly more expressed in both females vs NF_{IVS} and males vs NF_{IVS}. The functional protein interaction clusters are illustrated in Supplementary Figure 6. The 74 proteins that are significantly higher in females compared to controls result in clusters related to response to unfolded protein, chylomicron assembly, membrane organization, regulation of cell migration, negative regulation of microtubule polymerization or depolymerization, positive regulation of cellular component organization, sarcomere organization, glycophagy, muscle organ development and carboxylic acid biosynthetic process (Figure 6A). With the cluster response to unfolded protein and negative regulation of microtubule polymerization or depolymerization the results of this approach are in line with the direct comparison of female and male HCM samples in which these proteins were represented by the cluster chaperone-mediated protein complex assembly. 8 of the 74 proteins that are significantly higher expressed only in females (CRK, HSPA4, TUBB6, ALDH1B1, DMD, LMOD2, HNRNPA3 and TFRC) overlap with the 46 proteins significantly different in the direct male and female comparison and may represent important candidates to define the female group (Figure 7).

The 16 proteins that are only significantly higher in HCM males compared to NF_{IVS} did not form any functional protein cluster. Of these proteins, only the protein SLC27A6 (solute carrier family 27 member 6/long chain fatty acid transport protein 6) overlaps with the 46 proteins that are significantly different in the direct comparison of females and males. As being significantly higher expressed compared to both NF_{IVS} and females, SLC27A6, involved in long chain fatty acid uptake, may be an important candidate defining the male HCM patients.

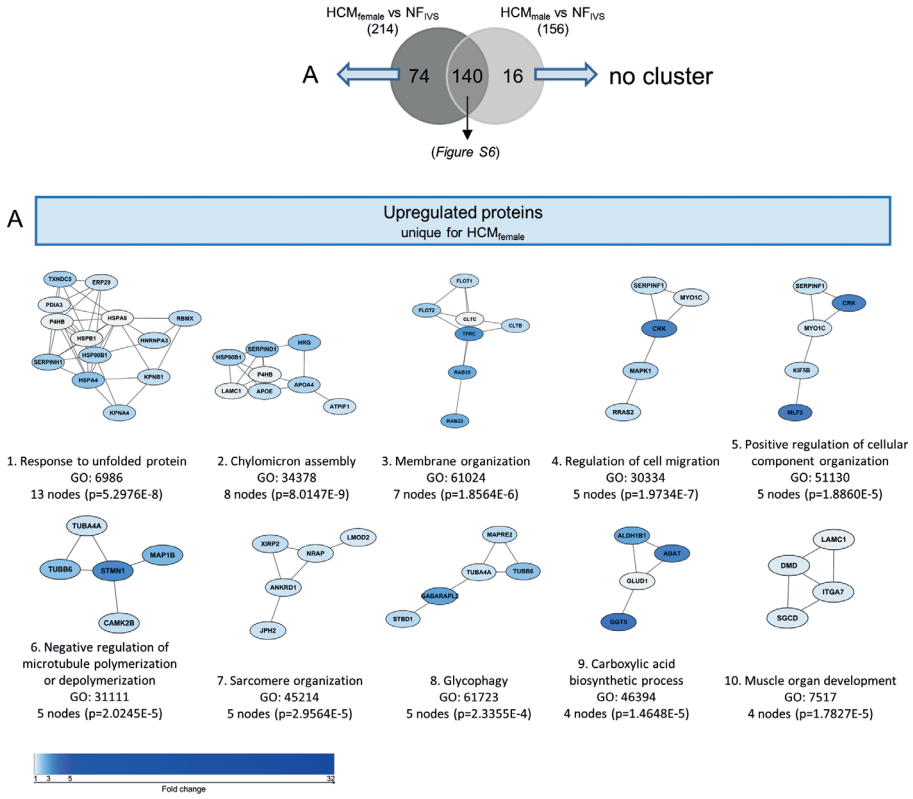

FIGURE 6. Functional protein cluster of the upregulated proteins that are unique for either HCM_{female} or HCM_{male} when compared separately to NF_{IVS}. A venn diagram was created with the significantly higher expressed proteins between HCM_{female} and NF_{IVS} and HCM_{male} and NF_{IVS}, to identify the upregulated proteins that are unique for either males or females or shared by both groups. Panel (A) illustrates the functional protein cluster of the proteins that are only significantly higher expressed in females when compared to NF_{IVS}. The proteins only significant for HCM_{male} did not give any functional protein cluster. For each protein cluster the most significant biological process is given. Proteins with a p-value <0.05 were used for the analysis.

Transcriptional Regulation of Significantly Different Proteins Between HCM_{female} and HCM_{male} Is Not Dominated by Sex Hormones

Since sex hormones also act as transcription factors, we analyzed if sex-hormone-related transcription factors can be responsible for the 46 significantly differentially expressed proteins of the direct comparison between female and male HCM samples (Figure 2). Possible transcription factor bindings sites were analyzed with the ToppFun database. Three hundred Seventy two transcription factors were identified that have binding-sites in the 46 proteins that are significantly different between female and male HCM patient samples. The 10 most significant transcription factors are

shown in Supplementary Table 2. Of these we found 7 to be sex-hormone related (Supplementary Table 3). These 7 transcription factors are involved in the regulation of 5 significantly different proteins between male and female HCM myocardium: HSPD1, PYGM, DMD, ENO3 and TFRC. Of these, DMD, ENO3 and TFRC are also significantly different when comparing females with NF_{IVS} (Figures 5, 6). With PYGM and ENO3 involved in carbohydrate metabolism, DMD involved in muscle organization and HSPD1 as a member of the PQC, we thereby identified candidate proteins that may be regulated by sex hormone-related transcription factors. However, the bioinformatical analysis revealed that the 5 proteins also have binding sites for another 258 of the 372 identified transcription factors. Based on this we can conclude that the differences found between female and male samples may be partly due to transcriptional regulation by sex hormones but that this is not the dominant mechanism driving sex-dependent differential protein expression.

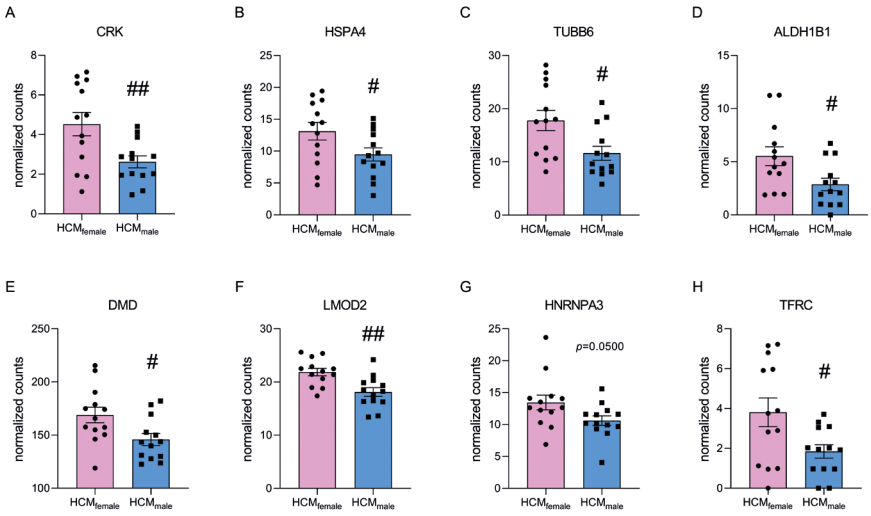

FIGURE 7. Normalized counts of proteins that are significantly upregulated in HCM_{female} compared to HCM_{male} and are uniquely upregulated in females when compared to $NF_{IVS.}$ (A) CRK, (B) HSPA4), (C) TUBB6, (D) ALDH1B1, (E) DMD, (F) LMOD2, (G) HNRNPA3 and (H) TFRC. $^{\#}p<0.05$, $^{\#\#}p<0.01$, unpaired two-tailed t-test.

DISCUSSION

In this study we analyzed sex-differences at the protein level in proteomics data of HCM patient tissue to define sex-specific protein expression which may explain the difference in clinical presentation. The direct comparison of the male and female patient groups resulted in only a small number of significantly different proteins. Compared to males, female HCM patients display lower levels of myofilament proteins related to the biological process muscle filament sliding and have elevated levels of tubulin and HSPs. Consistently, by subtracting the baseline differences using an additional non-failing control group, we observed a more profound elevation of HSPs and the microtubule processes in female HCM patients.

Set of 8 Proteins Consistently Defines the Female HCM Patients

A study investigating sex-differences in gene expression at the mRNA level in idiopathic cardiomyopathy patients found 1837 differently expressed genes between male and female patients, of which the large majority of 1377 genes had a fold change <1.2 (37). Considering these low fold changes on a gene expression level, little changes at the protein level are to be expected. We found expression levels of 8 proteins significantly higher in females when directly compared to males, and also uniquely significant for females when compared to NF_{IVS} (Figure 7). Thereby, these proteins are disease-specific and may play an important role in defining the female patient group. One of these proteins is CRK, which is an adaptor protein with SH2 and SH3 domains but no catalytic region. It functions in signal transduction processes and has been shown to be involved in cardiac development (38). HSPA4 is a heat shock protein that acts as nucleotide exchange factor for HSP70 chaperones. Its expression is upregulated in response to pressure overload and in human heart failure, which is thought to be a beneficial response as it helps degrading misfolded proteins (39). TUBB6 is a b-tubulin subtype that forms microtubules together with a-tubulin. Elevated levels of tubulin have been observed in heart failure (40). ALDH1B1 is an aldehyde dehydrogenase that is involved in alcoholmetabolism and has been shown to function in glucose metabolism (41). DMD encodes for dystrophin and connects the actin cytoskeleton with the extracellular matrix. As actin crosslinker, it plays an important role for the mechanical properties of the cardiomyocyte. Elevated levels in females may be explained by its gene location on the X-chromosome. Mutations in DMD have been associated with muscular dystrophies and Xlinked dilated cardiomyopathy (42). LMOD2 is the cardiac isoform of leiomodin, an actin-binding protein involved in thin filament assembly. Studies in adult mice have shown that LMOD2 has an essential role in maintaining proper cardiac thin filament length and coinciding force generation (43). HNRNPA3 is a heterogeneous nuclear ribonucleoprotein that binds to single-stranded telomeric repeats to stabilize them (44), and TFRC encodes for the transferrin receptor that promotes iron uptake (45).

Elevated Levels of HSPs and Tubulin Are in Line With a More Severe Phenotype

The most prominent difference in our study were higher levels of tubulin and HSPs in female compared to male HCM patient samples taken at the time of myectomy. Interestingly, sex-differences in the expression of HSPs have been observed before. Higher levels of HSPA1A have been measured in healthy female rat hearts compared to male, and these increased levels were estrogen dependent (46). We also found by bio-informatical analysis that HSPD1, which is elevated in female compared to male HCM myocardium, can be regulated by the estrogen-related receptor α. It may be speculated that the estrogen-dependent HSP induction, that is known to be cardioprotective (47), has also beneficial effects in HCM, leading to lower disease penetrance and later disease onset in women. Indeed, HSP activation has been shown to have beneficial effects on heart function in a mouse model of desmin-related cardiomyopathy in which HSP expression was induced by geranylgeranylacetone (48). In our study we observed increased protein expression of HSPs in tissue samples from symptomatic stage II HCM patients, which raises the question if the optimal therapeutic window for HSP induction might already be at an earlier preclinical stage of the disease. This warrants further studies in iPSC-derived human heart models and other cardiomyopathy animal models.

Cytoskeletal proteins like tubulin and desmin are known to be elevated in heart failure (40). Our group has previously shown that tubulin protein levels are increased in HCM myectomy tissue compared to NF_{IVS} (24, 34). Interestingly, tubulin and desmin protein content has been shown to correlate well with left ventricular end-diastolic pressure (LVEDP) in heart failure (40). As increased LVEDP indicates diastolic dysfunction, cytoskeletal protein levels correlate directly with diastolic dysfunction. Furthermore, tubulin has in combination with its posttranslational modifications a direct effect on contractile function, as detyrosinated tubulin binds to desmin and causes a stiffening of the myofilament (49-51). As increased levels of tubulin in females compared to males correlate with more severe diastolic dysfunction (13), proof-of-concept studies in model systems have to show whether this is a causal relationship during HCM development.

Male Samples Display Lower Levels of Translational Proteins

Ribosomal and protein synthesis-related proteins, which form the cluster "translation", were significantly downregulated in male HCM patients compared to NF_{IVS}. Interestingly, it was recently shown that cMyBP-C protein synthesis and degradation rates were slowed down in induced pluripotent stem cell-derived cardiomyocytes harboring a heterozygous *MYBPC3* mutation (52). The authors proposed that cells harboring a *MYBPC3* truncating mutation may have the capacity to attain normal levels of cMyBP-C protein and thereby preserve cardiomyocyte function. On the other hand, protein turnover is needed to replace aged/damaged proteins. Thus, while reduced protein turnover may preserve protein stoichiometry and thereby cardiomyocyte

function, it may lead to accumulation of damaged proteins in the sarcomere. Our data are in line with the study of Helms and colleagues, and imply reduced protein turnover in particular in male HCM hearts at the time of myectomy. Increasing protein translation rate to maintain proper protein turnover represents an attractive avenue to further explore.

Sex-Specific Difference in Carbohydrate Metabolism

Downregulation of metabolic pathways is a general HCM disease hall mark (24, 53) and accordingly we did not find major differences in these pathways between males and females. However, females showed lower levels of proteins related to carbohydrate catabolic process (Figure 2A), including muscle associated glycogen phosphorylase (PYGM) and β-enolase (ENO3). Mutations in both of these genes have been associated with glycogen metabolism disorders (54). Consequently, reduced levels of PYGM and ENO3 impair glycogen metabolism in women. Our transcription factor analysis showed that both PYGM and ENO3 can be regulated by sex hormone transcription factors. The findings indicate that women may be less metabolically flexible to adapt to altered metabolic demand, at least during disease development. Imaging studies have shown that reduced cardiac efficiency occurs already at the early disease stage in asymptomatic male and female mutation carriers (55, 56) and may indicate that metabolic changes may be present in the very early stages before the onset of cardiac remodeling.

More Fibrosis in Female Patients Is Not Reflected at Protein Level

It has been observed that female HCM patient samples show more fibrosis compared to male samples (13). Interestingly, this difference is not reflected at protein level. Neither in the direct comparison of female and male HCM samples, nor in the analysis compared to NF_{IVS}, we observed a specific increase in extracellular matrix proteins for females. In the current proteomics analysis, increased expression of extracellular matrix proteins was a general disease hallmark, and common for both female and male group. The methodological difference between quantifying proteins involved in extracellular matrix organization in this proteomics analysis and measuring the actual fibrotic area in tissue sections as performed by Nijenkamp et al. may underlie the divergent findings.

STUDY LIMITATIONS

The findings in this study are observational and provide a starting point for further validation in an independent cohort and proof-of-concept studies in disease models. Due to the limited availability of non-failing heart tissues, the male control samples used in this study are not age-matched with the male HCM samples, whichmay contribute to observed differences in protein expression. Furthermore, the group

size of only female or male non-failing samples is too small to perform comparisons of HCM and controls of the same sex. Therefore, follow-up studies would benefit from age-matched and increased numbers of nonfailing controls to differentiate between sex- and disease-specific differences in protein expression. As our findings point toward a possible role of sex hormone regulation, information about the hormonal state of the female subjects should be collected for future studies.

CONCLUSION

This proteomic analysis of female and male SMP HCM tissue highlights that elevated protein levels of tubulin correlate with more severe diastolic dysfunction in females. Another aspect which warrants further research is reduced protein turnover, in particular in male HCM, which may represent an adaptive mechanism to maintain protein stoichiometry, though may also have a negative impact and result in "aged" sarcomeres. Further research in experimental model systems is needed to determine if targeting tubulin and protein quality control at an early disease stage prevent the progression of cardiac dysfunction.

DATA AVAILABILITY STATEMENT

The datasets presented in this study can be found in online repositories. The names of the repository/repositories and accession number(s) can be found below: ProteomeXchange consortium, identifier PXD012467, http://www.ebi.ac.uk/pride/archive/projects/PXD012467.

ETHICS STATEMENT

The studies involving human participants were reviewed and approved by Local medical ethics review committee of the Erasmus Medical Center, Rotterdam, Netherlands. Written informed consent to participate in this study was provided by the participants' legal guardian/next of kin.

AUTHOR CONTRIBUTIONS

MS, DK, and JV conceived, designed, and coordinated the study and wrote the manuscript. MS, LD, JK, TP, TS, and SP performed and/or analyzed the experiments. CR and MM were involved in patient data andmaterial acquisition. CJ provided supervision for proteomics experiments. All authors proof-read the manuscript and gave valuable input.

FUNDING

We acknowledge the support from the Netherlands Cardiovascular Research Initiative: An initiative with support of the Dutch Heart Foundation, CVON2014-40 DOSIS and NWO (NWO-ZonMW; 91818602 VICI Grant to JV).

CONFLICT OF INTEREST

The authors declare that the research was conducted in the absence of any commercial or financial relationships that could be construed as a potential conflict of interest.

REFERENCES

1. Maron BJ, Gardin JM, Flack JM, Gidding SS, Kurosaki TT, BildDE. Prevalence of hypertrophic cardiomyopathy in a general population of young adults: echocardiographic analysis of 4111 subjects in the CARDIA Study. Coronary Artery Risk Development in (Young) Adults. Circulation. (1995) 92:785–9. doi: 10.1161/01.CIR.92.4.785
2. Semsarian C, Jodie I, Martin Maron S, Barry JM. New perspectives on the prevalence of hypertrophic cardiomyopathy. J Am College Cardiol. (2015) 65:1249–54. doi: 10.1016/j.jacc.2015.01.019
3. Michels M, Olivotto I, Asselbergs F, van der Velden WJ. Life-long tailoring of management for patients with hypertrophic cardiomyopathy: awareness and decision-making in changing scenarios. Neth Heart J. (2017) 25:186–99. doi: 10.1007/s12471-016-0943-2
4. Authors/Task Force, Elliott PM, Anastasakis A, Borger MA, Borggrefe M, Cecchi F, et al. 2014 ESC Guidelines on diagnosis and management of hypertrophic cardiomyopathy: the task force for the diagnosis and management of hypertrophic cardiomyopathy of the european society of cardiology (ESC). Eur Heart J. (2014) 35:2733–79. doi: 10.1093/eurheartj/ehu284
5. Ho CY, Charron P, Richard P, Girolami F, Van Spaendonck-Zwarts KY, Pinto Y. Genetic advances in sarcomeric cardiomyopathies: state of the art. Cardiovasc Res. (2015) 105:397–408. do: 10.1093/cvr/cvv025
6. Ingles J, Burns C, Barratt A, Semsarian C. Application of genetic testing in hypertrophic cardiomyopathy for preclinical disease detection. Circ Cardiovasc Genet. (2015) 8:852–9. doi: 10.1161/CIRCGENETICS.115.001093
7. Olivotto I, Maron MS, Adabag AS, Casey SA, Vargiu D, Link MS, et al. Gender-related differences in the clinical presentation and outcome of hypertrophic cardiomyopathy. J Am Coll Cardiol. (2005) 46:480–7. doi: 10.1016/j.jacc.2005.04.043
8. Kubo T, Kitaoka H, OkawaM, Hirota T, Hayato K, Yamasaki N, et al. Gender-specific differences in the clinical features of hypertrophic cardiomyopathy in a community-based Japanese population: results from Kochi RYOMA study. J Cardiol. (2010) 56:314–9. doi: 10.1016/j.jjcc.2010.07.004
9. Maron BJ, Casey SA, Poliac LC, Gohman TE, Almquist AK, Aeppli DM. Clinical course of hypertrophic cardiomyopathy in a regional United States cohort. JAMA. (1999) 281:650–5. doi: 10.1001/jama.281.7.650
10. Maron BJ, Olivotto I, Spirito P, Casey SA, Bellone P, Gohman TE, et al. Epidemiology of hypertrophic cardiomyopathy-related death: revisited in a large non-referral-based patient population. Circulation. (2000) 102:858–64. doi: 10.1161/01.CIR.102.8.858
11. Marstrand P, Han L, Day SM, Olivotto I, Ashley EA, Michels M, et al. Hypertrophic cardiomyopathy with left ventricular systolic dysfunction: insights from the share registry. Circulation. (2020) 141:1371–83. doi: 10.1161/CIRCULATIONAHA.119.044366
12. Bos JM, Theis JL, Tajik AJ, Gersh BJ, Ommen SR, Ackerman MJ. Relationship between sex, shape, and substrate in hypertrophic cardiomyopathy. Am Heart J. (2008) 155:1128–34. doi: 10.1016/j.ahj.2008.01.005
13. Nijenkamp L, Bollen IAE, van Velzen HG, Regan JA, van Slegtenhorst M. Sex differences at the time of myectomy in hypertrophic cardiomyopathy. Circ Heart Fail. (2018) 11:e004133. doi: 10.1161/CIRCHEARTFAILURE.117.004133

14. Schulz-Menger J, Abdel-Aty H, Rudolph A, Elgeti T, Messroghli D, Utz W, et al. Gender-specific differences in left ventricular remodelling and fibrosis in hypertrophic cardiomyopathy: insights from cardiovascular magnetic resonance. Eur J Heart Fail. (2008) 10:850–4. doi: 10.1016/j.ejheart.2008.06.021
15. Leinwand LA. Sex is a potent modifier of the cardiovascular system. J Clin Invest. (2003) 112:302–7. doi: 10.1172/JCI200319429
16. Chen YZ, Qiao SB, Hu FH, Yuan JS, Yang WX, Cui JG, et al. Left ventricular remodeling and fibrosis: sex differences and relationship with diastolic function in hypertrophic cardiomyopathy. Eur J Radiol. (2015) 84:1487–92. doi: 10.1016/j.ejrad.2015.04.026
17. Borlaug BA, Redfield MM, Melenovsky V, Kane GC, Karon BL, Jacobsen SJ, et al. Longitudinal changes in left ventricular stiffness: a community-based study. Circ Heart Fail. (2013) 6:944–52. doi: 10.1161/CIRCHEARTFAILURE.113.000383
18. van Velzen HG, Schinkel AFL, Baart SJ R, Huurman, van Slegtenhorst MA, Kardys I, et al. Effect of gender and genetic mutations on outcomes in patients with hypertrophic cardiomyopathy. Am J Cardiol. (2018) 122:1947–54. doi: 10.1016/j.amjcard.2018.08.040
19. Geske JB, Ong KC, Siontis KC, Hebl VB, Ackerman MJ, Hodge DO, et al. Women with hypertrophic cardiomyopathy have worse survival. Eur Heart J. (2017) 38:3434–40.doi: 10.1093/eurheartj/ehx527
20. van Driel B, Nijenkamp L, Huurman RM, van der Velden MJ. Sex differences in hypertrophic cardiomyopathy: new insights. Curr Opin Cardiol. (2019) 34:254–9. doi: 10.1097/HCO.0000000000000612
21. Huurman R, Schinkel AFL, van der Velde N, Bowen DJ, Menting ME. Effect of body surface area and gender on wall thickness thresholds in hypertrophic cardiomyopathy. Neth Heart J. (2020) 28:37–43. doi: 10.1007/s12471-019-01349-1
22. Latchman DS. Heat shock proteins and cardiac protection. Cardiovasc Res. (2001) 51:637–46. doi: 10.1016/S0008-6363(01)00354-6
23. Golenhofen N, Perng MD, Quinlan RA, Drenckhahn D. Comparison of the small heat shock proteins alphaB-crystallin, MKBP. HSP25, HSP20, and cvHSP in heart and skeletal muscle. Histochem Cell Biol. (2004) 122:415–25. doi: 10.1007/s00418-004-0711-z
24. Schuldt M, Pei J, Harakalova M, Dorsch LM, Schlossarek S, Mokry M, et al. Proteomic and functional studies reveal detyrosinated tubulin as treatment target in sarcomere mutationinduced hypertrophic cardiomyopathy. Circ Heart Fail. (2021) 26:139–40. doi: 10.1161/CIRCHEARTFAILURE.120.007022
25. Pham TV, Piersma SR, Warmoes M, Jimenez CR. On the betabinomial model for analysis of spectral count data in label-free tandem mass spectrometry-based proteomics. Bioinformatics. (2010) 26:363–9. doi: 10.1093/bioinformatics/btp677
26. Warmoes M, Jaspers JE, Pham TV, Piersma SR, Oudgenoeg G, Massink MP, et al. Proteomics of mouse BRCA1-deficient mammary tumors identifies DNA repair proteins with potential diagnostic and prognostic value in human breast cancer. Mol Cell Proteomics. (2012) 11:M111013334. doi: 10.1074/mcp.M111.013334
27. Piersma SR, Broxterman HJM, Kapci, de Haas RR, Hoekman K, VerheulHM, et al. Proteomics of the TRAP-induced platelet releasate. J Proteom. (2009) 72:91–109. doi: 10.1016/j.jprot.2008.10.009
28. Perez-Riverol Y, Csordas A, Bai J, Bernal-Llinares M, Hewapathirana S, Kundu DJ, et al. The PRIDE database and related tools and resources in 2019: improving support for quantification data. Nucleic Acids Res. (2019) 47: D442–D50. doi: 10.1093/nar/gky1106

29. Shannon P, Markiel A, Ozier O, Baliga NS, Wang JT, Ramage D, et al. Cytoscape: a software environment for integrated models of biomolecular interaction networks. Genome Res. (2003) 13:2498–504. doi: 10.1101/gr.1239303
30. Maere S, Heymans K, Kuiper M. BiNGO: a cytoscape plugin to assess overrepresentation of gene ontology categories in biological networks. Bioinformatics. (2005) 21:3448–49. doi: 10.1093/bioinformatics/bti551
31. Nepusz T, Yu H, Paccanaro A. Detecting overlapping protein complexes in protein-protein interaction networks. Nat Methods. (2012) 9:471–2. doi: 10.1038/nmeth.1938
32. Heberle H, Meirelles GV, da Silva FR, Telles GP, Minghim R. InteractiVenn: a web-based tool for the analysis of sets through Venn diagrams. BMC Bioinform. (2015) 16:169. doi: 10.1186/s12859-015-0611-3
33. Chen J, Bardes EE, Aronow BJ, Jegga AG. ToppGene suite for gene list enrichment analysis and candidate gene prioritization. Nucleic Acids Res. (2009) 37:W305–11. doi: 10.1093/nar/gkp427
34. Dorsch LM M, Schuldt, dos Remedios CG, Schinkel AFL, de Jong PL, Michels M, et al. (2019). Protein quality control activation and microtubule remodeling in hypertrophic cardiomyopathy. Cells. 8:741. doi: 10.3390/cells8070741
35. Lang RM, Bierig M, Devereux RB, Flachskampf FA, Foster E, Pellikka PA, et al. Recommendations for chamber quantification: a report from the American Society of Echocardiography's Guidelines and Standards Committee and the Chamber Quantification Writing Group, developed in conjunction with the European Association of Echocardiography, a branch of the European Society of Cardiology. J Am Soc Echocardiogr. (2005) 18:1440–63. doi: 10.1016/j.echo.2005.10.005
36. Nagueh SF, Appleton CP, Gillebert TC, Marino PN, Oh JK, Smiseth OA, et al. Recommendations for the evaluation of left ventricular diastolic function by echocardiography. J Am Soc Echocardiogr. (2009) 22:107–33. doi: 10.1016/j.echo.2008.11.023
37. Fermin DR, Barac A, Lee S, Polster SP, Hannenhalli S, Bergemann TL, et al. Sex and age dimorphism of myocardial gene expression in nonischemic human heart failure. Circ Cardiovasc Genet. (2008) 1:117–25. doi: 10.1161/CIRCGENETICS.108.802652
38. Park TJ, Boyd K, Curran T. Cardiovascular and craniofacial defects in Crk-null mice. Mol Cell Biol. (2006) 26:6272–82. doi: 10.1128/MCB.00472-06
39. Mohamed BA, Barakat AZ, Zimmermann WH, Bittner RE, Muhlfeld C, Hunlich M, et al. Targeted disruption of Hspa4 gene leads to cardiac hypertrophy and fibrosis. J Mol Cell Cardiol/. (2012) 53:459–68. doi: 10.1016/j.yjmcc.2012.07.014
40. Heling A, Zimmermann R, Kostin S, Maeno Y, Hein S, Devaux B, et al. Increased expression of cytoskeletal, linkage, and extracellular proteins in failing human myocardium. Circ Res. (2000) 86:846–53. doi: 10.1161/01.RES.86.8.846
41. Singh S, Chen Y, Matsumoto A, Orlicky DJ, Dong H, Thompson DC, et al. ALDH1B1 links alcohol consumption and diabetes. Biochem Biophys Res Commun. (2015) 463:768–73. doi: 10.1016/j.bbrc.2015. 06.011
42. Pecorari I, Mestroni L, Sbaizero O. Current understanding of the role of cytoskeletal cross-linkers in the onset and development of cardiomyopathies. Int J Mol Sci. (2020) 21:16. doi: 10.3390/ijms21165865
43. Pappas CT, Farman GP, Mayfield RM, Konhilas JP, Gregorio CC. Cardiacspecific knockout of Lmod2 results in a severe reduction in myofilament force production and rapid cardiac failure. J Mol Cell Cardiol. (2018) 122:88–97. doi: 10.1016/j.yjmcc.2018.08.009

44. Tanaka E, Fukuda H, Nakashima K, Tsuchiya N, Seimiya H, Nakagama H. HnRNP A3 binds to and protects mammalian telomeric repeats in vitro. Biochem Biophys Res Commun. (2007) 358:608–14. doi: 10.1016/j.bbrc.2007.04.177
45. Hentze MW, Muckenthaler MU, Andrews NC. Balancing acts: molecular control of mammalian iron metabolism. Cell. (2004) 117:285–97. doi: 10.1016/S0092-8674(04)00343-5
46. Voss MR, Stallone JN, Li M, Cornelussen RN, Knuefermann P, Knowlton AA. Gender differences in the expression of heat shock proteins: the effect of estrogen. Am J Physiol Heart Circ Physiol. (2003) 285:H687–92. doi: 10.1152/ajpheart.01000.2002
47. Knowlton AA, Korzick DH. Estrogen and the female heart. Mol Cell Endocrinol. (2014) 389:31–9. doi: 10.1016/j.mce.2014.01.002
48. Sanbe A, Daicho T, Mizutani R, Endo T, Miyauchi N, Yamauchi J, et al. Protective effect of geranylgeranylacetone via enhancement of HSPB8 induction in desmin-related cardiomyopathy. PLoS ONE. (2009) 4:e5351. doi: 10.1371/journal.pone.0005351
49. Robison P, Caporizzo MA, Ahmadzadeh H, Bogush AI, Chen CY, Margulies KB, et al. Detyrosinated microtubules buckle and bear load in contracting cardiomyocytes. Science. (2016) 352:aaf0659. doi: 10.1126/science.aaf0659
50. Chen CY, Caporizzo MA, Bedi K, Vite A, Bogush AI, Robison P, et al. Suppression of detyrosinated microtubules improves cardiomyocyte function in human heart failure. Nat Med. (2018) 24:1225–33. doi: 10.1038/s41591-018-0046-2
51. Caporizzo MA, Chen CY, Bedi K, Margulies KB, Prosser BL. Microtubules increase diastolic stiffness in failing human cardiomyocytes and myocardium. Circulation. (2020) 141:902–15. doi: 10.1161/CIRCULATIONAHA.119.043930
52. Helms AS, Tang VT, O'Leary TS, Friedline S, Wauchope M, Arora A, et al. Effects of MYBPC3 loss-of-function mutations preceding hypertrophic cardiomyopathy. JCI Insight. (2020) 5:e133782. doi: 10.1172/jci.insight.133782
53. Coats CJ, Heywood WE, Virasami A, Ashrafi N, Syrris P, Dos Remedios C, et al. Proteomic analysis of the myocardium in hypertrophic obstructive cardiomyopathy. Circ Genom Precis Med. (2018) 11:e001974. doi: 10.1161/CIRCGENETICS.117.001974
54. Tarnopolsky MA. Myopathies related to glycogen metabolism disorders. Neurotherapeutics. (2018) 15:915–27. doi: 10.1007/s13311-018-00684-2
55. Guclu A, Knaapen P, Harms HJ, Parbhudayal RY, Michels M, Lammertsma AA, et al. Disease stage-dependent changes in cardiac contractile performance and oxygen utilization underlie reduced myocardial efficiency in human inherited hypertrophic cardiomyopathy. Circ Cardiovasc Imaging. (2017) 10:1249–54. doi: 10.1161/CIRCIMAGING.116.005604
56. Timmer SA, Germans T, Brouwer WP, Lubberink MJ, van der Velden AA. Carriers of the hypertrophic cardiomyopathy MYBPC3 mutation are characterized by reduced myocardial efficiency in the absence of hypertrophy and microvascular dysfunction. Eur J Heart Fail. (2011) 13:1283–9. doi: 10.1093/eurjhf/hfr135

THE SUPPLEMENTARY DATA IS AVAILABLE ONLINE:

https://www.frontiersin.org/articles/10.3389/fcvm.2021.612215/full#supplementary-material

METABOLOMIC SIGNATURES IN PRECLINICAL AND ADVANCED DISEASE STAGES OF HYPERTROPHIC CARDIOMYOPATHY

Maike Schuldt, Beau van Driel, Sila Algul, Rahana Y. Parbhudayal, Daniela QCM. Barge-Schaapveld, Ahmet Güçlü, Mark Jansen, Annette F. Baas, Mark A. van de Wiel, Evgeni Levin, Tjeerd Germans, Judith JM. Jans, Jolanda van der Velden

Manuscript in preparation

8

ABSTRACT

Objectives

To define if disturbed myocardial energetics are reflected in the serum metabolome in the preclinical stage of HCM with the potential to serve as biomarkers, we performed a metabolomics screen in serum of asymptomatic carriers in comparison to healthy controls and patients with obstructive HCM (HOCM).

Background

Hypertrophic cardiomyopathy (HCM) is the most common inherited heart disease but risk prediction is still poor due to incomplete penetrance and lack of clear genotype-phenotype correlations. Advanced imaging techniques have shown altered myocardial energetics already in preclinical mutation carriers.

Methods

We performed non-quantitative direct-infusion high-resolution mass spectrometry-based metabolomics on serum from fasted asymptomatic mutation carriers, symptomatic HOCM patients and healthy controls (n= 31, 14 and 9, respectively). We performed multivariate modelling with multiple gradient boosting classifiers to identify biomarker panels that discriminate the groups.

Results

For all 3 group-wise comparisons, we identified a panel of 30 serum metabolites that discriminate the groups. These metabolite panels perform equally good as advanced imaging techniques in distinguishing the groups.

Conclusions

This study reveals unique metabolic signatures in serum of preclinical Carriers and HOCM patients, which may be used for risk stratification and precision therapeutics.

INTRODUCTION

Hypertrophic cardiomyopathy (HCM) is the most common inherited heart disease with a prevalence ranging from 1:500 to 1:200 (1,2) and identification of a pathogenic gene variant in~50-60% of all patients. Genetic family screening enables to identify gene variant carriers (carriers) early in life, who are at risk to develop cardiac disease. However, risk prediction is still poor due to incomplete penetrance and lack of clear genotype-phenotype correlations (3). Based on current guidelines of the European Society of Cardiology, HCM is defined by a wall thickness ≥13 mm in first-degree family members (i.e. preclinical carriers) in one or more left ventricular (LV) myocardial segments (2). To diagnose cardiac hypertrophy and dysfunction, the American College of Cardiology Foundation/American Heart Association recommends long-term clinical evaluations (echocardiography and electrocardiography) every 12–18 months from the age of 12 to 18–21 years, and at least every 5 years at the age of >21 years, while the ESC does not recommend a specific interval.

Efforts have been made to find prognostic markers that can identify asymptomatic preclinical carriers who are at risk to develop overt HCM. The first study that identified a possible early disease marker in blood was done by Ho et al. who provided evidence for a pro-fibrotic response in carriers without hypertrophy illustrated by significantly elevated levels of the C-terminal pro-peptide of type I procollagen (4). Furthermore, elevated levels of NT-proBNP have been linked with heart failure-related death and transplantation (5). Identification of markers at preclinical disease stage may allow early treatment to prevent and/or delay disease.

Here we performed a metabolic analyses in blood samples from carriers based on studies showing altered energetic state of the heart at preclinical HCM disease stage. Phosphorus-31 magnetic resonance spectroscopy showed an abnormal cardiac energetic state, evident from a decrease in the phosphocreatine to adenosine triphosphate ratio (PCr/ATP), in carriers independent of the presence of hypertrophy (6). In accordance, analysis of *in vivo* myocardial external efficiency by combined ^{11}C-acetate positron emission tomography (PET) and cardiovascular magnetic resonance (CMR) imaging showed increased myocardial oxygen consumption (MVO_2) and decreased myocardial efficiency in preclinical carriers compared to healthy controls (7,8). At a cellular level, studies in human cardiac HCM samples showed that pathogenic gene variants increase myofilament calcium sensitivity, kinetics, and tension cost and alter myosin sequestration (9-14), which may alter cardiomyocyte energetics and underlie the increase in MVO_2. In patients with obstructive HCM (HOCM), a decrease in MVO_2 is observed compared to controls and carriers (15), which may be explained by secondary changes in metabolism and mitochondrial function in the hypertrophied myocardium. Indeed, proteomic analyses recently revealed lower levels of metabolic pathway proteins in myectomy samples from HOCM patients

(16,17). Overall, these studies show that metabolic changes (i.e. energetic state of the heart) are central in the early (preclinical) and advanced disease stages of HCM, and may be used as biomarker for disease stage-dependent diagnosis and the design of treatment strategies.

While advanced *in vivo* tools to monitor energy status and metabolism of the heart are available, such imaging modalities are expensive and limited to specialized medical centers. There is an urgent need to find easily accessible serum biomarkers for better risk prediction that can be tested in standard diagnostic laboratories. To define if changes in the metabolic serum profile are already evident at a preclinical stage of HCM, we performed a metabolomics screen in serum of asymptomatic carriers in comparison to healthy controls. To establish if the metabolic serum profile is altered at the advanced disease stage, a comparison was made between carriers and individuals with HOCM.

METHODS

Study population

The study protocol was in agreement with the principles outlined in the Declaration of Helsinki. Inclusion of individuals was part of the Engine study (18), and approval for this study was given by the local Medical Ethics Review Committees. Written informed consent was obtained from each individual prior to inclusion in this study. The study population consisted of 31 asymptomatic carriers without hypertrophy (carrier). Maximal wall thickness for the carrier group was based on the ESC criterion of LV thickness of ≥13 mm in first-degree family members. In addition, 14 patients with symptomatic HOCM. Criteria of exclusion were: aortic regurgitation more than grade 1, presence of coronary artery disease (coronary artery stenosis >30%), previous septal reduction therapy, poor LV function (ejection fraction <50%), a history of diabetes mellitus or hypertension (defined as a systemic blood pressure ≥140/90 mm Hg), and significant renal dysfunction defined as an estimated glomerular filtration rate <30 mL/min per 1.73·m2 (15). Table S1 provides an overview of the specific mutations of both preclinical carriers and HOCM patients. Nine healthy related and mutation-negative participants served as control group (Ctrl). PET-CMR data for these groups have been published previously (7,18). Clinical parameters of the different groups are shown in Table 1.

Blood serum preparation

Patients fasted overnight prior to collection of blood samples. The samples were collected by venous puncture and allowed to clot for 1 hour at 37°C. Following this incubation period, clotted samples were left to contract for at least 30 minutes at 4°C. The serum was centrifuged (4000 rpm, 20 minutes, 4°C) and separated. Sodium azide (0.01%) was added to the supernatant. All samples were stored at -20°C until use.

TABLE 1. Demographic and clinical characteristics of the study population[1].

	Carriers (n=31)	HOCM patients (n=14)	Ctrl (n=9)
Age (years)	38 ± 14*	50 ± 13#	51 ± 8
Male sex (no. (%))$	7 (22.6)	10 (71.4)	6 (66.7)
LVM (g)	70.3 ± 16.8	193.7 ± 68.7*,#	102.5 ± 17.8
LVM_i	38.6 ± 7.3	95.4 ± 33.0*,#	49.5 ± 6.1
LVEF (%)	67 ± 5	71 ± 10*	61 ± 6
Systolic BP (mmHg)	111 ± 14	118 ± 17	124 ± 13
Diastolic (mmHg)	66 ± 9	69 ± 13	69 ± 4
MAP (mmHg)	81 ± 10	85 ± 14	88 ± 5
HR (bpm)	61 ± 8	60 ± 4	66 ± 9
NT-proBNP (pg/l)	77 ± 55	1533 ± 2976#	54 ± 55

[1]Values are given as mean ± SD. Abbreviations: HOCM, hypertrophic obstructive cardiomyopathy; Ctrl, control; LVM, left ventricular mass; LVM_i, LVM indexed for body surface area; LVEF, left ventricular ejection fraction; BP; blood pressure; MAP, mean arterial pressure; HR, heart rate. *p<0.05 compared to Ctrl; #p<0.05 compared to Carrier, one-way ANOVA with Tukey's multiple comparisons test. $p<0.05 Chi-square test.

Metabolomics profiling

Analysis of the metabolites was conducted as previously described (19). Briefly, a non-quantitative direct-infusion high-resolution mass spectrometry (DI-HRMS) based metabolomics method was applied in combination with a nano-electrospray ionization source. The mean peak intensities of the technical triplicates were calculated and annotated by matching the m/z of these mass peaks with a range of two parts per million to metabolite masses that are found in the Human Metabolome Database (20). Accordingly, mass peaks were identified.

Data analysis and modelling

We identified panels of metabolic biomarkers in order to discriminate between the following groups of subjects: Carrier vs Ctrl, Carrier vs HOCM and HOCM vs Ctrl. In brief, we used a combination of multiple gradient boosting classifiers (21,22) to improve prediction accuracy. To avoid over-fitting, we used a 5-fold stratified cross-validation over the training partition of the data (80%), while the remaining data (20%) was used as the test dataset. We conducted a rigorous stability selection procedure (22) to ensure the reliability and robustness of the biomarker signatures. This was repeated 10 times and Receiver-Operating-Characteristics Area-Under-Curve (ROC AUC) scores were computed each time and averaged for the final test ROC AUC. A permutation (randomization test) (23) was used to evaluate statistical validity of the results. In the permutation test, the outcome variable (e.g. Carrier vs HOCM) was randomly reshuffled 1000 times while the corresponding -omics profiles were kept intact. We used Python v. 3.8 (www.python.org), with packages Numpy, Scipy and Scikits-learn for implementing the model and R version 3.5.3 for visualizations.

Prediction model

The prediction model combining MEE and MVO2.beat is a standard logistic regression model as fit with R's glm() function. As this is a low-dimensional model, predictions were simply obtained from the model fit. These probabilistic predictions define the possible cut-offs for a positive test. Sensitivity and specificity are determined for these cut-offs, and then visualized by the receiver operating characteristic (ROC) curve. Area-under-the-ROC-curve (AUC) is determined as well. ROC and AUC were computed using R's pROC package.

Correlation analysis

Pearson correlation with Benjamini-Hochberg correction was performed to check if top 30 metabolites correlate with clinical parameters.

Analysis of metabolite-protein links

For identification of functional links between metabolites and significantly different expressed proteins in HCM, the directly interacting enzymes of the top 30 metabolites of each pairwise comparison were identified using MetaBridge v1.2 based on the KEGG database. Consequently, proteins were overlapped with significantly different proteins in HCM compared to control, derived from a proteomics study of our group (17). Additionally, we identified metabolite-protein links by manual literature search.

Statistics

Graphpad Prism v8 software was used for statistical analysis of clinical data. Data were statistically analyzed using one-way ANOVA with Tukey's multiple comparisons *post hoc* test or Chi-square test if appropriate. All values are shown as mean ± standard error of the mean. A p-value ≤0.05 was considered as significantly different.

RESULTS

Characteristics of study population

Metabolomic serum profiling was performed in 31 Carriers, 14 HOCM patients and 9 Ctrl. Gene variants in the Carriers were present in *MYH7*, *MYBPC3* and troponins (Figure 1A; Table S1), whereas HOCM patients displayed a mixed genetic background and 28.6% of patients were sarcomere mutation negative (Figure 1B). Figure 1A-B shows an overview of the affected genes in our study groups. Figure S1 highlights the location of all gene variants in this study. Patient characteristics are summarized in Table 1. The Carrier group was on average approximately 10 years younger than the HOCM and Ctrl group and is dominated by females, whereas HOCM and Ctrls have more males. The HOCM group showed significantly higher LV mass, a slightly increased LV ejection fraction and highly elevated NT-proBNP levels compared to Carriers and Ctrls, which is characteristic for the obstructive nature of the disease.

Changes in energetic status of the heart of included individuals, measured by PET-CMR imaging (8,15), are illustrated in Figure 1. Compared to Ctrls, Carriers showed increased MVO_2 and both Carriers and HOCM showed reduced myocardial external efficiency (MEE) (Figure 1C-D).

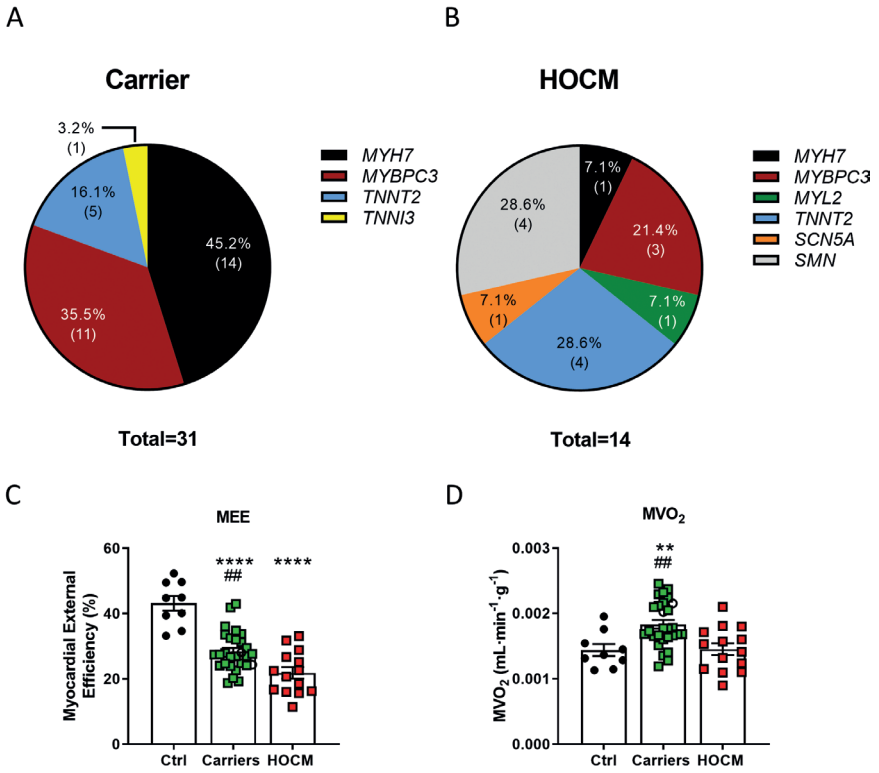

FIGURE 1. Distribution of affected genes in the (A) Carrier and (B) HOCM group. (C) Myocardial external efficiency (MEE) and (D) myocardial oxygen consumption normalized to tissue weight (MVO_2) in Ctrls, Carriers and HOCM patients (data have been published in Guclu et al. and Parbhudayal et al. (8,15). ****p<0.0001, **p<0.01 compared to Ctrls, ##p<0.01 compared to HOCM, one-way ANOVA with Tukey's multiple comparisons test.

Multivariate modeling reveals altered metabolic profile in preclinical stage of HCM

Multivariate modelling was performed for the Carrier vs Ctrl group, the Carrier vs HOCM group and the HOCM vs Ctrl group to determine if the serum metabolome profiles could distinguish the groups. Principal component analysis (PCA) (Figure S2A) and partial least squares-discriminant analysis (PLS-DA) (Figure 2A) indeed showed distinct patterns in all group comparisons. Notably, the Carrier group clusters more tightly than the control and HOCM group, indicating less variability within the Carrier group compared to HOCM and Ctrl. The 30 most predictive metabolites for all three

group comparisons are presented with their relative importance in Figure 2B, and their corresponding –log10(p) values are presented in Figure S2C. Some metabolites cannot be uniquely identified because they share the same mass with other metabolites. The possible identifications of these metabolites are listed in Table S2. The radar plots in Figure 2C show the 15 most important metabolites that differentiate the two respective groups, and illustrate the differential serum metabolite profile in the different group comparisons. With this analysis we established metabolic signatures that define the three groups.

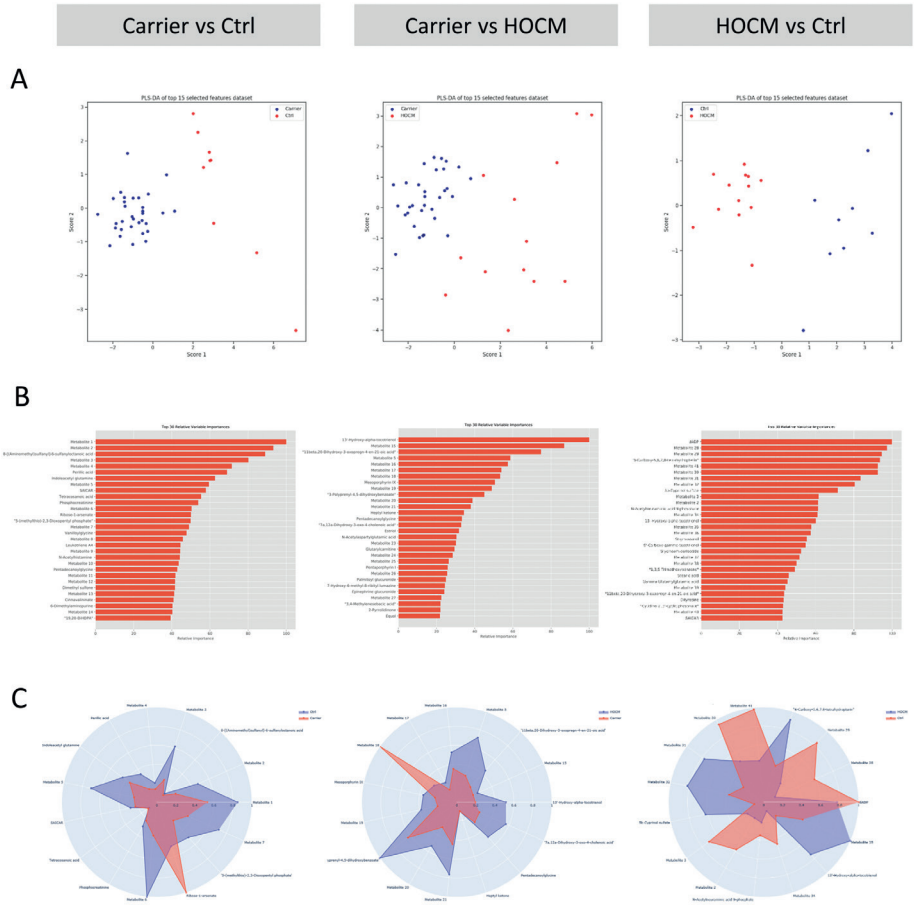

FIGURE 2. Multivariate modelling. (A) Partial least square-discriminant analysis plots for the three group-wise comparisons Carrier vs Ctrls, Carrier vs HOCM and HOCM vs Ctrls. (B) Top 30 most predictive metabolites sorted based on their relative importance in distinguishing the two groups. (C) Radar plots of the top 15 most predictive metabolites, illustrating the differences in the serum metabolite profile between the groups.

Distinct metabolic signatures at preclinical and symptomatic stage of HCM

We listed and grouped the 30 most predictive metabolites of each comparison into different subgroups based on their chemical taxonomy super class (Table 2). The bar graphs with the individual data points are provided in Figure S3A-C for Carrier vs Ctrl, in Figure S4A-C for Carrier vs HOCM and in Figure S5A-C for HOCM vs Ctrl (data from the third group is included in all comparisons). The number of metabolites per subgroup are shown in Table 2, and illustrate that the majority of changes are in the "lipids and lipid-like molecules" and "organic acids and derivatives".

TABLE 2. Top 30 most important metabolites of the three pairwise comparisons categorized based on their chemical taxonomy super class[2].

Carrier vs Ctrl	Carrier vs HOCM	HOCM vs Ctrl
	Benzenoids	
2	**1**	**2**
Metabolite 2		**Metabolite 2**
Vanilloylglycine	3-Polyprenyl-4,5-dihydroxybenzoate	1,3,5-Trimethoxybenzene
	Lipids and lipid-like molecules	
10	**14**	**13**
	11beta,20-Dihydroxy-3-oxopregn-4-en-21-oic acid	**11beta,20-Dihydroxy-3-oxopregn-4-en-21-oic acid**
	13′-Hydroxy-alpha-tocotrienol	**13′-Hydroxy-alpha-tocotrienol**
Metabolite 3		**Metabolite 3**
Metabolite 5	**Metabolite 5**	
8-[(Aminomethyl)sulfanyl]-6-sulfanyloctanoic acid	3,4-Methylenesebacic acid	5b-Cyprinol sulfate
19,20-DIHDPA	7a,12a-Dihydroxy-3-oxo-4-cholenic acid	9′-Carboxy-gamma-tocotrienol
Metabolite 1	Glutarylcarnitine	Metabolite 28
Metabolite 6	Metabolite 15	Metabolite 30
Metabolite 7	Metabolite 16	Metabolite 34
Metabolite 14	Metabolite 18	Metabolite 39
Perillic acid	Metabolite 22	Metabolite 40
Tetracosanoic acid	Metabolite 25	Metabolite 41
	Metabolite 26	Stearic acid
	Metabolite 27	Stigmastanol
	Palmitoyl glucuronide	
	Nucleosides, nucleotides and analogues	
1	**0**	**3**
SAICAR		**SAICAR**
		dADP
		Glycineamideribotide

TABLE 2. Continued.

Carrier vs Ctrl	Carrier vs HOCM	HOCM vs Ctrl
	Organic acids and derivatives	
10	**7**	**8**
Pentadecanoylglycine	**Pentadecanoylglycine**	
5-(methylthio)-2,3-Dioxopentyl phosphate	Metabolite 17	Cytidine 2′,3′-cyclic phosphate
Indoleacetyl glutamine	Metabolite 19	Dityrosine
Metabolite 4	Metabolite 20	Gamma Glutamylglutamic acid
Metabolite 9	Metabolite 21	Metabolite 29
Metabolite 11	Metabolite 24	Metabolite 31
Metabolite 12	N-Acetylaspartylglutamic acid	Metabolite 32
Metabolite 13		Metabolite 36
N-Acetylhistamine		Metabolite 38
Phosphocreatinine		
	Organic oxygen compounds	
3	**2**	**2**
Metabolite 8	Epinephrine glucoronide	Metabolite 33
Metabolite 10	Heptyl ketone	Metabolite 35
Ribose-1-arsenate		
	Organoheterocyclic compounds	
2	**5**	**2**
6-Dimethylaminopurine	2-Pyrrolidinone	6-Carboxy-5,6,7,8-tetrahydropterin
Cinnavalininate	7-Hydroxy-6-methyl-8-ribityl lumazine	Metabolite 37
	Mesoporphyrin IX	
	Metabolite 23	
	Pentaporphyrin I	
	Organosulfur compounds	
1	**0**	**0**
Dimethyl sulfone		
	Phenylpropanoids and polyketides	
0	**1**	**0**
	Equol	

[2]The numbers indicate the number of metabolites in the different metabolite categories. Metabolites that are significant in 2 pairwise comparisons are highlighted in bold.

Most metabolites that belong to the category "organic acids and derivatives" in all three comparisons are dipeptides. The dipeptides differ between the different comparisons but represent a common finding. Lipids and lipid-like molecules are also among the top 30 metabolites of all three comparisons. Among these metabolites are fatty acids and conjugates, indicating changes in the fatty acid metabolism, but also eicosanoids that represent metabolites involved in the inflammatory response. The number of metabolites belonging to the category "lipids and lipid-like molecules" is largest in the comparisons with the HOCM group, suggesting that changes in lipid metabolism are predominant in the advanced disease stage.

Notably, 7 of the 30 most important metabolites are predictive in two different comparisons (Figure 3). Pentadecanoylglycine and Metabolite 5 are amongst the 30 most important metabolites in the Carrier vs Ctrl comparison and the Carrier vs HOCM comparison. This indicates that a decrease in these two metabolites may be an early change defining the Carrier group (Figure 3A). Levels of 11beta,20-Dihydroxy-3-oxopregn-4-en-21-oic acid and 13'-Hydroxy-alpha-tocotrienol are higher in the HOCM group and may therefore define an advanced disease stage (Figure 3B). Among the 30 most important metabolites in the Carrier vs Ctrl and the HOCM vs Ctrl comparison are SAICAR, Metabolite 2 and Metabolite 3. These metabolites show lower levels in both the Carrier and the HOCM group compared to Control and may characterize myocardial disease from early to late stages (Figure 3C).

Taken together, the 7 metabolites that are predictive in two different comparisons may play an important role in defining the disease stage.

Metabolic signature versus in vivo energetic status of the heart

To define if the top metabolites reflect energetic changes in the heart, a correlation was made between metabolites and MEE and MVO_2. Correlation analyses showed that 15 metabolites of all three sets of top 30 metabolites significantly correlated with MEE, and 20 metabolites correlated with MVO_2, but this correlation was not significant after correcting for multiple testing (p values are included in Table S2). This indicates that one single metabolite alone is not powerful enough as a predictive biomarker. To evaluate if the complete metabolic signature could be used to identify preclinical Carriers that show already an altered energetic status of the heart, we compared the performance of the imaging parameters MEE and MVO_2 with the metabolite signature in sensitivity and specificity curves (Figure 4). In all three group-wise comparisons the metabolite profile as well as the imaging parameters perform equally well in distinguishing the groups. As this analysis is driven by the 30 most important metabolites from our multivariate analysis, a biomarker panel derived from a selection of the 30 metabolites could potentially represent a suitable tool for clinical practice and has to be validated in an independent cohort.

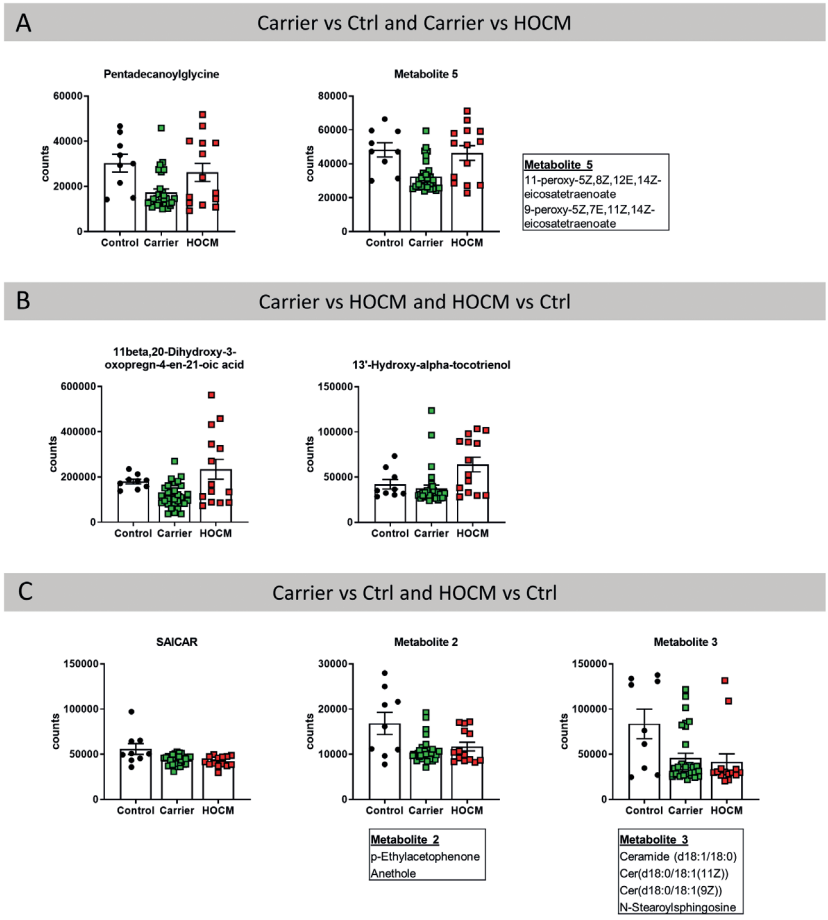

FIGURE 3. Metabolites that are among the 30 most important metabolites in distinguishing the groups in the (A) Carrier vs Ctrl and Carrier vs HOCM comparison, (B) Carrier vs HOCM and HOCM vs Ctrl comparison and (C) Carrier vs Ctrl and HOCM vs Ctrl comparison.

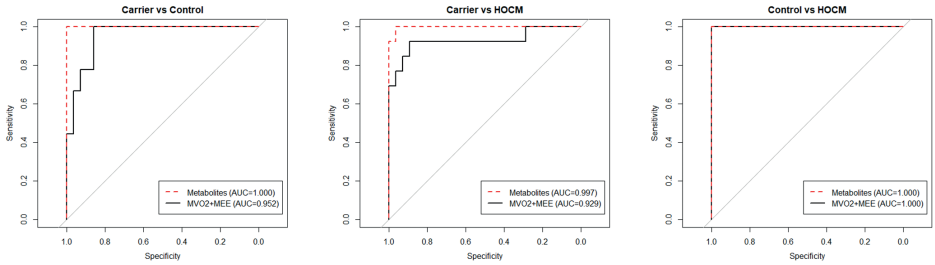

FIGURE 4. Sensitivity and specificity curves comparing the performance of the metabolomics data and the clinical imaging data in distinguishing the groups.

DISCUSSION

In this study we investigated the ability of serum metabolites to discriminate preclinical carriers from healthy controls and HOCM patients. For each comparison we obtained a set of 30 metabolites that are together most predictive in distinguishing these groups. Based on the number of metabolites per category in each comparison (Table 2) we can hypothesize that changes in organic compounds are an early event in HCM pathogenesis and already present in asymptomatic carriers, while changes in lipid metabolism are pronounced at the advanced disease stage. Our study reveals unique metabolic signatures in serum of preclinical Carriers and HOCM patients, which may have potential for risk stratification and precision therapeutics.

Altered inflammatory signature at preclinical disease stage

Several inflammatory metabolites show a different expression pattern in the serum of preclinical carriers compared to controls or HOCM. Metabolite 2 (p-Ethylacetophenone; Anethole), which has lower levels in the carriers and HOCM, has anti-inflammatory properties that are mediated by either inhibition of production and/or release of inflammatory mediators like tumor necrosis factor (TNF), nitric oxide, prostaglandins, interleukin-1, and interleukin-17 (24,25). The anti-inflammatory effects of Mesoporphyrin, which is lower in carriers compared to HOCM, are suggested to be mediated by inhibition of cytokine production like interferon-gamma and interleukin 6 (26). Leukotrienes and prostaglandins, that can be summarized as eicosanoids, are more difficult to interpret since they can have pro-inflammatory as well as anti-inflammatory functions, which are dependent on the particular immunological context (27,28). Metabolite 6 has Leukotriene A4 as a possible metabolite identification and shows reduced levels in carriers vs controls and intermediate levels in HOCM. Overall, the preclinical carriers show an altered inflammatory blood signature.

Altered metabolic blood profile reflects changes in the HOCM heart

The metabolic signatures in serum from Carriers and HOCM may reflect disease mechanisms in the heart, the signature in Carriers may especially reflect early disease changes. To validate the biological relevance of the identified metabolites in the context of HCM, we looked for common pathways and direct links of the top 30 metabolites and significantly changed proteins of our recent proteomics study in myectomy tissue of HCM patients (17). Indeed, several top metabolites could be linked to altered changes in the heart of HOCM patients. Our recent proteomics analysis of 50 HOCM samples showed significantly lower levels of Leukotriene A4 hydrolase, the enzyme that converts Leukotriene A4 to Leukotriene B4 (17). The catalytic reaction inactivates the enzyme which is notable by a change in molecular weight. Therefore, reduced levels of Leukotriene A4 and the Leukotriene A4 hydrolase could indicate increased conversion to Leukotriene B4 which is implicated in inflammatory conditions (29). Asymmetric dimethylarginine is directly linked to the enzyme dimethylarginine

dimethylaminohydrolase 1. This enzyme is increased in myocardial tissue of HCM patients and plays a role in nitric oxide generation, which is a key molecule in the process of inflammation (30).

Next to the inflammatory response, we also identified links between the serum metabolites and tissue proteins in the lipid and fatty acid metabolism. Tetracosanoic acid, a very long chain fatty acid, has lower serum levels in carriers and HOCM compared to controls. In tissue of HOCM patients we found reduced expression of Long-chain-fatty-acid-CoA ligase 1 (17) which catalyzes a step in the fatty acid beta-oxidation. Increased tissue protein levels of the long chain fatty acid transport protein 6 (17), that translocates long-chain fatty acids across the plasma membrane (31), are in line with elevated serum levels of stearic acid in HOCM compared to Ctrls. Reduced Monoacylglycerol (Metabolite 18 and 34) serum levels in HOCM compared to Ctrls with intermediate levels in Carriers are in line with lower protein levels of monoglyceride lipase in heart tissue of HOCM patients (17), which is the enzyme that can hydrolyze the reaction to fatty acids and glycerol. The metabolite Glycerylphosphorylethanolamine is directly linked to Lysophospholipase 1, which hydrolyzes fatty acids, and is decreased in the tissue of HCM patients. The top 30 metabolites Indoleacetic acid and 5-Hydroxyindoleacetaldehyde from the HOCM vs Ctrl comparison have the aldehyde dehydrogenases ALDH9A1, ALDH3A2 and ALDH7A1 as directly interacting enzymes, of which ALDH3A2 is increased in HCM tissue, whereas ALDH9A1 and ALDH7A1 have lower levels in HCM. Since ALDH3A2 catalyzes the oxidation of medium and long chain aliphatic aldehydes to fatty acids, also this finding points towards an altered fatty acid metabolism.

As we can identify direct links of serum metabolites with protein changes in the heart, mainly regarding fatty acid metabolism, the top serum metabolites may reflect pathologic changes in the heart underlining their biological relevance.

Disease stage-dependent changes in metabolic signatures

A shift from fatty acids to glucose as substrate for mitochondrial oxidation is reported in acquired forms of cardiac hypertrophy and disease (32,33). Accordingly, changes in serum levels of fatty acids may derive from substrate changes in the heart. One of the fatty acids elevated in the HOCM group compared to the carrier is glutarylcarnitine. It belongs to the class of acylcarnitines that play a key role in transporting fatty acids across the mitochondrial membrane for subsequent fatty acid beta-oxidation (34). Lower acylcarnitine levels have been observed in the serum of asymptomatic or mildly symptomatic idiopathic HCM patients compared to controls in a study by Nakamura (35). Since our HOCM patients are already in an advanced disease stage, levels of acylcarnitines could differ dependent on the disease stage, with lower levels in asymptomatic patients and higher levels in symptomatic patients. Differences in levels of carnitines in the blood can also point towards fatty acid oxidation disorders.

Carnitine palmitoyltransferase II deficiency, one of the most common inherited disorders of mitochondrial fatty acid oxidation, is diagnosed by calculating the $(C_{16:0}+C_{18:1})/C_2$ ratio in the blood (36,37). Since we found an elevated carnitine in the HOCM group, we calculated the $(C_{16:0}+C_{18:1})/C_2$ ratio for our samples but did not find differences between groups (data not shown), excluding that one of the patients suffered from carnitine palmitoyltransferase II deficiency.

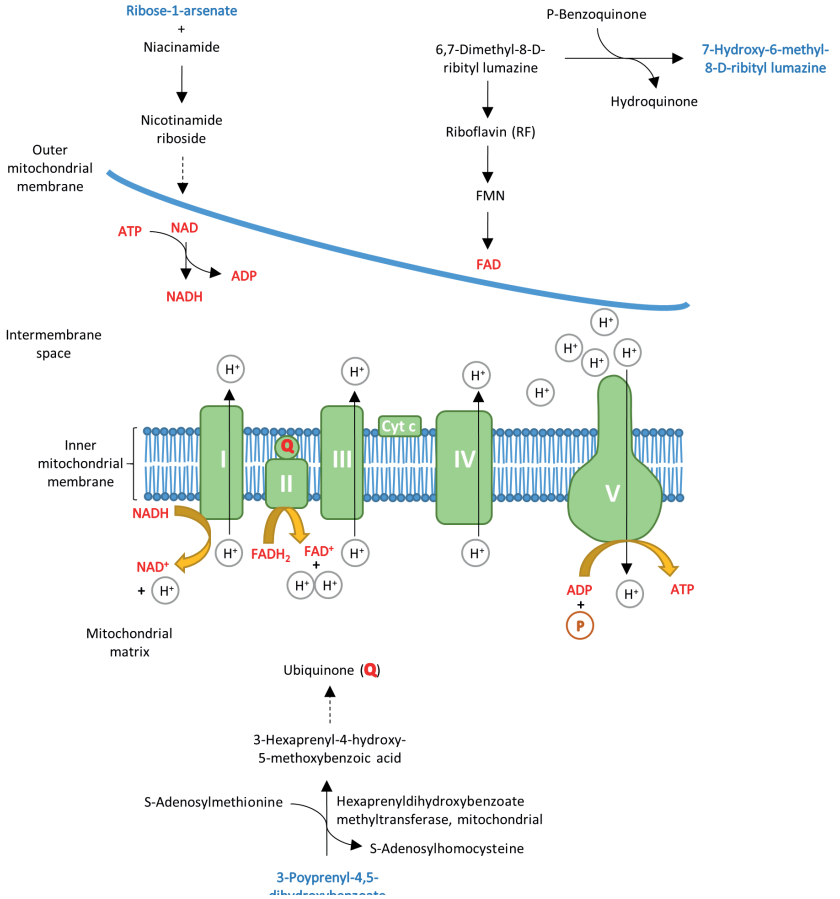

FIGURE 5. Schematic overview of the mitochondrial electron transport chain. Some of the top 30 metabolites (highlighted in blue) can be linked to energy metabolism, as they are involved in pathways that lead to essential molecules of the electron transport chain, which are highlighted in red.

Previous studies have shown different stages of energy deficiency in the myocardium of preclinical carriers and HOCM patients (15). Interestingly, when comparing the serum of the carrier and HOCM group, we also find alterations of metabolites that can be linked to energy metabolism (highlighted in Figure 5). 7-Hydroxy-6-methyl-8-ribityl

lumazine is an intermediate in the riboflavin metabolism which is important for building the enzyme cofactors flavin-adenine dinucleotide (FAD) and flavin mononucleotide (FMN) (38,39). 3-Polyprenyl-4,5-dihydroxybenzoate, also elevated in the HOCM group, is a substrate for the mitochondrial enzyme hexaprenyldihydroxybenzoate methyltransferase which is involved in the ubiquinone biosynthesis pathway and important for the electron transport chain (40). Carriers have elevated levels of the carbohydrate Ribose-1-arsenate compared to controls. Ribose-1-arsenate is an intermediate in the arsenate detoxification pathway, and is formed by the enzyme purine nucleoside phosphorylase (41). We also found other components of the purine metabolism being altered. Purine is not only a building block for the nucleotide bases adenosine and guanosine, but also a component of the molecules ATP, GTP, cyclic AMP, NADH and coenzyme A that are involved in cellular energy transmission. Although the metabolites are not directly involved in the electron transport chain, they are intermediates of pathways that lead to essential components of the electron transport chain (Figure 5).

Altered protein homeostasis in HCM

We found peptide alterations in both the carriers and the HOCM patients. Most of these peptides are dipeptides that are supposedly incomplete breakdown products of proteins. We can speculate that these changes are associated with the presence of mutant protein in carriers and HOCM patients causing increased protein degradation and protein synthesis to renew proteins. This would match findings of activated protein quality control in tissue of HOCM patients (42,43). The dipeptide Metabolite 11 (Alanyl-Leucine), which belongs to the branched chain amino acids, is significantly elevated in carriers and HOCM compared to controls. This is in line with previous findings of increased levels of branched chain amino acids in a Finnish HCM cohort (44). Interestingly, the first step of branched chain amino acid catabolism occurs not in the liver, but in the heart (45). Hence, this may point to derailed branched chain amino acid catabolism in the heart at preclinical disease stage.

STUDY LIMITATIONS AND CLINICAL IMPLICATIONS

As shown in Figure 4, the serum metabolites perform as good as the advanced imaging modalities MEE and MVO_2 in identifying preclinical Carriers and HOCM patients in our study cohort. Therefore, serum metabolites have the potential to serve as diagnostic biomarkers. As serum can be sampled repeatedly and minimal invasively from individuals, a metabolite panel could be used to detect energetic changes in the heart to monitor carriers and to determine the right time for therapeutic intervention. This study shows that there are serum biomarker candidates which can as a combined set distinguish healthy controls, preclinical carriers with an altered energetic status of the heart and obstructive HCM patients. The findings in this study are derived from

relatively small groups and provide a starting point for the ultimate goal to define a set of blood biomarkers that is predictive for identifying asymptomatic gene variant carriers that will transition into a symptomatic state and are in need of preventive treatment. The top 30 metabolites that are driving our multivariate model will need to be validated in follow-up studies with independent data sets with the ultimate goal to define a clinically feasible biomarker panel of 4-6 prognostic markers.

ACKNOWLEDGEMENTS

We thank Vasco Sequeira for the design of Figure S1.

FUNDING SOURCES

We acknowledge the support from the Netherlands Cardiovascular Research Initiative: An initiative with support of the Dutch Heart Foundation, CVON2014-40 DOSIS and NWO (NWO-ZonMW; 91818602 VICI grant to Jolanda van der Velden).

REFERENCES

1. Semsarian C, Ingles J, Maron MS, Maron BJ. New Perspectives on the Prevalence of Hypertrophic Cardiomyopathy. Journal of the American College of Cardiology 2015;65:1249-1254.
2. Authors/Task Force, Elliott PM, Anastasakis A et al. 2014 ESC Guidelines on diagnosis and management of hypertrophic cardiomyopathy: the Task Force for the Diagnosis and Management of Hypertrophic Cardiomyopathy of the European Society of Cardiology (ESC). Eur Heart J 2014;35:2733-79.
3. Ho CY, Charron P, Richard P, Girolami F, Van Spaendonck-Zwarts KY, Pinto Y. Genetic advances in sarcomeric cardiomyopathies: state of the art. Cardiovasc Res 2015;105:397-408.
4. Ho CY, Lopez B, Coelho-Filho OR et al. Myocardial fibrosis as an early manifestation of hypertrophic cardiomyopathy. N Engl J Med 2010;363:552-63.
5. Coats CJ, Gallagher MJ, Foley M et al. Relation between serum N-terminal pro-brain natriuretic peptide and prognosis in patients with hypertrophic cardiomyopathy. Eur Heart J 2013;34:2529-37.
6. Crilley JG, Boehm EA, Blair E et al. Hypertrophic cardiomyopathy due to sarcomeric gene mutations is characterized by impaired energy metabolism irrespective of the degree of hypertrophy. J Am Coll Cardiol 2003;41:1776-82.
7. Witjas-Paalberends ER, Guclu A, Germans T et al. Gene-specific increase in the energetic cost of contraction in hypertrophic cardiomyopathy caused by thick filament mutations. Cardiovasc Res 2014;103:248-57.
8. Parbhudayal RY, Harms HJ, Michels M, van Rossum AC, Germans T, van der Velden J. Increased Myocardial Oxygen Consumption Precedes Contractile Dysfunction in Hypertrophic Cardiomyopathy Caused by Pathogenic TNNT2 Gene Variants. J Am Heart Assoc 2020;9:e015316.
9. Sequeira V, Wijnker PJ, Nijenkamp LL et al. Perturbed length-dependent activation in human hypertrophic cardiomyopathy with missense sarcomeric gene mutations. Circ Res 2013;112:1491-505.
10. Witjas-Paalberends ER, Piroddi N, Stam K et al. Mutations in MYH7 reduce the force generating capacity of sarcomeres in human familial hypertrophic cardiomyopathy. Cardiovasc Res 2013;99:432-41.
11. Witjas-Paalberends ER, Ferrara C, Scellini B et al. Faster cross-bridge detachment and increased tension cost in human hypertrophic cardiomyopathy with the R403Q MYH7 mutation. J Physiol 2014;592:3257-72.
12. Piroddi N, Witjas-Paalberends ER, Ferrara C et al. The homozygous K280N troponin T mutation alters cross-bridge kinetics and energetics in human HCM. J Gen Physiol 2019;151:18-29.
13. McNamara JW, Li A, Lal S et al. MYBPC3 mutations are associated with a reduced super-relaxed state in patients with hypertrophic cardiomyopathy. PLoS One 2017;12:e0180064.
14. Toepfer CN, Garfinkel AC, Venturini G et al. Myosin Sequestration Regulates Sarcomere Function, Cardiomyocyte Energetics, and Metabolism, Informing the Pathogenesis of Hypertrophic Cardiomyopathy. Circulation 2020;141:828-842.
15. Guclu A, Knaapen P, Harms HJ et al. Disease Stage-Dependent Changes in Cardiac Contractile Performance and Oxygen Utilization Underlie Reduced Myocardial Efficiency in Human Inherited Hypertrophic Cardiomyopathy. Circulation Cardiovascular imaging 2017;10.

16. Coats CJ, Heywood WE, Virasami A et al. Proteomic Analysis of the Myocardium in Hypertrophic Obstructive Cardiomyopathy. Circ Genom Precis Med 2018;11:e001974.
17. Schuldt M, Pei J, Harakalova M et al. Proteomic and Functional Studies Reveal Detyrosinated Tubulin as Treatment Target in Sarcomere Mutation-Induced Hypertrophic Cardiomyopathy. Circ Heart Fail 2021:CIRCHEARTFAILURE120007022.
18. Guclu A, Germans T, Witjas-Paalberends ER et al. ENerGetIcs in hypertrophic cardiomyopathy: traNslation between MRI, PET and cardiac myofilament function (ENGINE study). Neth Heart J 2013;21:567-71.
19. Haijes HA, Willemsen M, Van der Ham M et al. Direct Infusion Based Metabolomics Identifies Metabolic Disease in Patients' Dried Blood Spots and Plasma. Metabolites 2019;9:12.
20. Wishart DS, Feunang YD, Marcu A et al. HMDB 4.0: the human metabolome database for 2018. Nucleic Acids Res 2018;46:D608-d617.
21. Caruana R, Niculescu-Mizil A, Crew G, Ksikes A. Ensemble selection from libraries of models. Proceedings of the twenty-first international conference on Machine learning. Banff, Alberta, Canada: ACM, 2004:18.
22. Chen T, Guestrin C. XGBoost: A Scalable Tree Boosting System. Proceedings of the 22nd ACM SIGKDD International Conference on Knowledge Discovery and Data Mining. San Francisco, California, USA: ACM, 2016:785-794.
23. Meinshausen N, Bühlmann P. Stability selection. Journal of the Royal Statistical Society: Series B (Statistical Methodology) 2010;72:417-473.
24. Domiciano TP, Dalalio MM, Silva EL et al. Inhibitory effect of anethole in nonimmune acute inflammation. Naunyn Schmiedebergs Arch Pharmacol 2013;386:331-8.
25. Chainy GB, Manna SK, Chaturvedi MM, Aggarwal BB. Anethole blocks both early and late cellular responses transduced by tumor necrosis factor: effect on NF-kappaB, AP-1, JNK, MAPKK and apoptosis. Oncogene 2000;19:2943-50.
26. Takaoka Y, Matsuura S, Boda K, Nagai H. The effect of mesoporphyrin on the production of cytokines by inflammatory cells in vitro. Jpn J Pharmacol 1999;80:33-40.
27. Ricciotti E, FitzGerald GA. Prostaglandins and inflammation. Arterioscler Thromb Vasc Biol 2011;31:986-1000.
28. Esser-von Bieren J. Immune-regulation and -functions of eicosanoid lipid mediators. Biol Chem 2017;398:1177-1191.
29. Haeggstrom JZ, Kull F, Rudberg PC, Tholander F, Thunnissen MM. Leukotriene A4 hydrolase. Prostaglandins Other Lipid Mediat 2002;68-69:495-510.
30. Coleman JW. Nitric oxide in immunity and inflammation. Int Immunopharmacol 2001;1:1397-406.
31. Schwenk RW, Holloway GP, Luiken JJ, Bonen A, Glatz JF. Fatty acid transport across the cell membrane: regulation by fatty acid transporters. Prostaglandins Leukot Essent Fatty Acids 2010;82:149-54.
32. Neubauer S. The failing heart--an engine out of fuel. N Engl J Med 2007;356:1140-51.
33. Ingwall JS. Energy metabolism in heart failure and remodelling. Cardiovasc Res 2009;81:412-9.
34. Stephens FB, Constantin-Teodosiu D, Greenhaff PL. New insights concerning the role of carnitine in the regulation of fuel metabolism in skeletal muscle. J Physiol 2007;581:431-44.
35. Nakamura T, Sugihara H, Kinoshita N et al. Serum carnitine concentrations in patients with idiopathic hypertrophic cardiomyopathy: relationship with impaired myocardial fatty acid metabolism. Clin Sci (Lond) 1999;97:493-501.
36. Gempel K, Kiechl S, Hofmann S et al. Screening for carnitine palmitoyltransferase II deficiency by tandem mass spectrometry. J Inherit Metab Dis 2002;25:17-27.

37. Tajima G, Hara K, Yuasa M. Carnitine palmitoyltransferase II deficiency with a focus on newborn screening. J Hum Genet 2019;64:87-98.
38. Henriques BJ, Olsen RK, Bross P, Gomes CM. Emerging roles for riboflavin in functional rescue of mitochondrial beta-oxidation flavoenzymes. Curr Med Chem 2010;17:3842-54.
39. Eckle SB, Corbett AJ, Keller AN et al. Recognition of Vitamin B Precursors and Byproducts by Mucosal Associated Invariant T Cells. J Biol Chem 2015;290:30204-11.
40. Jonassen T, Clarke CF. Isolation and functional expression of human COQ3, a gene encoding a methyltransferase required for ubiquinone biosynthesis. J Biol Chem 2000;275:12381-7.
41. Gregus Z, Roos G, Geerlings P, Nemeti B. Mechanism of thiol-supported arsenate reduction mediated by phosphorolytic-arsenolytic enzymes: II. Enzymatic formation of arsenylated products susceptible for reduction to arsenite by thiols. Toxicol Sci 2009;110:282-92.
42. Dorsch LM, Schuldt M, dos Remedios CG et al. Protein Quality Control Activation and Microtubule Remodeling in Hypertrophic Cardiomyopathy. Cells 2019;8.
43. Lim DS, Roberts R, Marian AJ. Expression profiling of cardiac genes in human hypertrophic cardiomyopathy: insight into the pathogenesis of phenotypes. J Am Coll Cardiol 2001;38:1175-80.
44. Jorgenrud B, Jalanko M, Helio T et al. The Metabolome in Finnish Carriers of the MYBPC3-Q1061X Mutation for Hypertrophic Cardiomyopathy. PLoS One 2015;10:e0134184.
45. Huang Y, Zhou M, Sun H, Wang Y. Branched-chain amino acid metabolism in heart disease: an epiphenomenon or a real culprit? Cardiovasc Res 2011;90:220-3.

SUPPLEMENTAL FIGURES

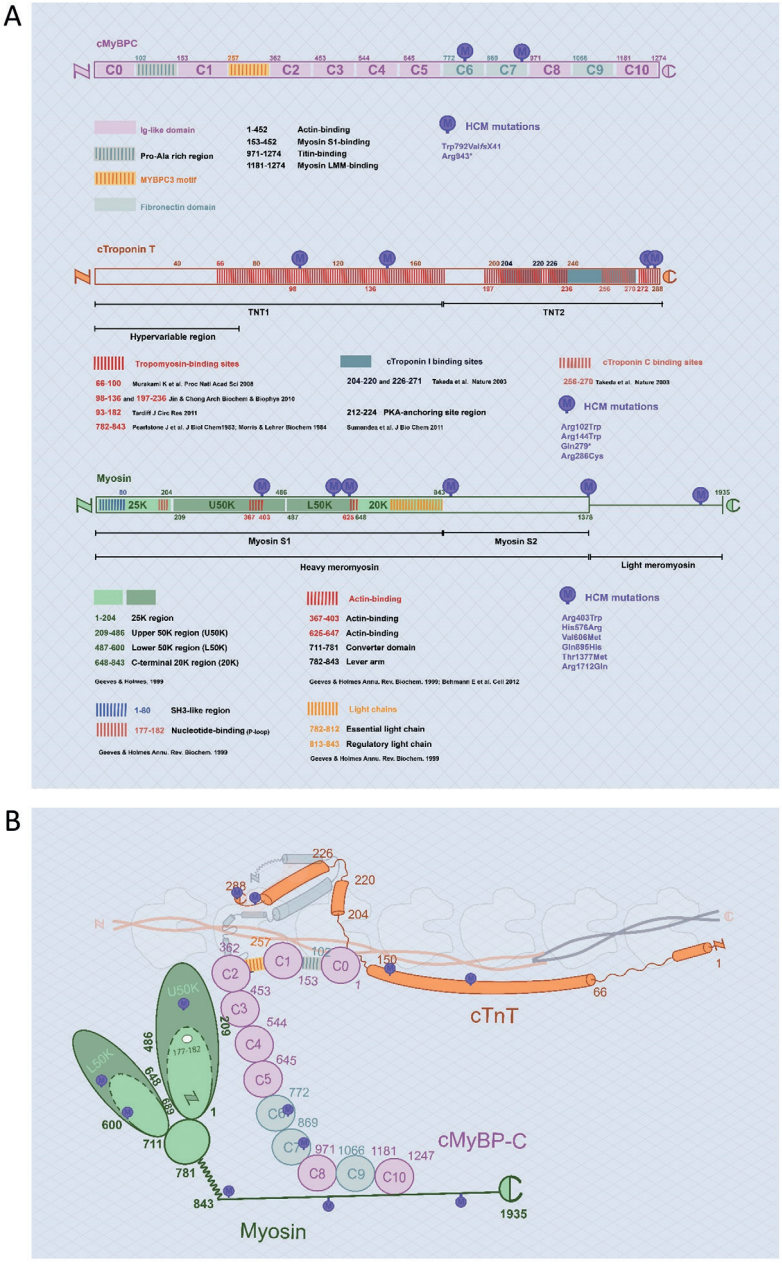

FIGURE S1. Overview of gene variants in this study. (A) shows the protein domains in which the gene variants are located. Image with permission granted by Vasco Sequeira. (B) indicates the location of the gene variants in the structural context. Image adapted from Sequeira et al. Circ Res 2013 with permission Circ Res.

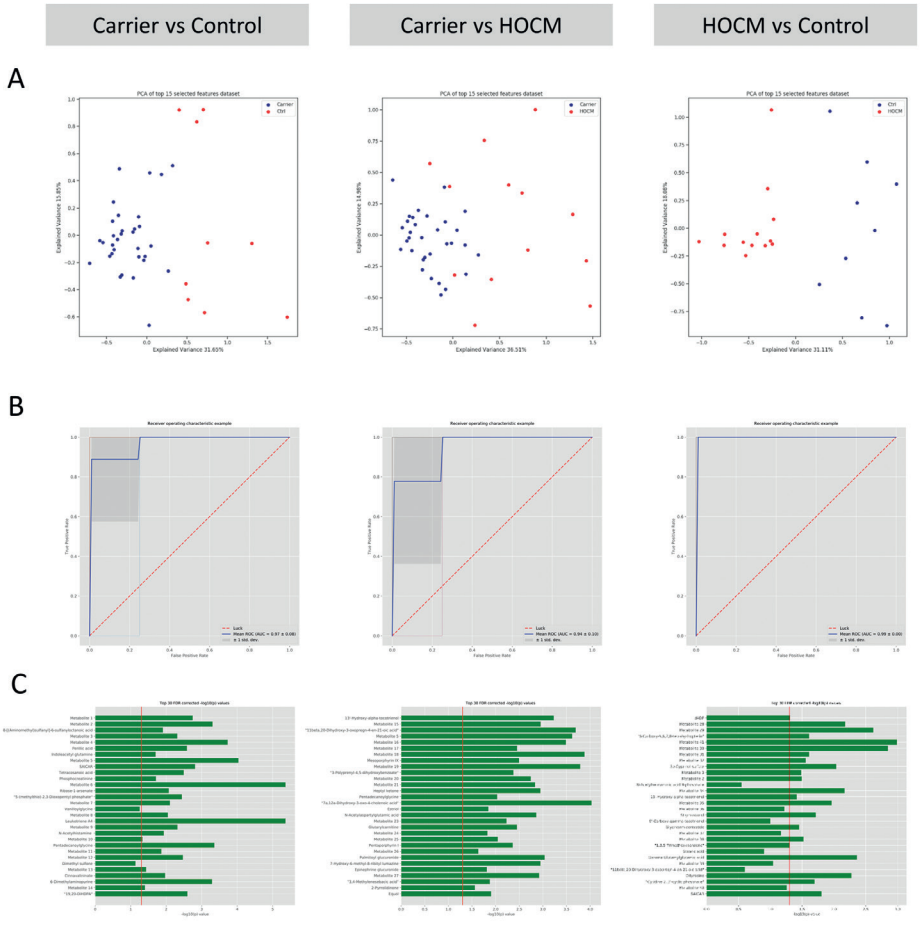

FIGURE S2. Multivariate modelling. (A) Principal component analysis (PCA) for the three group-wise comparisons Carrier vs Ctrls, Carrier vs HOCM and HOCM vs Ctrls. (B) ROC curves of the three group-wise comparisons presenting the performance of the metabolomics data in distinguishing the groups. (C) Top 30 most predictive metabolites with corresponding –log10(p)-values.

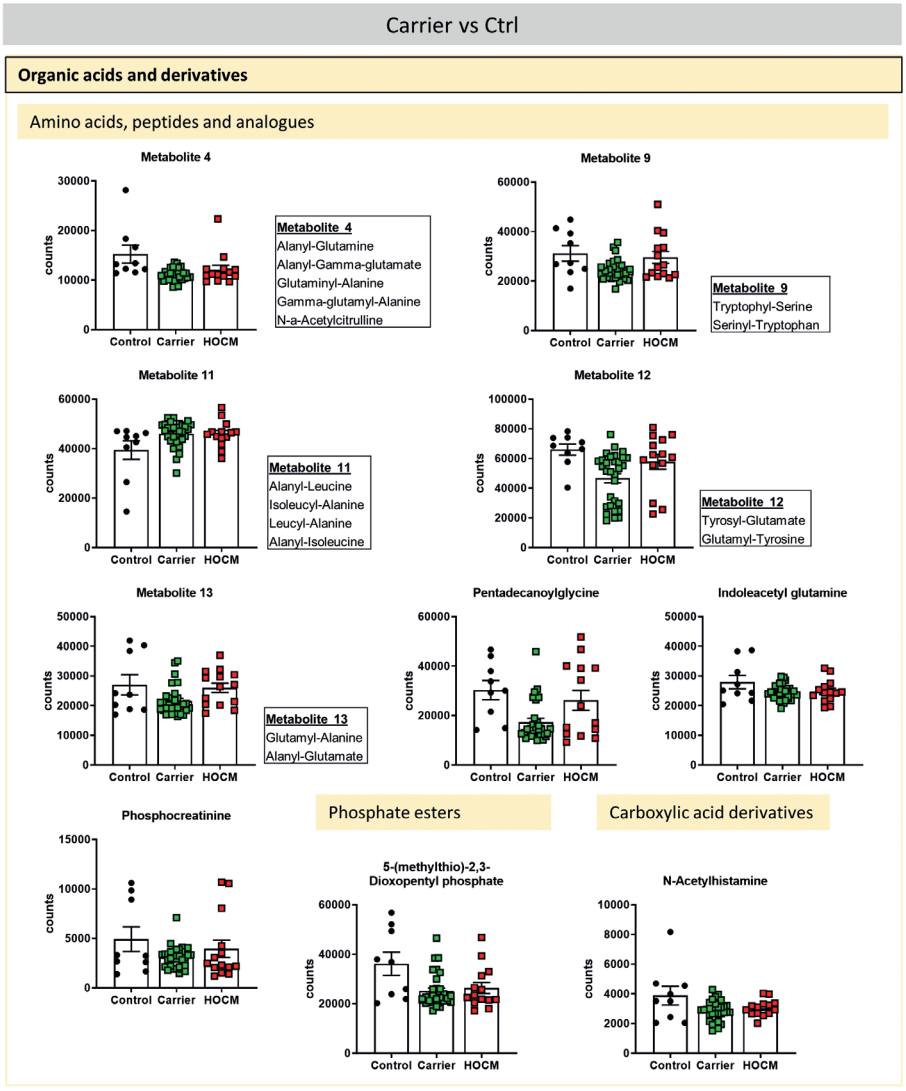

FIGURE S3. Bar graphs with individual data points of the top 30 most important metabolites in distinguishing the Carrier vs Ctrl group. Data from the third group is included in all graphs.

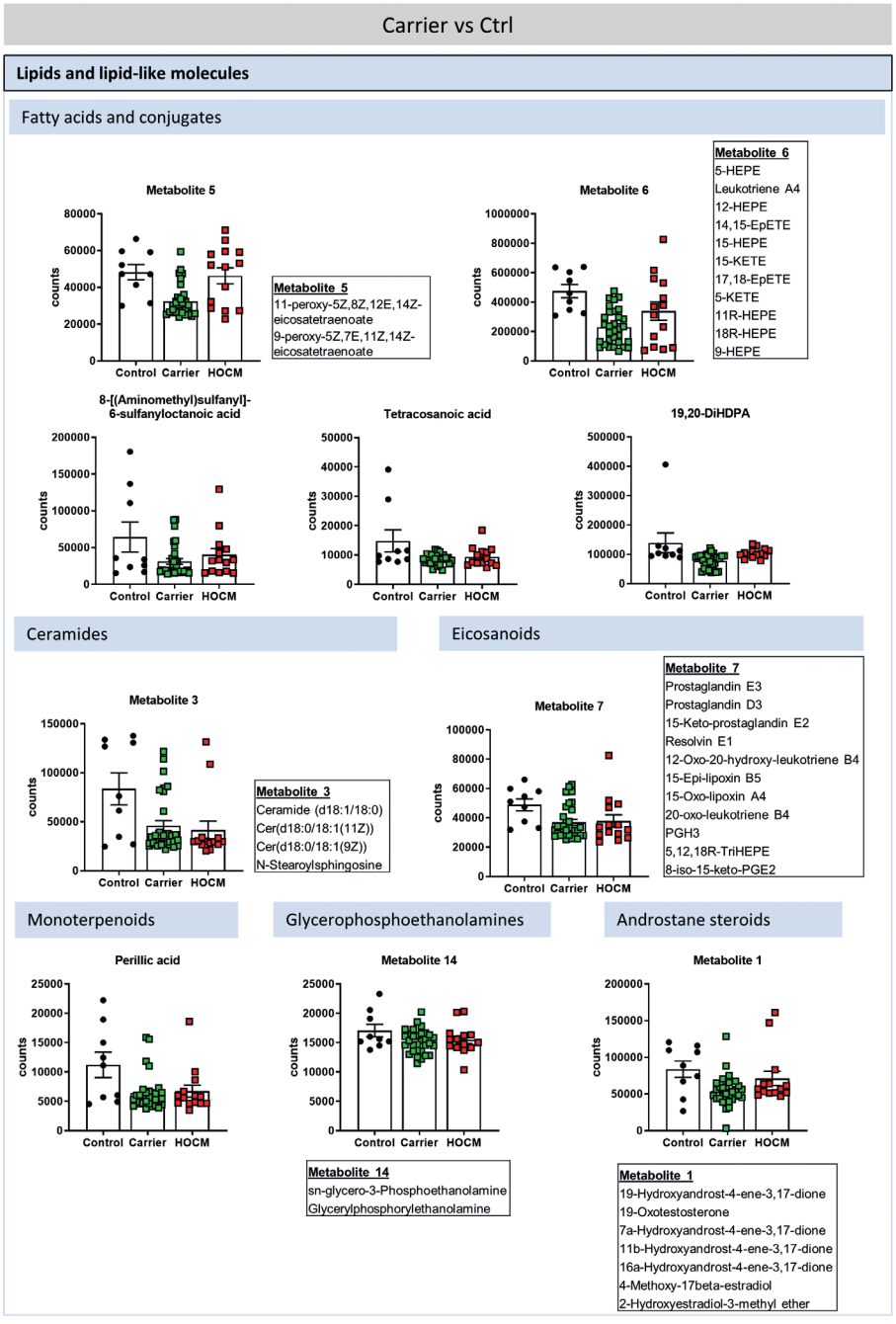

FIGURE S3. Continued.

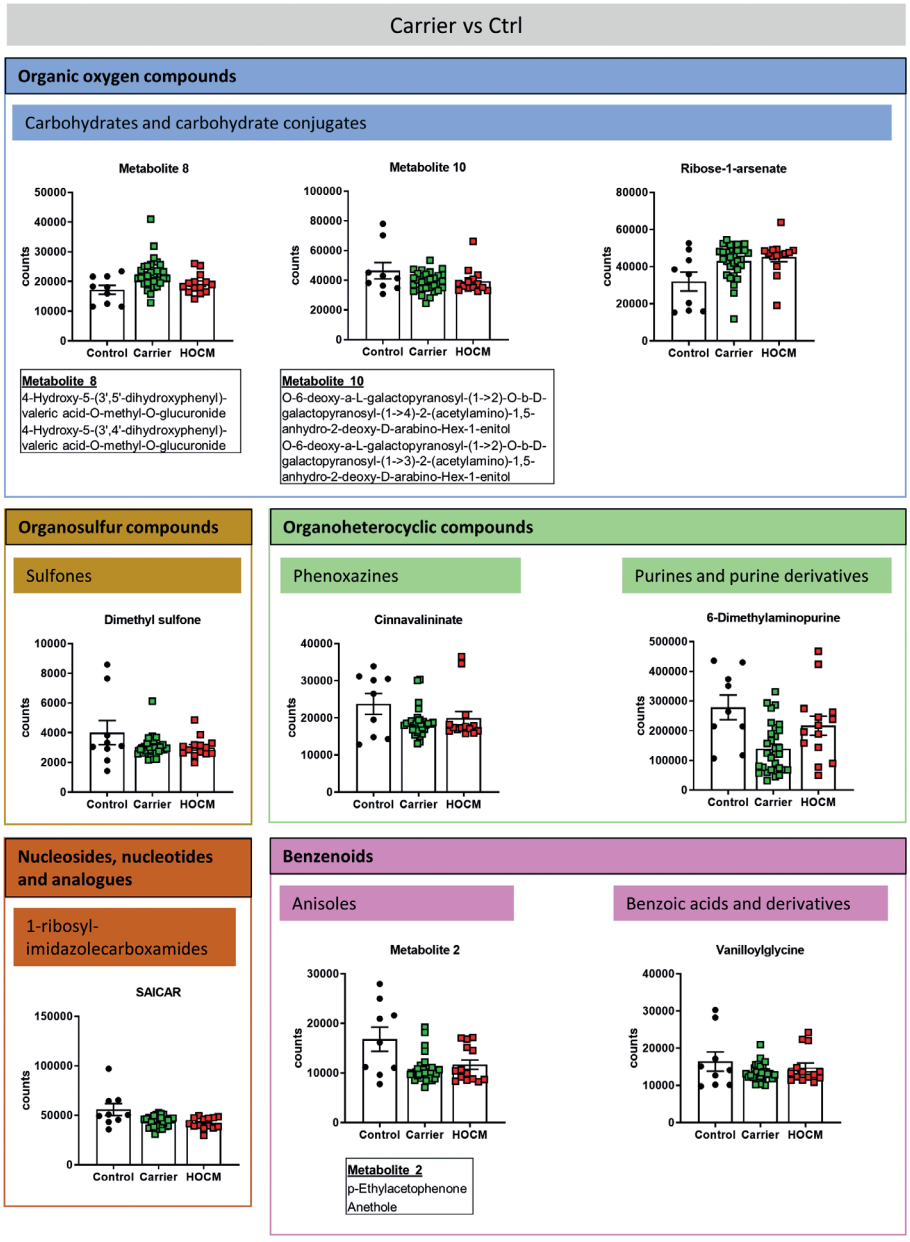

FIGURE S3. Continued.

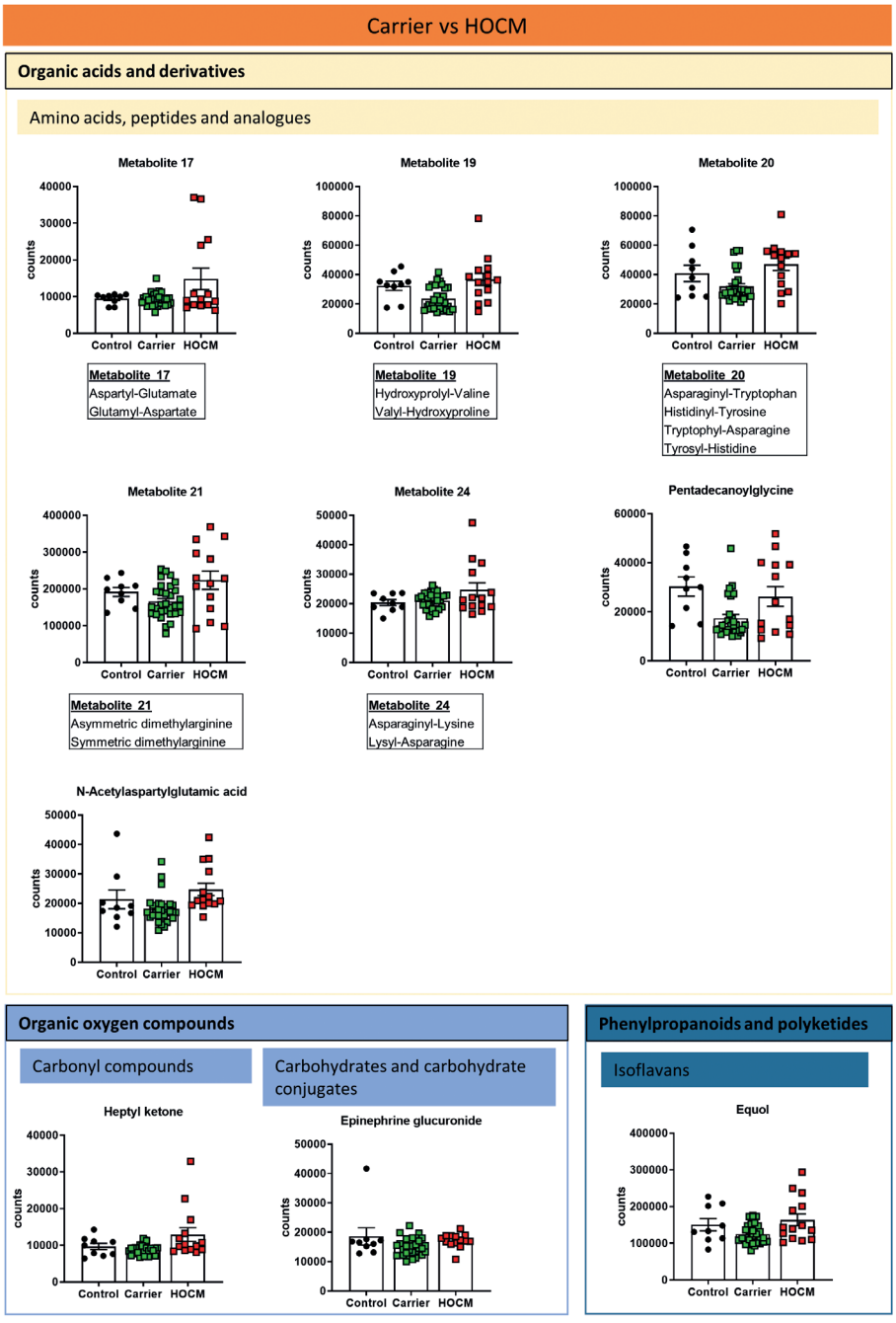

FIGURE S4. Bar graphs with individual data points of the top 30 most important metabolites in distinguishing the Carrier vs HOCM group. Data from the third group is included in all graphs.

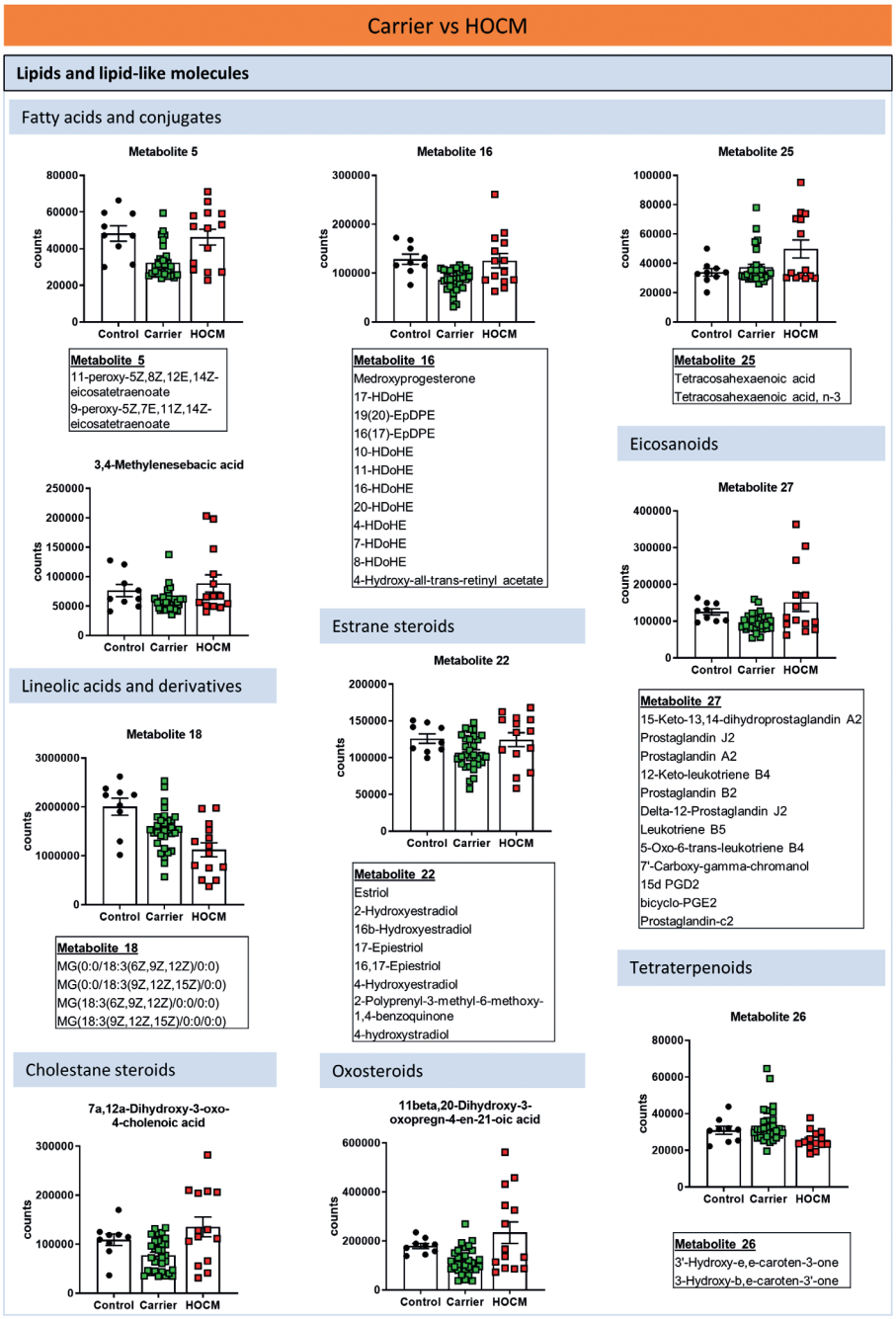

FIGURE S4. Continued.

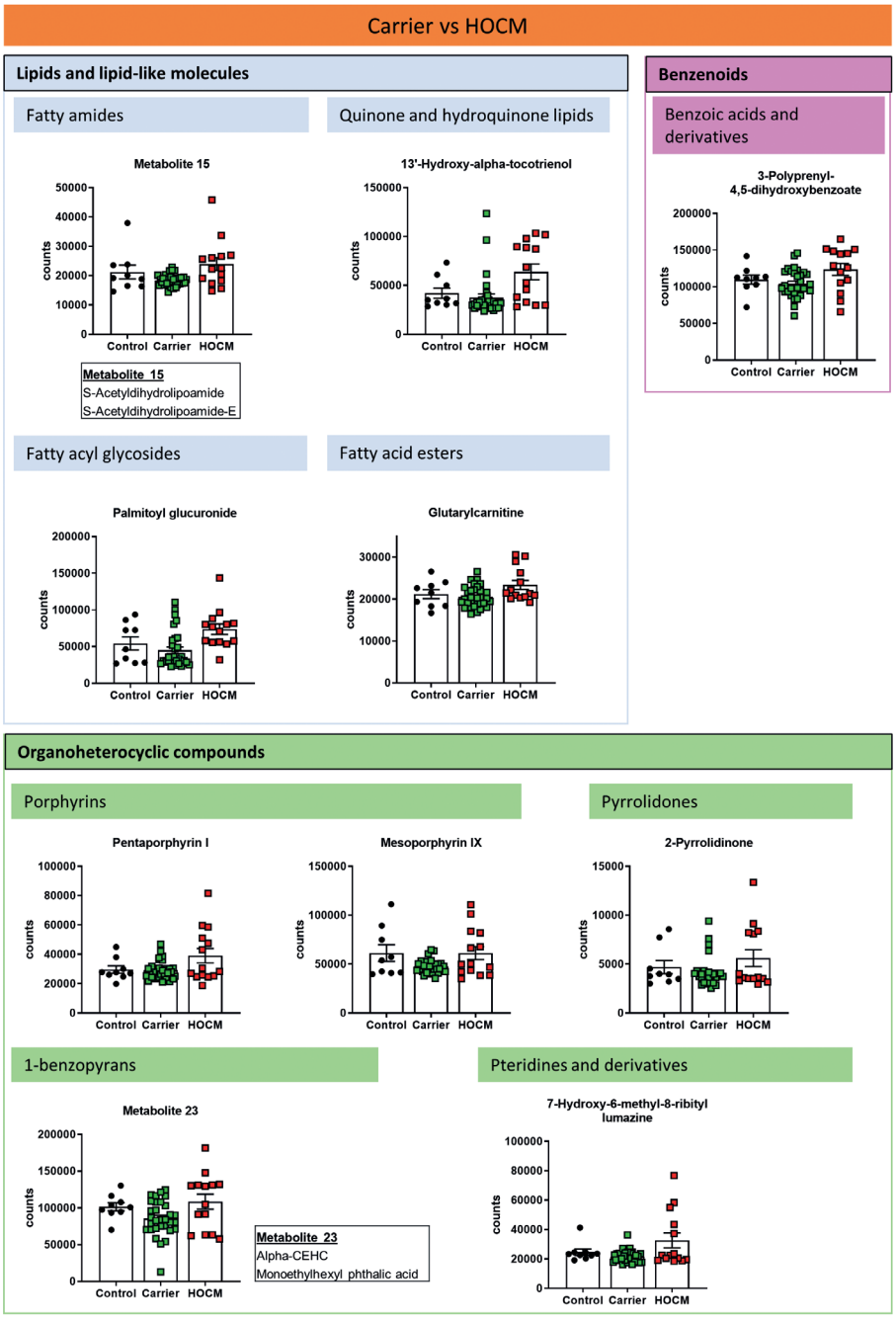

FIGURE S4. Continued.

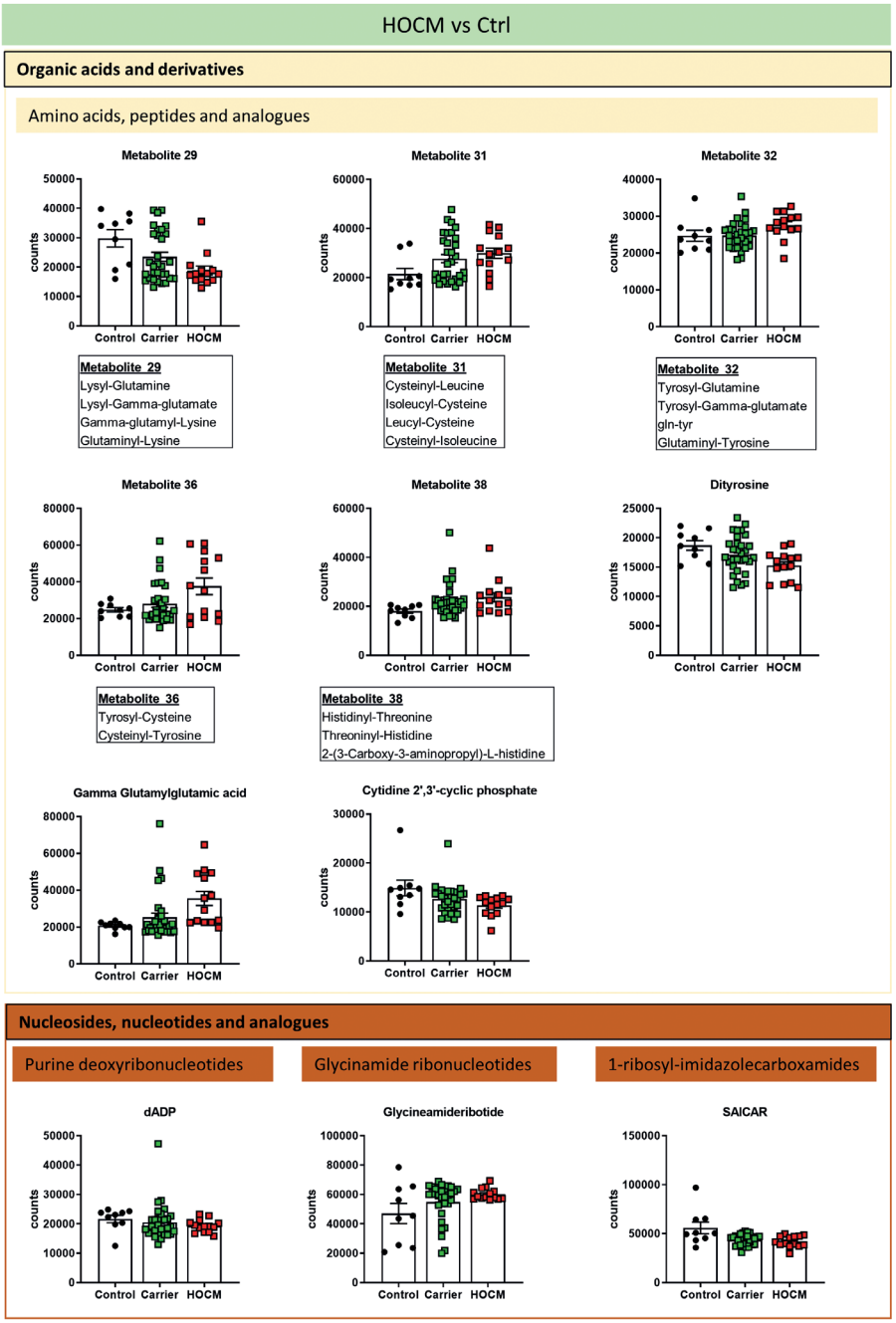

FIGURE S5. Bar graphs with individual data points of the top 30 most important metabolites in distinguishing the HOCM vs Ctrl group. Data from the third group is included in all graphs.

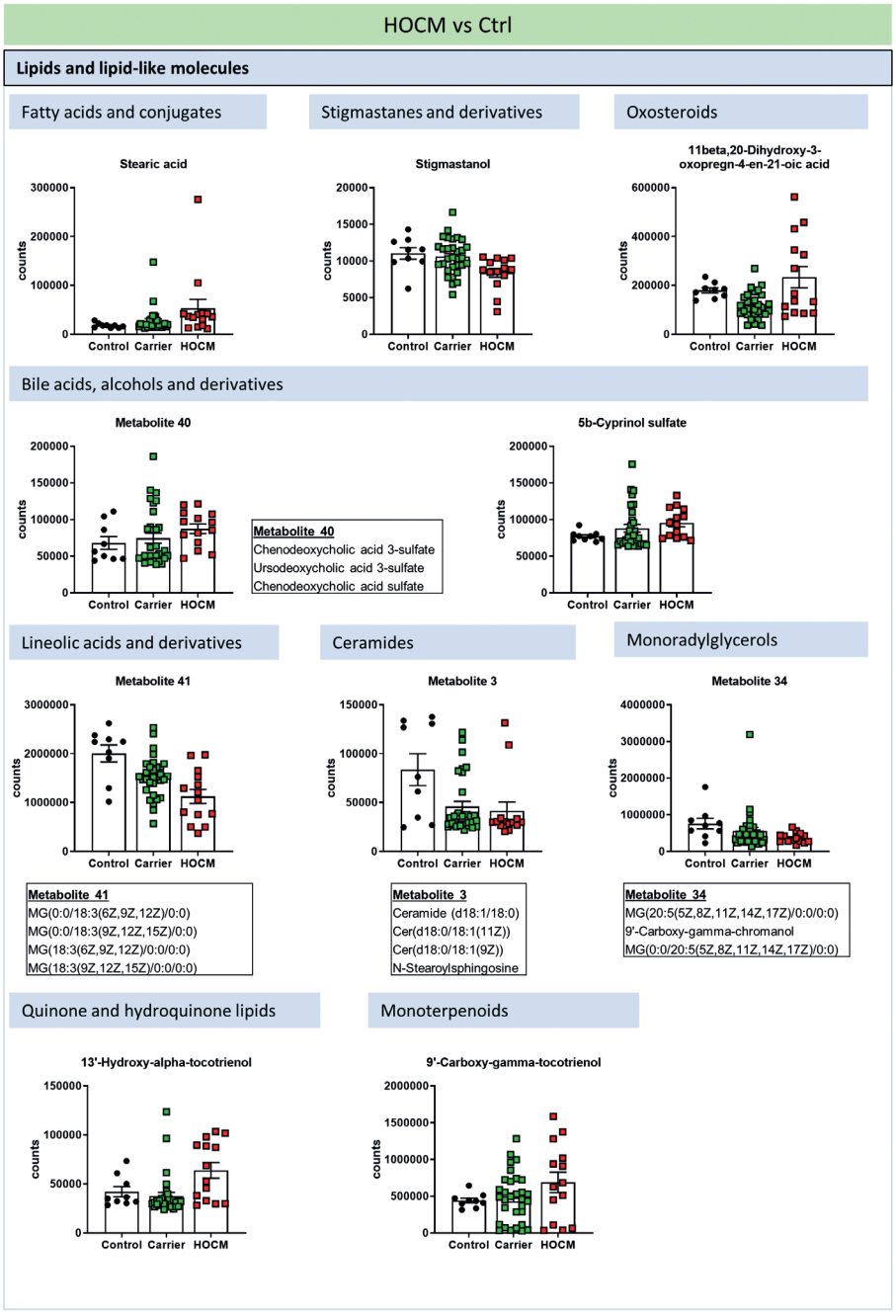

FIGURE S5. Continued.

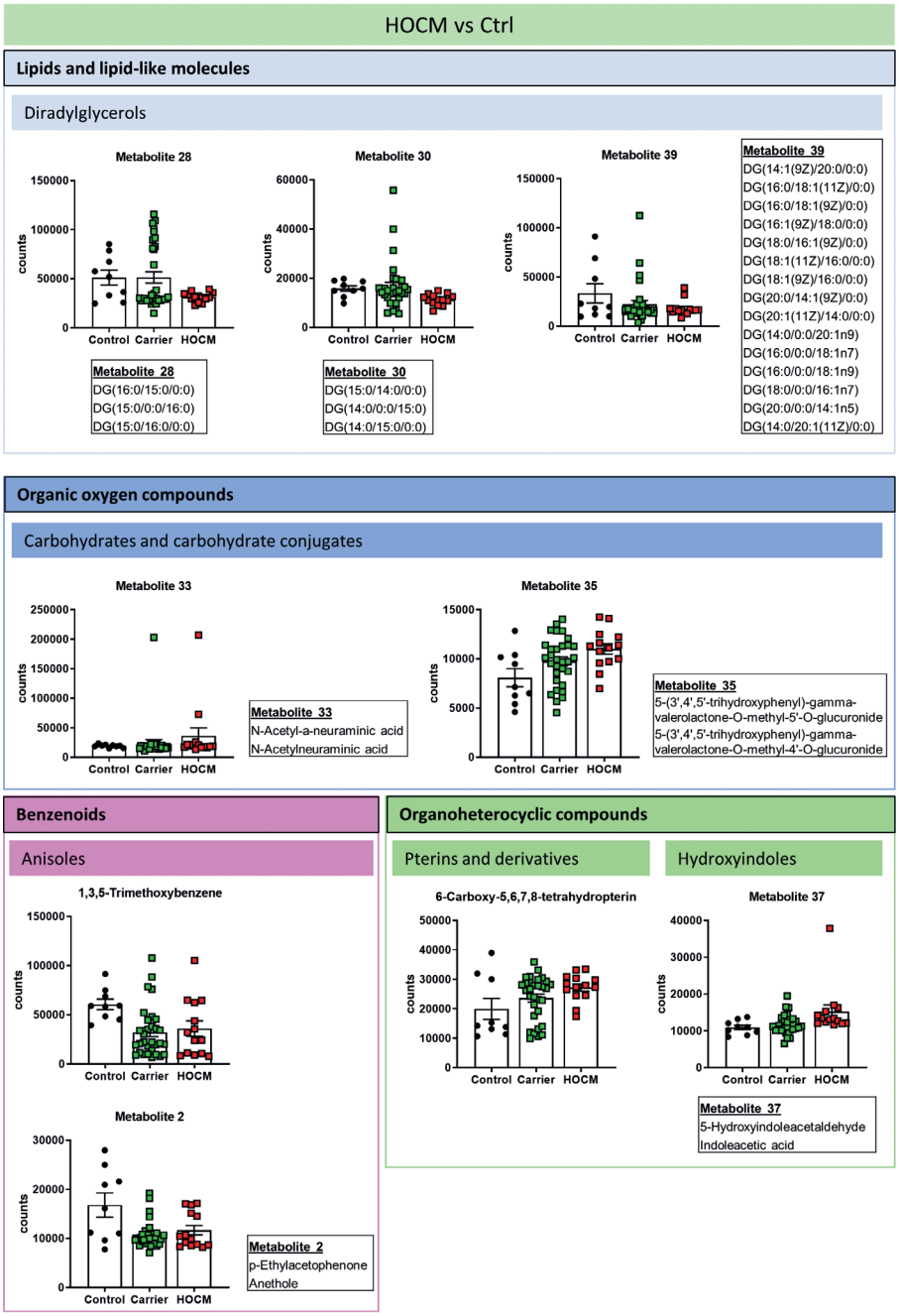

FIGURE S5. Continued.

TABLE S1. Gene variants of preclinical Carriers and HOCM patients including mutation type, sex and age of the individuals.

Gene	Mutation	Type	Age	Sex
Preclinical Carriers				
MYH7	p.His576Arg	missense	34	F
MYH7	p.Arg403Trp	missense	35	F
MYH7	p.Val606Met	missense	30	M
MYH7	p.Thr1377Met	missense	58	F
MYH7	p.Thr1377Met	missense	36	F
MYH7	p.Thr1377Met	missense	21	M
MYH7	p.Arg403Trp	missense	21	F
MYH7	p.Arg403Trp	missense	65	F
MYH7	p.Thr1377Met	missense	44	F
MYH7	p.Arg1712Gln	missense	45	F
MYH7	p.Arg1712Gln	missense	33	M
MYH7	p.Thr1377Met	missense	18	F
MYH7	p.Thr1377Met	missense	31	F
MYBPC3	p.Trp792ValfsX41	truncation	60	F
MYBPC3	p.Trp792ValfsX41	truncation	28	F
MYBPC3	p.Trp792ValfsX41	truncation	30	F
MYBPC3	p.Trp792ValfsX41	truncation	22	M
MYBPC3	p.Trp792ValfsX41	truncation	34	F
MYBPC3	p.Trp792ValfsX41	truncation	60	F
MYBPC3	p.Trp792ValfsX41	truncation	24	F
MYBPC3	p.Trp792ValfsX41	truncation	56	F
MYBPC3	p.Trp792ValfsX41	truncation	26	M
MYBPC3	p.Trp792ValfsX41	truncation	43	F
MYBPC3	p.Trp792ValfsX41	truncation	31	F
MYBPC3	p.Lys301fs	frame shift	41	F
TNNT2	p.Arg102Trp	missense	59	F
TNNT2	p.Arg102Trp	missense	58	F
TNNT2	p.Arg286Cys	missense	48	F
TNNT2	p.Arg144Trp	missense	40	F
TNNT2	p.Arg285Cys	missense	32	M
TNNI3	p.Ser166Phe	missense	22	M

TABLE S1. Continued.

Gene	Mutation	Type	Age	Sex
HOCM patients				
MYH7	p.Gln895His	missense	66	M
MYBPC3			54	F
MYBPC3	p.Trp792ValfsX41	truncation	18	M
MYBPC3	p.Arg943*	truncation	54	F
TNNT2	p.Arg285Cys	missense	43	M
TNNT2	p.Arg102Trp	missense	27	M
TNNT2	p.Arg286Cys	missense	53	M
TNNT2	p.Gln279*	truncation	54	M
MYL2	p.Glu134Ala	missense	57	F
SCN5A			64	M
Sarcomere mutation negative			52	M
Sarcomere mutation negative			68	F
Sarcomere mutation negative			46	M
Sarcomere mutation negative			47	M

TABLE S2. Metabolite identifications and functional classes of the top 30 metabolites of all three group-wise comparisons[3].

Metabolite	Possible identifications	Functional class	p value MEE	padj_BH MEE	p value MVO_2	padj_BH MVO_2
Metabolite 1	19-Hydroxyandrost-4-ene-3,17-dione; 19-Oxotestosterone; 7a-Hydroxyandrost-4-ene-3,17-dione; 11b-Hydroxyandrost-4-ene-3,17-dione; 16a-Hydroxyandrost-4-ene-3,17-dione; 4-Methoxy-17beta-estradiol; 2-Hydroxyestradiol-3-methyl ether	Lipids and lipid-like molecules				
Metabolite 2	p-Ethylacetophenone; Anethole	Benzenoids				
Metabolite 3	Ceramide (d18:1/18:0); Cer(d18:0/18:1(11Z)); Cer(d18:0/18:1(9Z)); N-Stearoylsphingosine	Lipids and lipid-like molecules	**0.0203**	0.9617		
Metabolite 4	Alanyl-Glutamine; Alanyl-Gamma-glutamate; Glutaminyl-Alanine; Gamma-glutamyl-Alanine; N-a-Acetylcitrulline	Organic acids and derivatives	**0.0226**	0.9617	**0.0039**	0.2924
Metabolite 5	11-peroxy-5Z,8Z,12E,14Z-eicosatetraenoate; 9-peroxy-5Z,7E,11Z,14Z-eicosatetraenoate	Lipids and lipid-like molecules			**0.0010**	0.2875
Metabolite 6	5-HEPE; Leukotriene A4; 12-HEPE; 14,15-EpETE; 15-HEPE; 15-KETE; 17,18-EpETE; 5-KETE; 11R-HEPE; 18R-HEPE; 9-HEPE	Lipids and lipid-like molecules			**0.0010**	0.2875
Metabolite 7	Prostaglandin E3; Prostaglandin D3; 15-Keto-prostaglandin E2; Resolvin E1; 12-Oxo-20-hydroxy-leukotriene B4; 15-Epi-lipoxin B5; 15-Oxo-lipoxin A4; 20-oxo-leukotriene B4; PGH3; 5,12,18R-TriHEPE; 8-iso-15-keto-PGE2	Lipids and lipid-like molecules				

TABLE S2. Continued.

Metabolite	Possible identifications	Functional class	p value MEE	padj_BH MEE	p value MVO_2	padj_BH MVO_2
Metabolite 8	4-Hydroxy-5-(3',5'-dihydroxyphenyl)-valeric acid-O-methyl-O-glucuronide; 4-Hydroxy-5-(3',4'-dihydroxyphenyl)-valeric acid-O-methyl-O-glucuronide	Organic oxygen compounds				
Metabolite 9	Tryptophyl-Serine; Serinyl-Tryptophan	Organic acids and derivatives				
Metabolite 10	O-6-deoxy-a-L-galactopyranosyl-(1->2)-O-b-D-galactopyranosyl-(1->4)-2-(acetylamino)-1,5-anhydro-2-deoxy-D-arabino-Hex-1-enitol; O-6-deoxy-a-L-galactopyranosyl-(1->2)-O-b-D-galactopyranosyl-(1->3)-2-(acetylamino)-1,5-anhydro-2-deoxy-D-arabino-Hex-1-enitol	Organic oxygen compounds				
Metabolite 11	Alanyl-Leucine; Isoleucyl-Alanine; Leucyl-Alanine; Alanyl-Isoleucine	Organic acids and derivatives				
Metabolite 12	Tyrosyl-Glutamate; Glutamyl-Tyrosine	Organic acids and derivatives				
Metabolite 13	Glutamyl-Alanine; Alanyl-Glutamate	Organic acids and derivatives				
Metabolite 14	sn-glycero-3-Phosphoethanolamine; Glycerylphosphorylethanolamine	Lipids and lipid-like molecules				
Metabolite 15	S-Acetyldihydrolipoamide; S-Acetyldihydrolipoamide-E	Lipids and lipid-like molecules				
Metabolite 16	Medroxyprogesterone; 17-HDoHE; 19(20)-EpDPE; 16(17)-EpDPE; 10-HDoHE; 11-HDoHE; 16-HDoHE; 20-HDoHE; 4-HDoHE; 7-HDoHE; 8-HDoHE; 4-Hydroxy-all-trans-retinyl acetate	Lipids and lipid-like molecules			**0.0009**	0.2875

TABLE S2. Continued.

Metabolite	Possible identifications	Functional class	p value MEE	padj_BH MEE	p value MVO_2	padj_BH MVO_2
Metabolite 17	Aspartyl-Glutamate; Glutamyl-Aspartate	Organic acids and derivatives				
Metabolite 18	MG(0:0/20:3(5Z,8Z,11Z)/0:0); MG(0:0/20:3(8Z,11Z,14Z)/0:0); MG(20:3(11Z,14Z,17Z)/0:0/0:0); MG(20:3(5Z,8Z,11Z)/0:0/0:0); MG(20:3(8Z,11Z,14Z)/0:0/0:0); MG(0:0/20:3(11Z,14Z,17Z)/0:0)	Lipids and lipid-like molecules	**0.0012**	0.9617		
Metabolite 19	Hydroxyprolyl-Valine; Valyl-Hydroxyproline	Organic acids and derivatives				
Metabolite 20	Asparaginyl-Tryptophan; Histidinyl-Tyrosine; Tryptophyl-Asparagine; Tyrosyl-Histidine	Organic acids and derivatives				
Metabolite 21	Asymmetric dimethylarginine; Symmetric dimethylarginine	Organic acids and derivatives			**0.0045**	0.2924
Metabolite 22	Estriol; 2-Hydroxyestradiol; 16b-Hydroxyestradiol; 17-Epiestriol; 16,17-Epiestriol; 4-Hydroxyestradiol; 2-Polyprenyl-3-methyl-6-methoxy-1,4-benzoquinone; 4-hydroxystradiol	Lipids and lipid-like molecules			**0.0014**	0.2875
Metabolite 23	Alpha-CEHC; Monoethylhexyl phthalic acid	Organoheterocyclic compounds			<0.0001	0.1720
Metabolite 24	Asparaginyl-Lysine; Lysyl-Asparagine	Organic acids and derivatives				
Metabolite 25	Tetracosahexaenoic acid; Tetracosahexaenoic acid, n-3	Lipids and lipid-like molecules			**0.0043**	0.2924

TABLE S2. Continued.

Metabolite	Possible identifications	Functional class	p value MEE	padj_BH MEE	p value MVO_2	padj_BH MVO_2
Metabolite 26	3′-Hydroxy-e,e-caroten-3-one; 3-Hydroxy-b,e-caroten-3′-one	Lipids and lipid-like molecules			**0.0076**	0.3950
Metabolite 27	15-Keto-13,14-dihydroprostaglandin A2; Prostaglandin J2; Prostaglandin A2; 12-Keto-leukotriene B4; Prostaglandin B2; Delta-12-Prostaglandin J2; Leukotriene B5; 5-Oxo-6-trans-leukotriene B4; 7′-Carboxy-gamma-chromanol; 15d PGD2; bicyclo-PGE2; Prostaglandin-c2	Lipids and lipid-like molecules			**0.0190**	0.5463
Metabolite 28	DG(16:0/15:0/0:0); DG(15:0/0:0/16:0); DG(15:0/16:0/0:0)	Lipids and lipid-like molecules				
Metabolite 29	Lysyl-Glutamine; Lysyl-Gamma-glutamate; Gamma-glutamyl-Lysine; Glutaminyl-Lysine	Organic acids and derivatives	**0.0107**	0.9617		
Metabolite 30	DG(15:0/14:0/0:0); DG(14:0/0:0/15:0); DG(14:0/15:0/0:0)	Lipids and lipid-like molecules			**0.0117**	0.4829
Metabolite 31	Cysteinyl-Leucine; Isoleucyl-Cysteine; Leucyl-Cysteine; Cysteinyl-Isoleucine	Organic acids and derivatives				
Metabolite 32	Tyrosyl-Glutamine; Tyrosyl-Gamma-glutamate; gln-tyr; Glutaminyl-Tyrosine	Organic acids and derivatives				
Metabolite 33	N-Acetyl-a-neuraminic acid; N-Acetylneuraminic acid	Organic oxygen compounds				
Metabolite 34	MG(20:5(5Z,8Z,11Z,14Z,17Z)/0:0/0:0); 9′-Carboxy-gamma-chromanol; MG(0:0 /20:5(5Z,8Z,11Z,14Z,17Z)/0:0)	Lipids and lipid-like molecules	**0.0110**	0.9617		

TABLE S2. Continued.

Metabolite	Possible identifications	Functional class	p value MEE	padj_BH MEE	p value MVO_2	padj_BH MVO_2
Metabolite 35	5-(3′,4′,5′-trihydroxyphenyl)-gamma-valerolactone-O-methyl-5′-O-glucuronide; 5-(3′,4′,5′-trihydroxyphenyl)-gamma-valerolactone-O-methyl-4′-O-glucuronide	Organic oxygen compounds	**0.0200**	0.9617		
Metabolite 36	Tyrosyl-Cysteine; Cysteinyl-Tyrosine	Organic acids and derivatives				
Metabolite 37	5-Hydroxyindoleacetaldehyde; Indoleacetic acid					
Metabolite 38	Histidinyl-Threonine; Threoninyl-Histidine; 2-(3-Carboxy-3-aminopropyl)-L-histidine	Organic acids and derivatives				
Metabolite 39	DG(14:1(9Z)/20:0/0:0); DG(16:0/18:1(11Z)/0:0); DG(16:0/18:1(9Z)/0:0); DG(16:1(9Z)/18:0/0:0); DG(18:0/16:1(9Z)/0:0); DG(18:1(11Z)/16:0/0:0); DG(18:1(9Z)/16:0/0:0); DG(20:0/14:1(9Z)/0:0); DG(20:1(11Z)/14:0/0:0); DG(14:0/0:0/20:1n9); DG(16:0/0:0/18:1n7); DG(16:0/0:0/18:1n9); DG(18:0/0:0/16:1n7); DG(20:0/0:0/14:1n5); DG(14:0/20:1(11Z)/0:0)	Lipids and lipid-like molecules				

TABLE S2. Continued.

Metabolite	Possible identifications	Functional class	p value MEE	padj_BH MEE	p value MVO_2	padj_BH MVO_2
Metabolite 40	Chenodeoxycholic acid 3-sulfate; Ursodeoxycholic acid 3-sulfate; Chenodeoxycholic acid sulfate	Lipids and lipid-like molecules				
Metabolite 41	MG(0:0/18:3(6Z,9Z,12Z)/0:0); MG(0:0/18:3(9Z,12Z,15Z)/0:0); MG(18:3(6Z,9Z,12Z)/0:0/0:0); MG(18:3(9Z,12Z,15Z)/0:0/0:0)	Lipids and lipid-like molecules	**0.0012**	0.9617		
1,3,5-Trimethoxybenzene		Benzenoids				
2-Pyrrolidinone		Organoheterocyclic compounds				
3-Polyprenyl-4,5-dihydroxybenzoate		Benzenoids			**0.0042**	0.2924
3,4-Methylenesebacic acid		Lipids and lipid-like molecules				
5-(methylthio)-2,3-Dioxopentyl phosphate		Organic acids and derivatives	**0.0013**	0.9617		
5b-Cyprinol sulfate		Lipids and lipid-like molecules				
6-Carboxy-5,6,7,8-tetrahydropterin		Organoheterocyclic compounds				
6-Dimethylaminopurine		Organoheterocyclic compounds				
7-Hydroxy-6-methyl-8-ribityl lumazine		Organoheterocyclic compounds				
7a,12a-Dihydroxy-3-oxo-4-cholenoic acid		Lipids and lipid-like molecules			**0.0003**	0.1957
8-[(Aminomethyl) sulfanyl]-6-sulfanyloctanoic acid		Lipids and lipid-like molecules				

TABLE S2. Continued.

Metabolite	Possible identifications	Functional class	p value MEE	padj_BH MEE	p value MVO_2	padj_BH MVO_2
9′-Carboxy-gamma-tocotrienol		Lipids and lipid-like molecules			**0.0486**	0.6320
11beta,20-Dihydroxy-3-oxopregn-4-en-21-oic acid		Lipids and lipid-like molecules			**0.0086**	0.4078
13′-Hydroxy-alpha-tocotrienol		Lipids and lipid-like molecules				
19,20-DiHDPA		Lipids and lipid-like molecules				
Cinnavalininate		Organoheterocyclic compounds				
Cytidine 2′,3′-cyclic phosphate		Organic acids and derivatives				
dADP		Nucleosides, nucleotides and analogues	**0.0459**	0.9617		
Dimethyl sulfone		Organosulfur compounds				
Dityrosine		Organic acids and derivatives	**0.0208**	0.9617		
Epinephrine glucuronide		Organic oxygen compounds				
Equol		Phenylpropanoids and polyketides				
Gamma Glutamylglutamic acid		Organic acids and derivatives	**0.0447**	0.9617		
Glutarylcarnitine		Lipids and lipid-like molecules				
Glycineamideribotide		Nucleosides, nucleotides and analogues				

TABLE S2. Continued.

Metabolite	Possible identifications	Functional class	p value MEE	padj_BH MEE	p value MVO_2	padj_BH MVO_2
Heptyl ketone		Organic oxygen compounds				
Indoleacetyl glutamine		Organic acids and derivatives			**0.0469**	0.6225
Mesoporphyrin IX		Organoheterocyclic compounds				
N-Acetylaspartylglutamic acid		Organic acids and derivatives			**0.0251**	0.5533
N-Acetylhistamine		Organic acids and derivatives				
Palmitoyl glucuronide		Lipids and lipid-like molecules			**0.0239**	0.5533
Pentadecanoylglycine		Organic acids and derivatives			**0.0197**	0.5463
Pentaporphyrin I		Organoheterocyclic compounds	**0.0379**	0.9617		
Perillic acid		Lipids and lipid-like molecules				
Phosphocreatinine		Organic acids and derivatives				
Ribose-1-arsenate		Organic oxygen compounds				
SAICAR		Nucleosides, nucleotides and analogues	**0.0126**	0.9617		
Stearic acid		Lipids and lipid-like molecules				
Stigmastanol		Lipids and lipid-like molecules				
Tetracosanoic acid		Lipids and lipid-like molecules	**0.0119**	0.9617	**0.0318**	0.5549
Vanilloylglycine		Benzenoids	**0.0386**	0.9617		

[3]Metabolites in bold are significant in 2 comparisons. P value is given for metabolites that correlate significantly with myocardial external efficiency (MEE) or myocardial oxygen consumption (MVO_2), together with the adjusted p value for multiple testing.

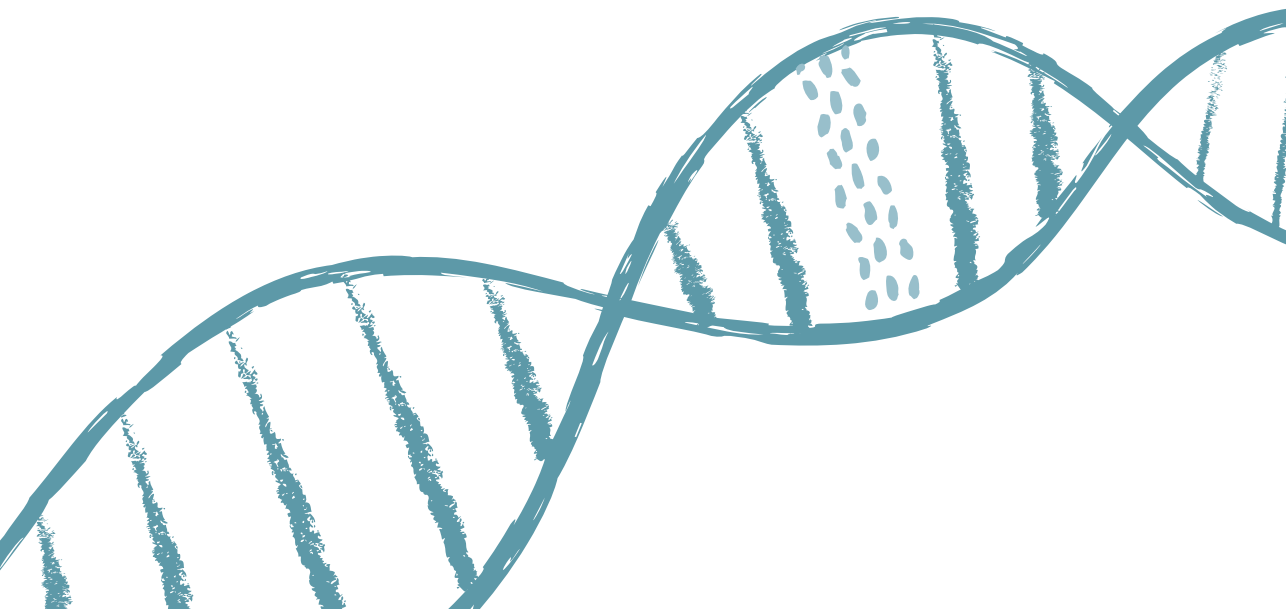

DISCUSSION AND SUMMARY

DISCUSSION AND FUTURE PERSPECTIVES

9

SUMMARY AND DISCUSSION

Hypertrophic cardiomyopathy (HCM) is a clinically heterogeneous disease with large differences in disease penetrance and severity between patients [1]. This is partly due to the presence of 2 major patient populations, the one with an identified gene mutation (sarcomere mutation-positive, SMP) and the one in which a pathogenic gene mutation is not identified (sarcomere mutation-negative, SMN) [2]. But also within these groups variation is large. The variability between the SMP patients is not only explained by the large number and variety of identified pathogenic gene variants termed mutations [2], as even patients with the exact same mutation can have a very different disease course and outcome [3]. Therefore, we hypothesize that a variety of disease modifiers can contribute and influence the clinical disease course in patients. Potential disease modifiers could be environmental factors, such as rural or urban residence, differences in lifestyle, including diet and exercise, and additional gene mutations or (epi)genetic modifiers. In this thesis we explored the mutant protein dose and mutation location and the cellular protein quality control (PQC) as potential disease modifiers. We further used -omics techniques to identify differences at the RNA and protein level between different genetic groups to identify novel disease modifiers and potential novel treatment targets. Additionally, we have shown with a metabolomics study that asymptomatic mutation carriers have a metabolic profile which is distinct from healthy controls, which may be used in the future to identify mutation carriers at risk.

Mutant protein dose and location

One of the proposed disease modifiers that we explored in this thesis is the mutation location and the mutant protein dose. Different mutation locations can be defined as mutations in different genes, and studies in the past aimed to establish a relationship between disease severity and symptoms and the different affected genes. Although some genes have been associated with a more or less severe phenotype, no clear genotype-phenotype correlations were established [4-6]. In addition to gene-specific differences, he mutation location effect can also be assessed for mutations in different protein domains of the same gene. Some functional correlations have been described for mutations in *MYH7* [7, 8], but overall this is poorly investigated. Therefore, we focused in this thesis on the mutation location effect in the *TNNT2* gene, encoding for cardiac troponin T (cTnT).

Especially in individuals with the exact same mutation, differences in the mutant protein dose could contribute to the differences in clinical disease outcome. As most HCM-causing gene mutations are heterozygous, which means that the patient has one healthy and one mutant allele, a ratio of 50% wild-type and 50% mutant protein would be expected. However, different factors could change this expected ratio of healthy and mutant protein. Differences in mRNA and/or protein stability between the healthy and mutant mRNA or protein could alter the ratio. A less stable mutant protein which is prone for degradation and removal by the PQC system could result

in a lower percentage of mutant protein compared to the wild type form, whereas a more stable protein could accumulate resulting in an increased dose of mutant protein. Also the PQC might be an important player regulating the amount of mutant protein in the cell. A healthy well-working PQC might be able to keep the mutant protein dose low. Translating this to the clinical situation, it could imply that patients with a high percentage of mutant protein may present with more severe symptoms and earlier disease onset, whereas patients with a low dose of mutant protein may have only mild symptoms. Timely activation of the PQC to keep the mutant protein dose low may provide a new treatment option.

In HCM, the role of the mutant protein dose is poorly investigated. It is not known how much mutant protein is present in the myocardium of patients as this is difficult to determine. Only for patients with a truncating mutation in *MYBPC3* it is known that the truncated mutant protein is not present, but that the levels of the healthy protein are reduced to ~70% compared to healthy controls [9], which is called haploinsufficiency.

In **Chapter 2** we investigated the mutant protein dose and location effect of different *TNNT2* mutations on cardiomyocyte function. For this we introduced different doses of recombinant mutant cTnT into single permeabilized cardiomyocytes from healthy donors by performing troponin exchange experiments. Strikingly, we observed for two of the mutations, I79N and R94C, that a low dose of mutant protein (<15%) is already sufficient for the maximal increase in myofilament Ca^{2+}-sensitivity, while the effect size is determined by the mutation location. For the R278C mutation, however, we observed increased myofilament Ca^{2+}-sensitivity at low and intermediate dose, whereas a high mutant dose led to decreased myofilament Ca^{2+}-sensitivity. Although we only looked at 3 different cTnT mutations, we have evidence that the mutant protein dose effect is mutation location-specific and not applicable in the same way for every mutation. As the R278C mutation shows a mutant protein dose-dependent functional effect on Ca^{2+}-sensitivity, this could indeed underlie clinical differences between patients. In 2 myectomy samples of HCM patients with the R278C mutation we determined the mutant protein content with mass spectrometry. With 28% and 36% the amount of mutant protein was quite similar in the samples, and could not be directly linked to differences in function. As clinical outcome is most likely dependent on a combination of disease modifiers, *in vitro* results may not be directly reflected in the complex *in vivo* setting.

Protein quality control

The PQC, comprising heat shock proteins (HSPs), the ubiquitin-proteasome system (UPS) and autophagy [10], has already been investigated in a variety of cardiac diseases and often derailment of the PQC has been found. The PQC is crucial for cellular proteostasis as it maintains a healthy balance of protein synthesis and degradation [11]. While it assists in protein folding of newly synthesized proteins, it also recognizes

damaged and defective proteins and ensures their degradation and is crucial for cardiac health [10, 11].

In HCM, a malfunctioning PQC could lead to accumulation of mutant protein which in turn could cause disease onset or a more severe phenotype. As the function of the PQC declines with age, patients may exceed a toxic mutant protein threshold in late adulthood explaining the average disease in the later stages of life. But a defective PQC may not only lead to the accumulation of the mutant protein, also the normal protein turnover will be hampered, so that other aged and defective proteins accumulate which will increase the overall cell stress.

In **Chapter 3** we reviewed the current knowledge about the role of the PQC in the pathogenesis of inherited cardiomyopathies. In human cardiomyopathies, HSP expression has been poorly studied, but upregulation of HSPs has been described in different cardiomyopathy animal models and is generally considered as a beneficial compensatory effect [12, 13]. UPS derailment has already been described in human heart disease [14, 15] and may aggravate disease as decreased proteasome function leads to accumulation of toxic mutant protein. Therefore, modulating different components of the PQC system may provide a novel treatment strategy for inherited cardiomyopathies. The pharmacological induction of HSPs in an animal model of desmin-related cardiomyopathy provides promising evidence for its effectiveness, as it reduced protein aggregation and improved heart function [16].

In **Chapter 4** we determined the expression levels of several PQC key players in our large HCM patient cohort. Compared to healthy controls, we found increased levels of the stabilizing HSPs HSPB1 and HSPB7 and the ATP-dependent HSPD1 and HSPA2, that have refolding capacity. Additionally, we observed increased levels of α-tubulin that correlated with its acetylation level and with the HSP expression levels. This is in line with previous work showing elevated levels of microtubules in failing myocardium [17], which is thought to increase cellular stability. In summary, we showed that HSP levels are indeed elevated in the myocardium of HCM patients and may act as disease modifiers.

Deregulated energy metabolism proteome

In part 2 of this thesis we performed omics-techniques to identify novel disease modifiers in an unbiased manner on different cellular levels. In **Chapter 5** we performed a proteomics screen of a large number of well-characterized human myectomy samples. One of our main findings was reduced expression of proteins involved in energy metabolism. We found lower levels of proteins related to glucose metabolism as well as fatty acid metabolism. Also proteins of the mitochondrial respiratory chain were consistently lower expressed, matching observations of energy deficiency in patients and animal models [18-20]. As energy deficiency has been proposed as the

primary mutation-induced pathomechanism leading to compensatory hypertrophy [21], our study supports ongoing clinical trials investigating the therapeutic effect of targeting the metabolism in early stages of the disease [22].

Detyrosinated tubulin provides novel treatment target in HCM

In **Chapter 5** we also identified increased levels of detyrosinated tubulin as the main difference between SMP and SMN HCM samples. In line with previous studies by the Prosser group [23, 24], we could show in our novel *MYBPC3*$_{2373insG}$ mouse model that detyrosinated tubulin has a negative effect on diastolic function of isolated cardiomyocytes. Lowering tubulin detyrosination by treatment with parthenolide increased relaxation time and improved diastolic function. As our mouse model replicated the increase in detyrosination of tubulin, but not the increase in total levels of α-tubulin as we found in the human samples, we speculate that the increase in detyrosination may happen before the increase in levels of α-tubulin. Hence, detyrosinated tubulin may be an early treatment target and inhibition of detyrosination could potentially halt or slow disease progression.

As we found the elevated levels of detyrosinated tubulin mainly in SMP samples and only to a lower extent in SMN samples, targeting detyrosination is thought to be a promising therapeutic target only in SMP patients. As HCM is clinically heterogeneous, patient-specific or at least genotype-specific treatment strategies may characterize future therapies.

Sex differences at the protein level

As we also see differences in clinical presentation between male and female patients [25-33], we defined sex-specific differences in our proteomics data in **Chapter 7** to identify differences at the protein level between male and female SMP HCM samples. Interestingly, we found higher levels of tubulin in females compared to males. As females show more severe diastolic dysfunction [29, 31, 33], we propose that this is (at least partly) due to elevated levels of tubulin. Furthermore, we found increased levels of HSPs in females compared to males. Studies have shown that the estrogen-dependent induction of HSPs has cardio-protective effects [34]. This could explain why females have a later disease onset compared to males. Follow-up studies are needed to determine whether the female-specific increase in HSPs may be estrogen regulated.

Identification of novel candidate regulators

In **Chapter 6** we integrated different layers of cellular regulation, namely the histone acetylome, the transcriptome and the proteome, to identify key players that drive pathological changes in HCM patients with a mutation in *MYBPC3*. We identified 36 upregulated and 17 downregulated protein-coding genes that were changed in all three levels of analysis, DNA, RNA and protein. Consequently, these candidates may belong to the main disease drivers.

Due to the characteristics and limitations of the different methodologies, integration and direct translation to the clinic is challenging. As the analysis is performed on bulk tissue, not only the mutation-carrying cardiomyocytes are analyzed, but also other cell types like fibroblasts, endothelial cells and immune cells. The larger proportion of cells in the heart are non-cardiomyocytes. As ChIP-seq and RNA-seq is performed on nuclear material, these data are highly influenced by the non-cardiomyocytes. Proteomics on the other hand is a stronger representation of the cardiomyocytes as these are responsible for most of the cell volume. While ChIP-seq and RNA-seq provide a good coverage of the whole histone acetylome and transcriptome, proteomics is prone to the more abundant proteins covering only a fraction of the proteome. Different levels of regulation at all stages further complicate the direct integration and translation of these findings.

Further studies are needed to validate whether the identified candidates have a functional effect in HCM pathogenesis. Induced pluripotent stem cell-derived cardiomyocytes from HCM patients carrying a pathogenic mutation can provide a screening platform to test the functional role of the candidate genes in overexpression and knock-down experiments.

Metabolic signature

For early treatment that may be able to halt or slow disease progression, it is of importance to identify mutation carriers at risk before the onset of symptoms and irreversible cardiac remodeling. Imaging studies have shown that asymptomatic mutation carriers show already reduced cardiac efficiency [19]. However, these advanced imaging techniques are not suitable for periodic screening of patients due to their high costs, and because they can only be performed in specialized centers. Since changes in metabolism may be reflected in the serum metabolite profile, we performed serum metabolomics on healthy controls, asymptomatic mutation carriers and obstructive HCM patients in **Chapter 8**. Interestingly, we found a very distinct serum metabolite profile between asymptomatic carriers and healthy controls, that can distinguish the two groups in our patient cohort. Our statistical model revealed a panel of 30 metabolites that drives the model and provides a starting point for further validation in a different independent cohort. If a set of these candidates can be validated, a simple serum biomarker panel can be developed and used for periodic screening. In the future, this may provide a tool to determine the correct time point for therapeutic intervention and identifying mutation carriers at risk to develop cardiac dysfunction.

FUTURE PERSPECTIVES

The findings from the omics-studies that are described in this thesis serve as a starting point for follow-up studies to validate their functional relevance in HCM pathogenesis. Thereto, different animal models and cellular model systems are available. As many animal models lack some of the key characteristics of human HCM, advances have been made in the generation of 3D engineered heart tissues (EHTs) [35]. EHTs allow for the assessment of both functional and structural changes upon genetic manipulations, drug treatment and other interventions [36]. These EHTs can be generated from patient-derived induced pluripotent stem cells (ipsc), that are differentiated into cardiomyocytes. For the last few years, many efforts have been put into optimizing the differentiation protocols to improve purity, maturity and yield. Recently, Buikema et al. published a cardiomyocyte expansion protocol [37], that allows for the generation of a very large number of cardiomyocytes in a short amount of time. We could show that these cells are also functional in the EHT model [37]. Being able to produce a large amount of cardiomyocytes provides the opportunity to generate EHTs in a large scale for e.g. drug screening purposes. These EHTs can be used to test novel treatment strategies, but also to study disease modifiers, like the mutant protein dose effect, in a more complex cellular system. For these purposes, viral gene expression systems can be used to introduce the mutant gene into the EHT.

The current treatment of HCM patients is only symptomatic to relieve left ventricular outflow tract obstruction and heart failure symptoms. Omics-studies in well characterized patient cohorts and patient tissues form a basis to unravel genotype-specific pathomechanisms that can ultimately lead to patient-specific treatment approaches. Identification of disease modifiers will further help to improve risk prediction in mutation carriers and novel biomarker panels may aid in determining the proper time point for therapeutic intervention.

REFERENCES

1. Ingles, J., et al., *Application of Genetic Testing in Hypertrophic Cardiomyopathy for Preclinical Disease Detection.* Circ Cardiovasc Genet, 2015. **8**(6): p. 852-9.
2. Ho, C.Y., et al., *Genetic advances in sarcomeric cardiomyopathies: state of the art.* Cardiovasc Res, 2015. **105**(4): p. 397-408.
3. Maron, B.J., et al., *Epidemiology of hypertrophic cardiomyopathy-related death: revisited in a large non-referral-based patient population.* Circulation, 2000. **102**(8): p. 858-64.
4. Page, S.P., et al., *Cardiac myosin binding protein-C mutations in families with hypertrophic cardiomyopathy: disease expression in relation to age, gender, and long term outcome.* Circ Cardiovasc Genet, 2012. **5**(2): p. 156-66.
5. Coppini, R., et al., *Clinical phenotype and outcome of hypertrophic cardiomyopathy associated with thin-filament gene mutations.* J Am Coll Cardiol, 2014. **64**(24): p. 2589-2600.
6. Anan, R., et al., *Prognostic implications of novel beta cardiac myosin heavy chain gene mutations that cause familial hypertrophic cardiomyopathy.* J Clin Invest, 1994. **93**(1): p. 280-5.
7. Rai, T.S., et al., *Genotype phenotype correlations of cardiac beta-myosin heavy chain mutations in Indian patients with hypertrophic and dilated cardiomyopathy.* Mol Cell Biochem, 2009. **321**(1-2): p. 189-96.
8. Tanjore, R.R., et al., *Genotype-phenotype correlation of R870H mutation in hypertrophic cardiomyopathy.* Clin Genet, 2006. **69**(5): p. 434-6.
9. van Dijk, S.J., et al., *Cardiac myosin-binding protein C mutations and hypertrophic cardiomyopathy: haploinsufficiency, deranged phosphorylation, and cardiomyocyte dysfunction.* Circulation, 2009. **119**(11): p. 1473-83.
10. Wang, X., H. Su, and M.J. Ranek, *Protein quality control and degradation in cardiomyocytes.* J Mol Cell Cardiol, 2008. **45**(1): p. 11-27.
11. Latchman, D.S., *Heat shock proteins and cardiac protection.* Cardiovasc Res, 2001. **51**(4): p. 637-46.
12. Min, T.J., et al., *The protective effect of heat shock protein 70 (Hsp70) in atrial fibrillation in various cardiomyopathy conditions.* Heart Vessels, 2015. **30**(3): p. 379-85.
13. Niizeki, T., et al., *Relation of serum heat shock protein 60 level to severity and prognosis in chronic heart failure secondary to ischemic or idiopathic dilated cardiomyopathy.* Am J Cardiol, 2008. **102**(5): p. 606-10.
14. Predmore, J.M., et al., *Ubiquitin proteasome dysfunction in human hypertrophic and dilated cardiomyopathies.* Circulation, 2010. **121**(8): p. 997-1004.
15. Day, S.M., et al., *Impaired assembly and post-translational regulation of 26S proteasome in human end-stage heart failure.* Circ Heart Fail, 2013. **6**(3): p. 544-9.
16. Sanbe, A., et al., *Protective effect of geranylgeranylacetone via enhancement of HSPB8 induction in desmin-related cardiomyopathy.* PLoS One, 2009. **4**(4): p. e5351.
17. Heling, A., et al., *Increased expression of cytoskeletal, linkage, and extracellular proteins in failing human myocardium.* Circ Res, 2000. **86**(8): p. 846-53.
18. Luedde, M., et al., *Decreased contractility due to energy deprivation in a transgenic rat model of hypertrophic cardiomyopathy.* J Mol Med (Berl), 2009. **87**(4): p. 411-22.
19. Guclu, A., et al., *Disease Stage-Dependent Changes in Cardiac Contractile Performance and Oxygen Utilization Underlie Reduced Myocardial Efficiency in Human Inherited Hypertrophic Cardiomyopathy.* Circ Cardiovasc Imaging, 2017. **10**(5).

20. Crilley, J.G., et al., *Hypertrophic cardiomyopathy due to sarcomeric gene mutations is characterized by impaired energy metabolism irrespective of the degree of hypertrophy.* J Am Coll Cardiol, 2003. **41**(10): p. 1776-82.
21. Ashrafian, H., et al., *Hypertrophic cardiomyopathy:a paradigm for myocardial energy depletion.* Trends Genet, 2003. **19**(5): p. 263-8.
22. van Driel, B.O., et al., *Extra energy for hearts with a genetic defect: ENERGY trial.* Neth Heart J, 2019. **27**(4): p. 200-205.
23. Robison, P., et al., *Detyrosinated microtubules buckle and bear load in contracting cardiomyocytes.* Science, 2016. **352**(6284): p. aaf0659.
24. Chen, C.Y., et al., *Suppression of detyrosinated microtubules improves cardiomyocyte function in human heart failure.* Nat Med, 2018. **24**(8): p. 1225-1233.
25. Olivotto, I., et al., *Gender-related differences in the clinical presentation and outcome of hypertrophic cardiomyopathy.* J Am Coll Cardiol, 2005. **46**(3): p. 480-7.
26. Marstrand, P., et al., *Hypertrophic Cardiomyopathy With Left Ventricular Systolic Dysfunction: Insights From the SHaRe Registry.* Circulation, 2020. **141**(17): p. 1371-1383.
27. Kubo, T., et al., *Gender-specific differences in the clinical features of hypertrophic cardiomyopathy in a community-based Japanese population: results from Kochi RYOMA study.* J Cardiol, 2010. **56**(3): p. 314-9.
28. Bos, J.M., et al., *Relationship between sex, shape, and substrate in hypertrophic cardiomyopathy.* Am Heart J, 2008. **155**(6): p. 1128-34.
29. Nijenkamp, L., et al., *Sex Differences at the Time of Myectomy in Hypertrophic Cardiomyopathy.* Circ Heart Fail, 2018. **11**(6): p. e004133.
30. Schulz-Menger, J., et al., *Gender-specific differences in left ventricular remodelling and fibrosis in hypertrophic cardiomyopathy: insights from cardiovascular magnetic resonance.* Eur J Heart Fail, 2008. **10**(9): p. 850-4.
31. Chen, Y.Z., et al., *Left ventricular remodeling and fibrosis: Sex differences and relationship with diastolic function in hypertrophic cardiomyopathy.* Eur J Radiol, 2015. **84**(8): p. 1487-1492.
32. Geske, J.B., et al., *Women with hypertrophic cardiomyopathy have worse survival.* Eur Heart J, 2017.
33. van Velzen, H.G., et al., *Effect of Gender and Genetic Mutations on Outcomes in Patients With Hypertrophic Cardiomyopathy.* Am J Cardiol, 2018. **122**(11): p. 1947-1954.
34. Knowlton, A.A. and D.H. Korzick, *Estrogen and the female heart.* Mol Cell Endocrinol, 2014. **389**(1-2): p. 31-9.
35. Mannhardt, I., et al., *Human Engineered Heart Tissue: Analysis of Contractile Force.* Stem Cell Reports, 2016. **7**(1): p. 29-42.
36. Hansen, A., et al., *Development of a drug screening platform based on engineered heart tissue.* Circ Res, 2010. **107**(1): p. 35-44.
37. Buikema, J.W., et al., *Wnt Activation and Reduced Cell-Cell Contact Synergistically Induce Massive Expansion of Functional Human iPSC-Derived Cardiomyocytes.* Cell Stem Cell, 2020. **27**(1): p. 50-63 e5.

APPENDIX

German summary/Deutsche Zusammenfassung

Curriculum Vitae

List of Publications

Acknowledgements

A

GERMAN SUMMARY/DEUTSCHE ZUSAMMENFASSUNG

Hypertrophe Kardiomyopathie ist eine genetische Erkrankung des Herzmuskels, die zu einer asymmetrischen Verdickung des Septums führt. Während der Diastole haben Patienten Schwierigkeiten, die Herzkammer ausreichend mit Blut zu füllen. Zudem haben sie ein erhöhtes Risiko, einen plötzlichen Herztod zu erleiden. Da es zurzeit noch keine heilenden Therapiemöglichkeiten gibt, werden Patienten nur symptomatisch behandelt, um die Krankheitssymptome zu lindern.

Ein wichtiges Merkmal der hypertrophischen Kardiomyopathie ist der individuell sehr unterschiedliche Krankheitsverlauf, der zum Teil dadurch erklärt werden kann, dass es zwei verschiedene Patientenpopulationen gibt. Etwa die Hälfte aller Patienten hat eine Genmutation in einem der kontraktilen Proteine des Herzens, während die Krankheitsursache in der anderen Hälfte der Patienten unbekannt ist. Inzwischen sind mehr als 1500 krankheitsauslösende Mutationen bekannt, selbst Patienten mit einer identischen Mutation können stark variierende Krankheitsverläufe zeigen. Es wird vermutet, dass eine Vielzahl an Faktoren den Schweregrad der Erkrankung beeinflussen. Zu diesen potenziellen Faktoren zählen unter anderem äußere Lebenseinflüsse, wie städtischer oder ländlicher Wohnort, unterschiedliche Lebensstile einschließlich Ernährung und sportliche Betätigung, sowie zusätzliche Genmutationen oder (epi)genetische Modifikationen.

Im ersten Teil dieser Doktorarbeit wurde der Einfluss der vorhandenen Menge an mutiertem Protein und die Mutationsstelle im Gen auf die Funktion von Herzmuskelzellen untersucht, da angenommen wird, dass Patienten mit mehr mutiertem Protein einen schwereren Krankheitsverlauf aufweisen. Interessanterweise konnte für zwei Mutationen im Protein Troponin T gezeigt werden, dass schon eine sehr geringe Menge an mutiertem Protein ausreichend ist, um die Funktion der Zelle negativ zu beeinflussen. Das Ausmaß dieses Effekts war dabei von der Mutationsstelle abhängig. Wie genau sich diese Beobachtungen auf Patienten übertragen lassen, müssen weitere Studien zeigen.

In Herzgewebeproben von Patienten wurde zudem die Menge an Hitzeschockproteinen untersucht, um zu bestimmen, ob es Unterschiede in der Aktivität der zellulären Proteinqualitätskontrolle gibt. Die Proteinqualitätskontrolle ist dazu da, defekte oder mutierte Proteine abzubauen, um eine normale Zellfunktion zu gewährleisten. Im Vergleich mit Kontrollproben konnten wir erhöhte Mengen an Hitzeschockproteinen in den Patientenproben feststellen. Dies ist vermutlich eine Reaktion der Zelle, um die mutierten Proteine abzubauen und dem generellen erhöhten Zellstress entgegenzuwirken. Weitere Studien müssen zeigen, ob eine gezielte Aktivierung der Proteinqualitätskontrolle als Therapiemöglichkeit genutzt werden kann, um einen Abbau der mutierten und fehlerhaften Proteine zu fördern.

Im zweiten Teil dieser Doktorarbeit wurden sogenannte omics-Techniken verwendet, um nach neuen krankheitsmodifizierende Faktoren auf Protein und RNA Basis zu suchen und neue therapeutische Angriffspunkte zu finden.

Dazu wurde das Proteom und das Transkriptom im Herzgewebe von Patienten untereinander und mit gesunden Kontrollproben verglichen. Alle Patientenproben hatten gemeinsam, dass sie weniger Proteine exprimiert haben, die für die zelluläre Energiegewinnung von Bedeutung sind. Diese Beobachtung stützt laufende klinische Studien, die zu therapeutischen Zwecken im frühen Krankheitsstadium in den Energiemetabolismus eingreifen.

Zudem haben die Studien ergeben, dass Patienten mit einer Genmutation, im Vergleich zu Patienten ohne Mutation, stark erhöhte Mengen α-Tubulin aufweisen, besonders von der detyrosinierten Form des Proteins. In einem Mausmodell mit einer krankheitsauslösenden Mutation konnte gezeigt werden, dass eine pharmakologische Verringerung der detyrosinierten Form dieses Proteins zu einer verbesserten Funktion der Herzmuskelzellen führt. Dementsprechend ergibt sich daraus ein vielversprechender neuer Therapieansatz für Patienten mit einer krankheitsverursachenden Mutation.

Ein Vergleich der Proben von Frauen und Männern hat zudem gezeigt, dass besonders Frauen mehr α-Tubulin sowie höhere Mengen an Hitzeschockproteinen haben.

In einem weiteren Ansatz wurden das Proteom, das Transkriptom und die Histonmodifikationen integriert, um neue potenzielle Regulatoren zu identifizieren, die einheitlich auf allen drei Ebenen verändert sind und dadurch besonders krankheitsrelevant sein könnten. Mehrere Kandidaten wurden identifiziert und weitere Studien werden zeigen, ob diese tatsächlich einen funktionellen Effekt in der Krankheitsentstehung haben.

Zusätzlich wurde in einer Metabolomics Studie gezeigt, dass asymptomatische Mutationsträger, verglichen zu gesunden Probanden, bereits ein anderes Profil an Metaboliten im Blutserum aufweisen. Dies könnte in der Zukunft als Biomarker genutzt werden, um Mutationsträger, bei denen sich der Krankheitsverlauf verschlechtert, zeitnah zu erkennen und rechtzeitig zu behandeln.

Die Ergebnisse dieser Doktorarbeit bestätigen, dass der Krankheitsverlauf der hypertrophischen Kardiomyopathie aus einem komplexen Zusammenspiel vieler Faktoren bestimmt wird. Die Ergebnisse dieser Studien bilden einen Ausganspunkt für weitere Validierungsstudien und legen den Grundstein für neue und patientenspezifische Therapieansätze.

CURRICULUM VITAE

Maike Schuldt was born in Einbeck, Germany, in 1991. After she obtained her university entrance qualification from the Goetheschule Einbeck in 2010, she started a bachelor of science degree in Molecular Medicine at the Georg-August University in Göttingen, Germany. During this bachelor program she performed an internship at the Beatson Institute for Cancer Research in Glasgow, United Kingdom, in the group of Prof. Olson. She performed her bachelor thesis with Dr. Muriel Lizé at the department of Molecular Oncology at the University of Göttingen and graduated in 2013. Maike continued her education with a master of science degree in Molecular Medicine at the same University and performed an internship at the institute of pharmacology and toxicology of the University Medical Center Göttingen with Prof. Lutz. During this internship she worked with engineered heart tissue and got in touch with Dr. Diederik Kuster from the department of physiology in Amsterdam, the Netherlands. She visited the lab for her master thesis research project and studied the role of glucocorticoids in hypertrophic cardiomyopathy. Because of her growing interest in cardiovascular research, she returned to Amsterdam after graduating from her master studies and started her PhD under the supervision of Prof. Jolanda van der Velden and Dr. Diederik Kuster. Maike worked within the national CVON-DOSIS consortium and studied disease modifiers in hypertrophic cardiomyopathy. Therefore she worked with human myectomy tissues and performed single-cell studies, as well as large scale proteomics, transriptomics and metabolomics studies. She collaborated with Dr. Jose Pinto from the Florida State University, Prof. Connie Jimenez from the Onco-proteomics laboratory of the Amsterdam UMC and the group of Prof. Folkert Asselbergs at the UMC Utrecht. In August 2020 Maike started working on a research project using a high-throughput screening to identify novel regulators of cardiac contraction and relaxation under the supervision of Dr. Diederik Kuster.

LIST OF PUBLICATIONS

Schuldt M, van Driel B, Algul S, Parbhudayal RY, Barge-Schaapveld DQCM, Güçlü A, Jansen M, Baas AF, Levin E, Germans T, Jans JJM, and van der Velden J. Metabolomics shows different blood marker profiles in preclinical and advanced disease stages of hypertrophic cardiomyopathy. *Manuscript in preparation*

van Driel B, **Schuldt M**, Algul S, Levin E, Güclü A, Germans T, van Rossum A, Pei J, Harakalova M, Baas AF, Jans JJM, and van der Velden J. Metabolomics in severe aortic stenosis reveals intermediates of nitric oxide synthesis as most distinctive markers. *Int J Mol Sci, 2021. In press*

Wildung M, Herr C, Riedel D, Wiedwald C, Tasena H, Heimerl M, Alevra M, Movsisian N, **Schuldt M**, Volceanov-Hahn L, Provoost S, Noethe-Menchen T, Urrego D, Freytag B, Wallmeier J, Beisswenger C, Bals R, van den Berge M, Timens W, Hiemstra P, Bradsma CA, Maes T, Andreas S, Heijink I, Pardo L, and Lize M. miR449 protects airway cilia and healthy lung aging. *Submitted*

Pei J*, **Schuldt M***, Nagyova E*, Gu E, el Bouhaddani S, Yiangou L, Jansen M, Calis JJA, Dorsch LM, Snijders Blok C, van den Dungen NAM, Lansu N, Boukens BJ, Efimov IR, Michels M, Verhaar MC, de Weger R, Vink A, van Steenbeek FG, Baas AF, Davis RP, Uh HW, Kuster DWD, Cheng C, Mokry M, van der Velden J, Asselbergs FW, and Harakalova M. Multi-omics integration identifies key upstream regulators of pathomechanisms in hypertrophic cardiomyopathy due to truncating MYBPC3 mutations. *Clinical Epigenetics, 2021. 13(1): p.61.*

Schuldt M, Dorsch LM, Knol JC, Pham TV, Schelfhorst T, Piersma SR, dos Remedios CG, Michels M, Jimenez CR, Kuster DWD, and van der Velden J. Sex-related differences in protein expression in sarcomere mutation-positive hypertrophic cardiomyopathy. *Frontiers in Cardiovascular Medicine, 2021. 8(129).*

Schuldt M, Pei J, Harakalova M, Dorsch LM, Schlossarek S, Mokry M, Knol JC, Pham TV, Schelfhorst T, Piersma SR, dos Remedios CG, Dalinghaus M, Michels M, Asselbergs FW, Moutin MJ, Carrier L, Jimenez CR, van der Velden J, and Kuster DWD. Proteomic and Functional Studies Reveal Detyrosinated Tubulin as Treatment Target in Sarcomere Mutation-Induced Hypertrophic Cardiomyopathy. *Circ Heart Fail, 2021: p. CIRCHEARTFAILURE120007022.*

Schuldt M, Johnston JR, He H, Huurman R, Pei J, Harakalova M, Poggesi C, Michels M, Kuster DWD, Pinto JR, and van der Velden J. Mutation location of HCM-causing troponin T mutations defines the degree of myofilament dysfunction in human cardiomyocytes. *J Mol Cell Cardiol, 2020. 150: p. 77-90.*

de Boer RA, Nijenkamp LLAM, Silljé HHW, Eijgenraam TR, Parbhudayal RY, van Driel B, Huurman R, Michels M, Pei J, Harakalova M, van Lint FHM, Jansen M, Baas AF, Asselbergs FW, van Tintelen JP, Brundel BJJM, Dorsch LM, **Schuldt M**, Kuster DWD, and van der Velden J (DOSIS consortium). Strength of patient cohorts and biobanks for cardiomyopathy research. *Neth Heart J. 2020 Aug; 28(Suppl 1):50–56.*

Buikema JW, Lee S, Goodyer WR, Maas RG, Chirikian O, Li G, Miao Y, Paige SL, Lee D, Wu H, Paik DT, Rhee S, Tian L, Galdos FX, Puluca N, Beyersdorf B, Hu J, Beck A, Venkamatran S, Swami S, Wijnker P, **Schuldt M**, Dorsch LM, van Mil A, Red-Horse K, Wu JY, Geisen C, Hesse M, Serpooshan V, Jovinge S, Fleischmann BK, Doevendans PA, van der Velden J, Garcia KC, Wu JC, Sluijter JPG, and Wu SM. Wnt Activation and Reduced Cell-Cell Contact Synergistically Induce Massive Expansion of Functional Human iPSC-Derived Cardiomyocytes. *Cell Stem Cell, 2020. 27(1): p. 50-63 e5.*

Dorsch LM, **Schuldt M**, dos Remedios CG, Schinkel AFL, de Jong PL, Michels M, Kuster DWD, Brundel BJJM, and van der Velden J. Protein Quality Control Activation and Microtubule Remodeling in Hypertrophic Cardiomyopathy. *Cells, 2019. 8(7).*

Najafi A, van de Locht M, **Schuldt M**, Schonleitner P, van Willigenburg M, Bollen IAE, Goebel M, Ottenheijm CA, van der Velden J, Helmes M, and Kuster DWD. End-diastolic force pre-activates cardiomyocytes and determines contractile force; role of titin and calcium. *J Physiol, 2019.*

Dorsch LM*, **Schuldt M***, Knezevic D, Wiersma M, Kuster DWD, van der Velden J, and Brundel BJJM. Untying the knot: protein quality control in inherited cardiomyopathies. *Pflugers Arch, 2018.*

Bollen IAE, **Schuldt M**, Harakalova M, Vink A, Asselbergs FW, Pinto JR, Kruger M, Kuster DWD, and van der Velden J. Genotype-specific pathogenic effects in human dilated cardiomyopathy. *J Physiol, 2017. 595(14): p. 4677-4693.*

Gabrielsen M, **Schuldt M**, Munro J, Borucka D, Cameron J, Baugh M, Mleczak A, Lilla S, Morrice N, and Olson MF. Cucurbitacin covalent bonding to cysteine thiols: the filamentous-actin severing protein Cofilin1 as an exemplary target. *Cell communication and signaling : CCS, 2013. 11(1): p. 58-58.*

ACKNOWLEDGEMENTS

The only part that is left to finish this book is to write down this last - and probably most read - chapter of my thesis and thank everybody who helped me in one way or another to accomplish it. The past 5 years have been a wonderful journey and left me with lots of great memories.

Dear Jolanda, thank you for letting me be part of your research group and doing my PhD on the DOSIS project. I immediately felt welcome in the department and learned a lot during the last years. Thank you for all the opportunities to go to summer schools, conferences and other labs to learn new techniques, have scientific exchange and develop myself further. Thank you for all the scientific discussions, feedback on manuscripts and overall supervision. Despite your full agenda you always made time if needed. Your enthusiasm and passion for science always inspired me.

Dear Diederik, my chapter in Amsterdam started with my master internship that you supervised. At that time I did not know that these 6 months would become more than 5 years, but I am glad that I decided to stay! Thank you for your trust and the opportunity to start this PhD. I am really grateful for all your help and advice in and outside the lab and appreciated that your door was always open. It was a great to work with you and also conferences and borrels were always a lot of fun!

Dear members of the thesis committee, Bianca, Connie, Reinier, Rudolf, Annette and Magdalena, thank you for your time and effort to critically evaluate my thesis.

My dear paranymphs Max and Larissa, I am so happy to have you both at my side during my defense. Max, from day one you were my German buddy showing me around the lab and Amsterdam. I have so many great memories from the past years. Working in the lab was never boring with you and all the borrels, parties, boat rides and not to forget the wintersport holidays were a lot of fun. You always had an open ear and I could always count on you. Larissa, my Amsterdam sister, ich bin froh, dass du auch sowas mit Science machst und in unser DOSIS Team gekommen bist. Es hat einfach geklickt und wir haben Submissions und Publikationen bei einem Dinner gefeiert, aber uns auch über Rejections bei einem Cappuccino aufgeregt. Und was hätte ich nur ohne unsere Koch- und Netflix-sessions, Likörchenabende und vor allem „Nachbesprechungen" gemacht. Thank you for your company that made the last years so memorable.

I also want to thank all the other members from Jolanda's group.

Ilse, you were such a big help in the beginning of my PhD, helping me to find my way around the department, teaching me how to isolate pretty cardiomyocytes and

so much more. You would always sponge when necessary and we maintained our emergency chocolate cabinet very well. Thanks for everything and all the fun things we did. The goat yoga was definitely one of my highlights!

Aref, you are one of a kind and it was great to have you in the office. Let me know if you find Mr. Schnee!

Vaishali, I am so happy that I got to know you and won't forget our a**-burning coffeebreaks with Max in the old MF building and cocktail nights (or brunches) with Ilse. You still need to teach me how to make a proper Indian curry!

Elza, I really missed your energy after you left. It was great working with you.

Vasco, I inherited your spot in the old MF office, which looked so empty after you removed all your "wallpaper". You always impressed me with your knowledge about science history, knowing all the publications from 40 years ago in and out.

Ruud, what should I have done without you! You were such a big help with all the blots and I guess most of us just realized after you left how much you took care of the protein lab. Rammstein at 8 am was always a nice surprise when entering the lab in the morning!

Paul, thank you for teaching me the troponin exchange and how to make EHTs. You could sometimes surprise me with making unexpected jokes!

Kim, I have to say I was a bit jealous when you left for your world trip but so cool that you did it! It was always fun with you and maybe we can go on another horse riding trip with Anoek one day!

Louise, with you it was never boring in our office and I enjoyed the music and spontaneous singing of you! If there was a moment for an inappropriate joke then you were usually the one to make it causing a good laugh!

Rahana and Beau, thanks for your input from the clinical side and the collaboration on the metabolomics study.

Leo, it was great having you in our group for a while. Thanks for teaching me some real Italian Carbonara!

Edgar, I was happy that you moved to our office after Ilse left and I had another person to share the ups and downs of cardiomyocyte measurements with. Thanks for sponging and being my backup for the myectomies. I enjoyed it so much when you were speaking German and won't forget our epic dance for Xu's defense!

Pedro, you have only been here for a year but it already feels like you have been part of this group for a long time. I am happy that you joined our group and became such a good friend! Your positive energy definitely lightens up the office!

Rafi and Qianliang, we do not know each other for that long yet but I wish you good luck with the ipsc-cardiomyocytes and your PhDs!

Zubayda, I am happy that I got to know you and could always listen to a funny story or Disney songs when we were in the lab.

Valentijn, you certainly mastered the art of isolating cardiomyocytes! Thank you for all the pretty cells, your help and the nice conversations in the lab.

A big thank you also to all secretaries! Aimée, you were really the heart of the department. You always knew how to help and I just loved your humor! Jessica, Sjoukje and Eva, thank you for taking care of all the orders and help with administrative questions. Isabelle, thank you for all your support regarding the PhD programme.

Duncan and Andreas, thank you for all the help with the myocyte setups and your patience in explaining the electronics and software. You saved more than one experiment with your immediate help in case of problems.

Thanks to all my office-roommates that made the PhD time so much more fun! It all started with Ilse, Manon, Joana and Michiel in the old MF building, where I inherited the famous paper-covered spot from Vasco, and continued with Ilse, Aref, Louise, Leo, Jin, Edgar, Nicole, Rafi, Pedro and Qianliang after moving to O2. Thanks for your company, all the fun conversations, the secret -actually not so secret- chocolate stocks, the Chinese lessons and the sponging when experiments did not work out as planned.

"Coffee is a hug in a mug" – Considering that, I guess we hugged quite a lot, and even our friend from the Science Café noticed when we were deviating from our normal coffee time :D Larissa, Eva, Laura, Pedro and Tatjana, thank you for the numerous cappuccino breaks that were always something to work towards! And I know what you are thinking now: "Thank you for saying thank you."

To the other "muscle" and 12th- floor people: Thanks for all the nice Friday lab meetings, the spontaneous chats in the hallway, the lunch company and the nice atmosphere on our floor.

Martijn, I think you are one of the only people that is still there from the moment I joined the department. We not only shared this PhD journey, but also our passion for troponology! Thanks for all the fun moments (Mmm-mm-mm-milk shake was

definitely one of them!). Stefan, I think I have never met somebody else who can eat so much cheese. With you it is never boring, and you have this ability to get people (me included) into discussions that they take very serious while you are already laughing inside. Always fun to watch when you are not the one who just got fooled :D Thanks for being always in a good mood! Marloes, you were always up for a joke and speaking out what everybody else was already thinking. Eva, I was instantly in a good mood when we said "Hallooo" to each other in the hallway. Will definitely miss that! Rowan, you are one of the kindest people I know. Sometimes we did not see each other for weeks but it was always nice talking to you! Kennedy, I hope one day we will be able to do the trip to Brazil! Thanks for letting us make a mess in your kitchen and the nice dinners at your place! Anoek, mijn schatje, thanks for your company and the distraction and entertainment in the office. Hope you can finish your PhD soon as well! Sylvia, thanks for the nice chats and always being helpful. Chris, you were somehow always there, and when you were not you showed up again for the drinks. Thanks for initiating many of the Vrijmibos! Mark, it was great having you in the department for a while. Won't forget the car ride to Austria :D

To all the other former and current colleagues: Josine, Barbara, Denise, Xu, Luciënne, Marit, Deli, Ricardo, Hua, Roselique, Yeszamin, Leon, Laura, Tatjana, Diewertje, Manon, Sun, Liza, Zeineb, Jeroen, Phat, Jisca, Xue, Fabienne, Igor, Pan, Robert, Rio, Aida, Natalija, Veerle, Vanessa, Albert, Karlijn, Emmy, Joana, Melissa, Nina, Anke, Jan, Michiel, Philippa, Reinier, Ed, Peter and Coen, thank you for the "gezelligheid" and the nice lunch breaks, borrels, labuitjes and other moments.

Martijn, Rowan and Denise, it was a lot of fun organizing TPO with you!

To my collaborators: Jose and Jamie, thank you for the troponin complexes and your help with the exchange study. Connie, thank you for your expertise and guidance on the proteomics study. Magdalena and Jiayi, thank you for performing the RNA sequencing and all your guidance in dealing with omics data. I definitely learned a lot from you! Jan-Willem and Renee, it was great that we could collaborate on the use of expanded cardiomyocytes in EHTs.

To all the members of the DOSIS consortium: It was great to be part of this team! Thanks for the nice meetings, the discussions and the joint projects that we accomplished.

Danae, Dorita, Lisa and Sila, thank you for doing your internships with me and helping me out with my projects.

Larissa, Laura, und Tatjana, die German-Trash-TV Abende mit euch waren immer das Highlight der Woche! In diesem Sinne möchte ich auch Sebastian, Melissa, Nico und Co für die wirklich unterhaltsamen Stunden danken, die durch Spinat-Lachs-Lasagne

und ein Likörchen perfekt gemacht wurden. Larissa, du kennst meine Küche inzwischen in- und auswendig. Laura, was für ein Timing, dass du immer pünktlich zur nächsten Likörrunde wieder wach warst. Tatjana, ich bin immer noch von deiner Coffee-map begeistert :D Ich freue mich schon auf die nächste Runde Floor-Workout und „Dj"enga mit euch. Ich sag nur: „Girl, do it for you!"

"You can always try and fail" – my motto in the bouldergym! Climbing people, thanks for the fun times! In the end Team Blue did not make it to the competitions but who knows what will happen in the future :D

A big thank you to all the people I met in the VU koor! It was so much fun singing with you, going to choir weekends and just hanging out! Niels G., Florine, Romé, Marthe, Joost, Anna L. and Niels N, I am so happy that I got to know you and look forward to more game nights with you!

Meine lieben Molmeds, ohne euch wäre das Studium nur halb so schön gewesen. Caro, Irina, Basti, Robin, Sarina, Rico, Sebi, und Neni, ich bin echt froh, dass wir uns gleich so gut verstanden haben und so eine gute Zeit hatten. Ich hoffe, dass wir unsere Traditionen wie Weihnachtsmarktbesuch und MMoT Reisen noch lange beibehalten und uns oft in der Skeipe treffen! Auf zum Atom!

Laura, Insa, Sonja und Hanna, es ist einfach schön, dass es mit euch immer so ist, als hätten wir uns erst gestern gesehen, auch wenn manchmal ein ganzes Jahr dazwischen liegt. Danke euch für die Besuche in Amsterdam, die Wichtelabende, Escaperooms und alles andere.

Zuletzt noch ein großes Danke an meine Familie. Mama & Papa, ihr habt mich immer unterstützt und mir alles ermöglicht. Auch die Entscheidung, für meinen PhD ins Ausland zu ziehen, habt ihr sofort bedingungslos unterstützt, obwohl wir uns dadurch manchmal monatelang nicht gesehen haben. Danke für alles!

Amsterdam Cardiovascular Sciences